Department of Mechanical Engineering

The modelling and analysis of hand arm vibration in order to reduce industrial vibration exposure

Amir Najafi Amin

This thesis is presented for the Degree of
Doctor of Philosophy
of
Curtin University

January 2017

Acknowledgements

I have been indebted in the preparation of this thesis to my supervisor, Professor Ian Howard, whose patience and kindness, as well as his academic experience, has been invaluable to me. His guidance helped me over the entire duration of my research. I could not have imagined having a better advisor and mentor for my PhD study.

Also, I would like to acknowledge the Department of Mechanical Engineering through the CIPRS scholarship and the following people for their generous assistance and support. My thesis committee, Dr. Rodney Entwistle and Dr. Andrew King for their support. Mr. David Collier and Mr. Graeme Watson and the rest of the technical officers in the Department of Mechanical Engineering at Curtin University.

Damione Wright from Glove Technologies, for providing financial support and supplying damping materials and anti-vibration gloves.

My parents, Hooshang and Nasrin, for their constant source of support, and this thesis would certainly not have existed without them.

Last but not least my wife Mahtab. She was always there cheering me up and standing by me through the good times and bad. I dedicated this thesis to her.

Nomenclature

Symbol	Name	Unit
A	Acceleration	m/s^2
A_o	Initial area	m^2
A_w	Area of wax	m^2
A_x	Acceleration in the X-direction	m/s^2
A_z	Acceleration in the Z-direction	m/s^2
A_{Axi}	Acceleration in the X-direction at the palm	m/s^2
A_{Ayi}	Acceleration in the Y-direction at the palm	m/s^2
A_{Azi}	Acceleration in the Z-direction at the palm	m/s^2
A_{Hxi}	Acceleration in the X-direction at the handle	m/s^2
A_{Hyi}	Acceleration in the Y-direction at the handle	m/s^2
A_{Hzi}	Acceleration in the Z-direction at the handle	m/s^2
A_{hxi}	Acceleration in the X-direction at the handle of a power tool	m/s^2
A_{hyi}	Acceleration in the Y-direction at the handle of a power tool	m/s^2
A_{hzi}	Acceleration in the Z-direction at the handle of a power tool	m/s^2
a_{hv}	Weighted value of total acceleration	m/s^2
b	Width	m
c	Coefficient of damping	$N.s/m$
E	Young's modulus	N/m^2
E_a	Apparent Young's modulus	N/m^2
F	Force	N
F_o	Force at the support	N
f_i	Frequency	Hz
f_n	Natural frequency	Hz
h	Height	m
h_o	Initial height	m
I_m	The second moment of area for the middle of the beam	m^4
I_s	The second moment of area for the side of the beam	m^4
j	Square root of minus one	[]
k	Stiffness	N/m
L	Length	m
L_o	Initial length	m

Symbol	Name	Unit
M_o	Bending moment at the support	$N.m$
M(x)	Bending moment at x	$N.m$
MI	Mechanical impedance	$N.s/m$
m	Mass	Kg
η	Loss factor	[]
$P_{E,1h}$	Point per hour	[]
PT_W	Predicted weighted acceleration of the glove for a tool	m/s^2
P_{ZZ}	Acceleration PSD	$(m/s^2)^2/Hz$
$q(x)$	Load	N/m
r_1	Outer radius	m
r_2	Inner radius	m
s	Length of plate at the two sides of the beam	m
T	Vibration transmissibility	[]
t	Thickness	m
V	Velocity	m/s
V(x)	Shear force at x	N
W	Weight	$gram$
w	Weighting factor	[]
ω	Angular frequency	rad/s
W_{hi}	Weighting factor	[]
W_{VPA}	Weighting factor based on vibration power absorption	[]
x	Displacement	m
$\dot{x}$	Velocity	m/s
$\ddot{x}$	Acceleration	m/s^2
y	Displacement of the handle	m
$\dot{y}$	Velocity of the handle	m/s
$\ddot{y}$	Acceleration of the handle	m/s^2
y_M	Deflection of the beam	m
Z	Mechanical impedance	$N.s/m$
Z_H	Mechanical impedance of hand	$N.s/m$
Z_M	Mechanical impedance of material	$N.s/m$
θ	Slope of the beam	[]
σ	Stress	N/m^2

Symbol	Name	Unit
ε	Strain	[]

List of Abbreviations

AM	Apparent Mass
BF	Biodynamic Force
BR	Biodynamic Response
CTS	Carpal Tunnel Syndrome
DAT	Data Acquisition Toolbox
DM	Displacement Mobility
DOF	Degree Of Freedom
EAV	Exposure Action Value
ECU	Extensor Carpi Ulnaris
ELV	Exposure Limit Value
EMG	Surface Electromyography
FWVT	Frequency Weighted Vibration Transmissibility
HAV	Hand-Arm Vibration
HAVS	Hand-Arm Vibration Syndrome
HAS	Hand-Arm System
LDPI	Laser Doppler Perfusion Imaging
LDV	Laser Doppler Vibrometer
MEMS	Micro-Electro Mechanical System
MI	Mechanical Impedance
MVT	Mean Vibration Transmissibility
PPE	Personal Protective Equipment
TPT	Thermal Perception Threshold
TTS	Temporary Threshold Shift
TVD	Traumatic Vasospastic Disease
VPA	Vibration Power Absorption
VPT	Vibration Perception Threshold
VT	Vibration Transmissibility
VWF	Vibration-induced White Finger
WBV	Whole Body Vibration
WMSD	Work-related Musculoskeletal Disorders

Abstract

Power tools facilitate many aspects of manufacturing and production. Unfortunately, the generated vibration in these tools, transmits to the hand and body of their operators, which over the long term can cause damage to joints, muscles, bones and etc. The health risk for these operators depends on many factors such as type, magnitude and time of vibration exposure. There are international standards regarding the measurement of this vibration transmissibility and for evaluating the performance of anti-vibration gloves for personal protective equipment; however, further investigation and review in this field is required for continued improvements in glove design.

This research investigates the vibration transmissibility from the vibrating handle to the hand-arm of the operator, and considers practical ways to attenuate the operator vibration exposure. For this purpose a novel handle was designed and utilized for simulating the vibration behaviour of the power tools' handle. This handle can measure the applied feed and grip forces by measuring the strains inside its structure, and by measuring the acceleration response at both the palm and fingers simultaneously.

The previous studies in this field have only investigated the vibration at one point of the hand, while this study suggests a practical way to measure vibration at different locations of the hand simultaneously. Measurement with this method generates a clearer picture of the vibration behaviour at the palm of the hand which provides more accurate evaluation of anti-vibration gloves.

Since any anti-vibration glove needs damping material, this study also investigated the vibration behaviour of three commercial damping materials experimentally. Analytical models for the tested materials were developed from the vibration measurements as a function of the coverage area and pressure of the samples. The results showed that a N-DOF lumped mass model with complex stiffness and damping can be developed to simulate the vibration behaviour of the material sample. Furthermore, the research showed that for high pressure load on the sample, only a 1-DOF model is required, and that the parameters of the model have linear relationship with the area of the sample. This model can be further combined with

the lumped-mass model of the hand-arm system for simulating the performance of the glove which uses the damping material.

Contents

1 Introduction

Power tools and machines serve the manufacturing industry by facilitating the level of operator's work and increasing the speed of production; therefore, for the last century, the industry has become completely dependent on them. These tools generate vibration due to their nature of design or by having unbalanced components. While operators hold the handles of these tools, the generated vibration transmits to the hand and arm of the operators. Vibration exposure over a long duration can harm the human body, and the health risk depends on the vibration level, frequency, duration of exposure and etc.

There are some regulations and standards for measuring and limiting the vibration transmissibility from the tools to the human body. For instance, ISO 10819 defines a procedure for measuring hand-arm vibration transmissibility from a vibrating handle to the hand. In addition, it defines a procedure for evaluating anti-vibration gloves. Studies showed there are many issues with the suggested testing setup and procedure. Although, in the last few decades, many researchers have studied in this field; however, still more investigation is required.

This study aims to further investigate the vibration transmissibility from a vibrating handle to the hand and arm, and to generate a clearer picture of this vibration behaviour for further reduction of vibration exposure. Therefore, this study designs and constructs an experimental apparatus suitable for measuring both hand-arm vibration transmissibility and for measuring mechanical impedance at the palm and finger sides. It suggests a more practical way for measuring vibration at the palm side which can be used for both laboratory and field tests, and improves the current standard's procedure for measuring vibration transmissibility. Later, it uses the

measured mechanical impedance of the palm and fingers sides, and generates lumped-mass models with multi degrees of freedom for simulating the vibration behaviour of the hand-arm system. In addition, this research investigates the vibration behaviour of damping materials and generates analytical models for simulating their vibration behaviour. It combines the lumped-mass models of the hand-arm system and damping materials, and develops models to simulate the performance of the resultant gloves which use the tested damping materials. With this simulation it suggests a proper amount for each of the tested materials inside the glove to satisfy the standard' criteria for evaluation as an anti-vibration glove.

The following chapter explores and reviews the previous studies in this field. Initially, it considers health risks regarding hand-arm vibration exposure and various related syndromes. It explorers the suggested testing setup and investigates each element in this testing procedure, including the excitation vibration spectra. In addition, this study reviews different approaches for evaluating anti-vibration gloves. Finally, it considers the analytical methods for simulating hand-arm vibration and explores different types of the suggested lumped-mass models for the simulation.

For simulating vibration of power tools and for measuring hand-arm vibration, a proper handle is required which does not have any resonance in the frequency range of the test. Since for analytical simulation, mechanical impedance of the system is required; therefore both acceleration and force at the driving point should be measured. As a result, the handle needs to measure the applied feed and grip forces as well as acceleration. Chapter three considers different approaches for measuring the applied forces. It designs a handle with the first natural frequency above 1400 Hz. This handle is equipped with strain gauges for measuring deformations in the handle, and later these strains can be translated into applied forces. Furthermore, this

study develops a data acquisition toolbox in the MATLAB environment for capturing data from all sensors, simulating the applied forces and plotting all necessary graphs.

Any anti-vibration glove needs damping material to operate as a cushion. Chapter four investigates the vibration behaviour of different damping materials. It shows the suggested procedure in the standard for measuring the vibration behaviour of damping materials for hand-arm vibration is not realistic, and suggests a practical method for this purpose. Later, it generates different types of lumped-mass models and selects a suitable model for each of the tested materials.

Chapter five utilizes the designed handle and measures the vibration transmissibility from the vibrating handle to the bare hand. This chapter compares the results of two different approaches for measuring vibration at the palm of the hand. First, it uses the suggested adaptor in the standard and then it uses a new approach, a strap with three embedded miniature accelerometers. The result of these tests show the adaptor cannot measure the vibration at the palm in the low frequency range, and it indicates the effects on the measured vibration. Later, this chapter measures the vibration transmissibility of a commercial glove and compares the result of the two methods.

Chapter six compares several lumped-mass models for the hand-arm vibration. It uses the measured mechanical impedance of the hand-arm from the participants in this study and finds the properties of the elements in the analytical models. Later, it uses the generated lumped-mass model of the tested damping material and combines them with the model of hand-arm system for simulating the performance of the resultant gloves which use these materials as cushion.

Chapter seven discusses the outcome of this study and different aspects of hand-arm vibration measurement, and finally chapter eight gives the conclusion and recommendations for the future work.

2 Literature review

Power tools have facilitated many aspects of modern human life. These tools usually create vibration which can be due to the unbalanced forces in the tool or it can be due to the operational nature and design of the tool. While an operator holds the handle of a running tool, the vibration of the tool transmits from the handle to the hand of the operator. This transmitted vibration is known as hand-arm vibration (HAV). If the vibration is transmitted to the whole body of the operator, it is referred to as whole body vibration (WBV). Being exposed to long term HAV can cause permanent damage and injury to the operator's body which is called hand-arm vibration syndrome (HAVS).

To reduce the risk of vibration exposure, there are some limitations for the maximum allowable exposure time based on the type and magnitude of the vibration. Table 2.1 shows the maximum allowable vibration exposure for the standard eight-hour work day [1]. The exposure limit value (ELV) is the maximum allowable vibration exposure on any single day, and the exposure action value (EAV) is a daily amount of vibration exposure which requires control action [2]. Studies show that workers are not usually aware of the level of vibration exposure to their body during each day and in many cases these levels are above the allowable limitation level [3].

Table 2.1 – Maximum allowable vibration exposure [1]

Type		Maximum (m/s^2)
HAV	ELV	5
	EAV	2.5
WBV	ELV	1.15
	EAV	0.5

The maximum vibration exposure time can also be calculated by using a "points" system. In this method the maximum limit value is 400 points and the maximum action value is 100 points. The value of one point for one hour of exposure is,

$$P_{E,1h} = 2a_{hv}{}^2 \,, \qquad \text{Eq. 2.1.1 [4]}$$

where a_{hv} is the weighted value of the total acceleration from the three orthogonal-axes. Table 2.2 shows the exposure limits of HAV based on the "points" system.

Table 2.2 – Exposure points table [4]

Acceleration (m/s²)	5m	15m	30m	1h	2h	3h	4h	5h	6h	8h	10h
20	67	200	400	800	1600	2400	3200	4000	4800	6400	8000
19.5	63	190	380	760	1500	2300	3050	3800	4550	6100	7600
19	60	180	360	720	1450	2150	2900	3600	4350	5800	7200
18.5	57	170	340	685	1350	2050	2750	3400	4100	5500	6850
18	54	160	325	650	1300	1950	2600	3250	3900	5200	6500
17.5	51	155	305	615	1250	1850	2450	3050	3700	4900	6150
17	48	145	290	580	1150	1750	2300	2900	3450	4600	5800
16.5	45	135	270	545	1100	1650	2200	2700	3250	4350	5450
16	43	130	255	510	1000	1550	2050	2550	3050	4100	5100
15.5	40	120	240	480	960	1450	1900	2400	2900	3850	4800
15	38	115	225	450	900	1350	1800	2250	2700	3600	4500
14.5	35	105	210	420	840	1250	1700	2100	2500	3350	4200
14	33	98	195	390	785	1200	1550	1950	2350	3150	3900
13.5	30	91	180	365	730	1100	1450	1800	2200	2900	3650
13	28	85	170	340	675	1000	1350	1700	2050	2700	3400
12.5	26	78	155	315	625	940	1250	1550	1900	2500	3150
12	24	72	145	290	575	865	1150	1450	1750	2300	2900
11.5	22	66	130	265	530	795	1050	1300	1600	2100	2650
11	20	61	120	240	485	725	970	1200	1450	1950	2400
10.5	18	55	110	220	440	660	880	1100	1300	1750	2200
10	17	50	100	200	400	600	800	1000	1200	1600	2000
9.5	15	45	90	180	360	540	720	905	1100	1450	1800
9	14	41	81	160	325	485	650	810	970	1300	1600
8.5	12	36	72	145	290	435	580	725	865	1150	1450
8	11	32	64	130	255	385	510	640	770	1000	1300
7.5	9	28	56	115	225	340	450	565	675	900	1150
7	8	25	49	98	195	295	390	490	590	785	980
6.5	7	21	42	85	170	255	340	425	505	675	845
6	6	18	36	72	145	215	290	360	430	575	720
5.5	5	15	30	61	120	180	240	305	365	485	605
5	4	13	25	50	100	150	200	250	300	400	500
4.5	3	10	20	41	81	120	160	205	245	325	405
4	3	8	16	32	64	96	130	160	190	255	320
3.5	2	6	12	25	49	74	98	125	145	195	245
3	2	5	9	18	36	54	72	90	110	145	180
2.5	1	3	6	13	25	38	50	63	75	100	125

Daily Exposure time

The acceleration of the tools can be measured with portable vibration monitors. Figure 2-1 shows a portable data-logging system with embedded accelerometers positioned inside an adaptor which is suitable for monitoring and measuring the vibration exposure during the operation of power-tools [5].

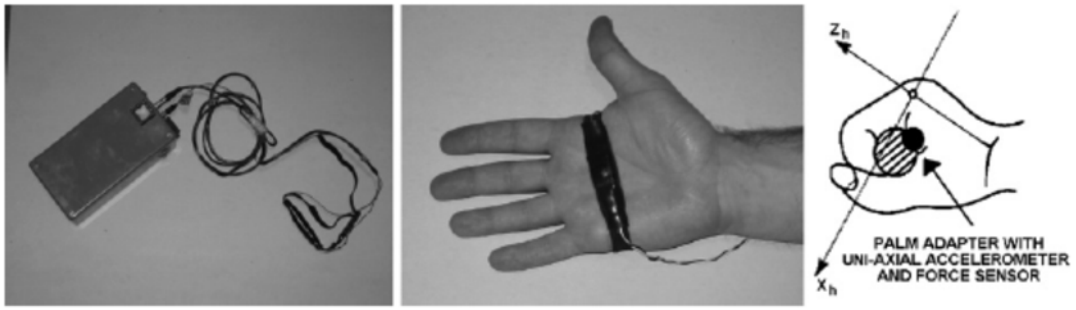

Figure 2-1 - Portable vibration exposure monitor [5]

Some of the manufacturers report the vibration level of their power tools; however, these levels may increase if the tools have faults [3] and studies have revealed that some of the tools have higher vibration levels in actual field tests than the vibration levels reported by the manufacturers; therefore, the reported vibration level cannot be used for calculating maximum exposure time [6]. Figure 2-2 shows the typical vibration magnitudes from common power tools [4].

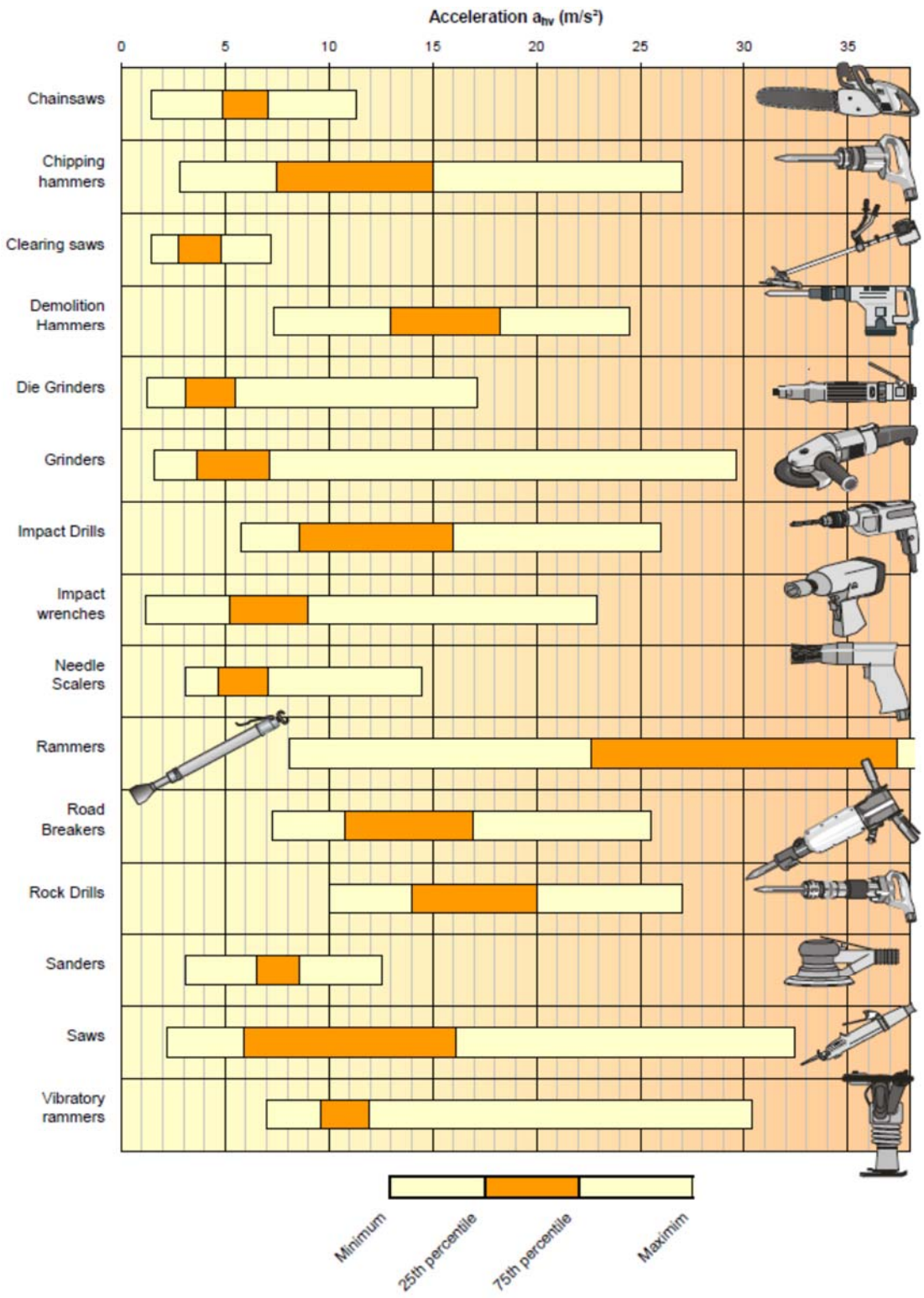

Figure 2-2 – Vibration magnitudes for common tools [4]

2.1 Hand-Arm Vibration Syndrome

Being exposed to long term HAV can cause damage to bones, joints and muscles which is known as hand-arm vibration syndrome (HAVS). The level and type of these injuries, depends on the type and duration of vibration exposure. These injuries can be categorized into three main subgroups which are vascular, neurological and musculoskeletal disorders [7, 8].

2.1.1 Vascular disorder

Vascular disorder is commonly known as dead or white finger and traumatic vasospastic disease (TVD) and is often described as vibration-induced white finger (VWF). White finger syndrome happens when the normal circulation of the blood in the fingers changes and there is a reduction or limitation of the blood flow to the fingers. It can also be triggered by cold temperature; therefore, it is suggested to warm the hand in order to return the blood circulation into the normal state [7, 9]. This syndrome has high prevalence among people who have been exposed to vibration. Workers can suffer from this syndrome even from their early years of exposure [10]. It is related to the frequencies of vibration and also to the biodynamic response (BR) of the hand and especially the fingers [11-13]. Tests on specific vibration frequencies have shown that anti-vibration gloves can reduce the drop in finger blood flow during HAV [14]. For assessing this syndrome, changes in the fingers' colour and blood pressure can be investigated by considering the resulting hand response to cold temperature [4]. Laser Doppler perfusion imaging (LDPI) is one of the advanced methods for measuring the temperature of the fingers without using traditional skin contact methods [15].

2.1.2 Neurological disorders

Neurological disorders include tingling, numbness in the fingers and hands, reduction in the normal sense of touch and temperature and reduction in the sensitivity of skin, etc. Statistics show that this syndrome has high prevalence among people who have been exposed to vibration [16]. In some study cases this prevalence was more than 80% [7]. There are several tests that can be used to assess this syndrome such as vibration perception thresholds (VPT), thermal perception thresholds (TPT) and Electromyography [4].

2.1.3 Musculoskeletal disorder

Work-related musculoskeletal disorders (WMSD) divides into two subgroups: skeletal and muscular. Skeletal disorders includes bone vacuoles and cysts in the hand, wrist and elbow osteoarthrosis, ossification at the sites of tendon insertion, carpal tunnel syndrome (CTS) and Dupuytren's contracture [4, 7, 8]. Muscular disorders includes weakness and pain in the hands, reduction of handgrip strength, muscle fatigue, tendinitis and tenosynovitis in the upper limbs [7]. These disorders are more related to the magnitude of displacement than the velocity of vibration or current frequency weighted acceleration; therefore, at low frequencies where the amplitude of the vibration is higher, the risk for these syndromes increases. It seems that for these disorders, separate kinds of weighting procedures other than that provided in ISO 5349 [7] are required [17].

2.2 Measurement

2.2.1 Vibration

In HAV tests, the vibration transmissibility (VT) from the vibrating handle to the hand should be measured. The ratio of the acceleration at the palm over the acceleration of the handle, shows the VT from the handle to the hand. These two accelerations are usually measured with two individual accelerometers and their difference in behaviour plays a noticeable role on the uncertainty of measurement [18]; however, some of them can have less than 2% uncertainty and due to their small sizes, they are suitable for both WBV and HAV tests [19].

ISO 10819 defines the frequency range of $25Hz$ to $1250Hz$ for vibrating the handle and divides this frequency range into medium and high frequency bands [20, 21]. The medium frequency band includes frequencies from $25Hz$ to $200Hz$ and the high frequency band is considered to be from $200Hz$ to $1250Hz$.

For each 1/3rd octave band in the test frequency range, the standard defines weighing factors which decreases as the frequency increases; however, the current weighting factors are not suitable for frequencies below $25Hz$ [22]. By finding the VT of the glove and the VT of the bare hand test, and by applying the weighting factor and finding the ratio of weighted VT of the glove test and bare hand test, the mean vibration transmissibility (MVT) can be calculated. According to the standard [20], a glove cannot be evaluated as an anti-vibration glove if the MVT of the glove for medium frequency band is above 1.0 or above 0.6 for the high frequency band. The recent version of this standard [21] reduces the criteria for medium frequency band from 1.0 down to 0.9 [21]. However, there are commercially available anti-vibration gloves in the market which cannot satisfy these criteria [23].

The standard also defines the power spectra for the HAV test. Figure 2-3 shows the power spectra diagram according to ISO 10819 in 1/3rd octave bands. Initially the standard defines two separate vibration amplitude diagrams for the medium and high frequency bands, later it combines these two into one diagram. This vibration can be generated either with random noise or sinusoidal signals [20, 21]. Studies also show that there is no significant difference in measured VT for impact or harmonic vibration [24].

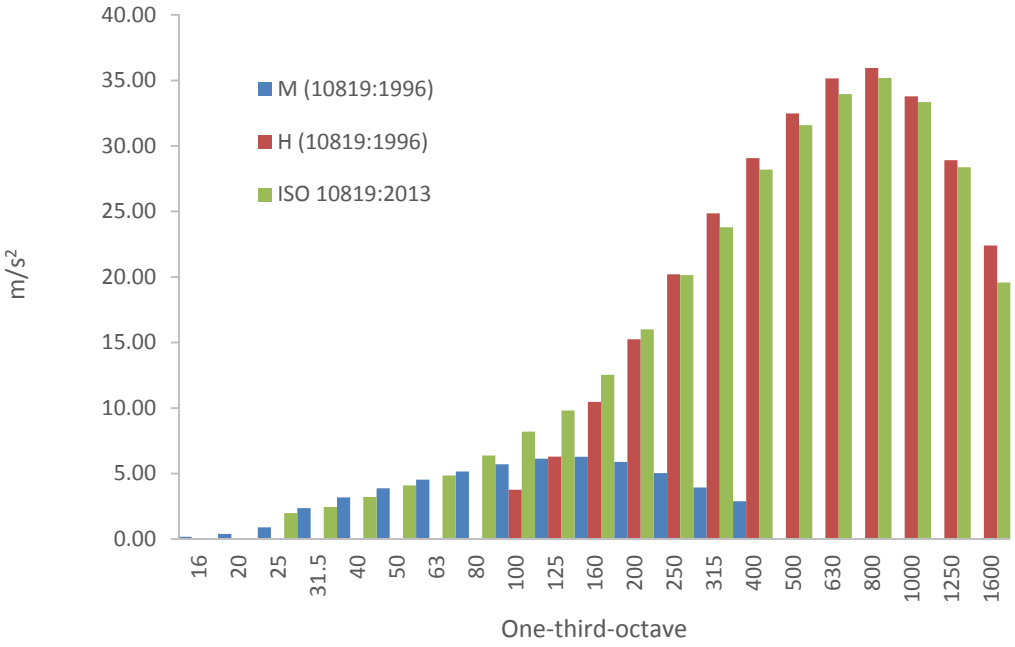

Figure 2-3 – HAV acceleration amplitude according to ISO 10819 [20, 21]

Figure 2-4 compares the defined power spectra in the standard with the power spectra of actual common tools [13]. It clearly shows that the defined spectra in the standard does not cover the vibration level of all power tools; therefore it is more practical to evaluate a glove for individual power tools [25, 26]. The power spectra and dominant frequency range of power tools changes for each type of tool; for instance, commonly used rotary and reciprocating tools, mainly vibrate in frequency ranges from $35Hz$ to $150Hz$ [27].

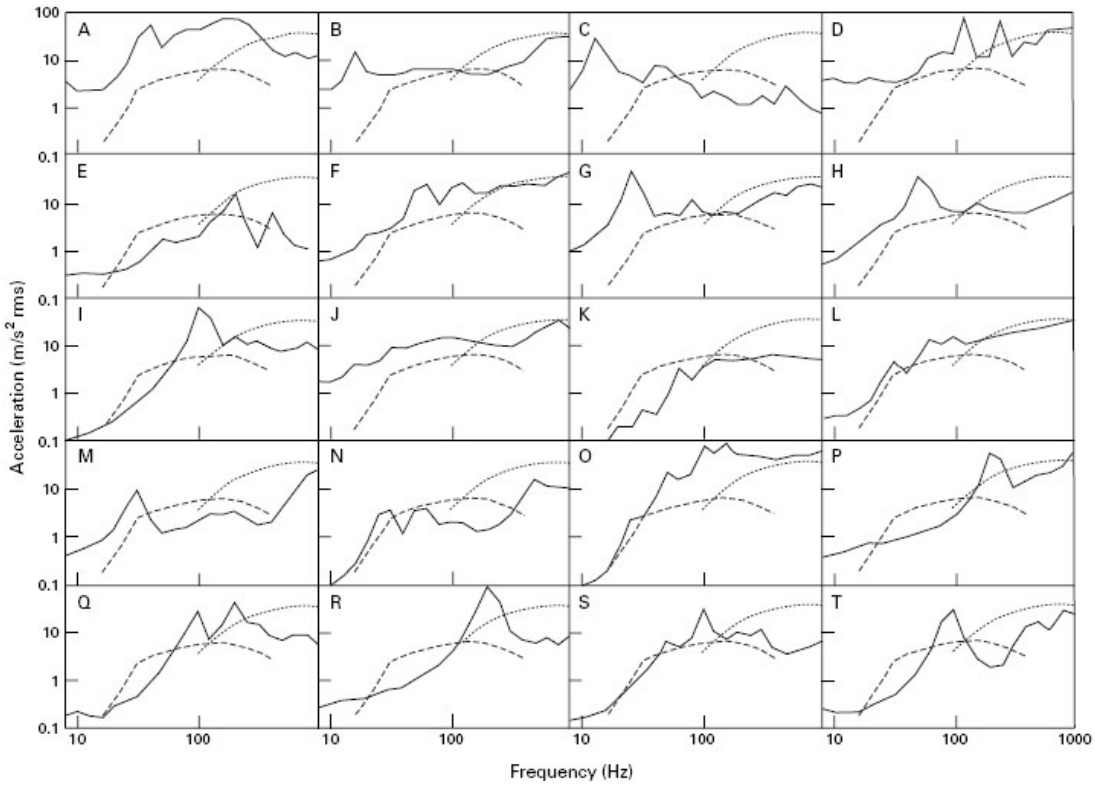

Figure 2-4 – Power tools frequency spectra [13]

Doted-lines are for ISO 10819 and continuous lines are for tools (A: pneumatic rock drill, B: pneumatic road breaker, C: petrol driven wackier compressing road surface after, D: a non-anti-vibration chain saw, E: an anti-vibration chain saw, F: a pneumatic metal chipping hammer, G: pole scrabblier, H: needle gun, I: random orbital sander, J: impact wrench, K: riveting gun, L: dolly used with riveting gun, M: nut runner, N:metal drill, O:wire swaging, P: etching pen, Q: electric 9 inch angle grinder, R: pneumatic rotary file, S: pneumatic 5 inch straight grinder, T: pneumatic 7 inch vertical grinder)

The standard defines vibration levels for one-directional vibration, typically the z-direction (Figure 2-5); however, for some tools such as a hand tractor, not only is the vibration in all directions, the highest vibration acceleration is in the x-direction and not the z-direction [28]. Furthermore, for the VT test the vibration should be generated with exciters and common electro-magnetic exciters can generate non-axial vibration due to their side-loads [29]; therefore, during VT measurements, the two accelerometers inside the handle and at the palm of the hand should be aligned together.

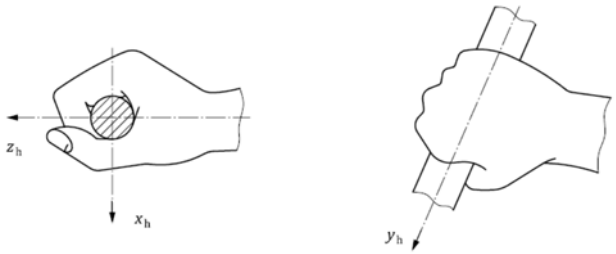

Figure 2-5 - Hand-arm vibration directions [30]

2.2.2 Handle

For measuring HAV, the standard [20, 21] requests the use of a solid handle which is mounted to an excitation system. The handle should have cylindrical shape with diameter of 40±0.5mm and minimum length of 110mm [20, 21]. During the HAV test, the operator should apply push and grip forces to the handle. The push force should be 50±8N and the grip force should be 30±5N. For maintaining these forces in the defined ranges, they should be measured and monitored by the operator during the test [20, 21]. There are two common ways for measuring push force, the sensors can be inside the handle [10, 21, 29, 31-37] or they can be inside the stand for the operator [12, 21, 38-48].

With force and acceleration data, the mechanical impedance (MI) of the hand can be calculated [32, 49-55]. By decreasing the distance between the sensors and the hand, the MI can be calculated to higher frequencies [54]; however, for measuring forces at the handle, the flexibility of the handle increases which decreases the natural frequency of the system. According to the standard, the handle should not have any resonance in the frequency of HAV tests which means the first natural frequency of the system should be above 1250Hz [21]. For the MI measurement, if the force data comes from the force sensors inside the fixture base, the first natural frequency of the system should be at least 5.4 times the highest desirable frequency for MI while

if the force data comes from sensors inside the handle, the first natural frequency of the handle should be at least 2.6 times the highest desirable frequency for MI [54, 56].

There are two common ways for measuring the push and grip forces. They could be measured directly by using load cells and force transducers [5, 25, 33-39, 41, 43-48]; or the strains inside the handle structure can be measured and translated to equivalent forces [29, 31, 32, 40, 49, 52, 57-67]. For force measurement, both strain gauges and piezoelectric sensors are suitable; however at low frequencies (below $25Hz$), the strain gauge shows better results than the piezoelectric sensor while at high frequencies (above $1000Hz$), it is reversed [11].

For static gripping of the handle, the concentration of the interface pressure is at the tips of the index and middle fingers and at the base of the thumb (Figure 2-6) [57, 60]; however, while the handle is vibrating, it shifts towards the middle of the fingers (Figure 2-7) [60].

The contact force between the hand and handle depends on many factors such as the feeding force, gripping force and diameter of the handle. The higher the feeding or gripping force or the lower the diameter of the handle leads to higher contact forces [35, 58, 68, 69]. The VT also depends of the location of the contact surface and the gripping force. For instance, for high gripping force, the vibration at the tip of the small fingers can be more than 2 times the source [70].

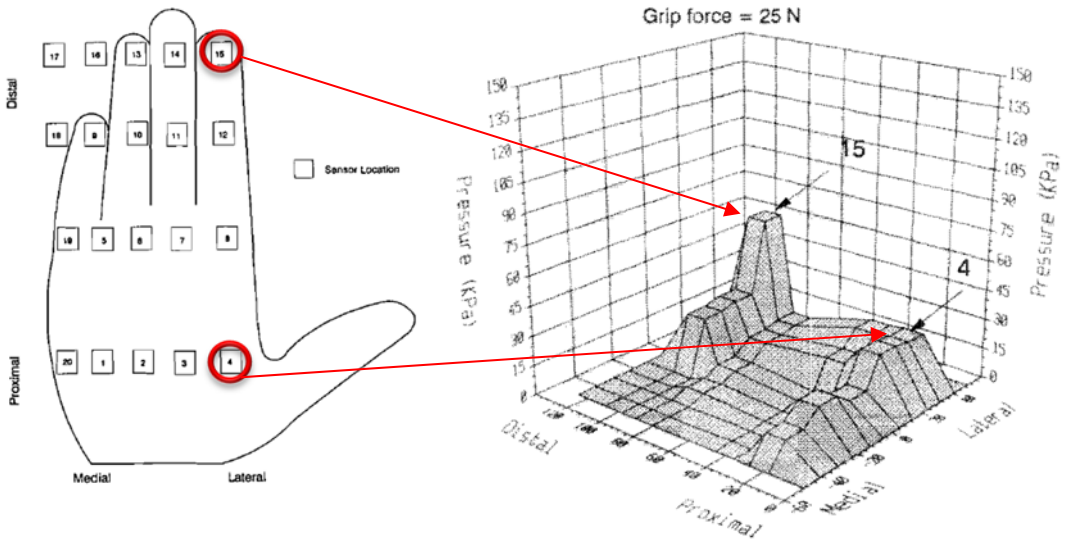

Figure 2-6 – Pressure distribution on the static handle [60]

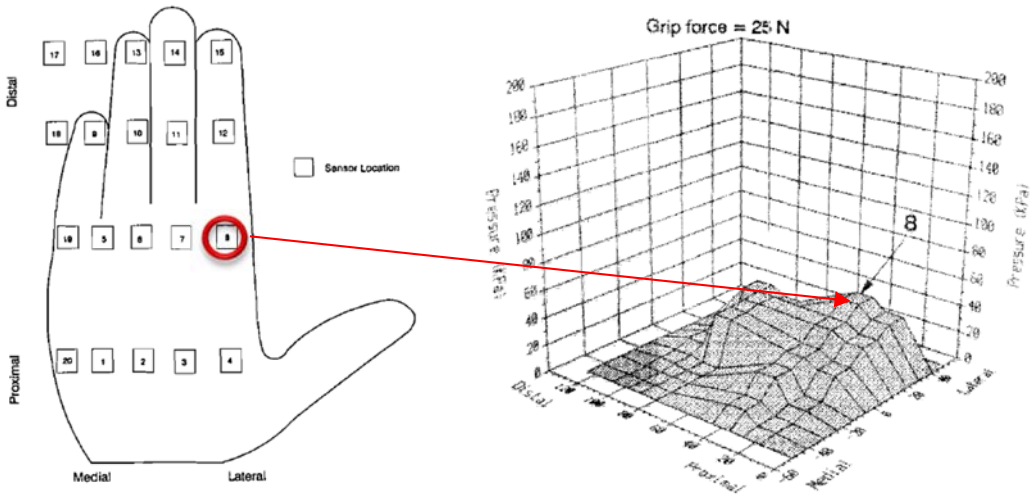

Figure 2-7 – Pressure distribution on vibrating handle [60]

By increasing the handle's diameter, the angle between the metacarpophalangeal and proximal interphalangeal increases and the angle between the distal interphalangeal and intermediate phalange remains constant [58]. Studies shows that for low levels of vibration, the increase of the handle's diameter could decrease the temporary threshold shifts (TTS) at the fingertip [71]. Figure 2-8 shows the variation of contact force of different parts of the hand as a function of diameter of the handle. As the figure shows, by increasing the diameter of the handle the total force decreases [72]. The diameter of the handle also affects the comfort of the operator and it depends on

the size of the operator's hand. Studies have shown that for female operators, the most comfortable feeling handle has a $35mm$ diameter, while for males, this is for a handle with $40mm$ diameter [73].

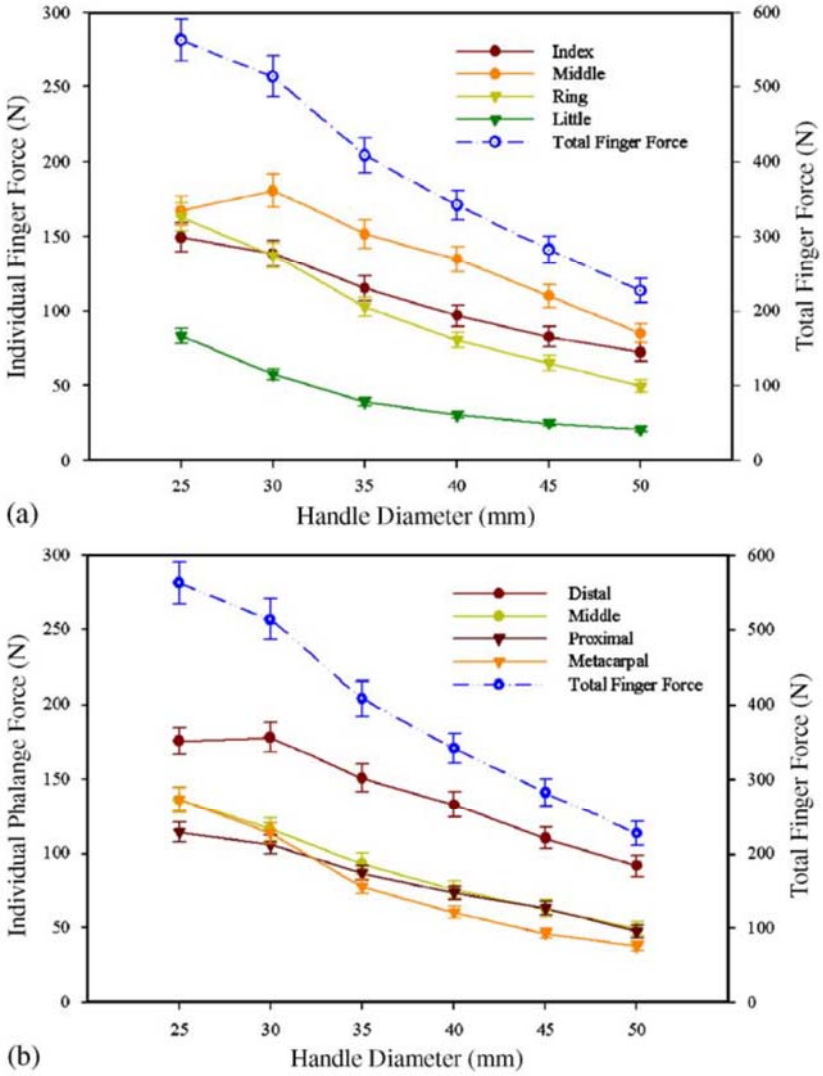

Figure 2-8 – Finger force vs handle diameter

(a) finger force vs. handle diameter; (b) phalange forces vs handle diameter [72]

2.2.3 Adaptor

For measuring vibration at the palm of the hand, the ISO standard requests the use of a rigid adaptor with embedded accelerometer with maximum weight of 15g (Figure 2-9). For increasing the accuracy of the measured acceleration inside the adaptor, it should be located closer to the handle [18]. For bare hand tests, this

adaptor should be placed between the handle and the palm of the hand and for glove tests, it should be located inside the glove at the palm side.

For ensuring the accuracy of the test rig, the adaptor should be affixed with the handle with contact force of 80±10N and the VT for all octave bands from 25Hz to 1250Hz should be measured to be a value of one with a tolerance of 5 percent [20, 21].

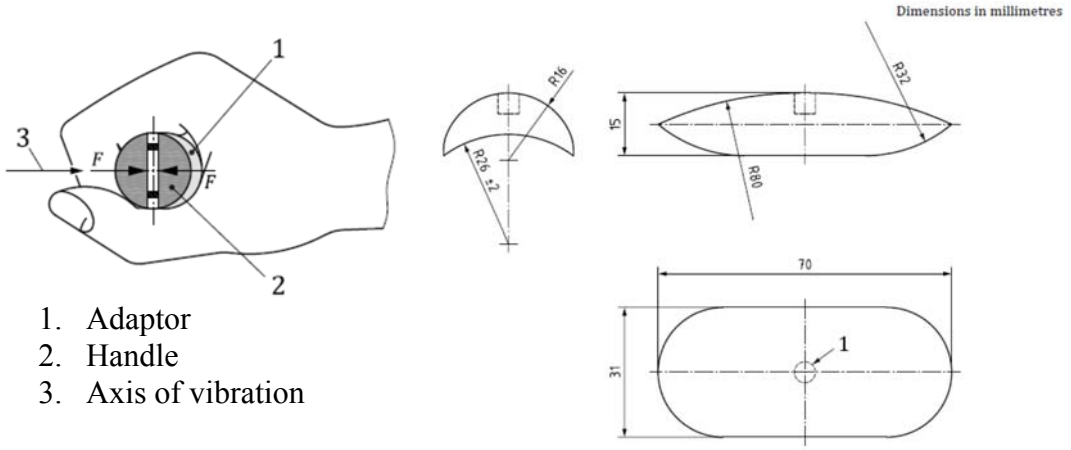

1. Adaptor
2. Handle
3. Axis of vibration

Figure 2-9 – Palm Adaptor for accelerate [21]

In the HAV test, the ratio of the captured data from two accelerometers (inside the adaptor and inside the handle) is defined as the VT; therefore, for minimizing the error, these two accelerometers should be aligned together. Studies show that by considering all three axes, the miss-alignment between these two accelerometers could be up to 60º which causes about 20% error in the measurement [29, 74]. Figure 2-10 shows the illustration of miss-alignment of the adaptor with or without a glove. For evaluating a glove as an anti-vibration glove, in the medium frequency range attenuation of 10% is required [21]; therefore, the error of measurement due to miss-alignment can lead to incorrect evaluation. However, there are other significant factors that can also effect the measurement such as subject variability, applied force, vibration magnitude and temperature [74].

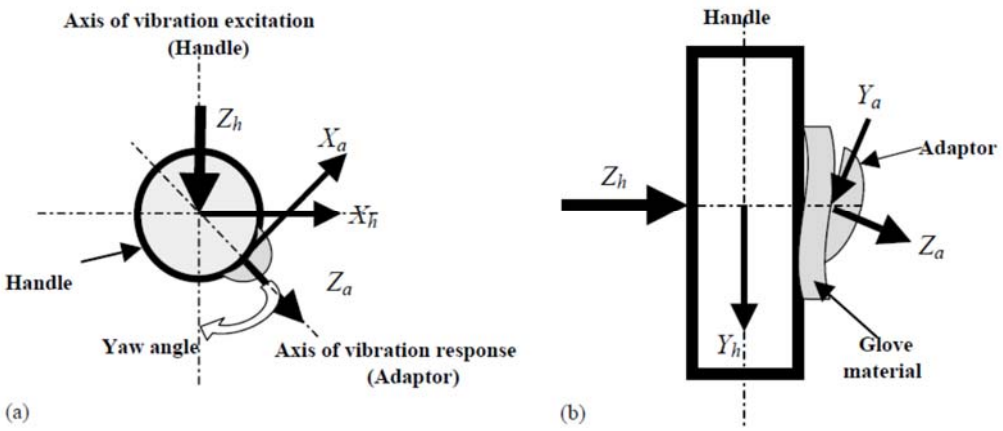

Figure 2-10 – Adaptor orientation and miss alignment [29]

Instead of using the adaptor for measuring acceleration, the VT to different parts of the hand can be measured by scanning with a laser Doppler vibrometer (LDV) which is free of misalignment and adaptor effects [75-78] .

Since the ISO standard requests the use of an adaptor, the position of the adaptor can be monitored for the operator for minimizing the misalignment error. One way for monitoring the position of the adaptor while the operator is wearing a glove is by putting a slit in the seam of the glove as shown in Figure 2-11 [44]. According to the standard, visible marks on both the handle and adaptor helps the operator to align the adaptor with the handle during both bare hand tests and glove tests [21]. However, this only works for the yaw angle and still the adaptor can have miss-alignment with the other axis. The yaw angle of the adaptor can be derived from,

$$tan(\alpha)_{t+\Delta t} = \frac{\int_t^{t+\Delta t} |A_x| dt}{\int_t^{t+\Delta t} |A_z| dt}, \qquad \text{Eq. 2.2 [79]}$$

where A_x and A_z are the acceleration in the x and z directions. By monitoring this angle for the operator during the test, the error due to this miss-alignment can be eliminated [79]. Another way for reducing miss-alignment is by calculating the overall acceleration from all three axes's for both adaptor and handle and use the ratio of these two as VT [21, 29, 44, 77].

Figure 2-11 – A slit cut on the glove to monitor alignment of Adaptor [44]

Although, the monitoring of the adaptor helps for maintaining position and orientation of the accelerometer at the palm side, it can heavily influence the result. The adapter is a solid object and its size, mass and location affects the resulting VT. Increasing the mass of the adaptor or decreasing the tightness of the adaptor to the skin, decreases the resonant frequency [77]. Furthermore, its resonance influences the resonance of the VT [25, 48]. Figure 2-11 shows various types of adaptors for measuring vibration at the hand. The adaptor can also be used for measuring the acceleration at the skin surface of the forearm and arm [77]. Comparison between the measurement results of the adaptor with the results of LDV, shows that the result from the adaptor can reveal the basic characteristic of VT and can be used for analytical modelling [77].

The palm adaptor should have proper contact with the handle; therefore the curvature of the bottom of it should be close to the curvature of the handle. In addition, the span's length should not be less than 70% of the width of the palm [40].

The palm adaptor affects the VT measurement for frequencies below $100Hz$ and the finger adaptor affects the VT measurement for frequencies between $25Hz$ to $80Hz$ [48]. Therefore, for measuring VT at low frequencies, the hand measurement is more suitable than the adaptor method; however, it suffers from poor repeatability. Especially for frequencies above $40Hz$, due to noticeable vibration attenuation at the

wrist, data from the third metacarpal has more reliability than vibration data measured from the wrist [80].

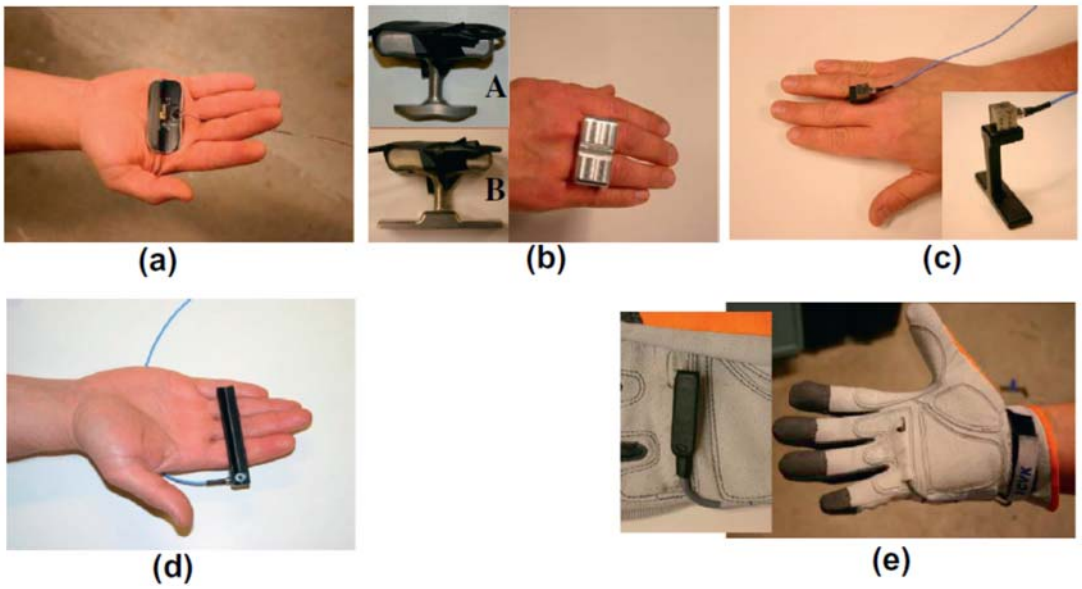

Figure 2-12 – Handheld adapters:

(a) Palm adapter; (b) Fingers-held dosimeter with foot; (c) Fingers-held adapter; (d) Beam adapter; (e) Glove-held adapter [48]

2.2.4 Mechanical Impedance

By measuring the force and acceleration at the driving point, the mechanical impedance (MI), displacement mobility (DM), or apparent mass (AM) of the hand-arm system (HAS) at the driving point can be derived.

$$MI = \frac{force\ excitation}{velocity\ response} \quad \text{Eq. 2.3}$$

$$DM = \frac{velocity\ response}{force\ excitation} \quad \text{Eq. 2.4}$$

$$AM = \frac{force\ excitation}{acceleration\ response} \quad \text{Eq. 2.5}$$

In HAV, the driving point can be either at the palm side or the fingers side. Therefore, both MIs of the palm and fingers are measureable. The summation of these two MIs gives the MI of the hand. Although, by measuring the total response

of the hand the distribution of MI in palm and fingers can be estimated; the most reliable approach is to measure each of these two individually [81]. Studies show that by knowing the MI of the handle alone and the total MI of the hand and handle, the MI of the hand can be calculated as,

$$Z_{Hand}(\omega) = Z_{Total}(\omega) - Z_{Handle}(\omega), \qquad \text{Eq. 2.6 [41]}$$

where Z_{Hand} is MI of the hand, Z_{Handle} is MI of the handle and Z_{Total} is the total measured MI while the operator is holding the handle.

The measurement for the force is only for one point, and there is a distributed force on the handle not a concentrated force. The distribution of the force varied due to the connection and structure flexibility and the effect of the hand on the handle which leads to increasing errors in the MI measurement [56].

In the HAV, many factors influence the measured MI such as diameter of the handle [53, 69, 82] and the posture [37, 53, 83, 84]. Measurements have shown that by changing the angle of the elbow from 90º to 180º and by extending the arm posture, the AM at low frequencies will increase by three times [53], and the VT to the upper-body will be amplified [85]. However, for frequencies above $25Hz$, this posture will lead to lower VT to the upper-arm [85]. Figure 2-13 shows that different postures will result in different MI of the HAS [37, 83, 86]; in spite to these alterations of MI for different postures, all results show high damping in the system [49]. Even for a particular posture, the shape and size of the body may alter the measured MI. In general, for frequencies above $20Hz$, the MI is largely influenced by the stiffness of the palm tissue, and larger hand-arm size leads to higher MI for frequencies below $40Hz$ and above $300Hz$ [87].

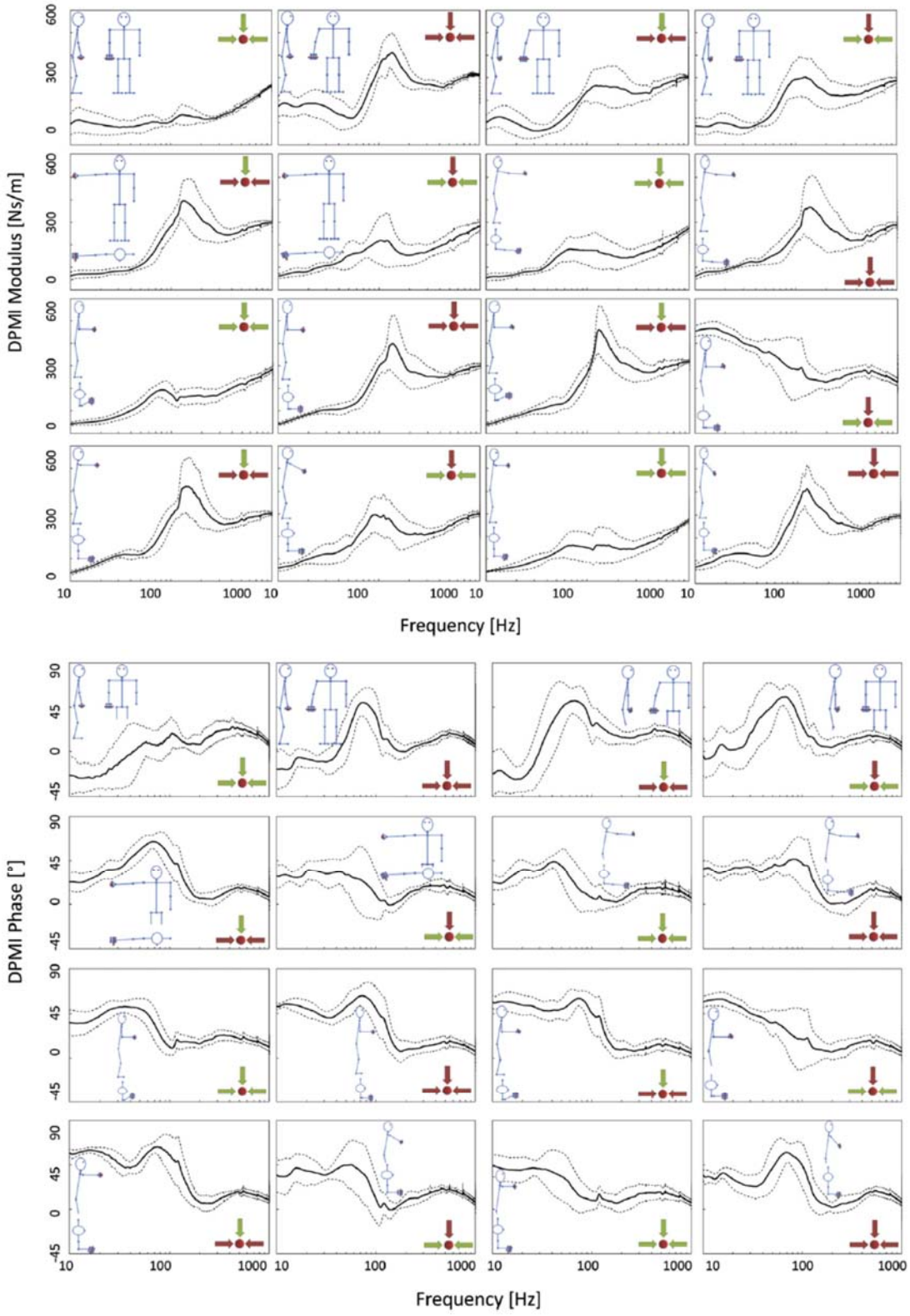

Figure 2-13 – Mechanical impedance for different posture [37]

Usually, the reported MI is the average of several measurements from different subjects. Since the frequency of resonance in these MI's is not unique, arithmetic

averaging of these MI introduces some error in the resultant MI [88]. Figure 2-14 shows different effects of arithmetic averaging on measured data which depends on number of subjects, closeness of resonance frequency and damping of the system.

MI has one resonance in the frequency range of $20Hz$ to $50Hz$ which varies by body characteristic and applied forces [87, 89, 90]. The frequency and magnitude of this resonance increases by increasing the push force [87, 89].

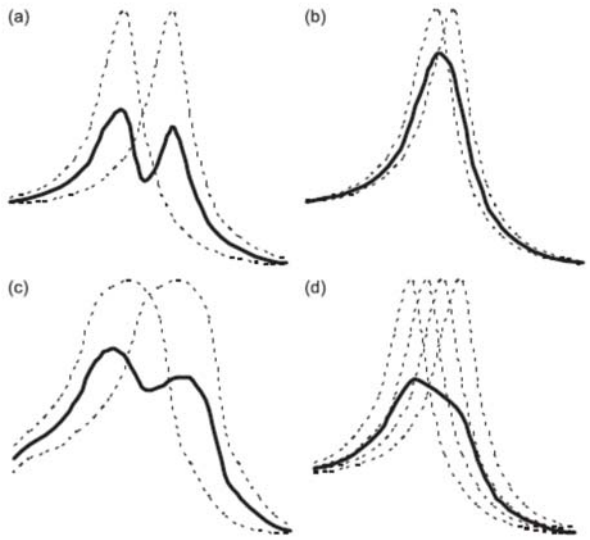

Figure 2-14 - Factors affecting the arithmetic averaging effects [88]

Studies have shown that for the same body characteristic, the MI is the highest when only the push force is applied, and the MI is the lowest when only the grip force is applied, [87, 89]. Furthermore, studies on the BR of different parts of the HAS reveals that the BR of the forearm is more sensitive to the push force and that the BR of the entire HAS is more sensitive to the grip force [24, 85].

The MI can be used for calculating the biodynamic force (BF). For this purpose the Eq. 2.3 can be written as,

$$MI(\omega_i) = \frac{F(\omega_i).j\omega_i}{A(\omega_i)}, \qquad \text{Eq. 2.7}$$

where $A(\omega_i)$ is the acceleration at driving point. By rearranging,

$$F(\omega_i) = MI(\omega_i).A(\omega_i)/j\,\omega_i\,, \qquad \text{Eq. 2.8 [91]}$$

where $F(\omega_i)$ shows the BF. Studies have shown that the dominant BF frequency is correlated with the dominant frequency of the power tool [91]. For frequencies below $100Hz$, the palm has a higher share of BF distribution than the fingers, while at higher frequencies these two have closer share of BF [91]. At the palm side and at frequencies below $40Hz$, the BF distribution is correlated with the applied force [91].

2.2.5 Power Absorption

Vibration power absorption (VPA), can be derived from,

$$VPA(\omega) = F(\omega).V(\omega) = F(\omega)\frac{A(\omega)}{j\omega}\,, \qquad \text{Eq. 2.9}$$

where F, V and A are force, velocity and acceleration at the contact point. Since, the MI can be written as,

$$Z = \frac{F}{V} = \frac{G_{FV}}{G_{VV}} = Re(Z) + j\,Im(Z)\,, \qquad \text{Eq. 2.10}$$

this results in,

$$VPA(\omega) = Re[Z(\omega)].|V(\omega)|^2 = Re[Z(\omega)].\left|\frac{A(\omega)}{\omega}\right|^2. \qquad \text{Eq. 2.11 [12]}$$

This equation shows how VPA is correlated with MI and the acceleration of vibration; therefore, for both palm and fingers by knowing MI, the VPA can be calculated. Since the palm and fingers have different MI characteristics, research has found that for injuries and disorders in the palm, wrist or arm structures, VPA at the palm and for injuries and disorders in fingers, VPA at the fingers should be investigated [92]. Although, it seems the vibration power absorption density (VPAD)

which is derived from the VPA at the fingers and the effective mass of the fingers soft tissue, may be a better factor for investigating vibration-induced disorders of fingers [93].

The dimensions of the hand and body weight correlated with the VPA [94, 95] while the square root of total VPA of the entire HAS was correlated with subjective sensation or discomfort [12, 96]. For instance, the higher handle size leads to higher VPA [24, 82].

At frequencies below $50Hz$, the VPA is the highest when there was only push force and it was the lowest when both push and grip forces were applied. For frequencies about $50Hz$, the VPA was not very sensitive to the type of force [89, 92, 94]. In addition, except for frequencies between $100Hz$ to $200Hz$ where the VPA was not very sensitive to the total force, for the rest of the frequencies, the VPA increases by increasing the total force, [94]. Since, the main part of VPA is for frequencies below $200Hz$, research showed that the VPA was more sensitive to the hand–handle coupling force than to the contact force [97].

For vibration in the x-direction (Figure 2-5) while the elbow has the 90º angle, the total VPA increases slightly by increasing the grip force, while increasing the push force does not show clear effect on it, and while the elbow has the 180º angle, the total VPA increases by increasing either of these two forces [82].

Studies showed that the distribution of the VPA depends on the dominant operating frequencies of the power tools. For tools with dominant low frequencies, such as rammers, the arm and shoulder have increased share of VPA [24, 98] and the defined ISO weighting factors in [7] correlates with this VPA distribution [12, 98]. For these

tools, the share of VPA for the upper body also increases by extending the arm posture, which could increase the risk of HAVS [85].

For tools with dominant high frequencies such as grinders, the fingers and hand have a higher share of VPA and the distribution in the fingers is more correlated with the unweighted acceleration [12, 24, 98].

The distribution of VPA at the fingers and palm is not equal and it depends on the frequency. For frequencies below $25Hz$, the palm has a higher share of VPA than the fingers while at high frequencies (between $250Hz$ to $1000Hz$) they have equal share of the VPA [99]. The resonance of the HAS also influences the distribution of VPA at the fingers [98].

2.2.6 Weighting Factors

ISO 5349 defines a frequency weighting for frequencies between $8Hz$ to $1000Hz$ to ascertain the effect of different frequencies in causing injury to the hand [7]. This weighting factor can be derived from,

$$W_{VPA}(\omega_i) = 0.958 \frac{\sqrt{Re[MI(\omega_i)]}}{\omega_i} \Big/ \frac{\sqrt{Re[MI(\omega_{REF})]}}{\omega_{REF}}, \qquad \text{Eq. 2.12 [12]}$$

where ω_{REF} is at 12.5 Hz which has the maximum weighting value[1] in the standard [12]. The defined weighting factor for either one-directional vibration or orthogonal directions at the palm, elbow and wrist is correlated with the measured vibration acceleration of many different power tools [42, 43, 98], while for the fingers it is more correlated with unweighted acceleration [98]. In addition, this weighting factor

[1] Maximum weighting value is 0.958.

agrees with the effect of vibration on developing disorders at the palm, wrist and arm structure for different frequencies [98]; while it is not the same for developing disorders at the fingers [12]. The current weighting factor has low ratio for high frequencies; therefore, it fades the effect and attenuation of anti-vibration gloves at high frequencies [74].

Since the change in MI for frequencies between 250Hz to 1000Hz is less than 10%, the current weighting factor underestimates the effect of high frequencies on developing finger disorders [12, 92, 94, 99-101]. On the other hand, the VPA in fingers at high frequencies is significantly higher than low frequencies; therefore, the current weighting could overestimate the effect of low-frequency vibration [12, 22, 98-100, 102]. The first resonant frequency of the fingers is in range of 80Hz to 250Hz, therefore, the high weighting factor for the fingers should be in this range [22]. The frequency weighted VPA at the fingers shows that vibration at frequencies between 16Hz to 500Hz may have higher risk for developing disorders in fingers [98].

2.2.7 Vibration Transmissibility Reduction

The vibration from power tools transmit to the hand and body of the worker; however, proper engineering modification on the tool such as changing the direction of the handle, balancing or supporting the weight of the tool could help to reduce the required force to lift and manoeuvre the tool, and as a result could reduce the VT from the tool to the hand of the worker [11, 103]. Furthermore, by using the BR of the operator and modelling the power tool as a vibration generator, the optimal suspension characteristics can be identified and used for designing a suspension system for the tool for reducing the VT [104]. Even for existing tools, the way the

operator holds the handles of the tools, could effect the level of VT; therefore the operators should be trained to correctly hold the handle of the tools and operate them [6, 105].

In order to reduce the hazard of VT, the handle of the tools can be covered with damping material [106], or anti-vibration gloves can be used as personal protective equipment (PPE). ISO 10819 defines a laboratory-based test for evaluating anti-vibration gloves. In this procedure, the ratio of VT with the glove and with the bare hand is defined as the VT of the glove which shows how the glove reduces vibration for each of the 1/3rd octave bands. Initially, this standard requests for the result of the test from three participants [20]; however due to the high variability of the glove VT results [107], the newer version of the standard increased the number of the participants to five persons [21]. According to the standard, if the average of the mean vibration transmissibility (MVT) for medium and high range in these tests are below 0.9 and 0.6, the glove can be evaluated as an anti-vibration glove [21]; however, even if a glove is evaluated as an anti-vibration glove, it is necessary to evaluate the vibration attenuation of the glove for individual tools, then use it as PPE [25, 26]. Furthermore, the performance of the glove depends on many factors such as vibration direction, posture of the operator and even push and grip forces [108].

For measuring VT at the hand a specific adaptor for the accelerometer should be used [21] which can affect the measurement result [48]; however, by using the MI of the hand while the operator is wearing the glove and the MI of the bare hand, the VT of the glove can be calculated without the need of using any adaptor [109]. Studies have shown that the VT of the glove for the frequency range of $40Hz$ to $200Hz$ is correlated with the MI of the hand and that the effectiveness of the glove increases by increasing the MI [110].

The anti-vibration gloves use damping materials as cushioning; therefore for designing these gloves, the choice of proper damping materials is crucial. These materials usually have non-linear stiffness and damping behaviour; therefore, the performance of the resultant gloves is non-linear and is a function of the applied push and grip forces [38, 39, 47, 110]. Materials with negative Poisson's ratio could be suitable for these gloves [111]. ISO 13753 [112, 113] defines a simple laboratory-based test for measuring the VT of a flat circular disk of resilient material. In this measurement, the material should be placed on the flat disk which is mounted on an exciter, and a mass with weight of $2.5kg$ should be placed on top of the material. By knowing the applied force to the material and accelerations of the top and bottom of the material, the MI of the material can be calculated. In addition, the VT of the resultant glove which uses this material as cushioning can be calculated as,

$$Glove\ Transmissibility = \frac{Z_M}{Z_H + Z_M}. \qquad \text{Eq. 2-13 [112, 113]}$$

In this equation Z_M and Z_H are the MI of the material and MI of the HAS respectively. Research has shown that the lower the VT of the material in this test, does not necessary lead to lower VT of the resultant glove which uses this material [114].

The trend of VT spectra depends on many factors such as thickness of the sample [115]. The measured VT includes at least one resonance and the frequency of it is a function of many factors such as temperature, humidity and etc. For some of the tested materials, this frequency increases by decreasing the temperature or increasing the humidity or material ageing [116]. Since after any resonance in the VT, the magnitude of the VT drops, by decreasing the resonance frequency, the overall VT

of the material decreases which could lead to better attenuation of the resultant glove.

Besides the property of the damping material, factors such as sewing pattern and kind of thread also affects the performance of the glove [114]. In addition, the standard emphasizes that the same material that is used at the palm side of the glove, should be used for the thumb and finger's side; however, this cannot guarantee the proper vibration attenuation at the fingers [47].

Research has shown that some gloves that are evaluated as anti-vibration gloves do not have proper vibration attenuation at the palm for frequencies below $25Hz$ and at the fingers for frequencies below $250Hz$ [39, 47, 108, 117]. Furthermore, for some of the tools with dominant low frequency behaviour, some anti-vibration gloves even increase the vibration [26].

The current procedure for evaluating gloves uses only one-directional measurement [21]; however, tri-axial measurement shows that some gloves that are not considered as anti-vibration gloves with the current procedure, actually have better performance than other gloves that are evaluated as anti-vibration gloves [118]. Furthermore, many tools such as the percussive chipping hammer generate shear axis vibration; while this procedure does not consider this type of VT [119]. This procedure only investigates the effect of the glove on VT at the palm of the hand and it ignores the effect of the glove on VT to the fingers and other parts of the body. Surface Electromyography (EMG) reveals that anti-vibration gloves may increase VT and fatigue at the Extensor Carpi Ulnaris (ECU) of the forearm [120].

Since the defined spectra in the standard does not cover the power spectra of all power tools [13], the performance of the glove can be estimated by using the vibration transfer function of the glove,

$$T(f_i) = \frac{\sqrt{{A_{Axi}}^2 + {A_{Ayi}}^2 + {A_{Azi}}^2}}{\sqrt{{A_{Hxi}}^2 + {A_{Hyi}}^2 + {A_{Hzi}}^2}}, \qquad \text{Eq. 2.14 [117]}$$

where $A_{Axi}, A_{Ayi}, A_{Azi}, A_{Hxi}, A_{Hyi}$ and A_{Hzi} are the measured accelerations at the adaptor and at the handle in three orthogonal directions. By knowing the acceleration of power tools in three orthogonal directions, the predicted weighted acceleration of the glove for the tool will be,

$$PT_W = \frac{\sum_{i=1}^{n} \sqrt{{A_{hxi}}^2 + {A_{hyi}}^2 + {A_{hzi}}^2}.T(f_i).w(f_i)}{\sum_{i=1}^{n} \sqrt{{A_{Hxi}}^2 + {A_{Hyi}}^2 + {A_{Hzi}}^2}.w(f_i)}, \qquad \text{Eq. 2.15 [117]}$$

where A_{hxi}, A_{hyi} and A_{hzi} are the measured accelerations at the handle of the tool and $w(f_i)$ is the weighting factor. Studies show that the result of this estimation could be used for field measurement [117, 121].

Research has shown that cotton gloves do not have vibration attention [122] and air bladder gloves are more effective when the operator only applies push forces and are least effective when only grip forces are involved [39]. Air-bladder gloves have better vibration attenuation at the palm compared to gel-filled gloves; however for high frequencies at the fingers side, gel-filled gloves have better performance [44, 47].

Evaluation of anti-vibration gloves is only based on their vibration attention; while there are other factors that need to be included in their effectiveness evaluation. For instance their effect on impaired manual dexterity of the workers and their effect of on temperature of the hand of the workers should also be investigated [119].

2.3 Hand-Arm Vibration Modelling

Analytical models of the hand-arm system (HAS) can be used for investigating HAV. Initial studies on MI reveal that the behaviour of the HAS can simply be modelled for three separate frequency zones. It can be modelled as a mass for frequencies below $50Hz$ and above $200Hz$ and it can be modelled as a spring for frequencies between $70Hz$ to $100Hz$ [123], while for frequencies between $16Hz$ to $63Hz$, it can be modelled as one degree of freedom (DOF) model [101]. However, it is more accurate to use a full lumped-mass model with all masses, springs and dampers and higher DOF for the analytical modelling. Furthermore, this model can be combined with finite element models to create a hybrid model for simulating both local effects such as stress and strain, and also for simulating global effects such as biodynamic response (Figure 2-15).

By knowing the biodynamic response of the system and in comparison with the response from the model, through optimization and reduction in error between the simulated and measured responses, the values of parameters for masses, springs and dampers can be derived. These biodynamic responses can be MI, VT or combinations of these two. Studies have shown that the values of parameters are strongly dependent on the target of the biodynamic responses. The MI is more correlated with the response of the whole system, while the VT is more related to the behaviour of small parts of the system such as tissues and muscles [83]. In addition, these parameters could have linear or nonlinear values [123].

There are a variety of these models in both number of components and connection between them. The most simple model of the HAS consists of only two DOF which only simulates contact between the skin of the palm and the upper body (Figure 2-16) while the more complex models can have higher DOF to simulate the

response of the skin of the fingers, skin of the palm and fingers (Figure 2-17 to Figure 2-22). These models usually simulate movement in only one-direction; however, more advanced models consisting of rotating parts can be used to simulate bending and can be used for different postures (Figure 2-21 and Figure 2-22).

The two DOF model (Figure 2-16) cannot reproduce all of the measured MI while the elbow has 90º angle [124]; however, for some postures while the elbow is straight, it could be an acceptable model [125]. The linear three and four DOF models (Figure 2-17 and Figure 2-18) have proper prediction for phase angles in the y-direction; while in x and z directions they are only valid for frequencies between $20Hz$ to $200Hz$ and $40Hz$ to $400Hz$ respectively [31]. These two models have proper prediction for magnitude of MI from $20Hz$ to $1000Hz$ [31]. The proposed three and four DOF models in the ISO standard [30] can reproduced the measured MI for both palm and fingers in the z-direction [46, 50, 124], while for the x and y directions they cannot reproduce the MI for the whole frequency range at all points [46].

The earlier models such as linear three DOF (Figure 2-17) simulates the palm and fingers as one part, while the newer models such as five DOF (Figure 2-20) separates the palm from the fingers. Energy analysis shows that these two models do not show the same power loss due to the way they model the HAS; however, the share of power for each individual part in these two models are comparable [126].

The parameters in these HAS models can be used for generating models with higher DOF to simulate the HAS with the glove. Some of these models only modelled the glove between the skin of the palm and the handle, and also between the skin of the

fingers and the handle (Figure 2-23) while others increase the accuracy by adding extra parts for modelling the glove between the palm and fingers (Figure 2-24).

The analytical response of these models shows several natural frequencies for the HAS. The first which is about $7Hz$ is correlated with the mass of the upper arm and shoulder, and the stiffness between these parts and the palm. The second natural frequency at about $31Hz$ is more associated with the mass of the palm and wrist, and the stiffness between these parts and the skin of the palm. The third natural frequency at around $228Hz$ is associated with the mass of the fingers and the stiffness between the fingers and the skin of the fingers [84].

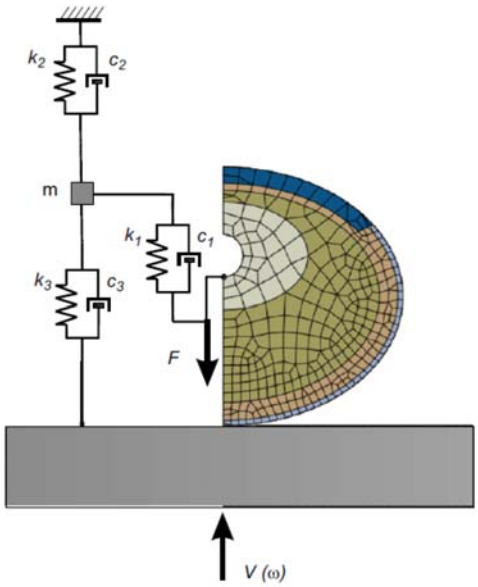

Figure 2-15 – Hybrid model of fingers [102]

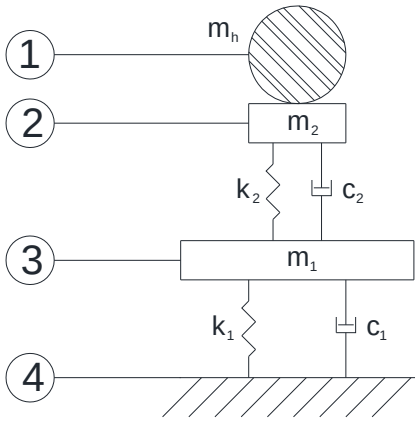

Figure 2-16 – Two-DOF model of hand-arm [30, 66, 125]

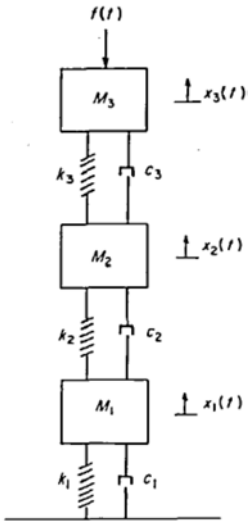

Figure 2-17 – Three-DOF model [49, 66, 123, 126]

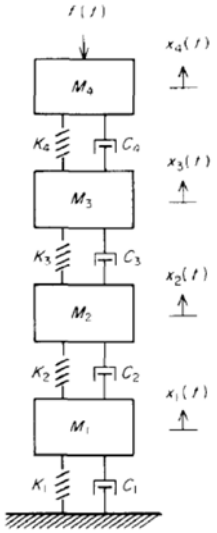

Figure 2-18 – Four-DOF model [31, 123]

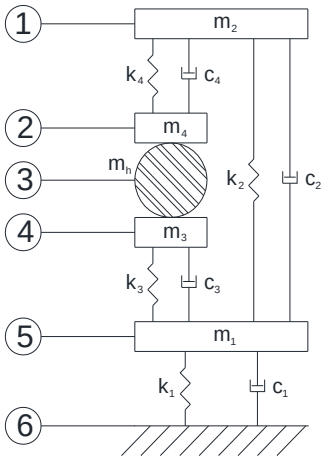

Figure 2-19 – Four-DOF model of hand-arm [30, 50]

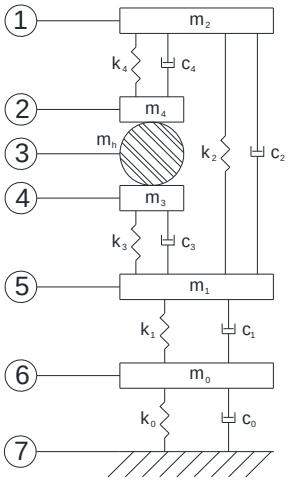

Figure 2-20 – Five-DOF model of hand-arm [30, 46, 50, 81, 88, 98, 126]

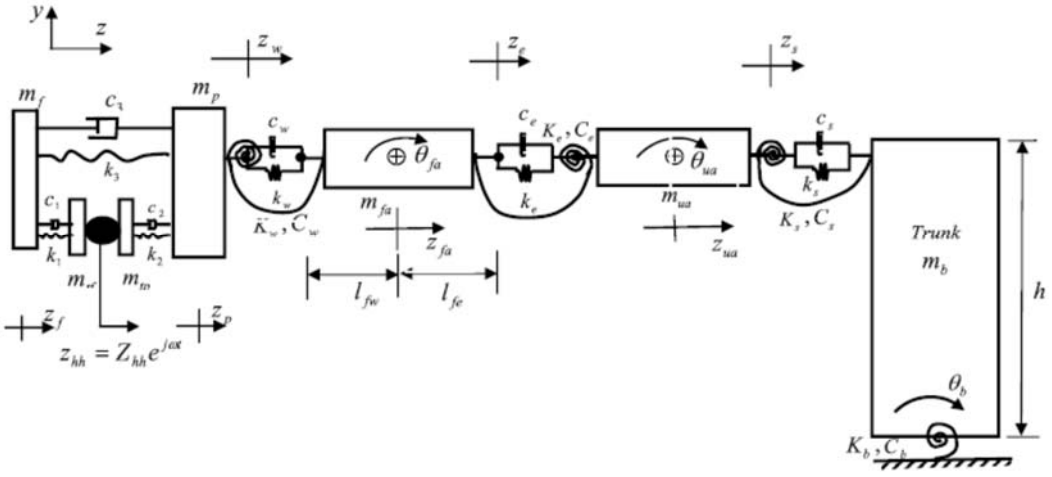

Figure 2-21 –Six-DOF model while the elbow has 180° angle [83]

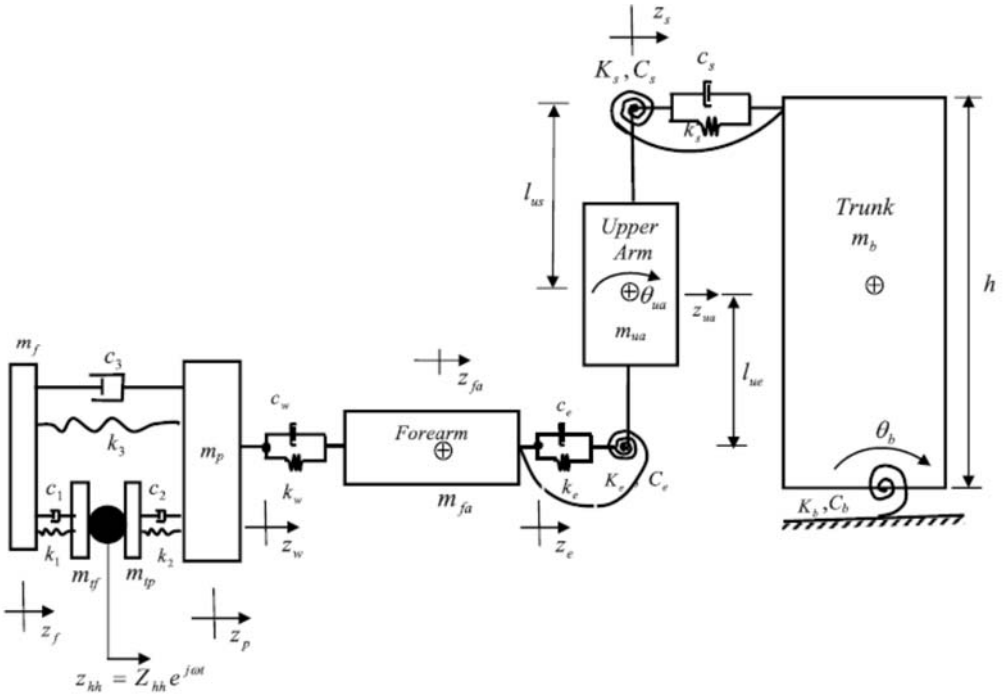

Figure 2-22 –Six-DOF model while the elbow has 90º angle [83]

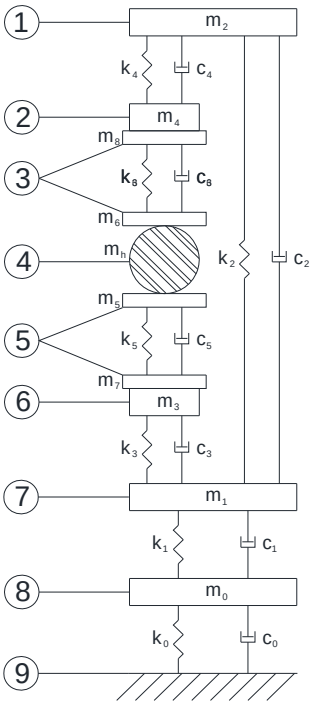

Figure 2-23 – Six-DOF model of hand-arm with glove [30, 46]

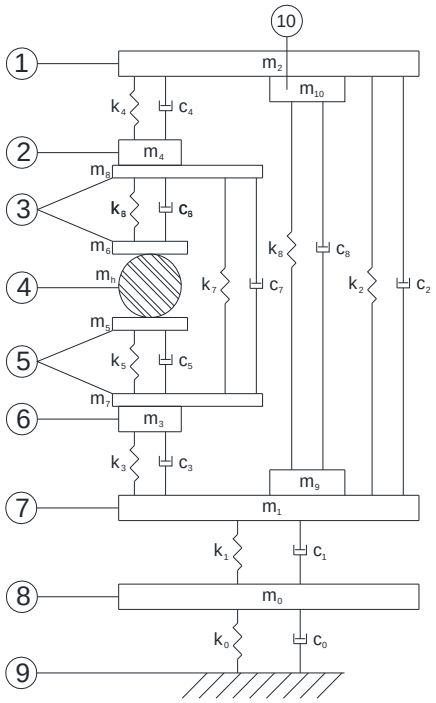

Figure 2-24 – Modified Six-DOF model of hand-arm with glove [84]

2.4 Summary

Vibration exposure from power tools to the human body involves significant potential health risks which depends on the vibration level, frequency, duration of exposure and etc. Anti-vibration gloves can be used for reducing this vibration exposure to the palm of the hand for certain frequencies. The ISO standard defines a procedure for measuring HAV and for evaluating anti-vibration gloves. Studies showed this procedure needs further improvement. This study investigates and improves some of the remaining issues with this procedure. In addition, it measures the VT at the different parts of the palm in order to generate a clearer picture of the VT at the palm of the hand.

Many researchers have used analytical models for simulating the vibration behaviour of the hand and arm. In addition, they combined this model with the analytical model of the glove, for simulating the performance of the glove. The properties of different elements of the glove model are usually derived from testing on an existing glove. This study uses the same analytical models with the opposite approach. It tries to find the proper amount of damping material inside the glove to achieve maximum vibration attenuation for both the palm and fingers sides before manufacturing the glove.

3 Experimental Setup

Power tools transmit vibration from their handles to the hands of workers. Being exposed to vibration can cause damage to the hands and arms of workers; therefore, in order to reduce this risk, the investigation on vibration transmissibility is crucial. Since each power tool has its own vibration behaviour, the frequency spectra of tools is not unique and varies by type and size of each tool [13]. Therefore, ISO 10819 [21] defines a practical procedure for standardizing vibration transmissibility tests and finding the vibration transmissibility from the vibrating handle to the hand of the operator. In addition, this standard can be used for evaluating gloves as to their anti-vibration properties.

The standard requests specific laboratory setup for simulating the vibration of power tools and measuring the resultant hand-arm vibration. In this setup a cylindrical handle which is attached to an exciter, simulates the vibration of the power tools' handles. According to this standard, the diameter of the test handle should be $40 \pm 0.5mm$ and it should be at least 110 mm in length. This standard also defines levels of vibration to be used for the frequency range from $25Hz$ to $1250Hz$. Table 3.1 shows the amplitude levels and weighting factors for the different frequencies in 1/3rd octave band for this test.

For the test, the operator should hold the handle and apply gripping and feeding forces while the handle is vibrating. The feeding force should be aligned to the direction of vibration. The gripping force during the test should be $30 \pm 5N$ and the feeding force should be $50 \pm 8N$. These forces should be monitored for the operator during the test.

The aim of this test is to measure the vibration transmissibility from the vibration handle to the hand of the operator; therefore, vibration at two points should be measured. One accelerometer inside the handle should measure the acceleration of the handle, the source of vibration, and the other accelerometer should measure the acceleration at the palm of the hand. For maintaining the position and orientation of the accelerometer at the palm, the standard has requested the use of a special adaptor for the accelerometer. Figure 3-1 shows the dimensions and shape of this adaptor.

Table 3.1 - Required handle acceleration [21]

Frequency Band	Acceleration PSD value	Acceleration tolerance in the 1/3rd octave band		1/3rd octave acceleration value	Weighting factor
f_i	P_{ZZ}	dB			
Hz	$(m/s^2)^2/_{Hz}$	-	+	m/s^2	W_{hi}
25	0.709	2	2	1.98	0.647
31.5	0.893	1	1	2.45	0.519
40	1.134	1	1	3.22	0.411
50	1.417	1	1	4.10	0.324
63	1.786	1	1	4.85	0.256
80	2.268	1	1	6.38	0.202
100	2.835	1	1	8.20	0.160
125	3.543	1	1	9.81	0.127
160	4.535	1	1	12.53	0.101
200	5.669	1	1	16.00	0.0799
250	7.087	1	1	20.14	0.0634
315	8.521	1	1	23.79	0.0503
400	9.179	1	1	28.19	0.0398
500	9.179	1	1	31.59	0.0314
630	8.555	1	1	33.96	0.0245
800	7.069	1	1	35.19	0.0186
1,000	4.994	1	1	33.35	0.0135
1,250	2.905	1E+12	2	28.37	0.00894
1,600	1.324	1E+12	3	19.58	-

For the test, the operator should stand straight; the elbow should have an angle of $90° \pm 15°$ while the forearm is to be aligned with the vibration direction. Figure 3-2 shows the experimental setup for this test according to ISO 10819.

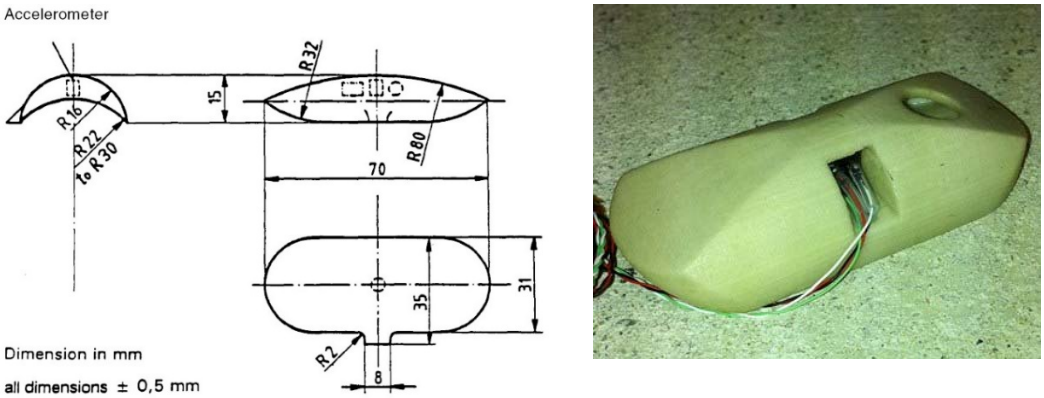

Figure 3-1 – Suggested adaptor for measuring the acceleration at the palm [21]

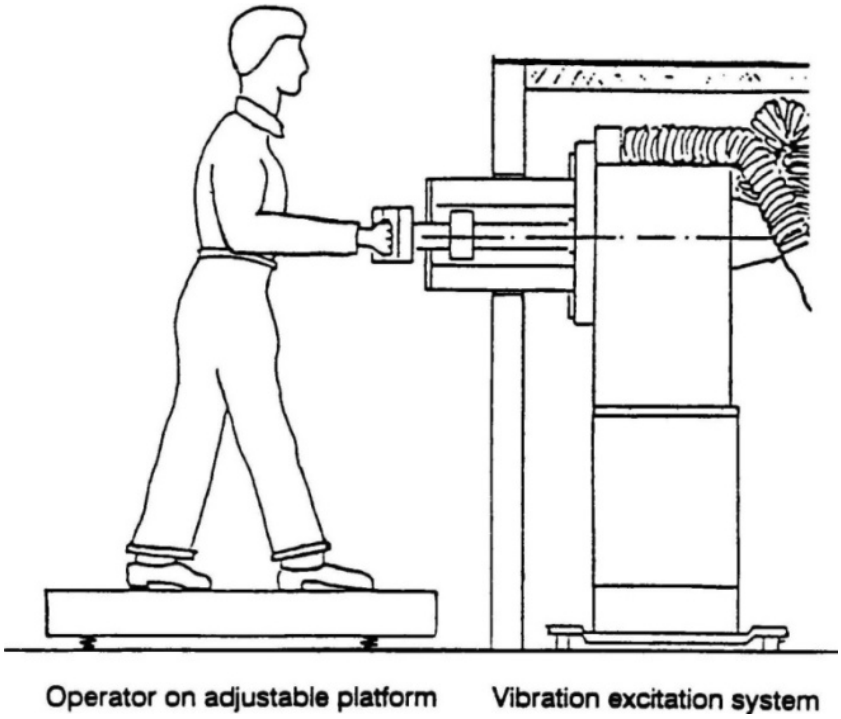

Figure 3-2 - ISO 10819 testing setup [21]

The first step in this procedure is to evaluate the testing rig. For this purpose, while the handle is vibrating according to the standard criteria, the operator should hold the handle without any glove and the vibration transmissibility from the handle to the hand should be measured. If the vibration transmissibility from the handle to the

hand over the whole frequency range is 1.0 with 5% tolerance, it indicates the testing setup is suitable for measuring the vibration transmissibility of the glove and evaluating the glove.

In the next step, by repeating the test while the operator is wearing the glove, the vibration transmissibility of the glove can be measured. This standard splits the frequency range of this test into two zones. The frequency range between 25Hz to 200Hz is called the Medium range and the frequency range between 200Hz to 1250Hz is called the High range. The mean vibration transmissibility for each range in this test is the summation of vibration transmissibility of each octave band multiplied by its weighting factor. The standard states that if the mean vibration transmissibility of a glove for the medium range is not below 0.9 and for the high range is not below 0.6, it cannot be classified as an anti-vibration glove.

3.1 Vibrating handle

The standard has defined the size and shape of the handle; however, there are other criteria that should also be considered. The frequency range for the hand-arm vibration test is from 25Hz to 1250Hz. Since the magnitude of vibration close to natural resonant frequencies of the system changes dramatically, if the system has any natural frequencies in the range of the hand-arm test, it can significantly affect the result. Therefore, the handle should be designed so that it will not have any resonance in the frequency range of the test. Even more importantly, the amplitude of vibration at frequencies close to the natural frequency can be higher than at other frequencies, therefore, the frequency of the first resonance of the handle should be as far as possible from the highest frequency in the test.

In addition, the handle needs proper sensors for measuring the feeding and gripping forces. Figure 3-3 shows two suggested handle designs from this standard. In the left design with two force transducers, the gripping force can be measured. For the feeding force an additional measuring system is required. In the second design both feeding and gripping forces can be measured with four force transducers in the front and back-side of the handle.

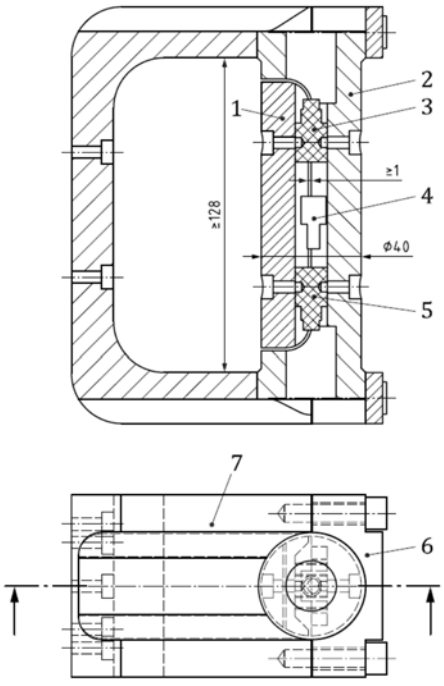

1.Measurement cap (aluminum or magnesium), 2.Handle base (aluminum) 3.Force transducer, 4.Accelerometer, 5.Force transducer, 6.Fixture clamp (aluminum) 7.Handle fixture (aluminum)

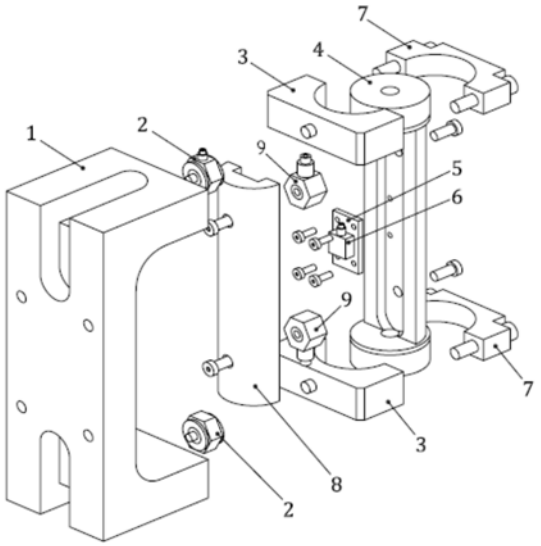

1.Base (aluminum), 2.Feed force transducer, 3.Read bracket, 4.Handle, 5.Accelerometer base, 6.Accelerometer, 7.Front bracket, 8.Handle cover, 9.Grip force transducer

Figure 3-3 – Suggested handle by ISO 10819:2013 [21]

Another way to measure the force is by measuring the amount of deformation of the system and translating it to the applied force. With the use of calibrated strain gauges, the strains at certain points of the system can be measured and the relevant force can be calculated. For measuring dynamic forces, force-transducers usually are suitable; however, for measuring the static force a complementary method is

required. In contrast, strain gauges are suitable for both static and dynamic measurement.

This study continues the previous research on hand-arm vibration at Curtin University. In the previous study, an aluminium cylindrical handle has been designed and manufactured for the B&K 4825 exciter. This exciter can apply a maximum 140N for random excitation with forced air-cooling. It has a single connecting shaft with 10mm diameter which the handle can be mounted to with a screw. This handle uses strain gauges for measuring feeding and gripping forces. The initial investigation showed that there were a number of problems with the handle design:

- The handle does not have any space inside for mounting the accelerometer; therefore, it is not possible to mount the accelerometer aligned to the excitation direction.
- The first natural frequency of the handle was around 500Hz, which is in the middle of the test frequency range. The amplitude of vibration at the natural frequency increases and after that decreases significantly; therefore, having the natural frequency in the test frequency range was shown to significantly affect the vibration transmissibility result.
- This handle was designed to attach to the exciter directly. The exciter[2] was found to be unsuitable for handling any bending force on the output shaft; therefore, during the tests, any misalignment of applied forces with the direction of movement, could cause damage to the system.

[2] B&K 4825

3.1.1 Handle design

In this study, for improving the performance of the handle, a new handle was designed and manufactured. The goal for this design was to increase the first natural frequency up to $1300Hz$. In addition, the aim was to design a support system for the handle to prevent it from applying any bending moment on the exciter.

In the design, strain gauges were utilized for monitoring the forces. In order to keep the resolution for strain measurement, the system needed to have proper flexibility at the measuring points; however, by increasing the flexibility, the frequency of the first resonance will be decreased. Therefore, the challenge was to find the acceptable shape of the handle to have high natural frequency, and high resolution of force measurement at the same time. For this purpose, a 3D-model of the handle was developed with SolidWorks and the dynamic behaviour of it was simulated with ANSYS. With the result of the simulation, the critical and affecting parameters on natural frequency and deflection at the measurement points with were identified. Later through several simulations finally the acceptable values for the parameters were identified and the model was finalized.

The new handle design was essentially a hollow cylindrical part; therefore, the mass of the handle decreased from $0.557kg$ to $0.480kg$ and consequently used less vibration power from the exciter than the previous one. On the other hand, the space inside of the handle gave enough room for the mounting of two accelerometers. One accelerometer was used for the vibration control system and the other for measuring the acceleration of the handle. The main accelerometer which was used for

measuring the acceleration of the handle was placed in the middle of the handle[3] aligned with the exciter and the second one which was used by the vibration controller for getting feedback from the system was mounted above it.

Table 3.2 shows the theoretical result of the first six natural frequencies of both the old and new handle design from the finite element modelling. As this table shows, the first natural frequency for the new handle occurred at 1461Hz, which was above the criteria range as required. In addition, with this design the strain deflection resolution for monitoring forces does not decrease. Figure 3-4 to Figure 3-9 show the mode shapes of the first three natural frequencies of the old and new handle.

Table 3.2 - Natural frequency comparison of handle design

	Existing handle (Hz)	New handle (Hz)
1	484	1,461
2	507	1,510
3	697	1,539
4	970	1,614
5	1,117	2,049
6	1,284	2,719

Two sets of strain gauges were designed for measure strain due to the feeding and gripping forces in the new handle. For feeding force measurement, two pairs of active-active strain gauges were mounted on the bottom and top of the base. For gripping force measurement, two pairs of active-dummy strain gauges were mounted on the bottom and top of the back-side of the cylindrical part of the handle.

[3] In the Hand-arm vibration tests, the adaptor should be aligned with this accelerometer (Figure 2-10 and Figure 2-11).

Since the exciter – B&K 4825 - cannot support any bending moment on the central axis, a support for the exciter central axis was required. Therefore, for this exciter a supporting system was designed to protect the exciter from applying any bending moment. This problem was solved by using a guiding system, which consisted of four connecting rods and two Teflon plates as bearings. With this support, even if an nonaligned force was applied from the operator to the handle, the applied force on the exciter would still be aligned with the central exciter rod. Figure 3-10 shows the handle attached to the guiding support system designed to prevent bending moments about the handle from damaging the exciter.

Although, the support system solved the bending moment problem, later results of the mechanical impedance of the handle showed there was significant non-linearity introduced into the system. This problem may be caused due to friction between the connecting rod and the Teflon bearing surface. This was found to not affect the vibration transmissibility measurement from the handle to the adaptor; however it was subsequently found to be unsuitable for measuring the mechanical impedance of the handle or operator. Finally, it was decided to buy a more robust exciter, which would not need the additional supporting system.

The new exciter, LDS V455 was able to apply maximum force up to 214N for random excitation. In addition, it had a connecting disk with 64 mm diameter with one M5 hole in the middle and five other M5 holes in a circle with 25 mm diameter around the centre of the first hole. With this exciter, the new handle could be mounted directly to the connecting disk without need of further support. This exciter was also driven by a LDS Laser $_{USB}$ Vibration Control System, which was very useful during the hand-arm vibration test for maintaining the vibration level according to the ISO criteria.

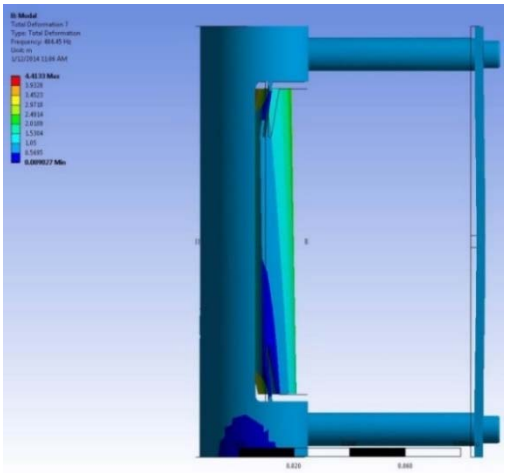

Figure 3-4 – Old handle - Mode Shape 1 at 484*Hz*

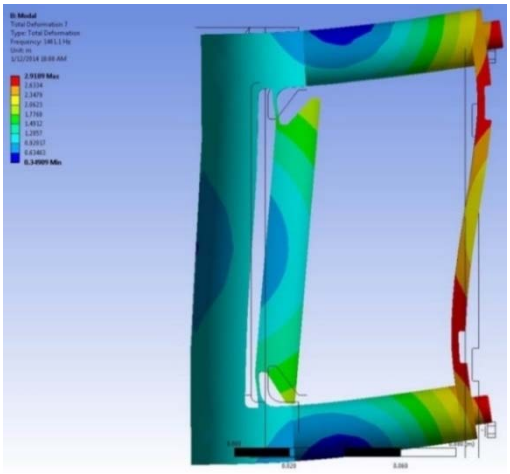

Figure 3-5 – New handle - Mode shape 1 at 1461Hz

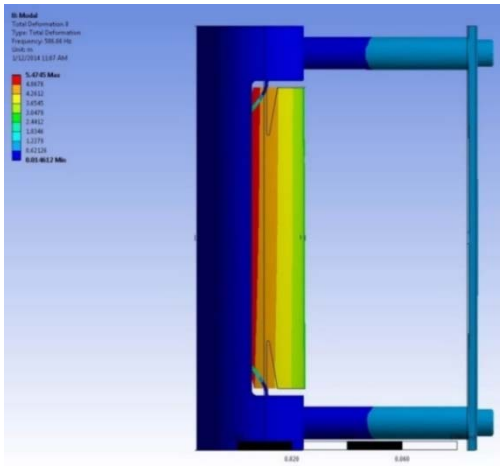

Figure 3-6 – Old handle - Mode Shape 2 at 507*Hz*

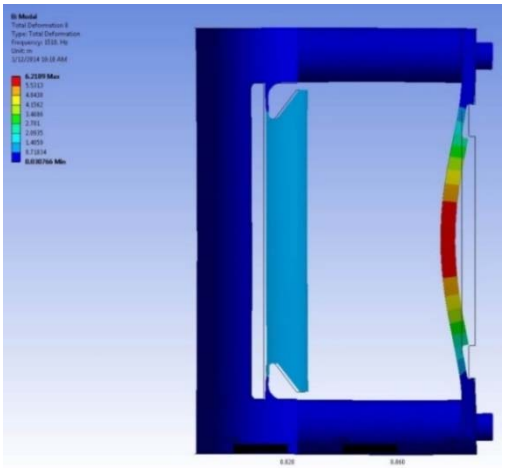

Figure 3-7- New handle - Mode shape 2 at 1510Hz

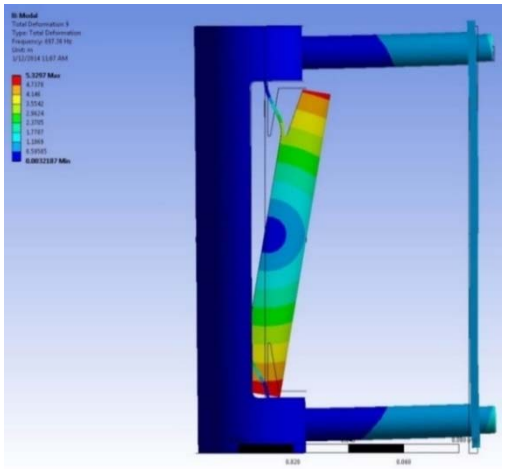

Figure 3-8 – Old handle - Mode Shape 3 at 697*Hz*

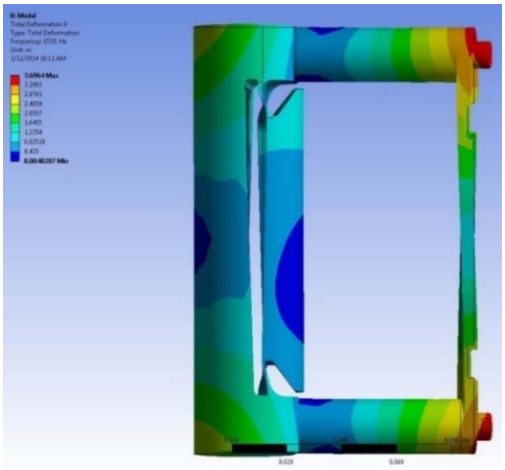

Figure 3-9- New handle - Mode shape 3 at 1539Hz

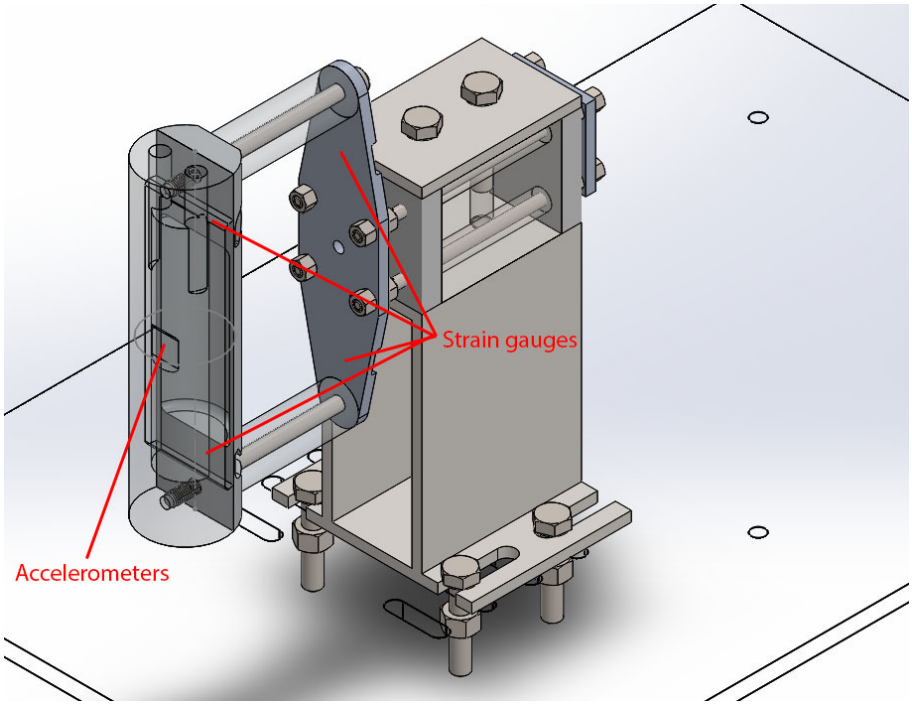

Figure 3-10 – First handle design with the support system

Therefore, the new approach for designing the handle became:

- Keeping the frequency of the first natural frequency above $1400Hz$
- Keeping the strain resolution for monitoring the feeding and gripping force
- Generate enough space inside the handle for three accelerometers where two of them could be aligned with the exciter direction of movement.
- Instead of measuring the feed force at the base of the handle, it was measured at the closest point to the handle which helps for measuring the mechanical impedance of the back side of the handle as well as the front side.

With these criteria and after optimization, another handle with better performance was designed and manufactured. In the final design, all of the measuring sensors were mounted inside the hollow cylindrical part where there was space for three accelerometers; one for the vibration controller system, one for measuring the acceleration of the handle at the palm side and one for measuring the acceleration of the handle at the fingers side.

For measuring the feeding force and gripping forces, for each half side of the handle, two pairs of active-active strain gauges were mounted at the bottom and top of the handle. All of these strain gauges were connected in a half-bridge circuit providing better resolution compared to the previous handle, which had an active-dummy pair. In addition, since the force measurement sensors were close to the palm and finger locations, they can be used to provide accurate data for calculating the impedance on each side of the handle. Since both accelerometers and strain gauges from the front and back-side of the handle work independently, the mechanical impedance of both sides of the handle can be measured simultaneously during the test.

Figure 3-11 shows the model for the final design of the handle[4]. As this figure shows the handle consists of two cylindrical parts, which are attached to the main frame. The cylindrical parts are made of aluminium and are hollow. In these parts, there were two accelerometers on the front-side and one on the back-side of the handle. On the top and bottom of each cylindrical part, there were flat plates where the strain gauges are attached. The main frame was made of steel and did not contain any sensor.

Figure 3-12 and Figure 3-13 show the first two modes shape of this handle. Similar to the previous design, the first natural frequency of this handle was above $1400Hz$.

[4] Figure A.3. 1 to Figure A.3. 10 in the Appendix show drawings of the handle.

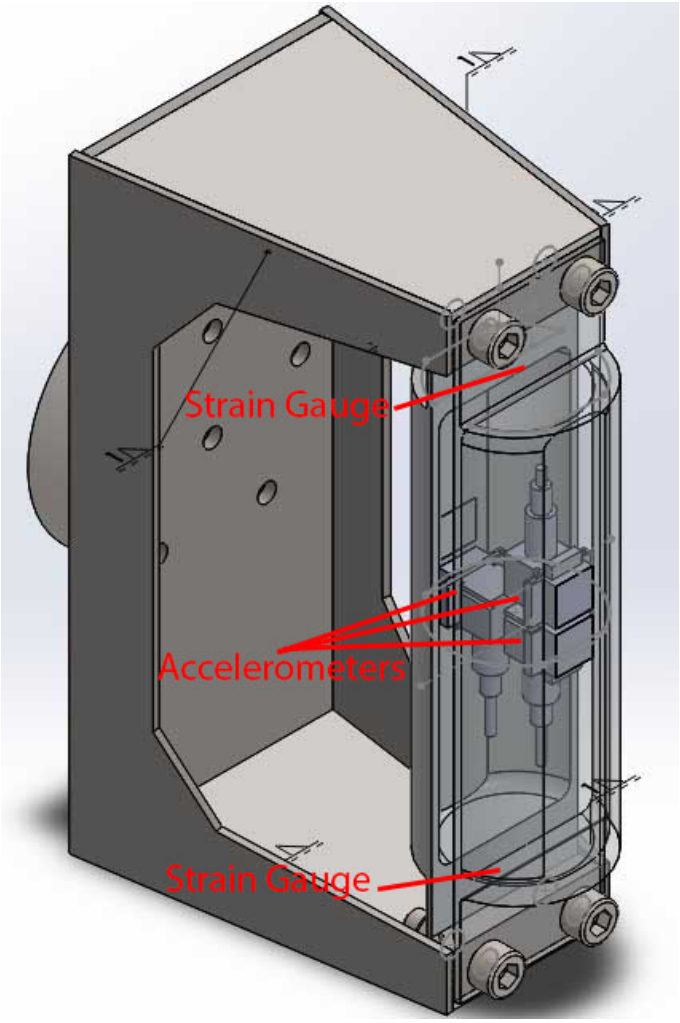

Figure 3-11 – The second handle

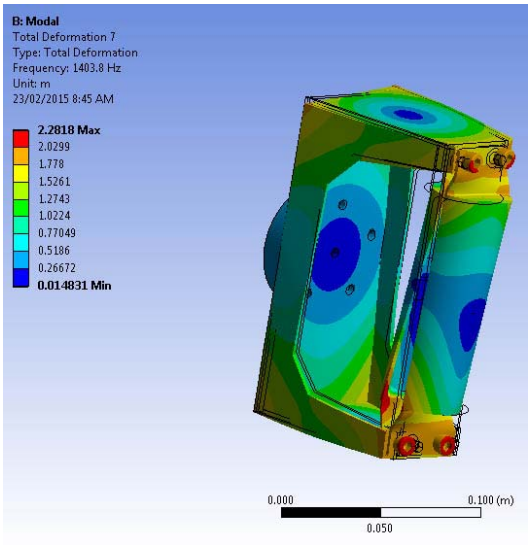

Figure 3-12 – Second handle
First Mode Shape at 1408Hz

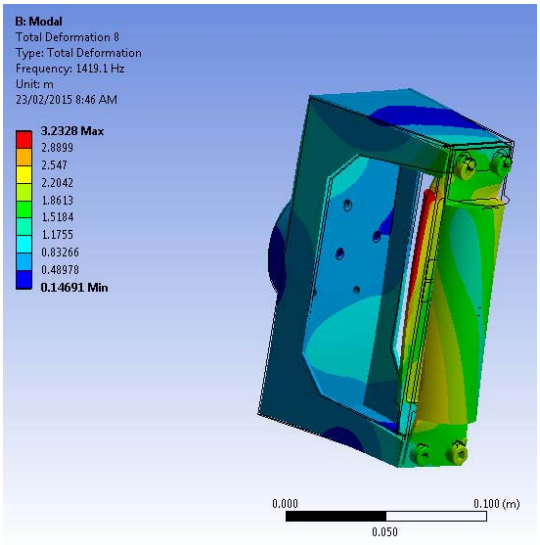

Figure 3-13 – Second handle
Second Mode shape at 1419Hz

3.1.2 Analytical modelling of the handle

Each half-cylindrical side of the handle can be modelled as a fixed beam. Figure 3-14 shows the schematic model of this beam with concentrated load and Figure 3-15 shows the similar model with distributed load. Each model consisted of two plates at the two ends and the hollow half-cylindrical part in the middle. The cross-sections of this beam were not uniform; therefore, for each section of the beam the second moment of area was given by,

$$I_s = \frac{bh^3}{12}, (x < s)\,, \qquad \text{Eq. 3-1}$$

$$I_m = \left[\frac{\pi}{8} - \frac{8}{9\pi}\right](r_1{}^4 - r_2{}^4) \simeq 0.1098(r_1{}^4 - r_2{}^4), \qquad (s < x < L - s), \qquad \text{Eq. 3-2}$$

$$I_s = \frac{bh^3}{12}, (L - s < x)\,, \qquad \text{Eq. 3-3}$$

where b is the width of the plate, h is the thickness of the plate and $r_1$and r_2 represent the outer and inner radius of the half-cylindrical part.

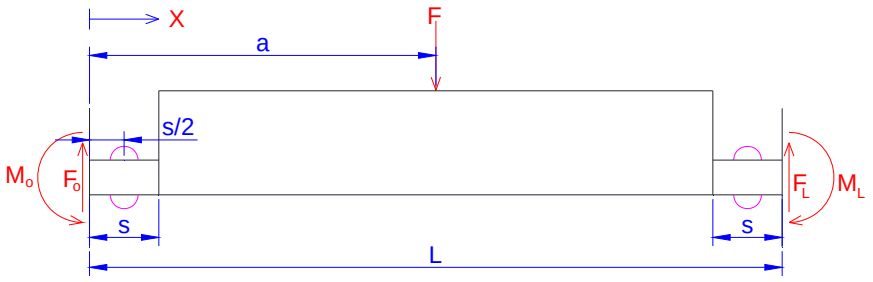

Figure 3-14- Schematic model of half-side of handle with concentrated load

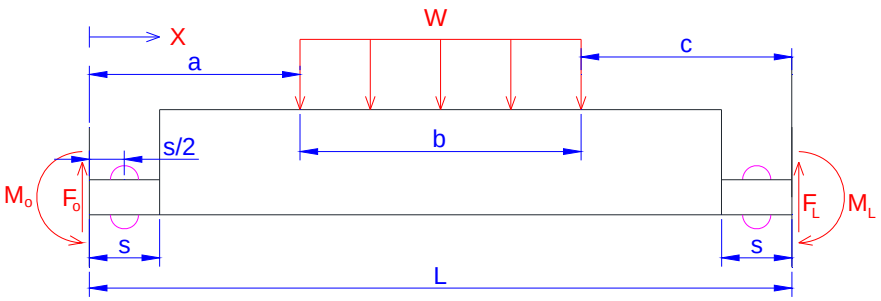

Figure 3-15- Schematic model of half-side of handle with distributed load

For a concentrated force, the equation for external loads can be defined as

$$q(x) = F_o < x >_{-1} - M_o < x >_{-2} - F < x - a >_{-1}, \quad \text{Eq. 3-4}$$

where F_o and M_o are support reactions, F is the loading at $x = a$ and $< \cdots >$ represents the bracket enclosing the arguments of the singularity function (Macaulays bracket). The singularity function has the following characteristics,

$$< x - a >^n = (x - a)^n \quad if\ x - a \geq 0\ and\ n > 0, \quad \text{Eq. 3-5}$$

$$< x - a >^n = 1 \quad if\ n = 0, \quad \text{Eq. 3-6}$$

$$< x - a >^n = 0 \quad if\ x - a < 0\ or\ n < 0, \quad \text{Eq. 3-7}$$

$$\int_{-\infty}^{x} < x - a >^n dx = \frac{1}{n + a} < x - a >^{n+1} \ if\ n > 0, \quad \text{Eq. 3-8}$$

$$\int_{-\infty}^{x} < x - a >^n dx = < x - a >^{n+1} \ if\ n \leq 0. \quad \text{Eq. 3-9}$$

The equation for shear force is,

$$V(x) = -\int q(x)\, dx = -F_o < x >^0 + M_o < x >_{-1} + F < x - a >^0. \quad \text{Eq. 3-10}$$

The bending moment inside the beam is,

$$M(x) = -\int V(x)\, dx = F_o < x >^1 - M_o < x >^0 - F < x - a >^1. \quad \text{Eq. 3-11}$$

The slope of the beam is,

$$\theta(x) = \int \frac{M(x)}{EI} dx. \quad \text{Eq. 3-12}$$

Since the beam does not have a uniform cross-section, the slope for each section is given by,

$$\theta_1 = \frac{F_o x^2 - 2M_o x}{2EI_s} + c_1, (0 < x < s), \quad \text{Eq. 3-13}$$

$$\theta_2 = \frac{F_o x^2 - F < x - a >^2 - 2M_o x}{2EI_m} + c_2, (s < x < L - s)\,, \quad \text{Eq. 3-14}$$

$$\theta_3 = \frac{F_o x^2 - F(x-a)^2 - 2M_o x}{2EI_s} + c_3, (L - s < x)\,. \quad \text{Eq. 3-15}$$

The deflection for each-section can be written as,

$$y_1 = \frac{F_o x^3 - 3M_o x^2}{6EI_s} + c_1 x + c_4, (0 < x < s)\,, \quad \text{Eq. 3-16}$$

$$y_2 = \frac{F_o x^3 - F < x - a >^3 - 3M_o x^2}{6EI_m} + c_2 x + c_5, (s < x < L - s)\,, \quad \text{Eq. 3-17}$$

$$y_3 = \frac{F_o x^3 - F(x-a)^3 - 3M_o x^2}{6EI_s} + c_3 x + c_6, (L - s < x)\,, \quad \text{Eq. 3-18}$$

The boundary conditions for the beam are assumed to be,

$$\theta(0) = 0\,, \quad \text{Eq. 3-19}$$

$$\theta_1(s) = \theta_2(s)\,, \quad \text{Eq. 3-20}$$

$$\theta_2(L - s) = \theta_3(L - s)\,, \quad \text{Eq. 3-21}$$

$$\theta(L) = 0\,, \quad \text{Eq. 3-22}$$

$$y(0) = 0\,, \quad \text{Eq. 3-23}$$

$$y_1(s) = y_2(s)\,, \quad \text{Eq. 3-24}$$

$$y_2(L - s) = y_3(L - s))\,, \quad \text{Eq. 3-25}$$

$$y(L) = 0\,. \quad \text{Eq. 3-26}$$

Therefore, the constant values for these equations become,

$$c_1 = 0\,, \quad \text{Eq. 3-27}$$

$$c_2 = \left[\frac{1}{EI_s} - \frac{1}{EI_m}\right]\left(\frac{F_o s^2}{2} - M_o s\right), \quad \text{Eq. 3-28}$$

$$c_3 = c_2 - \left[\frac{1}{EI_s} - \frac{1}{EI_m}\right]\left(\frac{F_o (L-s)^2}{2} - M_o (L - s) - \frac{F(L - s - a)^2}{2}\right), \quad \text{Eq. 3-29}$$

$$c_4 = 0\,, \quad \text{Eq. 3-30}$$

$$c_5 = -c_2 s + \left[\frac{1}{EI_s} - \frac{1}{EI_m}\right]\left(\frac{F_o s^3}{6} - \frac{M_o s^2}{2}\right), \quad \text{Eq. 3-31}$$

$$c_6 = c_2(L-s) - c_3(L-s) + c_5 - \left[\frac{1}{EI_s} - \frac{1}{EI_m}\right]\left(\frac{F_o(L-s)^3}{6} - \frac{M_o(L-s)^2}{2} - \frac{F(L-s-a)^2}{6}\right), \quad \text{Eq. 3-32}$$

For distributed loading the equation of load can be defined as,

$$q(x) = F_o < x >_{-1} - M_o < x >_{-2} - W < x-a >^0 + W < x-a-b >^0, \quad \text{Eq. 3-33}$$

where w is the distributed load. The shear force inside the beam is,

$$V(x) = -\int q(x)\, dx = -F_o < x >^0 + M_o < x >_{-1} + W < x-a >^1 - W < x-a-b >^1 \quad \text{Eq. 3-34}$$

The bending moment inside the beam is,

$$M(x) = -\int V(x)\, dx = F_o < x >^1 - M_o < x >^0 - \frac{W}{2} < x-a >^2 + \frac{W}{2} < x-a-b >^2. \quad \text{Eq. 3-35}$$

Since the beam has a non-uniform cross-section, the slope for each section is,

$$\theta_1 = \frac{F_o x^2 - 2M_o x}{2EI_s} + c_1, (0 < x < s), \quad \text{Eq. 3-36}$$

$$\theta_2 = \frac{F_o x^2 - \frac{W}{3} < x-a >^3 + \frac{W}{3} < x-a-b >^3 - 2M_o x}{2EI_m} + c_2, \quad (s < x < L-s), \quad \text{Eq. 3-37}$$

$$\theta_3 = \frac{F_o x^2 - \frac{W}{3}(x-a)^3 + \frac{W}{3}(x-a-b)^3 - 2M_o x}{2EI_s} + c_3, \quad (L-s < x), \quad \text{Eq. 3-38}$$

and the deflection for each-section is,

$$y_1 = \frac{F_o x^3 - 3M_o x^2}{6EI_s} + c_1 x + c_4, (0 < x < s), \quad \text{Eq. 3-39}$$

$$y_2 = \frac{F_o x^3 - \frac{W}{4} < x - a >^4 + \frac{W}{4} < x - a - b >^4 - 3M_o x^2}{6EI_m} + c_2 x + c_5, (s < x < L - s)\,, \quad \text{Eq. 3-40}$$

$$y_3 = \frac{F_o x^3 - \frac{W}{4}(x - a)^4 + \frac{W}{4}(x - a - b)^4 - 3M_o x^2}{6EI_s} + c_3 x + c_6, (L - s < x)\,. \quad \text{Eq. 3-41}$$

The same boundary conditions as concentrated load are assumed for the distributed load for this beam; therefore the constant values for these equations become,

$$c_1 = 0\,, \quad \text{Eq. 3-42}$$

$$c_2 = \left[\frac{1}{EI_s} - \frac{1}{EI_m}\right]\left(\frac{F_o s^2}{2} - M_o s\right), \quad \text{Eq. 3-43}$$

$$c_3 = c_2 - \left[\frac{1}{EI_s} - \frac{1}{EI_m}\right]\left(\frac{F_o (L-s)^2}{2} - M_o (L - s) - \frac{W(L-s-a)^3}{6} + \frac{W(L-s-a-b)^3}{6}\right), \quad \text{Eq. 3-44}$$

$$c_4 = 0, \quad \text{Eq. 3-45}$$

$$c_5 = -c_2 s + \left[\frac{1}{EI_s} - \frac{1}{EI_m}\right]\left(\frac{F_o s^3}{6} - \frac{M_o s^2}{2}\right), \quad \text{Eq. 3-46}$$

$$c_6 = c_2 (L - s) - c_3 (L - s) + c_5 - \left[\frac{1}{EI_s} - \frac{1}{EI_m}\right]\left(\frac{F_o (L-s)^3}{6} - \frac{M_o (L-s)^2}{2} - \frac{W(L-s-a)^4}{24} + \frac{W(L-s-a-b)^4}{24}\right). \quad \text{Eq. 3-47}$$

Now by knowing the bending moment at any point of this beam, the relevant stress for the point can defined as,

$$\sigma = -\frac{My}{I}\,, \quad \text{Eq. 3-48}$$

where M is the bending moment inside the beam, y is the distance of the point from the neutral axis and I is the second moment of area; therefore, the strain is given by,

$$\varepsilon = -\frac{My}{EI}\,. \quad \text{Eq. 3-49}$$

In this beam the strain gauges are placed at $x = \frac{s}{2}$ and $x = L - \frac{s}{2}$. When the position of the concentrated load or distributed load varies, the bending moment and the resultant strain at all points of the beam changes. Figure 3-16 shows the variation of strain for these two strain gauges as a function of load position. This graph shows strains for a concentrated load and distributed loads with 20, 40, 60 and 80mm length. All these curves have cubic equations and they are functions of load position and total load.

Therefore, the strain equation becomes,

$$Strain_{Left} = f * (-A\,x^3 + B\,x^2 - C\,x - D)\,, \qquad \text{Eq. 3-50}$$

$$Strain_{Right} = f * (A\,x^3 + B\,x^2 + Cx - D)\,, \qquad \text{Eq. 3-51}$$

By adding these two equations together, the strain relationship becomes,

$$Strain_{Right} + Strain_{Left} = 2 * f * (B\,x^2 - D). \qquad \text{Eq. 3-52}$$

Table 3.3 shows the parameters for this quadratic equation for different types of load on the beam.

Table 3.3 – Parameters in quadratic equation

Load	B	D
Concentrated load	33.9702	-0.12705
Distributed load (b=20 mm)	33.9702	-0.12592
Distributed load (b=40 mm)	33.9702	-0.12252
Distributed load (b=60 mm)	33.9702	-0.11686
Distributed load (b=80 mm)	33.9702	-0.10893

Figure 3-17 shows the ratio of two strains as a function of load position. These curves are almost linear and they are only a function of load position. Therefore, by knowing the ratio of two strains at the two ends of the each half-cylindrical part of

the handle, the position of the centre of load will be known. This study assumes the length of the distributed load on the handle is about $60mm$, and uses parameters of this type of load for calculating position of the load and the total load. Figure 3-18 shows the ratio of actual force over calculated force from two strains at the two ends of the beam for different types of load on the beam. Since, in HAV tests, the applied force is a distributed load, the calculated force can have up to 8% error for the distributed load with length less or greater than $60mm$. In the conduct of the laboratory hand-arm tests, by proper training, the operator should be able to apply the force almost in the middle of the handle; therefore, by considering the length of the applied force the expected error of the calculated force from the measured strains should be less than 5%.

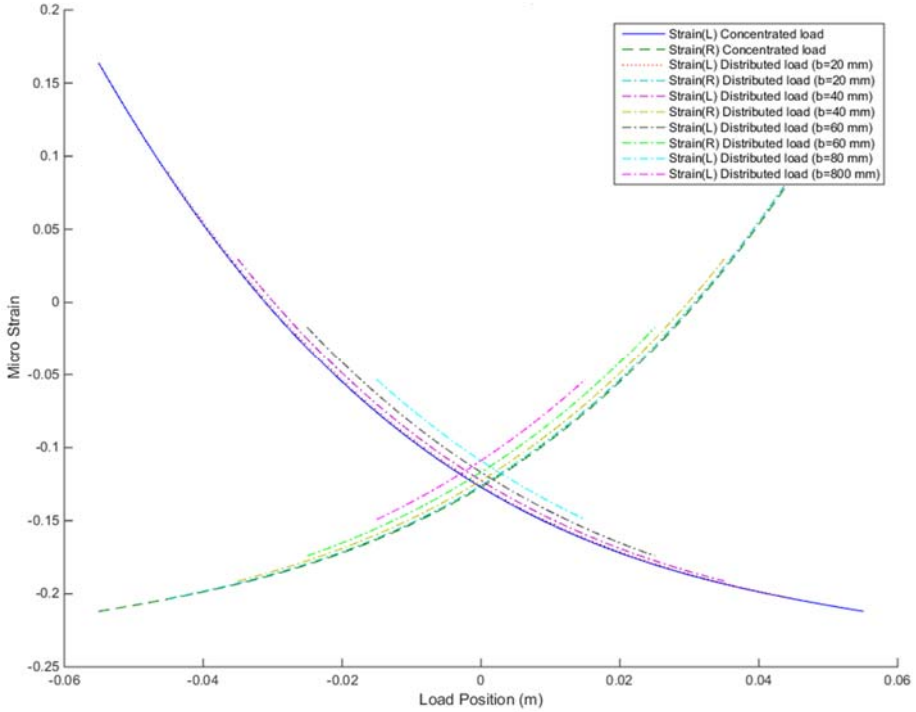

Figure 3-16- Calculated strain as a function of load position

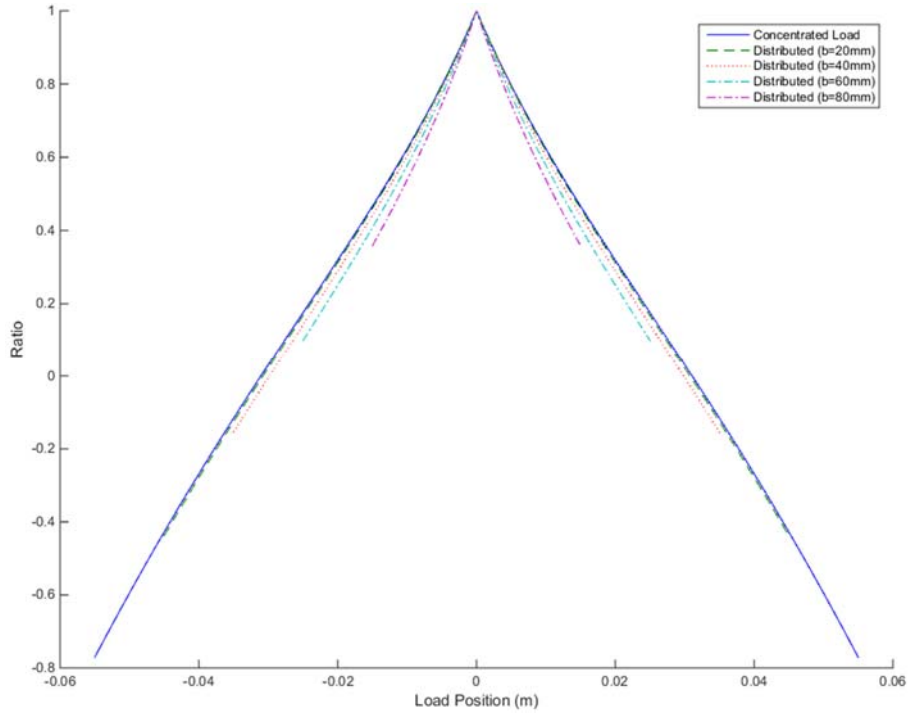

Figure 3-17- Difference of two calculated strains as a function of load position

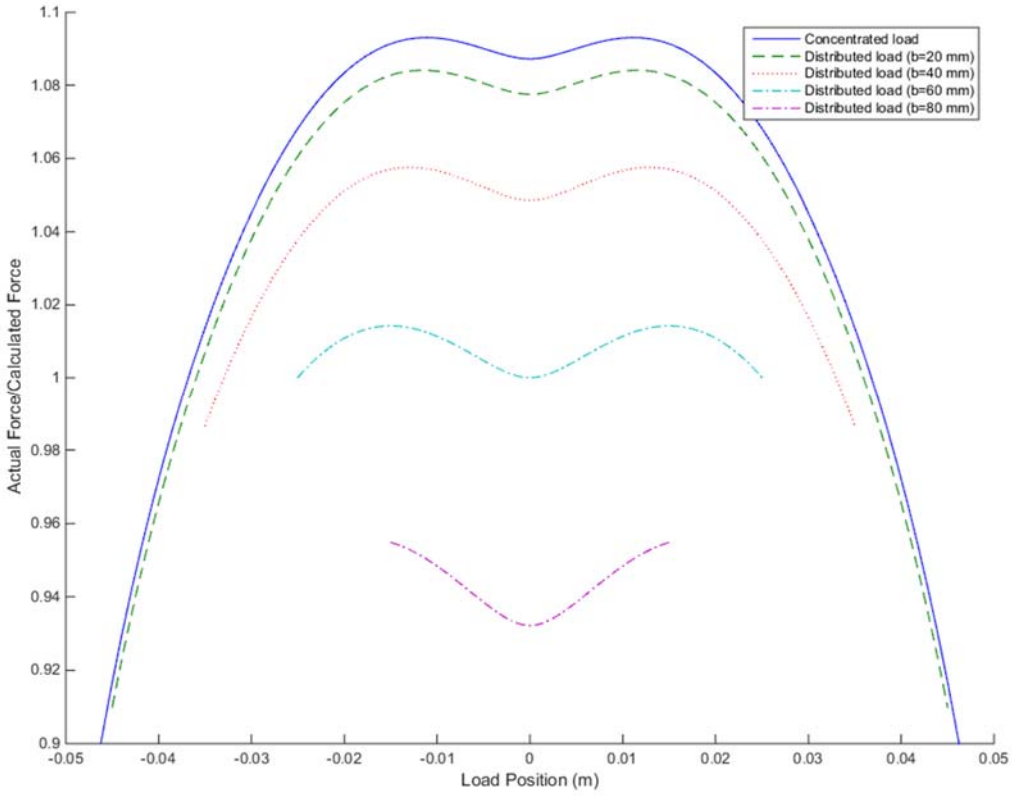

Figure 3-18- Actual force over calculated force as a function of load position

3.1.3 Strain gauge calibration

During the hand-arm vibration test, the operator should apply feeding and gripping forces and maintain these forces according to the ISO criteria. Therefore, it is necessary to measure and monitor these forces during the test. In the final design of the vibration handle, instead of using force-transducers for measuring the forces, strain gauges were used. Figure 3-19 shows the locations of these strain gauges on to the thin plates which are on the top and bottom of each half-cylindrical part on the handle. At each location, two strain gauges were used to create a half-bridge circuit. These two were active-active gauges, on the front and back-side of each plate.

By applying forces to each of the half-cylindrical parts, the top and bottom plates bend and with the strain gauges, the strain at each side is measureable. In order to monitor the applied forces for the operator, these strains should be translated to forces during the test. Therefore, a calibration function from strain to force is required and can be derived from a calibration test.

First the handle was calibrated when no force was applied to it; at this state it was assumed that the strain at all points were zero. Then static forces were applied to each side of the handle individually and the corresponding strains for each force for the top and bottom side were recorded. These forces were applied in the middle of the handle at each side. Later two sets of offset forces were applied to the handle. The first set was applied with 20mm offset above the centre to the top of the handle and the other set was applied with 20mm offset below the centre to the bottom of the handle. The RMS error in 1/3rd Octave band shows maximum value of 1 micro strain which is less than 2% of maximum strain measurement in HAV tests (Figure 3-24 and Figure 3-25).

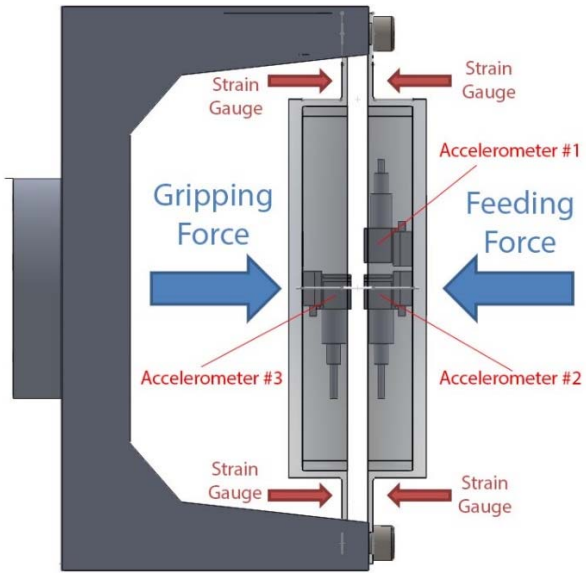

Figure 3-19 – Locations of strain gauges and accelerometers on the handle

Figure 3-20 to Figure 3-23 show the result for these three sets of forces for the top and bottom of the front side and for the top and bottom of the back-side of the handle respectively. In these figures the blue line with the circle shows the results for the force in the middle of the handle. The green line with star-marks shows the results for the force with $20mm$ offset to the top and the red line with the x-marks, shows the results for the force with $20mm$ offset to the bottom of the handle. The minor deviation from zero for some of the results is due to pre-stress inside the beam from previous tests. As these figures show, the relationship between the force and the strain in this handle is almost linear. Therefore, during the hand-arm vibration tests by measuring strain at top and bottom of the each side and using Eq. 3-52, the real time value of the force can be calculated. The strain from the bottom and top sides of each half-cylindrical part can be combined together to show the resultant strain at each part. Figure 3-24 and Figure 3-25 shows the resultant strain in the front and back side of the handle for normal and offset forces. In addition by using the difference of strains at the top and bottom of each side, the alignment of the applied force with the direction of movement can be monitored for the operator.

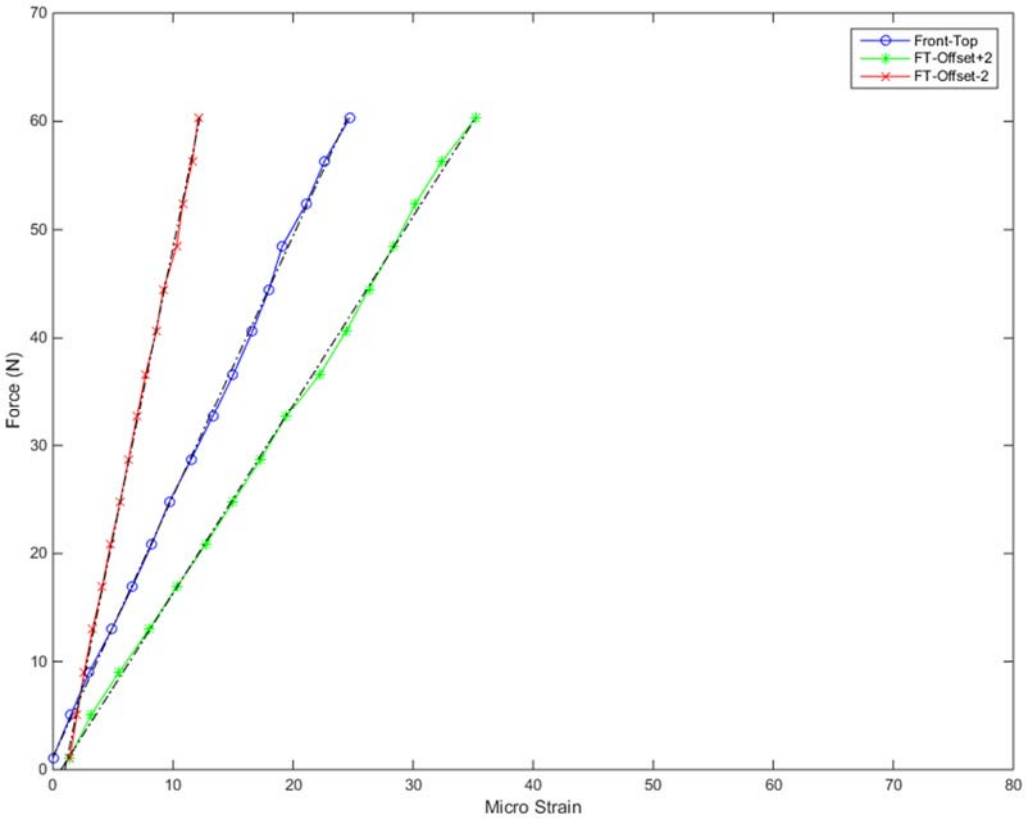

Figure 3-20 - Calibration front side - Top strain gauges

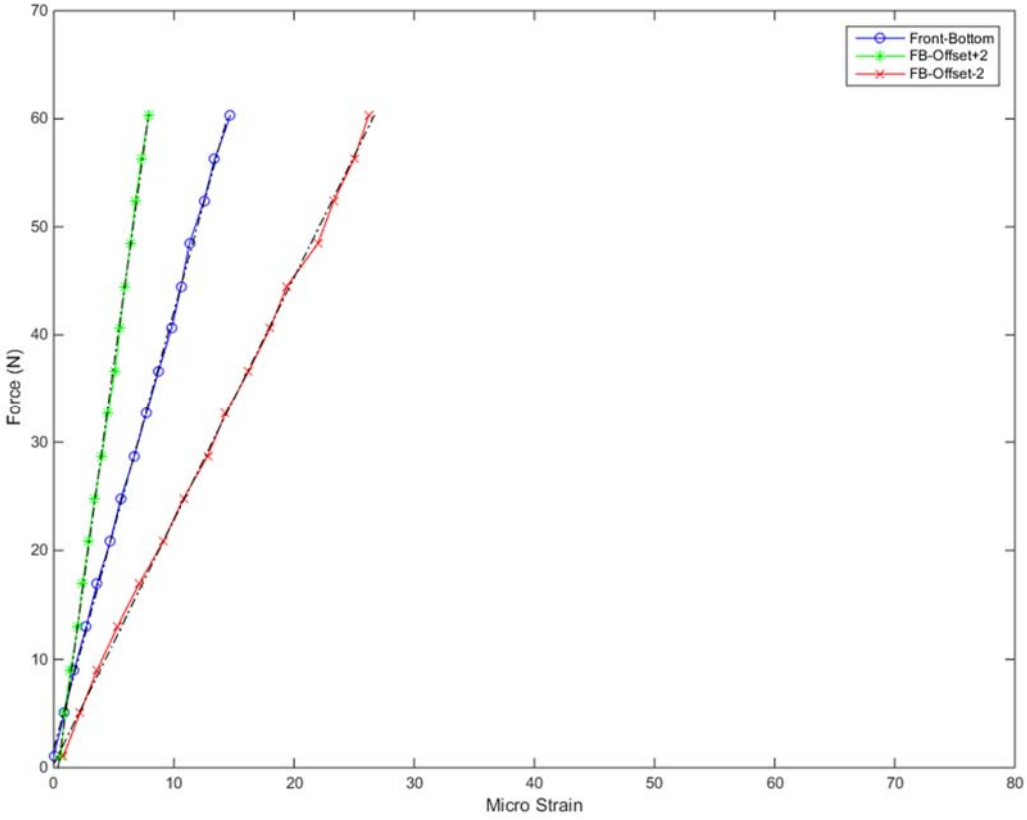

Figure 3-21 - Calibration front side - Bottom strain gauges

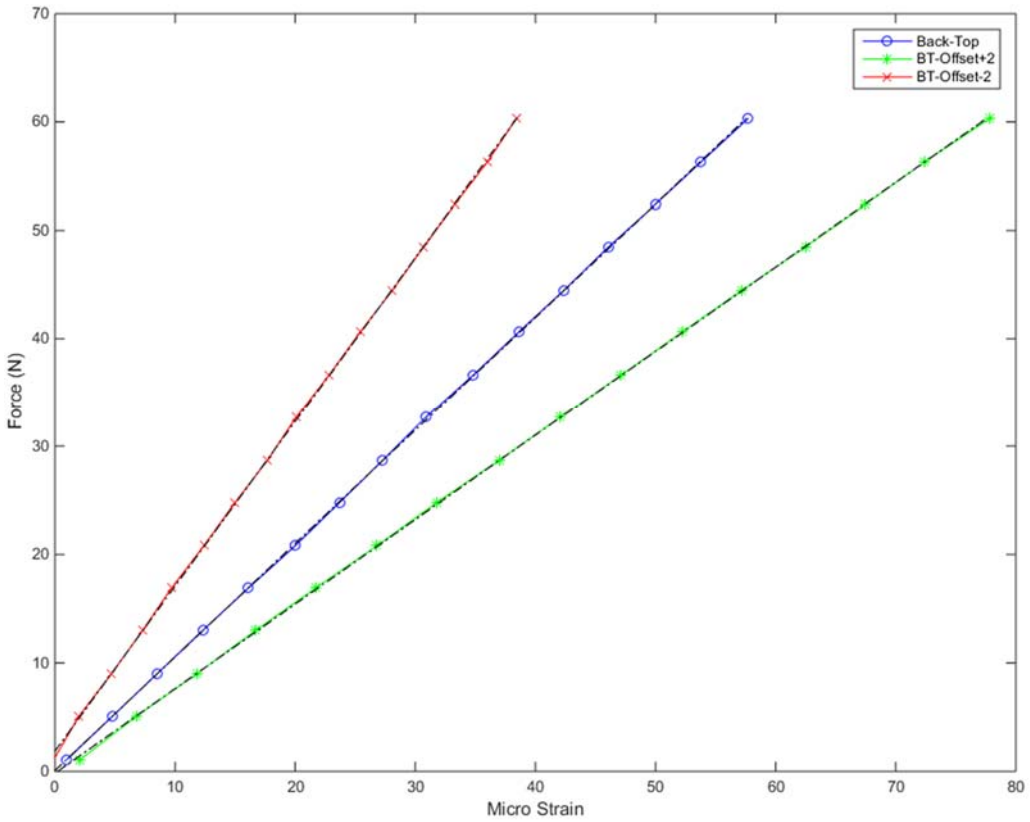

Figure 3-22 - Calibration back-side - Top strain gauges

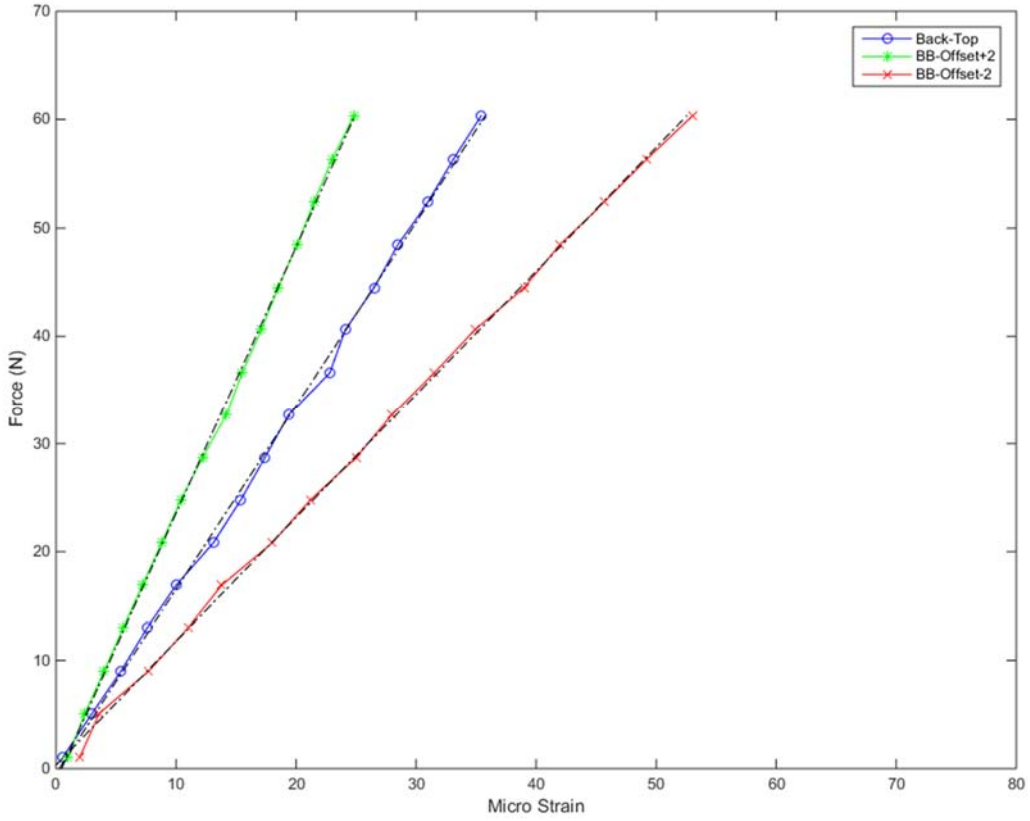

Figure 3-23- Calibration back-side - bottom strain gauges

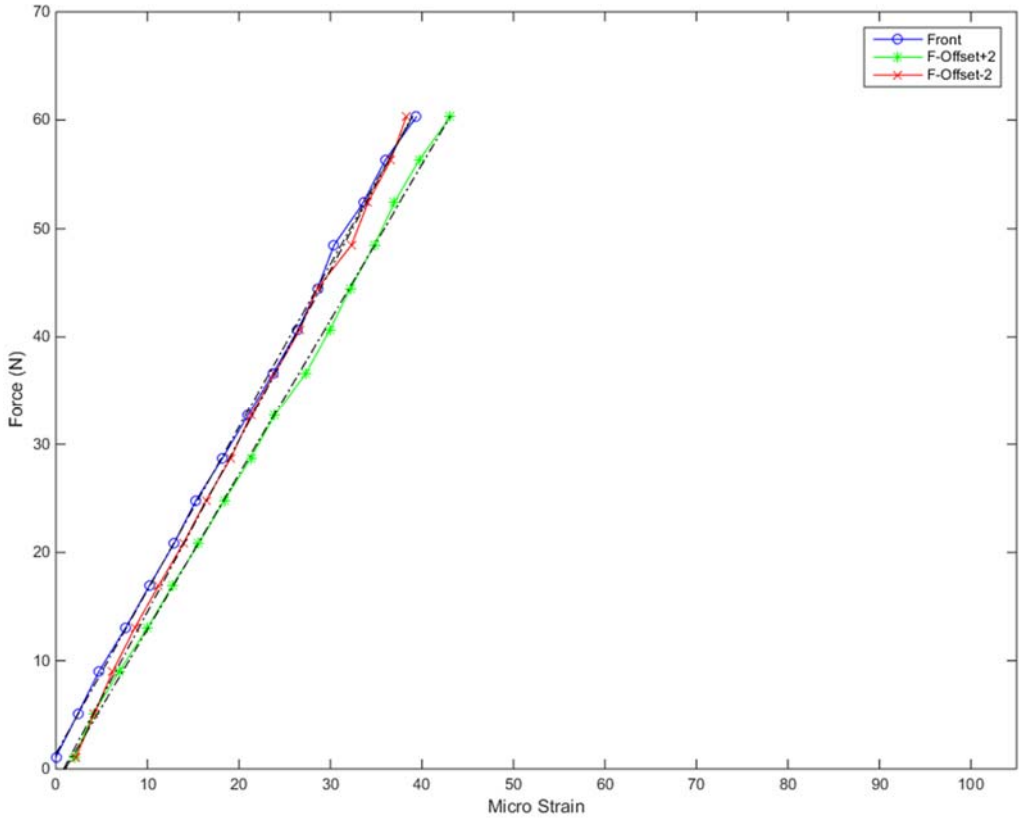

Figure 3-24- Calibration front side

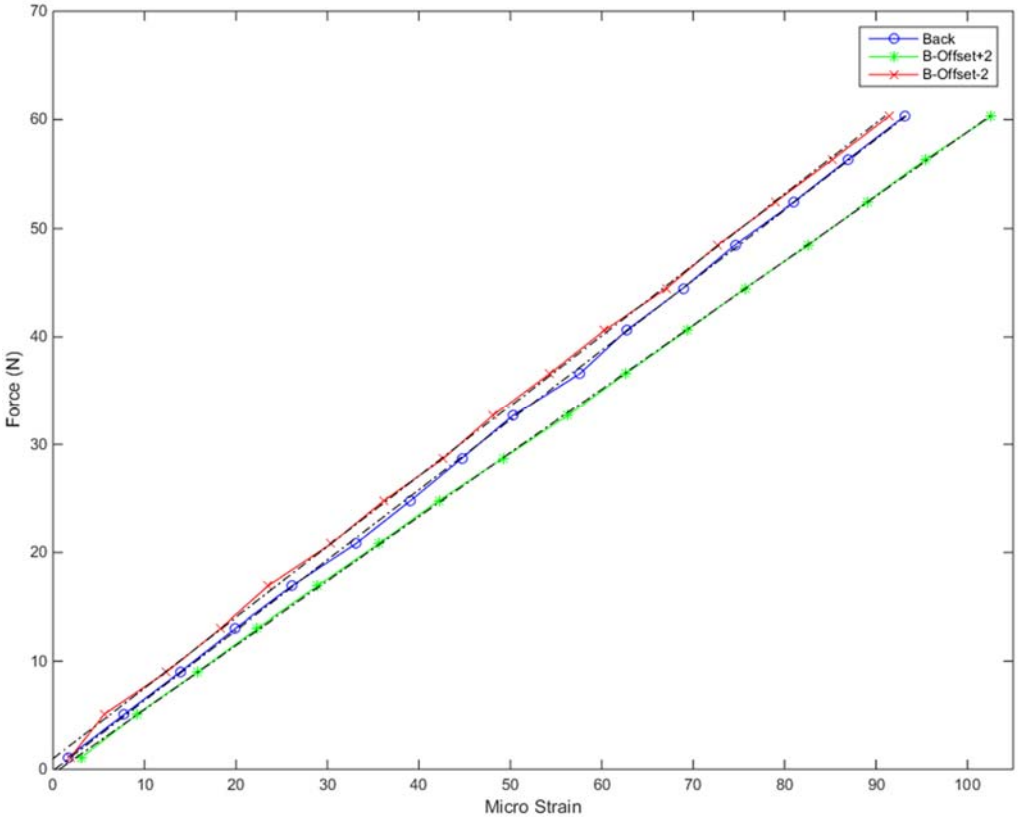

Figure 3-25- Calibration back-side

3.1.4 Accelerometer Calibration

For hand-arm vibration tests the acceleration at two points should be measured where the ratio of these show the vibration transmissibility. Therefore for having accurate and reliable data, first of all the accelerometers should be calibrated against a reference. In this study, different types and models of accelerometers were utilized. Table 3.4 shows the manufacturers properties of these accelerometers.

For the calibration test a "B&K 8305S" was used as the calibration accelerometer and reference. This accelerometer was screwed onto the B&K accelerometer calibrator type 4291, which excites at 80Hz. The B&K 8305S was connected to a B&K measurement amplifier type 2525. Figure 3-26 shows the test setup in this study for the calibration of all the test accelerometers.

Table 3.4 - Accelerometer properties

No	Manufacturer	Model	Direction	Sensitivity	Weight	Contact surface area
				V/ms^{-2}	g	mm^2
1	B&K	4507		0.0098850	4.8	100
2	B&K	4524B	X	0.0099490	4.4	100
3	B&K	4524B	Y	0.0100100	4.4	100
4	B&K	4524B	Z	0.0100700	4.4	100
5	ENDEVCO	35A	X	0.0004509	1.1	40
6	ENDEVCO	35A	Y	0.0003551	1.1	48
7	ENDEVCO	35A	Z	0.0003369	1.1	48
8	ENDEVCO	25A		0.0005880	0.2	11
9	ENDEVCO	25A		0.0005277	0.2	11
10	ENDEVCO	25A		0.0005296	0.2	11
11	ENDEVCO	25A		0.0006422	0.2	11

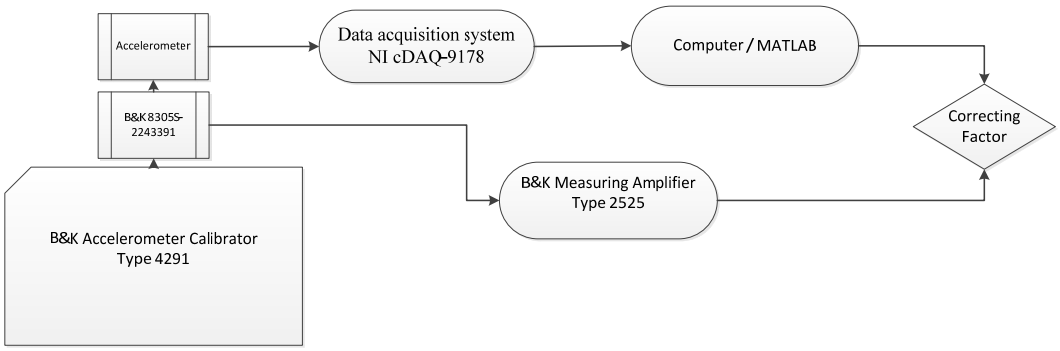

Figure 3-26 - Setup for accelerometer calibration

Each accelerometer was mounted on top of the reference accelerometer with wax. During the test, the measuring amplifier shows the amplitude of the vibration with reference accelerometer. The ratio between this amplitude and the measured amplitude of the other accelerometer was assumed to be the correcting factor for the accelerometer sensitivity. Table 3.5 shows the result of these tests. In further tests all of the accelerometers were tested at $159Hz$ and $500Hz$ to check the linearity of the sensitivity of the accelerometers.

Table 3.5 - Accelerometer sensitivity and sensitivity correcting factor after calibration

No.	Manufacturer	Model	Direction	Correcting Factor
1	B&K	4507		0.9711
2	B&K	4524B	X	0.9699
3	B&K	4524B	Y	0.9632
4	B&K	4524B	Z	0.9682
5	ENDEVCO	35A	X	1.0913
6	ENDEVCO	35A	Y	1.0722
7	ENDEVCO	35A	Z	1.2053
8	ENDEVCO	25A		1.0249
9	ENDEVCO	25A		1.0103
10	ENDEVCO	25A		1.0378
11	ENDEVCO	25A		0.9886

For these tests, wax was used to temporary mount the accelerometers on top of the reference accelerometers. With this method of mounting, the accelerometer and wax can create a lumped-mass system. The natural frequency for this 1-DOF model can be estimated as [127],

$$f_n = 0.159294\sqrt{\frac{A_w E}{tW}}, \qquad \text{Eq. 3-53}$$

where in this equation f_n is the mounted natural frequency in Hz, A_w is area of wax under the accelerometer base in mm^2, t is the thickness of wax in mm, E is the modulus of elasticity of wax[5] and finally W is the weight of the accelerometer in grams. The lowest natural frequency for these 1-DOF models of the accelerometers and wax was above 20,000Hz which is much higher than the frequency range for the hand-arm vibration testing. Therefore, the result of this calibration was determined to be acceptable for the hand-arm vibration tests.

3.1.5 Handle Impedance

Mechanical Impedance (MI) shows the resistance of the system to motion. MI can be used for simulating the behaviour of the system based on different input types. MI in the frequency domain can be defined as,

$$MI\ (\omega) = \frac{Force\ (\omega)}{Velocity\ (\omega)}. \qquad \text{Eq. 3-54}$$

Therefore, for measuring MI at a certain point, both applied force and velocity of the point are required. Instead of velocity, the acceleration of the point can be used and the MI can be defined as,

[5] Value of E was assumed to be $5*10^4$ Pa

$$MI\ (\omega) = j\omega \frac{Force\ (\omega)}{Acceleration\ (\omega)}. \qquad \text{Eq. 3-55}$$

As Figure 3-19 shows, three accelerometers are used in this handle. The first accelerometer measures the level of vibration for the vibration control system. The second accelerometer measures the vibration of the front-side and the third accelerometer measures the vibration of the back-side. Therefore, the accelerations at both front and back-side of the handle during the test are measureable. In addition, there are four sets of half-bridge strain gauges at the top and bottom of each half-cylindrical part. These strain gauges measure the strains at these points, which can be translated to the force at these points. With the acceleration and force data, the MI of the front and back-side of the handle can be calculated.

Figure 3-27 shows the MI of the system at the front of the handle as a function of frequency. In this graph, the results of two different tests are shown. During these tests, the vibration of the handle was controlled according to ISO 10819 criteria and the accelerometer that provides feedback from the handle to the controller, was mounted at the front-side of the handle. Since the first natural frequency of the handle was about $1400Hz$, the calculated MI for frequencies above $500Hz$ is not acceptable from this handle [54, 56].

Figure 3-28 shows that the MI of the system at the back-side is almost linear up to $1000Hz$ and it has one resonance at about $1100Hz$. Since the vibration controller controls the vibration amplitude and gets feedback from the front-side of the handle, this resonance was not visible in the front side result.

This measurement can be repeated while the operator is holding the handle. The calculated MI from the test shows the total MI of the operator and the whole system. The difference of MI from the whole system with the operator MI of the system

without the operator can show the MI of the operator [41]. This result is beneficial for deriving the parameters of the lumped-mass model of the hand-arm system.

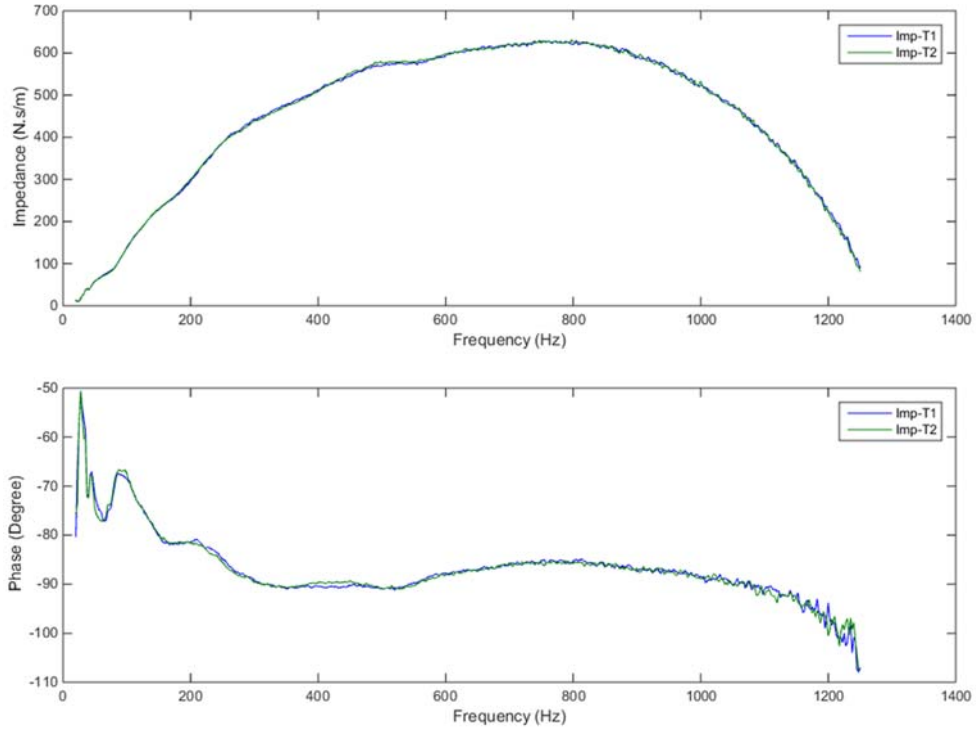

Figure 3-27 – Mechanical Impedance of front side

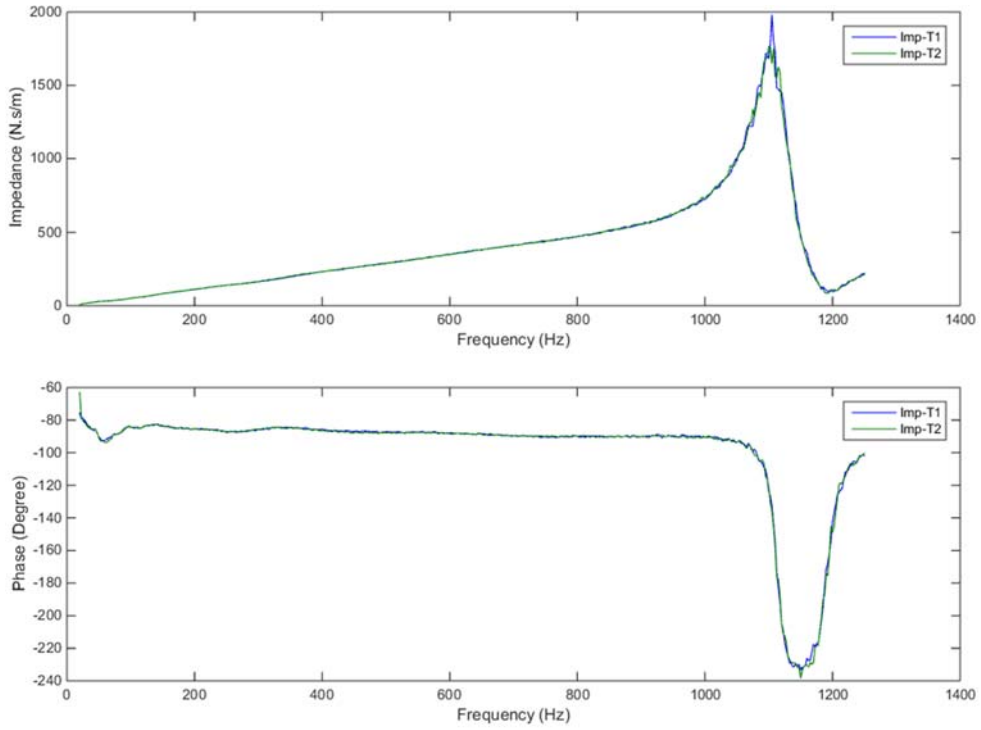

Figure 3-28 – Mechanical Impedance of back-side

3.2 Vibration controller

ISO 10819 defines the acceleration amplitude and tolerance for the frequency range from 25Hz to 1600Hz (Table 3.1). Since the MI of the whole system is not unique and depends on the MI of the operator, a dynamic controller is required for maintaining the acceleration level according to the criteria. For this purpose, the controller needs to get feedback from the system in order to change the input signal of the exciter; this feedback is provided by the first accelerometer inside the handle (Figure 3-19).

In this research, a LDS $LASER_{USB}$ Shaker Control System controlled the input signal of the shaker. This controller has hardware to get feedback from eight different channels with built-in digital signal processor with anti-alias filtering; in addition, it includes a Windows-based application for the user to define the system parameters and monitor the system during the operation. This controller needs to know the property of the shaker, channels and control parameters. With random profile setup in the software, the user can define the acceleration spectra and the acceptable tolerance ranges at the desired frequencies.

3.3 Data acquisition system

The measurement system for the hand-arm vibration tests includes data acquisition hardware for measuring all the vibrations and forces. Coupling and synchronizing these data is critical for further calculation and processing. Therefore, it is reasonable to use one data acquisition capturing device for digitizing all data.

3.3.1 NI cDAQ-9178

The National Instruments cDAQ-9178 is an interface chassis with eight separate slots for input and output modules. There are different modules available for capturing data from a variety of sensors including accelerometers and strain gauges. It has its own power supply and connects with a PC through a USB port. The chassis is designed to be portable; therefore, it is suitable for both lab and field tests. The driver of the device supports many software interfaces including LabVIEW and MATLAB.

3.3.2 NI 9234

NI 9234 is an input module with four channels for the NI compact DAQ. It is suitable for capturing data from integrated electronic piezoelectric (IEPE) and non-IEPE sensors. Table 3.6 shows the properties of this module.

Table 3.6 – NI9234

Measuring Type	Accelerometer, Microphone
Signal Conditioning	Current excitation, Anti-aliasing filter
Channels	4
Resolution	24 bits
Sample Rate	Max 51.2 kilo Sample/second/channel
Bandwidth	23.04 kHz
Max Voltage	5 V
Maximum voltage range	-5 V, 5 V
Input Impedance	305 k Ohm
Dynamic Range	102 dB
Excitation Current	2 mA

3.3.3 NI 9237

NI 9237 is an input module with four channels for the NI compact DAQ. It can be used for capturing data from strain gauges. Table 3.7shows the properties of this module.

Table 3.7 – NI9237

Measuring Type	Strain / Bridge-based sensor
Signal Conditioning	Anti-aliasing filter Bridge completion Voltage excitation
Single-Ended Channels	0
Differential Channels	4
Resolution	24 bits
Sample Rate	51.2 kilo Sample/second/channel
Maximum voltage range Range Accuracy	 -25 mV / V ~ 25 mV / V 0.0375 mV / V
Excitation Voltage	2 V, 2.5 V, 3.3 V, 5 V, 10 V

Figure 3-29 shows the circuit for this module. The solid lines in this figure show the circuit for the half-bridge mode and the dot-lines show the extra circuit for the full-bridge mode.

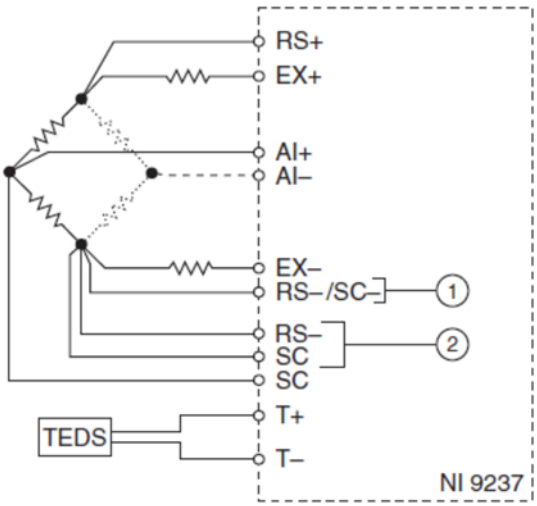

Figure 3-29 - Half bridge circuit

3.3.4 NI 9263

NI 9263 is an output module with four channels for generating analogue output signals. Table 3.8 shows the property of this module.

Table 3.8 – NI9263

Measuring Type	Voltage
Channels	4
Resolution	16 bits
Update Rate	100 kilo Sample/second
Bandwidth	23.04 kHz
Max Voltage	10 V
Maximum voltage range	-10 V, 10 V
Input Impedance	305 k Ohm
Current Drive Single	1 mA
Current Drive All	4 mA

3.4 MATLAB code for vibration measurement

The data acquisition system - NI cDAQ-9178 – can link with a PC through a USB cable and has its own driver for MATLAB. The data acquisition system can communicate with MATLAB directly by very simple commands. The code just

needs to initialize the system and defines the sample rate and sampling duration as follow:

```
v= daq.getVendors();
s= daq.createSession (v.ID);
d= daq.getDevices();
s.Rate = Sampling_Rate;
s.DurationInSeconds=Sampling_Time;
```

Each of the input/output channels should be defined with MATLAB individually. For each channel due to the type of channel, the appropriate properties of the channel are also required. For instance, for adding channels for capturing acceleration, the sensitivity of the sensor is required:

```
[~,idx] = s.addAnalogInputChannel(d(1).ID, 'ai0', 'Accelerometer');
s.Channels(idx).Sensitivity = Sensitivity;
```

and for the strain gauge, the type of the circuit and the nominal bridge resistance is required:

```
[~,idx] = s.addAnalogInputChannel(d(2).ID, 'ai0', 'Bridge');
s.Channels(idx).BridgeMode = 'Half';
s.Channels(idx).NominalBridgeResistance = Bridge_Resistance;
```

After defining all of the channels, the system is ready to capture data; the code should then wait until the end of the capturing time. The session should then be released and data acquisition system will then be ready for the next operation.

```
[data] = s.startForeground();
 while s.IsRunning
    % wait during capturing
end
```

```
s.release;
```

It is possible to obtain access to the measured data during the capturing time. By adding a *listener function* to this code, MATLAB calls the *listener function* whenever a package of data is ready. This method can be used for monitoring purposes during the data acquisition process. For instance, during hand-arm vibration tests, the feeding and gripping force should be monitored for the operator; therefore, by adding the *listener function* for MATLAB, the captured data from the strain gauges can be processed and used for monitoring the applied forces. The code for utilizing this option is as follows:

```
Listener_Handle = s.addlistener('DataAvailable', @Plot_Data);
```

3.4.1 Data Acquisition Toolbox (DAT)

Although the procedure of capturing data seems to be very simple, for capturing data from several channels, it is more appropriate to use a more comprehensive code. For this purpose, a toolbox was developed for this study. This Data Acquisition Toolbox (DAT) utilizes a GUI to develop user friendly software and facilitate the whole procedure of hand-arm vibration measurement tests. Figure 3-30 shows the flow chart that was used for developing the toolbox.

DAT is a MATLAB utility and has GUI interface. Figure 3-31 shows three screen shots of this Toolbox, which shows the main, channel property and chart property windows. The main window consists of two main lists for showing the input/output channels and charts. With this toolbox, the user can easily define different lists for input/output channels and plotting charts and save them; then depending on the type of the test, the user can load the relevant lists.

Below these lists, there is a setting section for capturing data, which includes information for sample rate, sampling time and some information about the test and operator. This utility has options to automatically save the data after each test; the saved data includes list of all channels, list of all of charts, setting for capturing data and time and date of test

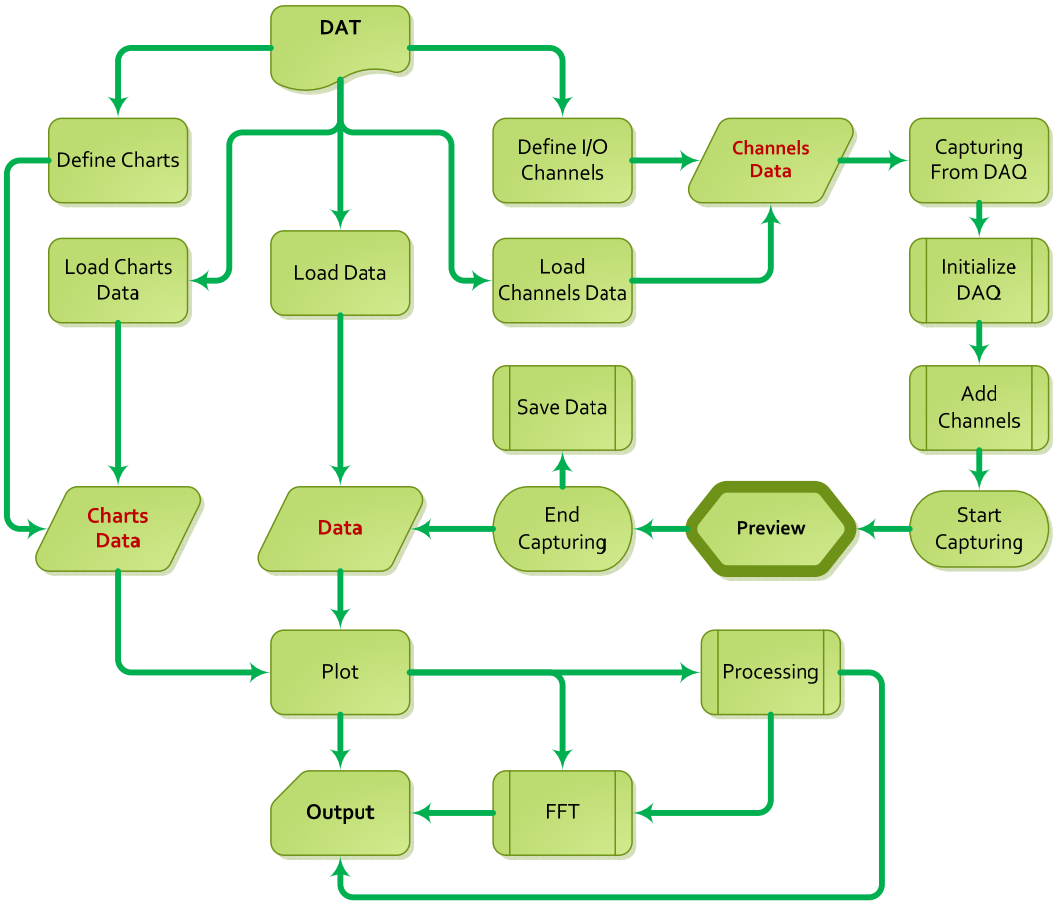

Figure 3-30– Flow chart for DAT

.

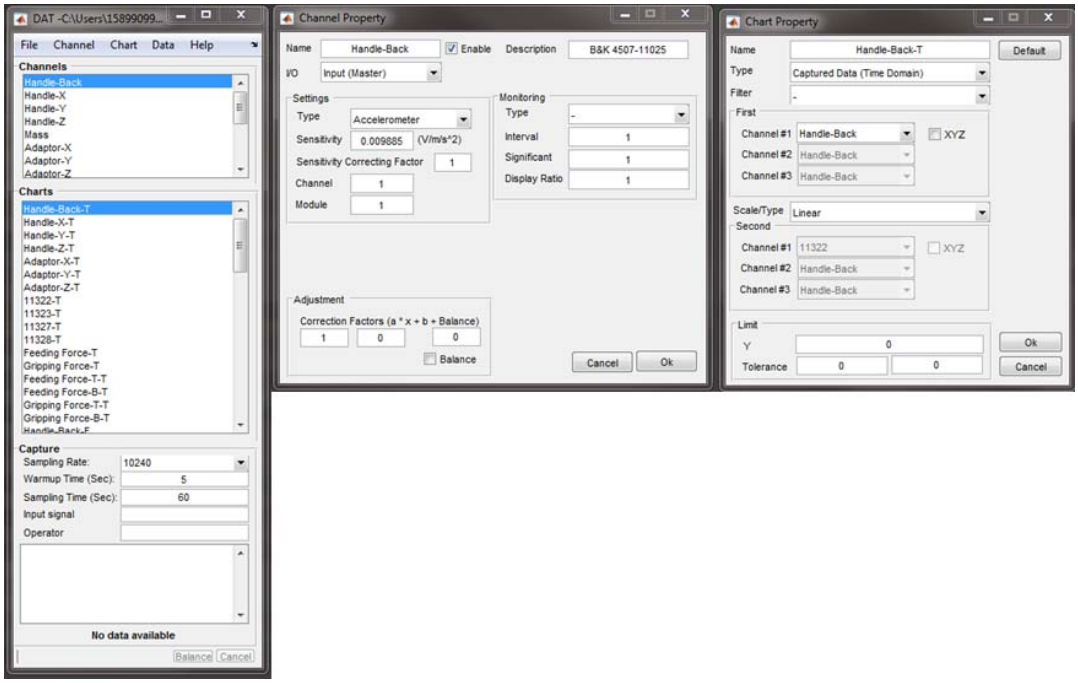

Figure 3-31– Screen shots of different windows of DAT

3.4.2 Input/output Channels

With the Channel Property window, both input and output channels can be defined. There is only one type of output channel in this toolbox, which is Voltage; however, there are several options for each type of input channel in this code, which includes:

- Accelerometer
- Voltage
- Thermocouple
- Current
- RTD
- Bridge
- Microphone
- IEPE

For each of these input/output channels the location of the channel of the module and location of the module on the chassis should be defined. In addition, depending on

the type of channel, the relevant property is also required. For the output channels, there are several options for the type of output waves which includes:

- Sine wave with multiple frequencies
- Saw-tooth wave with multiple frequencies
- Square wave with multiple frequencies
- Sine Sweep wave
- Random Noise with lower and upper frequency limit
- Random noise with spectra according to ISO 10819:2013 [21]
- Random noise with spectra according to ISO 13753:2008 [113]

In addition, for monitoring purposes, there are several options for input channels which includes:

- Graphical
- Digital
- Handle Force Indicator [6]

3.4.3 Plotting Charts

This toolbox includes several options for plotting charts. It can plot the raw data in the time domain or convert the data from the time into the frequency domain and then plot the spectra. For converting the data from the time domain into the frequency domain, the data can be divided into several sections, and then by using window averaging, the average amplitude or power spectra in the frequency domain can be calculated. This toolbox uses the Hanning function for windowing. These windows can also have overlaps to increase the number of frequency averages.

[6] Graphically shows the value and alignment of feeding and gripping forces

In addition, various processes can be applied to the raw data and then graphed. For instance, the strain from the strain gauges can be converted to the relative force and the resultant force can be plotted in either time or frequency domain. For the time and frequency domains this toolbox has the following options:

- Acceleration
- Strain
- Feed force (from strain)
- Gripping force (from strain)

For the frequency domain, the toolbox also has the following options:

- Transmissibility (from one accelerometer to second accelerometers)
- Glove Transmissibility (by dividing the mechanical impedance of the material by summation of mechanical impedance of the material and hand-arm system according to ISO 13753 [113])
- Power Spectra Density
- Coherence
- FRF
- System Impedance (by using force and acceleration data)
- Material Impedance (by using vibration transmissibility of the material according ISO 13753 [113])

3.5 Summary

For implementing HAV tests, a cylindrical shaped handle was designed and manufactured. The first natural frequency of the handle was above $1400Hz$. It consists of two hallow half-cylindrical shape made of Aluminium. These two parts were mounted on a base made of steel. Two thin flat plates were added on the top and bottom of each half-cylindrical part. These plates can bend due to applied forces. For measuring feeding and gripping force, four sets of active-active strain gauges

were mounted on these flat plates. The strain gauges were carefully calibrated with static loads in order to measure the total applied force and alignment of the force.

Inside the handle, there is space for mounting three accelerometers, one for vibration controller and two for measuring accelerations at front and back side of the handle. All of the accelerometers were calibrated with a reference accelerometer.

A comprehensive data acquisition toolbox was developed in MATLAB with a GUI interface with capability of capturing and monitoring data. In addition, it was equipped with post processor capability for calculating and plotting different charts such as frequency spectra, transmissibility and etc.

4 Material Vibration Transmissibility

Holding and working with power tools will lead to the transfer of vibration from the handle of the machine to the hand and arm of the worker. One practical way to reduce this vibration transmissibility (VT) is by using anti-vibration gloves. These gloves have damping-material as cushioning material. The VT, size and orientation of damping-materials inside these gloves can effect of the performance of them; therefore, identifying the VT behaviour of damping-materials is a key factor for designing and manufacturing more effective anti-vibration gloves.

4.1 Experimental Setup

For measuring VT of a damping-material ISO 13753 [113] defines a practical procedure. Figure 4-1 shows the setup for this measurement. In this test, the sample shall be flat and circular with 90mm diameter with constant thickness. The material shall be placed on a flat surface mounted to an exciter. A mass by weight of $2.5kg$ with flat surface and $90mm$ diameter shall be placed on top of the sample to simulate the force.

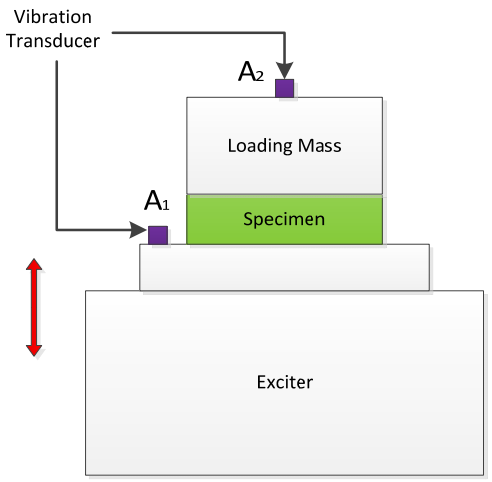

Figure 4-1 - Measurement setup (ISO 13753-2008)

Either random noise or sinusoidal excitation is usable for this test over the frequency range from $10Hz$ to $500Hz$. With random noise, the vibration amplitude shall be 0.025 $(m/s^2)^2/Hz$ with maximum 10% tolerance. For sinusoidal excitation, the magnitude shall be at least 1 m/s^2. Two accelerometers should measure the vibration behaviour of the bottom and top of the sample respectively. The ratio of these two accelerations in the frequency domain defines the VT of the sample and shows how much vibration is transmitted from the shaker to the top mass through the material. The VT result from this test can be used to calculate the Mechanical Impedance (MI) of the sample. Since the vibration impedance of the material can be defined as the ratio of force over velocity,

$$Z_M = \frac{F}{V}, \qquad \text{Eq. 4-1}$$

where Z_M is the MI of the sample, F is the force that was applied to the sample and V is the measured velocity. By assuming the material has a negligible mass and rearranging the equation,

$$m\ddot{x_2} = -Z_M(\dot{x_2} - \dot{x_1}), \qquad \text{Eq. 4-2}$$

where m is the mass of the weight on top of the sample, $\ddot{x}_2$ is the acceleration at the top of the sample and $\dot{x}_2$ and $\dot{x}_1$ are the velocity of the top and bottom of the sample respectively. By assuming harmonic excitation at the frequency ω, the response can be written as,

$$x(t) = Xe^{j\omega t}, \qquad \text{Eq. 4-3}$$

where j is square root of minus one and ω is angular frequency. The velocity can be defined as,

$$\dot{x} = \frac{\ddot{x}}{j\omega} \ . \qquad \text{Eq. 4-4}$$

By substituting this into Eq. 4-2, the MI can be found to be,

$$Z_M = \frac{j\omega m}{\frac{\dot{x}_1}{\dot{x}_2} - 1} \ . \qquad \text{Eq. 4-5}$$

Since,

$$\frac{\dot{x}_1}{\dot{x}_2} = \frac{\frac{\ddot{x}_1}{j\omega}}{\frac{\ddot{x}_2}{j\omega}} = \frac{A_1}{A_2} = \frac{1}{T} \ , \qquad \text{Eq. 4-6}$$

where T is the vibration transmissibility of the sample and by substituting this in Eq. 4-5,

$$Z_M = \frac{j\omega m}{\frac{1}{T} - 1} \ . \qquad \text{Eq. 4-7}$$

This equation defines how the MI of the sample can be calculated by using VT data. Furthermore, this result can be used for estimating the VT of the glove, which uses this material as cushion. For this glove,

$$Z_H \dot{x}_2 = -Z_M(\dot{x}_2 - \dot{x}_1) \ , \qquad \text{Eq. 4-8}$$

where Z_H is MI of hand-arm. By rearranging the equation, the following is found,

$$Glove\ Transmissibility = \frac{\dot{x}_2}{\dot{x}_1} = \frac{Z_M}{Z_H + Z_M} \ . \qquad \text{Eq. 4-9}$$

This equation estimates the VT of the glove by using the MI of the material and hand-arm system.

4.2 Experimental Test

This study investigates the dynamic behaviour and VT of three damping-materials for estimating their effectiveness in reducing the vibration transmission for operators

of power tools. Table 4.1 shows the properties of these materials. For measuring VT of these samples, this study follows the ISO 13753 [113] procedure. Figure 4-2 shows the setup for this test. In the setup two Brüel & Kjær 4507B accelerometers connected with a NI DAQ system measure the vibration accelerations of the top and bottom of the sample while the third accelerometer is connected with the LDS LASER$_{USB}$ Vibration Control System to control the vibration level according to the ISO criteria.

Table 4.1 - Sample properties

Sample Number	Name	Thickness (mm)	Density (kg/m^3)
1	D3O-A	6	915
2	D3O-B	4	435
3	GT6R	6	1050

Figure 4-2 - ISO 13753 Measurement Setup

Initially these samples were cut in circular shape with 90mm diameter according to standard specifications. With MATLAB code, the accelerations of the top and bottom of the sample were measured with sampling rate of 10240 sample per second

for a duration of 60 seconds. For converting the data from the time domain into the frequency domain, an FFT with a window length of 2048 was used.

The ratio of the two accelerations at the top and bottom of the sample in the frequency domain shows the VT of the sample. Figure 4-3 shows the magnitude and phase of VT for the whole disk of these three samples. Since the frequency range for the vibration excitation for these tests is from $10Hz$ to $500Hz$, the VT is also plotted for the same frequency range. This figure shows that both magnitude and phase of VT for all these samples are a function of frequency.

The VT spectra for all of these samples show one peak in the frequency range of the test. For the first sample, the frequency of the peak is about $200Hz$ and after that, the VT drops; however for the frequencies below $350Hz$, the VT is still above one and at $500Hz$, the VT becomes about 0.47.

For the second sample, the frequency of the peak is $155Hz$ and the VT drops after the peak. The VT for this sample at $265Hz$ goes below one and at $500Hz$ is about 0.24.

For the third sample, the frequency of the peak is $330Hz$ and the VT at $500Hz$ is one. For all of these samples the VT in the lower frequencies is above one and they do not show proper vibration attenuation in this test.

Eq. 4-7 calculates the MI of the samples by using the measured VT result. Figure 4-4 shows the resultant magnitude and phase of the MI of these samples. This figure shows that for all of these samples both magnitude and phase of MI are functions of frequency. For the gloves that use these materials as cushioning, Eq. 4-9 estimates the VT of the glove by using the MI data of the materials and the hand-arm MI.

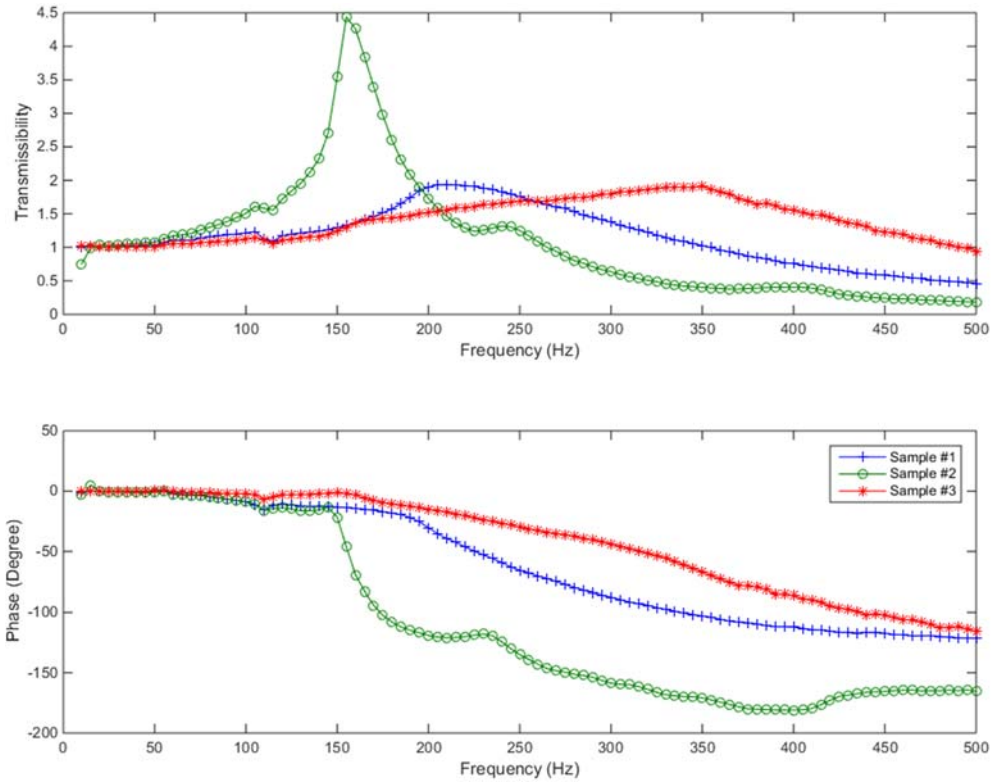

Figure 4-3 - VT (Whole disk)

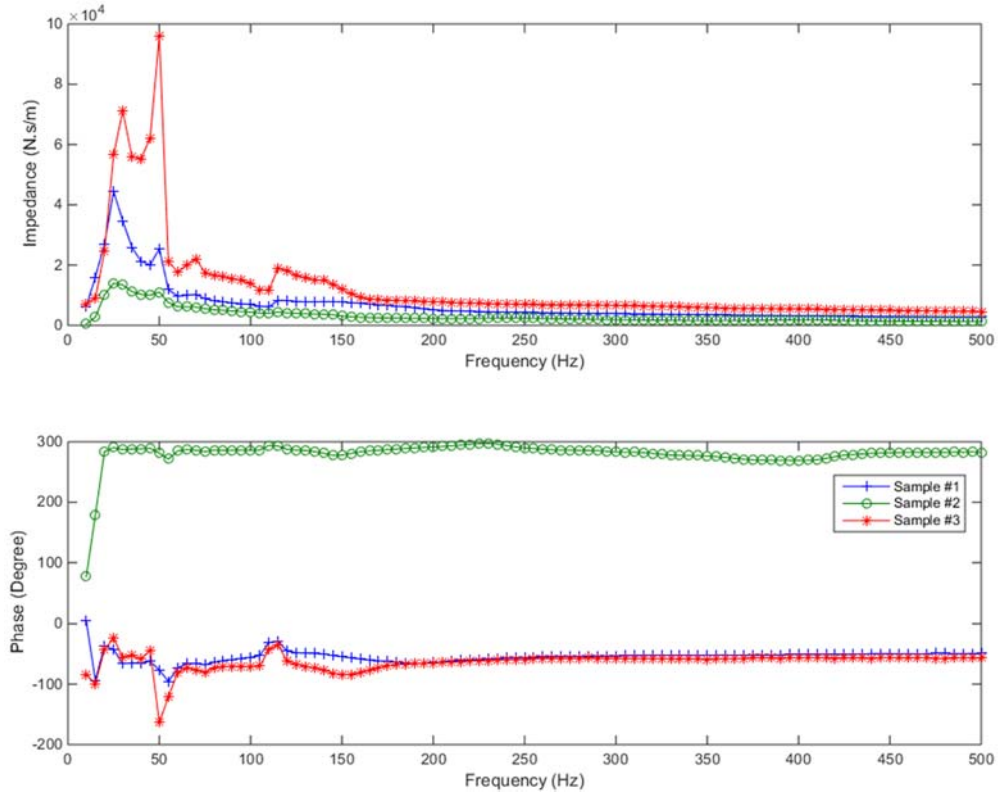

Figure 4-4 - Material Impedance (Whole disk)

For evaluating gloves as having anti-vibration properties, the mean VT across two frequency bands, being the medium band ($25Hz$ to $200Hz$) and the high frequency band ($200Hz$ to $1250Hz$), should be calculated and these values should be less than 0.9 for medium range and less than 0.6 for the high band according to ISO 10819 [21]. Table 4.2 shows the result for mean VT from these measured samples. As the result shows, ISO 13753 estimates that none of these three samples would have proper vibration attenuation if they been used inside the glove as cushioning material as tested. In the result, the estimation of ISO 13753 is that the gloves embedded with any of these materials will not be evaluated as anti-vibration gloves.

ISO 13753 is only concerned about VT of a specific size of the sample. In order to investigate the effect of size of the sample on VT and MI, instead of using one circular disk of each sample with $90mm$ diameter, a number of rectangular parts of the sample of size of $8mm$ by $8mm$ were used. The area of each of these rectangular parts is about 1% of the area of the whole disk. In separate tests, different numbers of these parts were tested to simulate different amount of coverage areas from three to fifty percent of the total area. Figure 4-5 shows the initial orientation for these tests. Since the orientation of these rectangular parts may affect the VT result, for each area coverage test, the average of at least three different tests with different orientations was measured and calculated to be the VT for that area coverage.

Table 4.2 – Mean VT of gloves

Sample No.	Medium Band (25Hz ~ 200Hz)	High Band (200Hz ~ 500Hz)
1	0.99	0.96
2	0.99	0.99
3	1.00	0.97

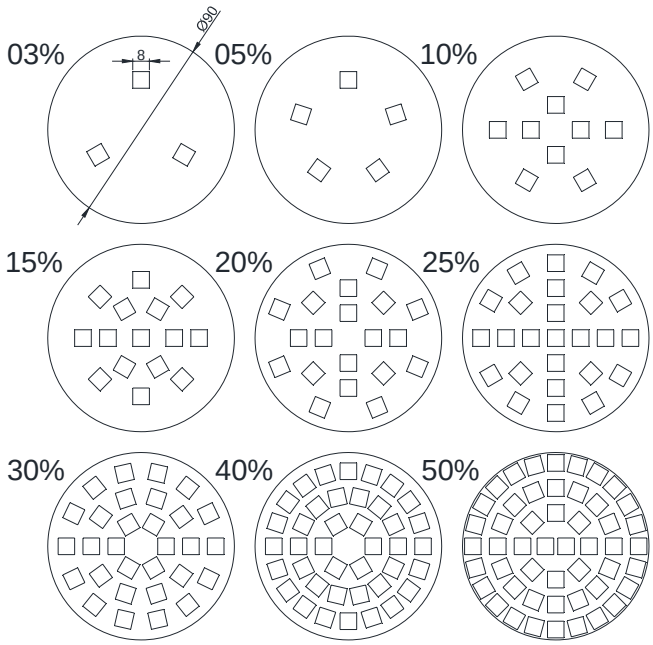

Figure 4-5 – Initial sample orientation

Figure A.4.1 to Figure A.4.3 in the Appendix show the magnitude and phase of VT for different area coverage of samples #1, #2 and #3 respectively. As these figures show, both magnitude and phase of VT are not only functions of frequency but they are also functions of coverage area and the corresponding amount of the sample.

Comparison between these results and the result from the circular disk shows the overall VT for the rectangular parts is significantly lower than the overall VT for the circular disk. These results show that all of these VT spectra have at least one resonance in the frequency range of the test. The frequency of the resonance of the rectangular parts is also lower than the resonance frequency for the circular disk. These trends show that the lower coverage area leads to lower resonance frequency in the VT spectra.

Figure A.4.4 to Figure A.4.6 in the Appendix shows the MI of these three samples for different coverage areas. These figures show that the magnitude of MI is also a function of coverage area and frequency; however, the phase of MI is only a function of frequency and not a function of coverage area. The sensitivity of MI phase to

frequency was found to be very low, in contrast to sensitivity of VT phase to the frequency. Similar to VT spectra, for all these three samples, it was found that by increasing the coverage area, the overall MI increases. These figures show that MI spectra of these samples has only one resonance in the frequency range of the test. Although the frequency of the resonance in MI spectra remains constant and does not change by variation of coverage area, the amplitude of MI increases by increasing the coverage area.

By dividing the result of MI by corresponding coverage area, the normalized MI per unit of area can be derived. Figure A.4.7 to Figure A.4.9 in the Appendix shows this normalized MI per unit of area of these three samples for different coverage areas. These figures show that for coverage area below 30%, the normalized MI is almost identical and it is independent of coverage area. For the rest of the coverage areas, the results are very close to the first region. This analysis illustrates that the MI spectra per unit of area shows a more practical result.

Subsequent analysis can consider the effect of using these samples inside gloves as cushioning materials where Eq. 4-9 can be used to estimate the VT of the resultant gloves. Figure 4-6 and Figure 4-7 show the mean VT of these gloves for both medium and high frequency band as a function of coverage area. Since in these tests, the vibration excitation frequency is limited to frequencies below $500Hz$, the mean VT for the high band cannot be calculated for frequencies above $500Hz$; therefore, instead of calculating the mean VT for frequencies between $200Hz$ to $1250Hz$ for the high band, these results were calculated for frequencies between $200Hz$ to $500Hz$. ISO 10819 defines a frequency weighting function for calculating the mean VT. In this function, the weight ratio for high frequencies compared to low frequencies is very low; therefore, since the level of VT of these samples decreases

with increasing frequency and the weight ratio for higher frequency for mean VT also decreases, ignoring the result of high frequency range in these tests is acceptable.

Although according to estimation of ISO 13753, none of these materials would have proper vibration attenuation inside the glove (Table 4.2); Figure 4-6 and Figure 4-7 show that when using smaller amounts of these samples as cushioning material inside the glove might lead to acceptable vibration attenuation. These figures show that with coverage area below 7% of the whole disk – with $90mm$ diameter - for the first sample, below 8% for the second sample and below 9% for the third sample, all of these materials should provide vibration attenuation according to ISO 10819 criteria. As a result, by proper design, the resultant glove could be evaluated as an anti-vibration glove.

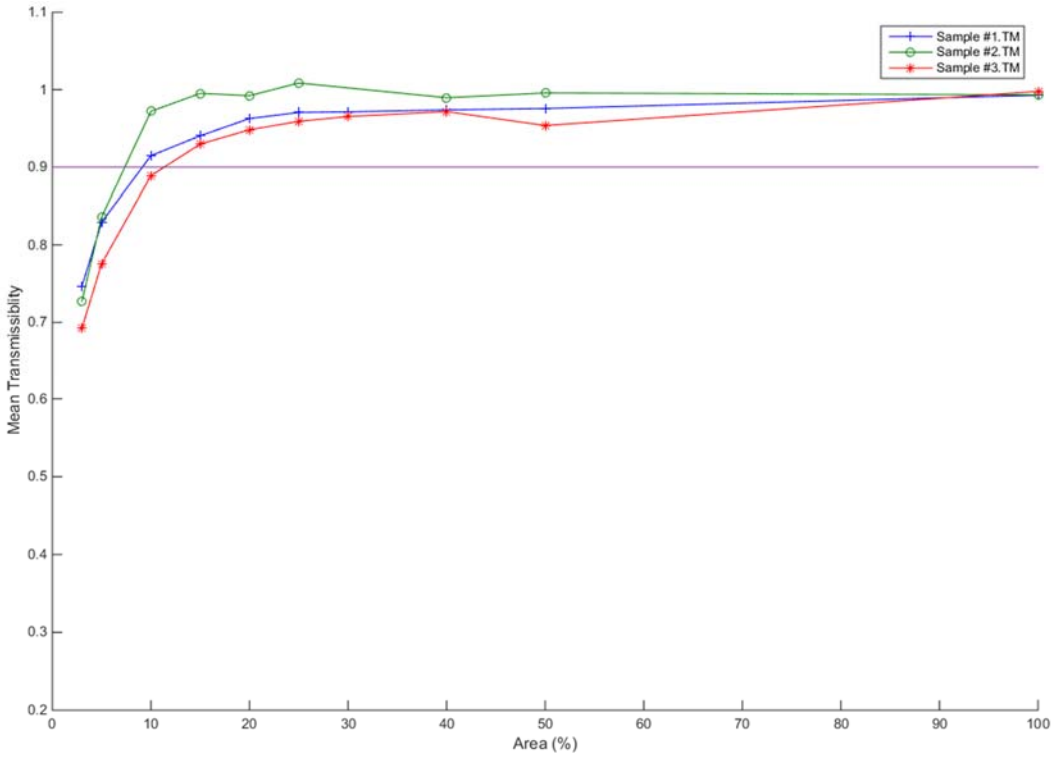

Figure 4-6 – Estimated Mean Vibration Transmissibility of Glove (Medium frequency)

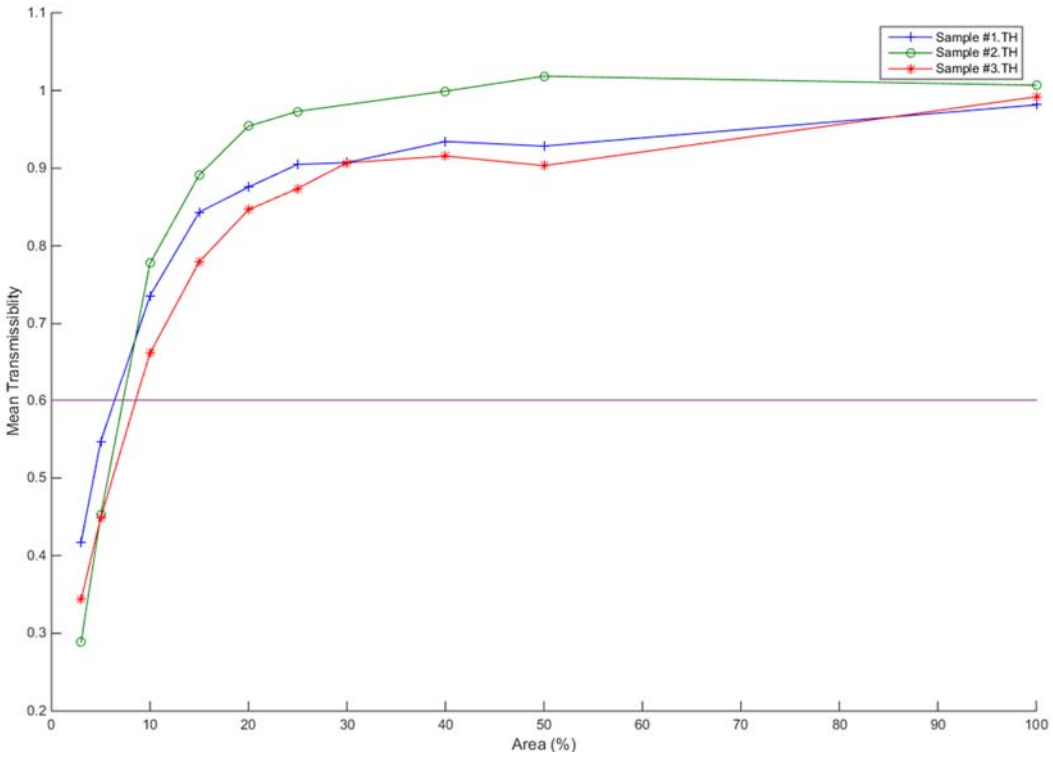

Figure 4-7 – Estimated Mean Vibration Transmissibility of Glove (High frequency)

4.3 Vibration Transmissibility Modelling

Lumped-mass models are useful for modelling vibration behaviour of materials. For this modelling, a block of material was assumed to consist of one, two or even multi separated masses which was attached together by springs and dampers (Figure 4-8). In vibration modelling, usually the vibration response of the system is of interest; however, in hand-arm vibration, the VT of the system is of interest. Modelling the vibration behaviour of different materials could help to understand the behaviour of the material and later the behaviour of the glove, which uses the same material for cushioning.

For each lumped-mass model a mathematical model can be developed and the resultant VT of the model can be calculated. This study assumes that a block of sample is placed on an exciter and a known mass is placed on top.

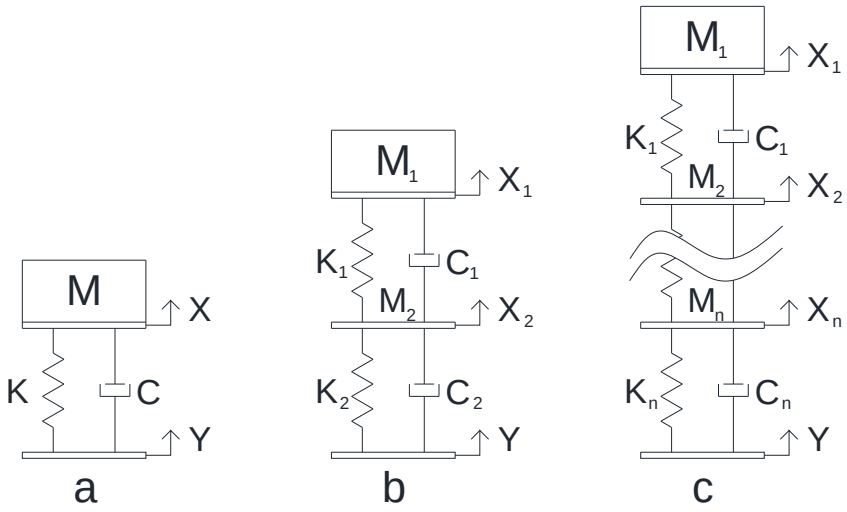

Figure 4-8 – Lumped mass models

4.3.1 One DOF Model of material

Figure 4-8.a shows a lumped-mass model with a single degree of freedom (DOF). In this model, the lower plate with displacement Y shows the lower part of the sample, which is in contact with the source of vibration. The upper plate with displacement of X, shows the upper part of the sample, which transfers the vibration to the top mass m. The mass of the sample is assumed to divide into two equal masses at the bottom and top of the sample. A string with stiffness k and damper with damping coefficient c is assumed to connect the lower plate and upper plate together. From the equation of motion,

$$m\ddot{x} + c(\dot{x} - \dot{y}) + k(x - y) = 0\,. \qquad \text{Eq. 4-10}$$

By assuming harmonic excitation and response,

$$y = Ye^{j\omega t}\,, \qquad \text{Eq. 4-11}$$

$$x = Xe^{(j\omega t+\varphi)}\,, \qquad \text{Eq. 4-12}$$

therefore,

$$\dot{y} = j\omega Ye^{j\omega t}\,, \qquad \text{Eq. 4-13}$$

$$\ddot{y} = -\omega^2 Y e^{j\omega t}\,, \qquad \text{Eq. 4-14}$$

$$\dot{x} = j\omega X e^{(j\omega t+\varphi)}\,, \qquad \text{Eq. 4-15}$$

$$\ddot{x} = -\omega^2 X e^{(j\omega t+\varphi)}\,. \qquad \text{Eq. 4-16}$$

By substituting Eq. 4-13 to Eq. 4-16 in Eq. 4-10,

$$k(X-Y) + i\omega c(X-Y) = \omega^2 mX\,. \qquad \text{Eq. 4-17}$$

The resulting transmissibility of the sample becomes,

$$T_{X/Y} = \frac{X}{Y} = \frac{k + j\omega c}{k + j\omega c - m\omega^2}\,. \qquad \text{Eq. 4-18}$$

4.3.2 Two DOF Model of material

Figure 4-8.b shows a 2-DOF model. In this model, there is one more DOF in the middle of the system compared with the 1-DOF model. Writing the equation of motion for each part of the model gives,

$$m_1\ddot{x_1} + c_1(\dot{x_1} - \dot{x_2}) + k_1(x_1 - x_2) = 0\,, \qquad \text{Eq. 4-19}$$

$$m_2\ddot{x_2} + c_2(\dot{x_2} - \dot{y}) + c_1(\dot{x_2} - \dot{x_1}) + k_2(x_2 - y) + k_1(x_2 - x_1) = 0\,, \qquad \text{Eq. 4-20}$$

where k_1 and k_2 are stiffness of the springs, c_1 and c_2 are damping coefficients of the dampers in the system. By assuming harmonic excitation and response,

$$y = Y e^{j\omega t}\,, \qquad \text{Eq. 4-21}$$

$$x_1 = X_1 e^{(j\omega t+\varphi_1)}\,, \qquad \text{Eq. 4-22}$$

$$x_2 = X_2 e^{(j\omega t+\varphi_2)}\,, \qquad \text{Eq. 4-23}$$

and substituting Eq. 4-21 to Eq. 4-23 into Eq. 4-19 and Eq. 4-20,

$$k_1(X_1 - X_2) + j\omega c_1(X_1 - X_2) = m_1\omega^2 X_1\,, \qquad \text{Eq. 4-24}$$

$$k_2(X_2 - Y) + k_1(X_2 - X_1) + j\omega c_2(X_2 - Y) + j\omega c_1(X_2 - X_1) = m_2\omega^2 X_2\,. \qquad \text{Eq. 4-25}$$

From Eq. 4-24,

$$T_{1/2} = \frac{X_1}{X_2} = \frac{k_1 + j\omega c_1}{k_1 + j\omega c_1 - m_1\omega^2}. \quad \text{Eq. 4-26}$$

By substituting in Eq. 4-25,

$$T_{2/Y} = \frac{X_2}{Y} = \frac{k_2 + j\omega c_2}{(k_1 + j\omega c_1)\left(1 - T_{1/2}\right) + k_2 + j\omega c_2 - m_2\omega^2}. \quad \text{Eq. 4-27}$$

Since,

$$\frac{X_1}{Y} = \frac{X_1}{X_2} * \frac{X_2}{Y}. \quad \text{Eq. 4-28}$$

The resulting transmissibility of the sample can be defined as,

$$\frac{X_1}{Y} = T_{1/2} * T_{2/Y}. \quad \text{Eq. 4-29}$$

4.3.3 Multi-DOF Model of material

Eq. 4-29 shows that the transmissibility of the whole system is the transmissibility of first part of the system multiplied by the transmissibility of the second part. By applying the same concept for a multi-DOF model, it can be easily shown that the resulting transmissibility can be defined as,

$$\frac{X_1}{Y} = T_{1/2} * T_{2/3} * \ldots * Tn_{/Y}. \quad \text{Eq. 4-30}$$

This shows that for finding the VT of a multi-DOF model, the VT of each part should be multiplied by the VT of the previous parts.

4.3.4 Lumped-mass modelling result for damping material

For generating lumped-mass models for a sample, the results from VT tests can be used. In this study by minimizing the difference between the measured VT and the simulated VT from the analytical model, the parameters for the model can be derived. Since for all these three samples, the VT is a function of coverage area, for

each sample and each coverage area an individual model was needed to be developed.

In lumped-mass models, for each DOF, three parameters are required. In this modelling, the assumption is that all parts of the model are in series and the mass of the sample is divided equally in each part of the model; except the top mass, where the mass of the loading mass should be added to it. Therefore, the mass of each part is assumed to be $1/n$ of the material mass; except m_1 which is assumed to be $1/n$ of the material mass plus the mass of the top weight. With the use of a Curve Fitting method, stiffness's and damping coefficients of the model can be found.

The simplest model is the 1-DOF lumped mass model, which consists of only one spring, one damper and one mass. In this model, both stiffness and damping coefficients are real numbers. Since this 1-DOF model is very simple, it cannot predict the vibration behaviour of these samples with acceptable accuracy. There are several ways for increasing the accuracy of these models:

- Increasing the DOF
- Having complex values for stiffness which consists of both real and imaginary parts
- Having complex values for damping coefficients which consists of both real and imaginary parts

In this study, different models with different DOF from one to three have been investigated to find the most appropriate model for these three samples. Table 4.3 shows the criteria for stiffness and damping coefficients in these models for each scenario.

Table 4.3 - Stiffness and damping coefficient criteria

Scenario	Stiffness		Damping coefficient	
	Real	Imaginary	Real	Imaginary
1	✓		✓	
2	✓	✓	✓	
3	✓	✓	✓	✓

Table 4.4 to Table 4.6 show the results of these simulations for samples #1, #2 and #3 respectively. In this simulation by reducing the least squares error, the parameters of the models were derived. The unusual high values in these tables show that the model could not converge for those cases. As these tables show, no single model was found which could be considered to provide an adequate best representation for all of the area coverage for all of the samples.

Table 4.4 – The least squares' error value for sample #1 models

DOF	Area	3%	5%	10%	15%	20%	25%	30%	40%	50%	100%
	Scenario	Least squares error									
1	1	1.4	0.2	0.4	0.2	1.1	1.5	4.0	6.2	16.6	6.0
1	2	0.3	0.1	0.3	0.5	0.3	0.6	0.8	1.5	6.5	6.7
1	3	0.3	0.1	0.1	0.5	0.2	0.2	0.5	0.9	4.3	5.1
2	1	1.4	0.2	0.4	0.2	1.1	1.5	4.0	6.2	16.7	6.1
2	2	0.3	0.1	0.3	0.5	0.3	0.6	0.8	1.5	6.5	6.5
2	3	0.7	0.4	0.3	0.7	0.3	0.2	0.3	0.8	3.3	7.6
3	1	2.0	0.2	0.6	0.6	0.5	1.1	0.8	2.0	8.6	3.1
3	2	0.3	0.1	0.3	0.3	0.4	0.6	1.5	2.3	8.4	4.3
3	3	5.1	0.3	1.6	1.3	1.9	2.3	1.1	0.8	1.3	9.8

Table 4.5 – The least squares' error value for sample #2 models

DOF	Area	3%	5%	10%	15%	20%	25%	30%	40%	50%	100%
	Scenario	Least squares error									
1	1	1.0	1.7	7.3	58.6	20.4	8.2	*[7]	32.3	74.1	19.0
1	2	1.7	1.1	4.0	59.7	10.0	4.2	*	20.4	55.0	9.6
1	3	1.6	1.6	3.5	51.0	11.5	1.9	*	12.8	41.8	4.1
2	1	9.4	1.2	2.2	54.7	26.7	7.7	*	51.3	105.5	34.4
2	2	1.7	1.1	4.1	59.8	10.1	4.2	*	20.5	55.1	9.8
2	3	3.8	2.2	1.8	17.4	11.8	3.3	*	24.6	61.5	12.7
3	1	1.0	1.2	6.4	67.5	12.1	2.3	*	17.9	46.3	23.3
3	2	2.5	1.7	3.4	58.1	7.7	3.8	*	22.2	55.0	30.5
3	3	3.1	2.2	2.5	51.1	9.8	1.0	*	9.5	26.3	43.7

Table 4.6 – The least squares' error value for sample #3 models

DOF	Area	3%	5%	10%	15%	20%	25%	30%	40%	50%	100%
	Scenario	Least squares error									
1	1	1.3	0.5	0.7	1.1	1.7	3.5	3.8	11.1	20.9	56.0
1	2	0.6	0.1	0.2	0.3	0.3	0.1	0.4	2.0	2.0	137.0
1	3	0.5	0.2	0.1	0.2	0.2	0.5	0.3	3.2	7.7	131.1
2	1	1.3	0.4	0.6	1.1	1.7	3.5	3.9	11.2	21.0	55.4
2	2	0.6	0.1	0.2	0.3	0.3	0.1	0.4	2.1	2.1	136.4
2	3	0.5	0.2	0.1	0.2	0.2	0.5	0.2	3.2	7.7	130.2
3	1	0.5	0.2	0.3	0.6	0.9	2.2	2.3	7.8	15.4	67.5
3	2	0.7	0.1	0.1	0.3	0.3	0.2	0.4	2.5	2.9	129.4
3	3	1.1	0.1	0.1	0.5	0.5	0.5	1.0	2.0	6.9	134.8

Furthermore, Figure A.4.14 and Figure A.4.15 in the Appendix also shows the same relationship for the third sample. Therefore, both real and imaginary parts of stiffness and damping coefficient for all of these samples can be defined as function of area.

Table 4.7 and Table 4.8 show values of stiffness and damping coefficient per unit of area for the first sample. Table 4.9 and Table 4.10 show the same results for second sample and Table 4.11 and Table 4.12 shows the results for the third sample.

[7] The coherence for the test was low, therefore the vibration transmissibility result was not acceptable.

Table 4.7 – Real and Imaginary coefficient for stiffness of models (sample #1)

DOF		1st Stiffness		2nd Stiffness		3rd Stiffness	
	Scenario	Real	Imaginary	Real	Imaginary	Real	Imaginary
1	1	5.95E+08					
1	2	5.97E+08	1.41E+08				
1	3	4.99E+08	1.39E+08				
2	1	5.94E+08		-1.17E+09			
2	2	5.96E+08	1.41E+08	-1.17E+09	0.00E+00		
2	3	5.42E+08	1.66E+08	-2.99E+09	-2.48E+04		
3	1	6.03E+08		-4.60E+09		4.56E+09	
3	2	5.87E+08	1.21E+08	-1.73E+09	4.22E+02	1.90E+09	3.76E+02
3	3	4.99E+08	1.38E+08	2.28E+06	1.41E+06	1.90E+09	4.73E+04

Table 4.8 - Real and Imaginary coefficient for damping coefficient of models (sample #1)

DOF		1st damping coefficient		2nd damping coefficient		3rd damping coefficient	
	Scenario	Real	Imaginary	Real	Imaginary	Real	Imaginary
1	1	4.22E+05					
1	2	2.06E+05					
1	3	2.09E+05	-1.54E+05				
2	1	4.21E+05		-2.32E+09			
2	2	2.06E+05		-2.32E+09			
2	3	1.69E+05	-9.07E+04	2.32E+07	-1.33E+07		
3	1	3.78E+05		-1.84E+10		1.87E+06	
3	2	2.30E+05		-6.23E+05		7.89E+05	
3	3	2.10E+05	-1.53E+05	4.90E+06	-5.14E+06	2.06E+06	1.00E+06

Table 4.9 - Real and Imaginary coefficient for stiffness of models (sample #2)

DOF		1st Stiffness		2nd Stiffness		3rd Stiffness	
	Scenario	Real	Imaginary	Real	Imaginary	Real	Imaginary
1	1	4.70E+08					
1	2	4.69E+08	1.12E+00				
1	3	5.12E+08	1.05E+08				
2	1	4.69E+08		-2.68E+09			
2	2	4.69E+08	1.12E+08	-2.69E+09	0.00E+00		
2	3	4.69E+08	1.12E+08	-2.68E+09	6.20E+03		
3	1	4.69E+08		-2.18E+09		2.20E+09	
3	2	4.68E+08	1.50E+08	-6.88E+08	-4.78E+01	6.97E+08	-2.47E+01
3	3	5.48E+08	1.44E+08	-6.88E+08	1.62E+02	6.97E+08	-7.04E+01

Table 4.10 - Real and Imaginary coefficient for damping coefficient of models (sample #2)

DOF		1st damping coefficient		2nd damping coefficient		3rd damping coefficient	
	Scenario	Real	Imaginary	Real	Imaginary	Real	Imaginary
1	1	2.17E+05					
1	2	-1.66E+04					
1	3	4.37E+02	7.77E+04				
2	1	1.95E+05		-7.24E+05			
2	2	-1.66E+04		-8.65E+09			
2	3	-1.59E+04	-1.27E+03	6.35E+05	5.72E+06		
3	1	1.95E+05		1.56E+06		6.29E+05	
3	2	-1.02E+05		-5.77E+04		5.85E+04	
3	3	-9.81E+04	1.58E+05	-5.72E+04	1.06E+03	5.94E+04	2.29E+03

Table 4.11 - Real and Imaginary coefficient for stiffness of models (sample #3)

DOF		1st Stiffness		2nd Stiffness		3rd Stiffness	
	Scenario	Real	Imaginary	Real	Imaginary	Real	Imaginary
1	1	4.51E+08					
1	2	4.53E+08	1.54E+08				
1	3	3.75E+08	1.50E+08				
2	1	4.51E+08		-3.46E+09			
2	2	4.52E+08	1.53E+08	-3.46E+09	0.00E+00		
2	3	3.74E+08	1.50E+08	4.05E+06	-8.56E+04		
3	1	4.55E+08		1.68E+08		0.00E+00	
3	2	4.61E+08	1.45E+08	-1.65E+09	3.27E+08	2.18E+09	1.20E+07
3	3	3.74E+08	1.50E+08	1.08E+07	2.13E+06	2.18E+09	1.56E+05

Table 4.12 - Real and Imaginary coefficient for damping coefficient of models (sample #3)

DOF		1st damping coefficient		2nd damping coefficient		3rd damping coefficient	
	Scenario	Real	Imaginary	Real	Imaginary	Real	Imaginary
1	1	3.42E+05					
1	2	6.85E+04					
1	3	7.34E+04	-1.43E+05				
2	1	3.41E+05		-1.17E+10			
2	2	6.84E+04		-1.17E+01			
2	3	7.32E+04	-1.43E+05	3.27E+05	4.00E+08		
3	1	2.93E+05		2.00E+07		-2.91E+12	
3	2	8.14E+04		-1.28E+10		8.17E+09	
3	3	7.32E+04	-1.42E+05	3.73E+07	-1.20E+08	4.56E+06	-7.21E+06

Figure A.4.16 to Figure A.4.25 in the Appendix show the resultant VT of these models with the measured data from coverage area 3% to 100%. In these figures, the continuous lines show the experimental VT of each sample. The dash-dot lines show the individual single degree of freedom for each sample and each area coverage. In these models, both stiffness and damping coefficient have both real and imaginary parts. The dash lines in these figures show the result of a single degree of freedom model of each sample, where both stiffness and damping coefficients of this model are linear functions of area.

Figure A.4.26 to Figure A.4.34 in the Appendix show the VT of sample #2 for different area coverage from 3% to 100%. Figure A.4.35 to Figure A.4.44 in the Appendix show the VT of sample #3 for different area coverage from 3% to 100%.

The results show that the mean VT of the gloves that use these samples as cushioning material can be estimated. Figure A.4.45 and Figure A.4.46 in the Appendix show the mean VT of the first material and the resultant mean VT from individual models for each coverage area and the resultant mean VT of the single model which is also a function of area. Figure A.4.47 and Figure A.4.48 in the Appendix show similar results for the second sample. Figure A.4.49 and Figure A.4.50 in the Appendix show the results for the third sample.

4.4 Apparent Young's Modulus and Loss Factor

Using apparent Young's modulus and loss factor is another method for modelling resilient material [128]. Young's modulus is the ratio of tensile stress over extensional strain,

$$E = \frac{\sigma}{\varepsilon}. \quad \text{Eq. 4-31}$$

The stress can be defined as,

$$\sigma = \frac{F}{A_o}, \quad \text{Eq. 4-32}$$

where F is the force and A_o is the initial area of the material and strain can be defined as,

$$\varepsilon = \frac{\Delta L}{L_o}, \quad \text{Eq. 4-33}$$

where ΔL is change in length and L_o is the initial length of material. Therefore, Young's modulus can be shown as,

$$E = \frac{FL_0}{A_0 \Delta L}. \quad \text{Eq. 4-34}$$

By assuming the material behaves as a single DOF model, extensional strain defines the difference in position between the top and bottom of the material,

$$E = \frac{m\ddot{x}_2 . L_o}{A_o(x_2 - x_1)}, \quad \text{Eq. 4-35}$$

where m is the mass of the top weight, $x_1$and x_2 are movements of the bottom and top of the sample. By rearranging,

$$m\ddot{x}_2 = \frac{A_o}{L_o} E(x_2 - x_1). \quad \text{Eq. 4-36}$$

For resilient material Young's modulus can have an imaginary part to show the loss factor in material,

$$E = E_a(1 + j\eta), \quad \text{Eq. 4-37}$$

where E_a is the apparent Young's modulus and η is the loss factor. By assuming harmonic excitation and response,

$$x(t) = Xe^{j\omega t}. \quad \text{Eq. 4-38}$$

By substituting Eq. 4-38 in Eq. 4-36,

$$m\ddot{x}_2 = \left(\frac{A_o}{h_o}\right) E_a(1 + j\eta)\left(\frac{\ddot{x}_2 - \ddot{x}_1}{-\omega^2}\right). \quad \text{Eq. 4-39}$$

By rearranging the transmissibility, it can be defined as,

$$\frac{\ddot{x}_2}{\ddot{x}_1} = \frac{E_a(1 + j\eta)}{E_a(1 + j\eta) + m\omega^2 h_o/A_o}. \quad \text{Eq. 4-40}$$

By defining P as,

$$P = \frac{m\omega^2 h_o}{A_o}, \quad \text{Eq. 4-41}$$

and substituting Eq. 4-41 in Eq. 4-40, gives,

$$\frac{\ddot{x}_2}{\ddot{x}_1} = \frac{E_a + jE_a\eta}{(E_a + P) + jE_a\eta}. \quad \text{Eq. 4-42}$$

By multiply $[(E_a + P) - jE_a\eta]$ on the numerator and denominator,

$$\frac{\ddot{x}_2}{\ddot{x}_1} = \frac{{E_a}^2 + E_aP + (E_a\eta)^2 + jPE_a\eta}{(E_a + P)^2 + (E_a\eta)^2}. \quad \text{Eq. 4-43}$$

Now by assuming that this transmissibility has both real and imaginary part,

$$I = \frac{PE_a\eta}{(E_a + P)^2 + (E_a\eta)^2}, \quad \text{Eq. 4-44}$$

$$R = \frac{{E_a}^2 + E_aP + (E_a\eta)^2}{(E_a + P)^2 + (E_a\eta)^2}. \quad \text{Eq. 4-45}$$

The ratio of these two parts is,

$$\frac{I}{R} = \frac{P\eta}{E_a(1+\eta^2)+P} \,. \qquad \text{Eq. 4-46}$$

Therefore the apparent Young's modulus can be defined as,

$$E_a = \frac{P(\eta R - I)}{I(1+\eta^2)} \,. \qquad \text{Eq. 4-47}$$

By rearranging,

$$E_a{}^2[(R-1)(1+\eta^2)] + E_a[P(2R-1)] + RP^2 = 0 \,. \qquad \text{Eq. 4-48}$$

By substituting Eq. 4-47 in Eq. 4-48,

$$\left(\frac{P(\eta R - I)}{I(1+\eta^2)}\right)^2[(R-1)(1+\eta^2)] + \frac{P(\eta R - I)}{I(1+\eta^2)}[P(2R-1)] + RP^2 = 0 \,. \qquad \text{Eq. 4-49}$$

By simplifying, the loss factor can be defined as,

$$\eta = \frac{-I}{R^2 + I^2 - R} \,. \qquad \text{Eq. 4-50 [128]}$$

Now by substituting Eq. 4-50 in Eq. 4-48,

$$E_a = \frac{-P(R^2 + I^2 - R)}{(R^2 + I^2 - 2R + 1)} \,. \qquad \text{Eq. 4-51}$$

By substituting Eq. 4-41 in Eq. 4-51, the apparent Young's modulus can be defined as,

$$E_a = -m\omega^2 \frac{h_o}{A_o} \frac{(R^2 + I^2 - R)}{(R-1)^2 + I^2} \,. \qquad \text{Eq. 4-52 [128]}$$

Eq. 4-50 and Eq. 4-52 show how the apparent Young's modulus and loss factor in this modelling can be defined as a function of the top mass, angular frequency, initial height, initial area and transmissibility data. Since the transmissibility of the resilient material is a function of frequency, the apparent Young' modulus and loss factor are also functions of frequency.

4.4.1 Young's Modulus and Loss Factor Result

The previous measured VT of samples can be used to derive the apparent Young's modulus and loss factor results. Figure A.4.51, Figure A.4.55 and Figure A.4.59 in the Appendix show the apparent Young's modulus for samples 1, 2 and 3 respectively and Figure A.4.53, Figure A.4.57 and Figure A.4.61 in the Appendix show the loss factor for these samples.

Figure A.4.51 shows that the apparent Young's modulus of the first sample is a function of both frequency and coverage area. By increasing the frequency, the apparent Young's modulus decreases. In addition, by increasing the coverage area the apparent Young's modulus decreases; however, Figure A.4.53 shows the Loss factor of the first sample is more sensitive to changing of frequency than changing of coverage area.

Figure A.4.55 shows that the apparent Young's modulus of the second sample is a function of both frequency and coverage area. For frequencies below $50Hz$, it is very sensitive to frequency; however, for frequencies above $50Hz$, the sensitivity decreases. By increasing the frequency, the apparent Young's modulus increases. Figure A.4.57 shows that the loss factor of the second sample has very low changes due to change of frequency or coverage area.

Figure A.4.59 shows that the apparent Young's modulus of the third sample is a function of both frequency and coverage area. Similar to the first sample, by increasing the frequency, it decreases and by increasing the coverage area, it increases. Figure A.4.61 shows that the loss factor for the third sample also has very similar behaviour to the loss factor of the first sample.

Figure A.4.52, Figure A.4.55 and Figure A.4.60 in the Appendix show the comparison between calculated apparent Young's modulus from material transmissibility tests and simulation using the 1-DOF model. As these figures shows the apparent Young's modulus of the models are only function of the frequency and not the coverage area.

Figure A.4.54, Figure A.4.58 and Figure A.4.62 in the Appendix show the comparison between calculated loss-factor from material transmissibility tests and simulation using the 1-DOF model. As these figures show, the loss-factor of the models are only function of the frequency and not the coverage area.

Figure A.4.63 in the Appendix shows that the resultant apparent Young's modulus of 1-DOF models has linear relationship with the frequency. Therefore, it can be derived from,

$$.E_{a_{S\#1}}(f) = -5{,}641\, f - 3{,}009{,}984\,, \qquad \text{Eq. 4-53}$$

$$.E_{a_{S\#2}}(f) = 1{,}894\, f - 2{,}039{,}386\,, \qquad \text{Eq. 4-54}$$

$$.E_{a_{S\#3}}(f) = -5{,}231\, f - 2{,}261{,}957, \qquad \text{Eq. 4-55}$$

where f is the frequency. Figure A.4.64 in the Appendix shows the resultant loss factor for the 1-DOF models. The loss factors of these models can be derived from,

$$\eta_{s\,\#1}(f) = (-1.4968e-6)f^2 - 0.00175\, f + 0.2889\,, \qquad \text{Eq. 4-56}$$

$$\eta_{s\#2}(f) = (3.2757e-7)\, f^2 - 0.00018\, f + 0.2057\,, \qquad \text{Eq. 4-57}$$

$$\eta_{s\#2}(f) = (-1.9309e-7)\, f^2 - 0.00021\, f + 0.4025\,. \qquad \text{Eq. 4-58}$$

4.5 Summary

Three damping material disks with $90mm$ diameter have been tested according to ISO 13753. Results of VT test for them show they cannot have proper vibration attenuation inside the glove. Future investigation shows that the VT of the glove was a function of coverage area of the damping material. By increasing the coverage area, the VT of the glove increases. When the whole contact area of the glove is covered with damping material, the VT of the glove became one.

Individual tests on different sizes of these samples show that the vibration behaviour of these samples for low coverage area (< 30%) can be modelled with 1-DOF lumped-mass having both stiffness and damping coefficients that are complex values.

Behaviour of the samples can also be shown by apparent Young's modulus and loss factor analysis. Results show that the apparent Young's modulus of these samples for high coverage area is a function of coverage area and frequency; while for the low coverage area it was only a function of frequency; however, the apparent Young's modulus derived from 1-DOF models, being only a function of frequency, did not alter by change of coverage area. The loss-factor of the material and 1-DOF models were also found to be functions of the frequency and were not very sensitive to coverage area.

5 Hand-Arm Vibration measurement

For HAV tests, the design handle in this study mounts directly to a LDS V455 exciter. A LDS Laser USB Vibration Control System controls and maintains the vibration level of the exciter according to the defined vibration level in the standard (Table 3.1). A National Instruments Compact DAQ system captures and digitizes all input data including accelerations and strains, and transfers them to the MATLAB workspace.

The Data Acquisition Toolbox (DAT) in MATLAB receives and saves the digitized data from 15 separate channels with 10,400 samples per second per channel for the duration of 60 seconds. In addition, DAT translates the measured strains into equivalent feed and grip forces, and monitors the value and direction of the applied forces for the operator during the test.

For measuring vibration at the palm of the hand, the standard [21] requests the use of a specific shape of a solid adaptor containing the accelerometer within the palm (Figure 2-9). For the bare hand test, this adaptor should be in contact with the vibrating handle and the palm of the hand, while for the glove test, it should be positioned inside the glove. For assessing the suitability and accuracy of the test rig for HAV tests, the VT from the handle to the adaptor while the adaptor is affixed to the handle with contact force $80\pm10N$ should be one with maximum 5% tolerance [21]. Figure 5-1 shows the result obtained from the handle developed for this test. This result indicates that the test rig was accurate and suitable for conducting the HAV test.

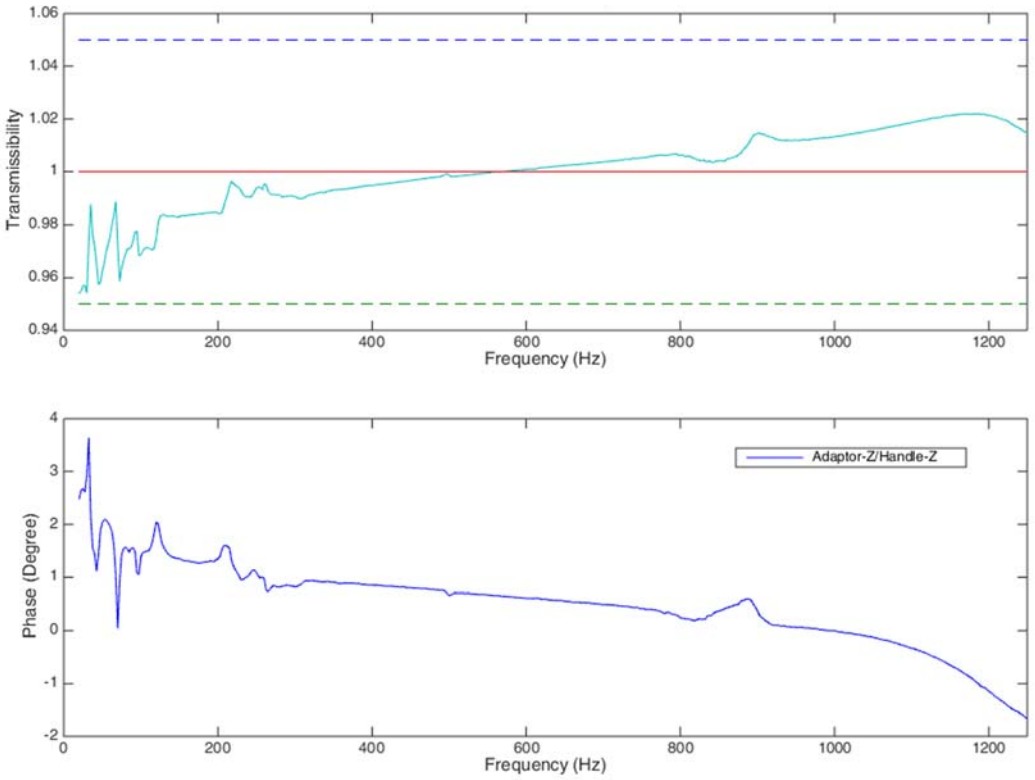

Figure 5-1 – VT from the handle to the adaptor

In this study, 10 male participants were involved in conducting the HAV tests. Table 6.1 shows some of the physical characteristics of the participants. For the first set of measurements, each of the participants held the handle with their bare hand and applied the defined push and grip forces while the handle was vibrating according to the standard vibration levels. The measured acceleration and force data from these tests can be used for calculating the mechanical impedance (MI). Since with this setup both acceleration and force data of the front and back sides of the handle can be measured simultaneously, the MIs at front and back side of the handle can be derived from a single test. By knowing the MIs of the front and back side of the handle, and MIs of the front and back side of the handle while the operator holds the handle, the MIs of the palm and fingers of the operator can be derived [41]. These results can be used for calculating biodynamic forces [91] or for generating analytical models of the HAS.

Table 5.1 – Participants body and hand characteristics

Operator No.	Height	Weight	Hand				Fingers	
			Length[8]	Breadth[9]	Circumference[10]	Volume[11]	Length[12]	Volume[13]
	m	kg	mm	mm	mm	ml	mm	ml
1	1.76	76	190	90	500	450	80	70
2	1.82	80	210	90	540	500	90	100
3	1.74	112	190	100	490	500	85	100
4	1.72	96	190	105	490	600	80	100
5	1.70	89	190	90	460	400	80	100
6	1.68	85	185	90	480	400	75	100
7	1.75	70	185	90	465	340	75	80
8	1.62	70	180	85	460	350	75	100
9	1.77	72	190	95	480	470	80	100
10	1.68	102	185	90	470	480	80	90
Min.	1.62	70	180	85	460	340	75	70
Max.	1.82	112	210	105	540	600	90	100
Average	1.72	85	190	93	484	449	80	94
Std. Deviation	0.06	14.5	8.0	5.9	24.0	78.8	4.7	10.7

5.1 Adapter vs. Strap

The proposed adaptor in the standard has an inner radius of 26 mm which is 6 mm larger than the outer radius of the proposed handle [21]. By assuming the anti-vibration gloves have about the same thickness, this difference in radius provides proper space for the glove to be in contact with both the handle and the adaptor;

[8] Tip of middle finger to crease at the wrist

[9] The width measured at metacarpal of the hand

[10] The circumference measured at metacarpal of the hand

[11] Water displaced by hand submerged to crease at the wrist

[12] Tip of middle finger to crease at the base of the finger

[13] Water displaced by fingers submerged to crease at the base of the middle finger

however, the solid shape of the adaptor may affect the orientation of the damping material inside the glove. It may seem that this adaptor design facilitates positioning and orienting the accelerometer at the palm side; however, it can have an effect on the VT measurement [25, 48].

In this study, with two different methods the VT at the palm has been investigated. In individual tests, either a plastic solid adaptor with an embedded tri-axial accelerometer or a thin flexible strap with three embedded miniature accelerometers has been used. Figure 5-2 compares positions of the accelerometers inside the strap with the position of the tri-axil accelerometer inside the adaptor.

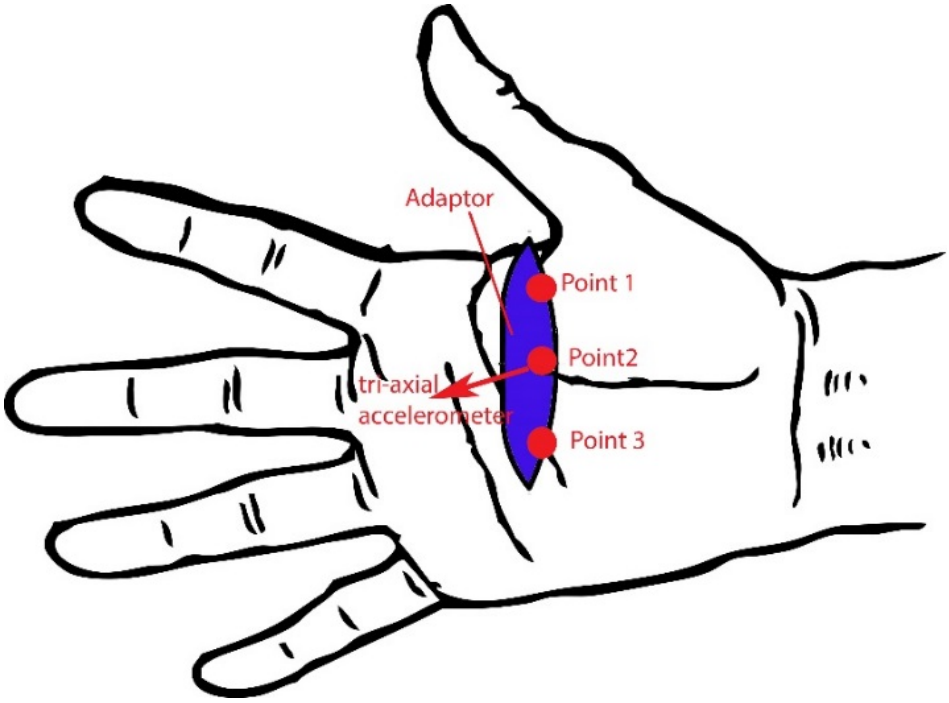

Figure 5-2 – Accelerometers location comparison (strap vs adaptor)

According to the standard, while the adaptor is affixed to the handle, if the accelerometer inside the adaptor shows the same acceleration as the accelerometer inside the handle shows, the test rig is accurate for the HAV tests [21]. Since the test adaptor in this study, has passed the accuracy criteria test (Figure 5-1), by comparing the result from the strap method with the adaptor method, while there is no damping

material between the accelerometer(s) at the palm side and the handle, the strap method can be evaluated.

With individual repeated tests by either the adaptor or the strap, the VT from the handle to the bare hand for each of the participants were measured. During these tests, the participants applied the defined push and grip force while the handle was vibrating.

Figure 5-3 compares the average[14] of the measured VT from the handle to the adaptor with the VT from the handle to either of the accelerometers in the strap for all participants in the frequency domain. The results show that for the frequencies between $125Hz$ and $1000Hz$, the top (A#1) and middle (A#2) accelerometers in the strap have the same vibration level as the accelerometer inside the handle. For frequencies above $1000Hz$, the accelerometer in the adaptor showed that the VT was measured to be 1.13 while the top (A#1), middle (A#2) and bottom (A#3) accelerometers in the strap gave the measured VT equal to 0.92, 1.08 and 1.14 respectively.

Since for frequencies below $1000Hz$, the VT of the adaptor is one, the higher VT for frequencies above $1000Hz$ cannot be due to miss-alignment of the adaptor. Therefore, it should be due to the effect of the hand-arm system on the VT. According to the standard [21], the adaptor has passed the accuracy test and the result of the middle (A#2) and bottom (A#3) accelerometers in the strap show less

[14] Figure A.5. 1 to Figure A.5. 10 in the Appendix compare the result of VT from the handle to the adaptor with the VT from the handle to either of the accelerometers on the strap for each of the participants in this study.

than 5% tolerance with the result from the adaptor; therefore, the results of these two accelerometers should also be correct for the frequencies above $1000Hz$.

Studies have shown that the hand-arm system has a few resonances at frequencies below $50Hz$ in the z-direction [84] and the result of all three accelerometers in the strap also showed high amplitude at these low frequencies; however, the accelerometer inside the adaptor does not show any resonance in this frequency region. The adaptor has a solid shape and in the bare hand test, it is in direct contact with the handle; therefore, it is more likely for the adaptor to show the vibration behaviour of the handle than the vibration of the palm of the hand. On the other hand, the strap is flexible and the accelerometers inside it can adapt them-self with the orientation and movement of the hand.

The bottom (A#3) accelerometer in the strap is in the middle of the palm. The surface curvature of the palm at this point is not parallel to the handle; therefore, the surface of the third accelerometer may also not be parallel to the handle. It seems that this part on the hand experiences lower levels of vibration for frequencies between $50Hz$ to $200Hz$ than the two other points.

The proposed length and width of the adaptor are 70 and $31mm$ [21] and the span's length of the adaptor should not be less than 70% of the width of the palm [40]. The adaptor covers most of the contact area in the z-direction at the palm side. Since it is solid, it can only provide a single vibration transmissibility measurement at the palm of the hand and sees the entire surface as one; therefore, it could be assumed that the measured vibration with the adaptor is the average of the vibration over the entire covered area. However the accelerometers in the strap can adapt their orientation with the orientation of the surface of the hand at their contact points and they can

adapt their movement with the movement of the surface of the palm at their contact points. As a result the measured vibration with the strap method can reveal more information about the vibration at different locations of the hand. Figure 5-4 compares the VT result from the adaptor and the average of all three accelerometers in the strap. The average vibration from the three accelerometers still shows high amplitude at low frequencies; therefore it still senses the resonances of the hand while for frequencies above $200Hz$, it has good agreement with the vibration level of the handle.

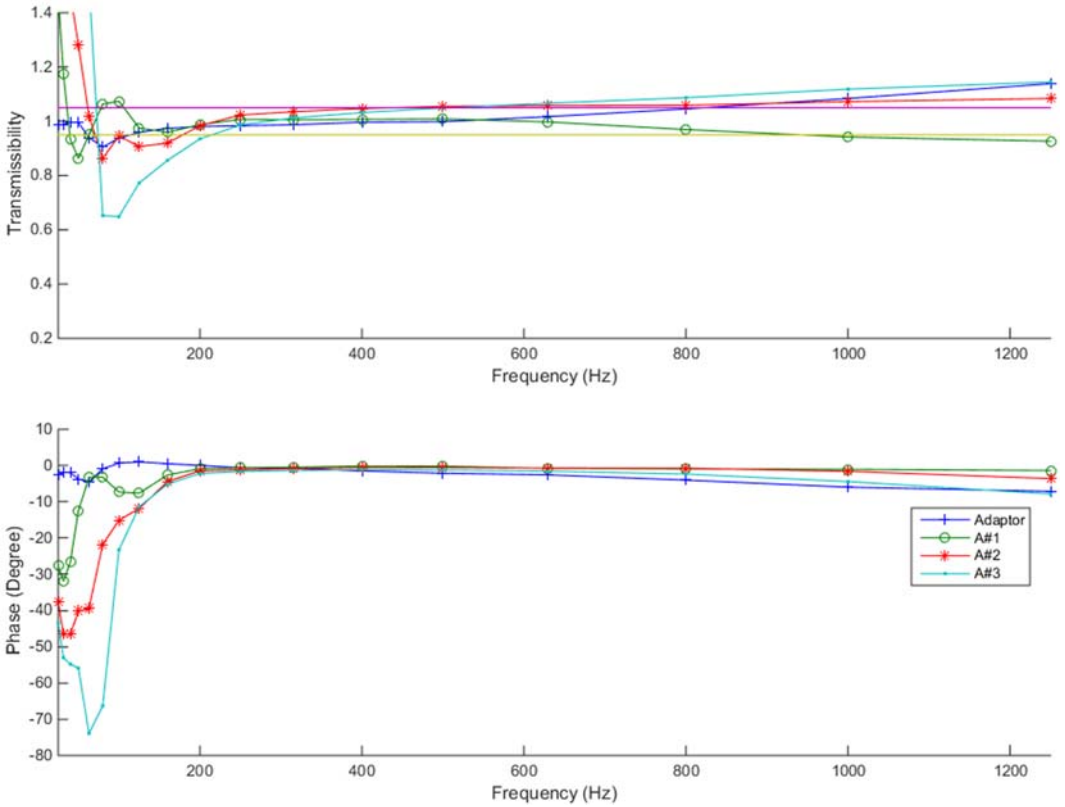

Figure 5-3 - Average VT to bare hand (Adaptor vs individual accelerometers on strap)

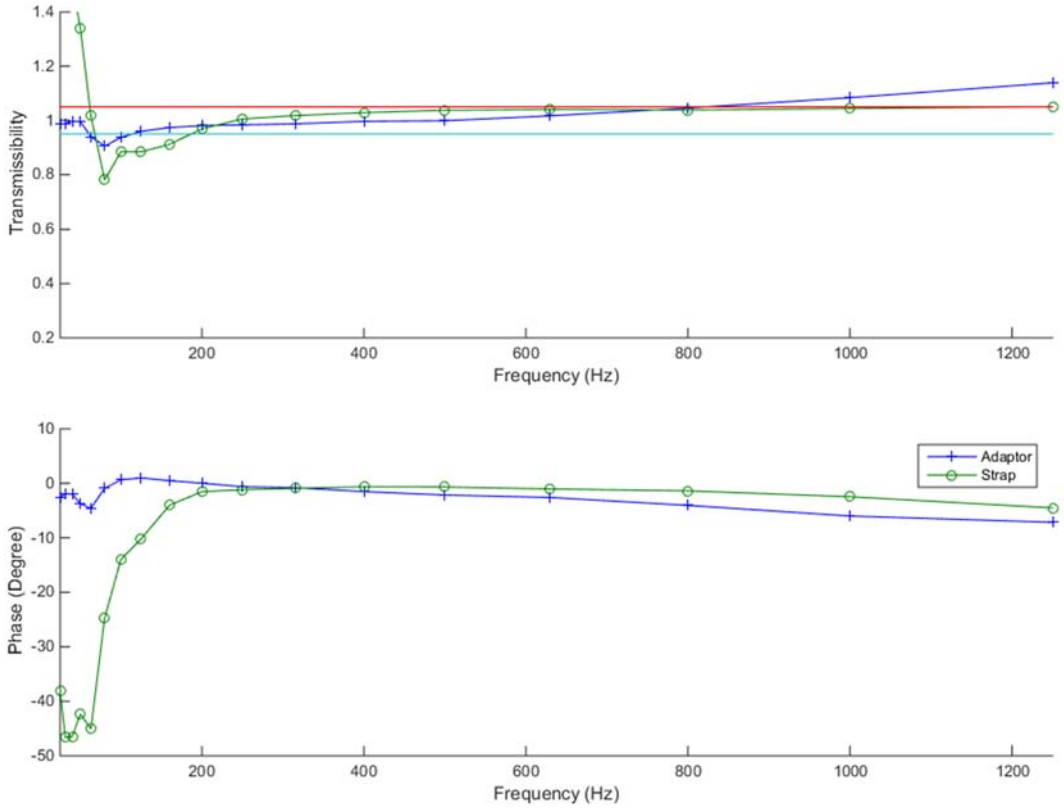

Figure 5-4 - Average VT to bare hand (Adaptor vs strap)

5.2 Glove Vibration Transmissibility

For evaluating a glove as an anti-vibration glove, the mean vibration transmissibility (MVT) of the glove for the medium[15] and high[16] frequency bands should not be above 0.9 and 0.6 respectively [21]. According to the standard the frequency weighted vibration transmissibility (FWVT) can be calculated from,

$$T = \frac{\sqrt{\sum_{i=i_L}^{i_u}[a_h(f_i)W_{hi}]^2}}{\sqrt{\sum_{i=i_L}^{i_u}[a_H(f_i)W_{hi}]^2}}\ , \qquad \text{Eq. 5-1 [21]}$$

[15] From 25 to 200Hz

[16] From 200 to 1250Hz

where $a_h(f_i)$ and $a_H(f_i)$ are the acceleration at the hand and at the handle respectively and W_{hi} is the weighting factor at frequency f_i. The MVT of the glove is the ratio of the FWVT of the glove test over the FWVT of the bare hand test. Since the adaptor is solid and it can only measure the average vibration of the hand, the standard requests the coverage of the entire area of the hand with damping material [21]; however, this could reduce the dexterity and comfort of the hand.

In this study, a commercial glove has been tested. The entire area of the palm side of this glove was not covered with the damping material; therefore, the standard does not evaluate it as anti-vibration glove. The hypothesis of this study was to compare the result of two different methods for measuring VT at the palm side and evaluating the measured VT at the palm side with the adaptor; therefore, this glove has been used for the glove test in this study.

In individual repeated tests while either the adaptor or the strap was inside the glove, the VT from the handle to the palm for each of the participants was measured. During these tests, the participants applied the defined push and grip forces while the handle was vibrating.

Figure 5-5 compares the average[17] of the measured VT in the glove tests with the adaptor and either of the accelerometers in the strap in the frequency domain. Since even without the glove, the VT from the handle to either the adaptor or the strap for all of the frequencies is not exactly one and properties of the hand-arm system effect on the VT, the actual VT of the glove should be the ratio of the VT from the glove test over the VT result measured from the bare hand test. Therefore, this figure

[17] Figure A.5. 11 to Figure A.5. 20 compare the result of the VT in the glove tests with the adaptor and the accelerometers in the strap for each of the participants in this study.

cannot show the actual VT of the glove. Figure 5-6 compares the average[18] of the actual VT of the glove with the adaptor and either of the accelerometers in the strap in the frequency domain of all participants. Each VT in this figure is derived from the ratio of the VT of the glove test over the VT of the bare hand test.

In the bare hand test, except at very low frequencies, all the accelerometers in the strap and the accelerometer in the adaptor have almost the same experience of vibration level; however, the result of the glove test reveals they have measured totally different levels of vibration.

The result from the adaptor shows that for frequencies below $50Hz$ and also for frequencies between $250Hz$ and $630Hz$, the glove increases the vibration level. For the frequency region of $400Hz$, the amplification of the glove is about 10%. For frequencies between $50Hz$ to $200Hz$, there is some vibration attenuation; however, in this frequency region the maximum vibration reduction which is at $80Hz$ is about 14%. In addition, for frequencies above $630Hz$, the VT decreases and it is about 0.44 at $1250Hz$. The accelerometer inside the adaptor does not sense the resonance of the HAS at low frequency ($< 50Hz$) in the bare hand test, and in the glove test it also shows amplification for the same frequency region; All the accelerometers in the strap sense the resonance of the HAS and in the results they all show that the glove has some vibration attenuation at this frequency region.

[18] Figure A.5. 21 to Figure A.5. 30 in the Appendix compare the result of VT of the glove with the adaptor and the accelerometers in the strap for each of the participants in this study.

In the glove tests, the top (A#1) accelerometer in the strap does not show any major change in the VT. For frequencies between 80Hz and 500Hz, the VT is almost one. After 500Hz, the VT increases slightly and at 1250Hz the VT becomes 1.07.

The middle (A#2) accelerometer in the strap for frequencies between 80 Hz and 160 Hz shows about 7% amplification in the VT and then for frequencies up to 500Hz it shows the VT is equal to one. For frequencies above 500Hz this accelerometer shows minor amplification of the VT.

The bottom (A#3) accelerometer in the strap shows amplification for frequencies between 80Hz and 160Hz with maximum of 10%. For frequencies above 200Hz it shows attenuation, and at 1250Hz it shows the VT is 0.64.

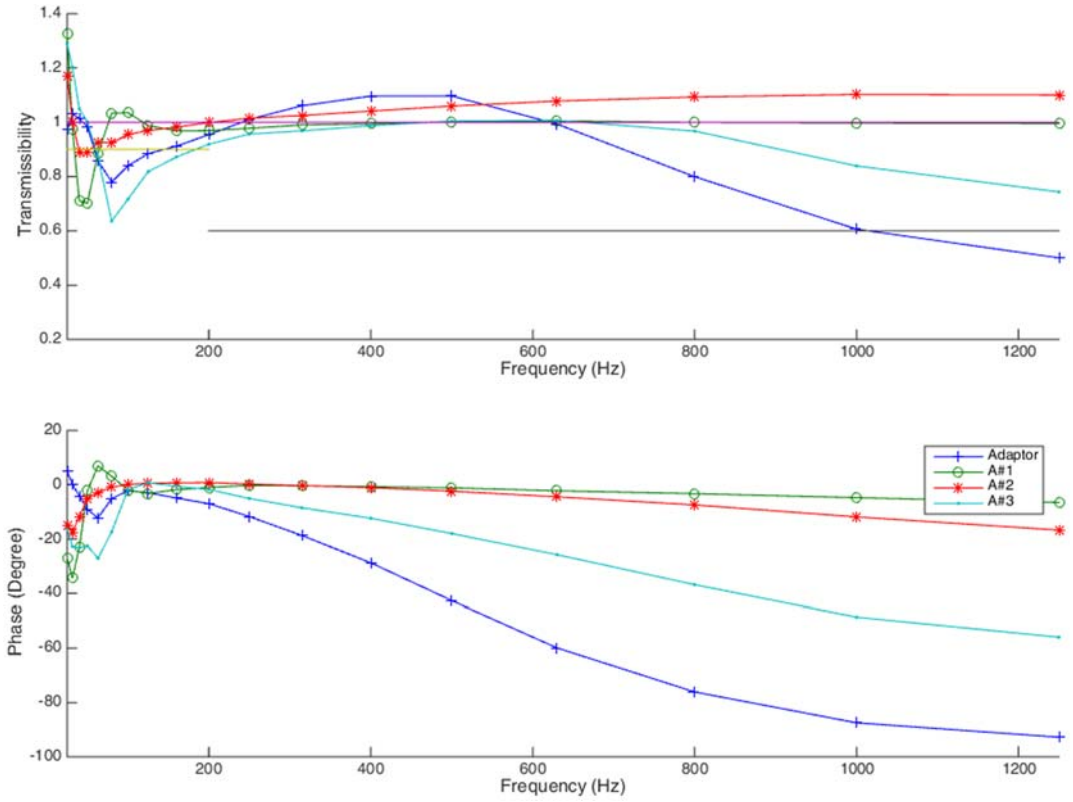

Figure 5-5 - Average measured VT from the glove tests (Adaptor vs individual accelerometers on strap)

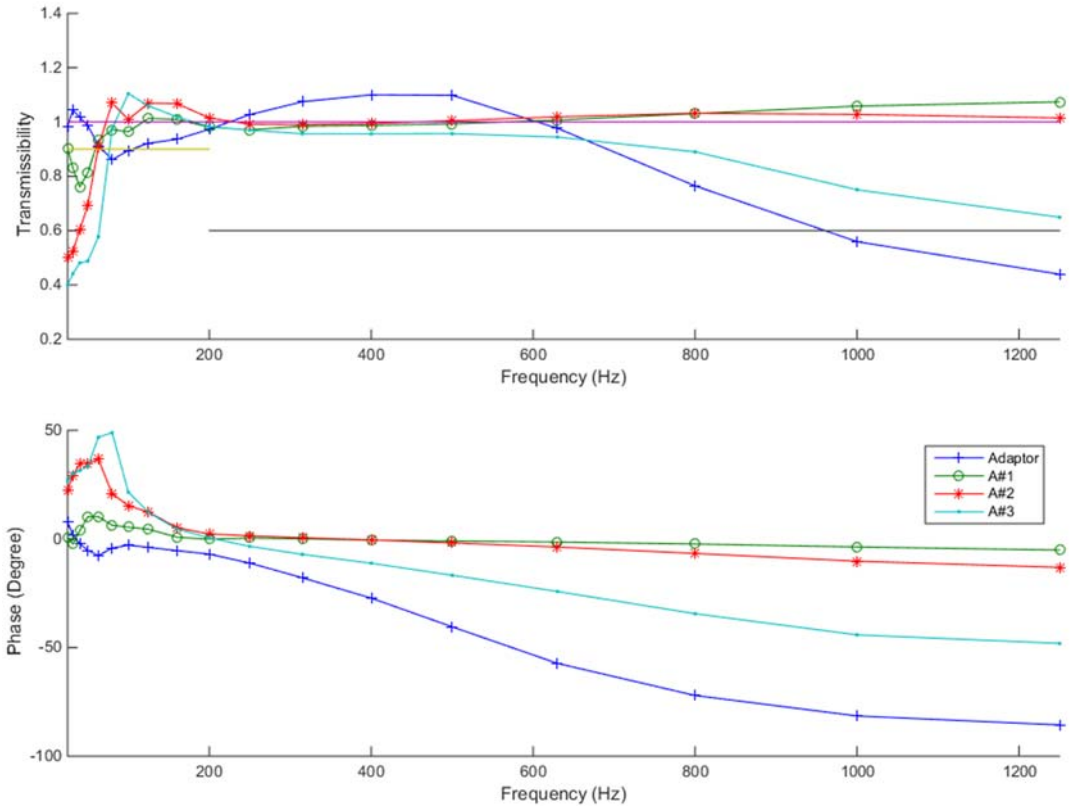

Figure 5-6 - Average of actual VT of the glove (ratio of glove test over bare hand test)

By using the measured data from the bare hand test and the glove test, the MVT of the glove for the medium and high frequency bands can be calculated. The result of the bare hand test shows that all the accelerometers inside the strap sense the resonance of the hand-arm system at the low frequencies; therefore, for excluding the effect of the resonance on the MVT result, the MVT of the medium frequency band has been calculated from $50Hz$ to $200Hz$. Table 5.2 compares the resultant MVT from the measured vibration with the adaptor and individual accelerometer in the strap. For the medium frequency band, the adaptor shows lower MVT than either of the accelerometers inside the strap while for the high frequency band it shows higher MVT than the others.

Table 5.2 – Mean Vibration Transmissibility

	Adaptor	Strap		
		A#1	A#2	A#3
Medium band (50^{19} $Hz \sim 200$ Hz)	0.92	0.98	1.01	0.93
High band (200 $Hz \sim 1250$ Hz)	1.03	1.01	0.99	0.94

The damping material inside the tested glove does not cover the entire area of the palm side; therefore, individual accelerometers in the strap have individual experiences of the transmitted vibration. They show both reduction and amplification at the same frequency at different locations of the hand; however, the adaptor due to its solid structure cannot sense these differences. As a result for evaluating the performance of a glove, using just the adaptor method provides an inaccurate estimation of the vibration transmitted to the hand.

5.3 Glove Power Absorption

The power absorption from the vibrating handle can be derived from,

$$PA(\omega) = Re[Z(\omega)].\left|\frac{A(\omega)}{\omega}\right|^2, \qquad \text{Eq. 5-2 [12]}$$

where $Z(\omega)$ is the mechanical impedance of the palm and $A(\omega)$ is the acceleration at the palm. Figure A.5. 31 to Figure A.5. 34 in the appendix compare the power absorption of the bare hand test with the glove test by using the result from the accelerometer inside the adaptor and the three accelerometers in the strap respectively. Table 5.3 shows the resultant power damping percentage of the glove according to the adaptor and individual accelerometers within the strap.

[19] Due to resonance at low frequencies, the MVT for medium band has been calculated from 50Hz instead of 25Hz)

The adaptor result shows that the maximum power damping with this glove is at 25 Hz, and it is about 37.6%. In addition, the maximum amplification is 16.5% at 100 Hz. The results from the top (A#1) and bottom (A#3) accelerometers in the strap, show the same frequency from maximum power damping of the glove with values of 50.6% and 22.5% respectively. The result from the middle (A#2) accelerometer in the strap shows the maximum power damping at that point is at slightly lower frequency with reduction of 34.7%. In general, the result from the strap in comparison with the result of the adaptor shows higher amplification of the glove but at lower frequency.

Table 5.3 – Percentage of Power Damping

Frequency (Hz)	% of Power damping			
	Adaptor	Strap		
		A#1	A#2	A#3
20	-1.2%	-37.0%	-34.7%	50.5%
25	-37.6%	-50.6%	-9.7%	-22.5%
31.5	-18.4%	-5.6%	-20.5%	3.6%
40	15.4%	31.4%	1.7%	20.9%
50	-7.5%	-41.4%	59.5%	-15.8%
63	-4.3%	19.4%	57.5%	63.0%
80	10.9%	49.8%	15.4%	25.4%
100	16.5%	-1.6%	5.0%	15.1%
125	9.4%	-9.0%	-25.9%	12.6%
160	9.2%	4.7%	14.1%	10.4%
200	-0.5%	7.5%	8.6%	13.7%
250	2.6%	1.7%	-3.2%	-4.3%
315	-29.3%	2.7%	-2.0%	-1.3%
400	-36.1%	6.0%	10.9%	59.6%
500	-12.1%	24.0%	14.9%	-72.8%

5.4 Summary

The ten participants in this study were involved with a series of tests for measuring the MI at the palm and fingers side, and the VT from the handle to the hand with either the adaptor method or the strap method. A commercial glove has been tested in this study and the VT from the handle to the hand through the glove has been tested.

The adaptor has a solid structure and has one embedded accelerometer, while the strap is flexible and has three embedded miniature accelerometers. As a result the strap method can reveal more information about different parts of the hand.

The results of the bare hand tests show that both the adaptor method and the strap method are acceptable; however, at low frequency the adaptor cannot sense the resonance of the hand-arm system.

The glove test results reveal that the adaptor, due to its solid structure, cannot measure the actual vibration of different points of the hand while the individual accelerometers in the strap can. The adaptor for the medium frequency band measures lower vibration and for the high frequency band measures higher vibration levels than the strap method.

6 Analytical modelling of Hand-arm system

Analytical models provide an important means for investigating the dynamic behaviour of hand-arm systems (HAS) and for simulating the response of HAS during hand-arm vibration (HAV) exposure. By knowing the mechanical impedance (MI) at the driving point, parameter values of the analytical model can be identified. For measuring MI, the adaptor is not involved, so this method is free of effects and errors that are usually introduced to the system by the adaptor [29, 74]. In addition, although many HAV tests for measuring VT can involve human interference, with MI method, the human interference effect can be minimized.

The HAS can be simulated using lumped-mass models with differing degrees of freedom (DOF). The simplest model of HAS consists of only two DOF. This model can only simulate the dynamic behaviour of the skin of the palm and the upper body while the more complex models with higher DOF's can simulate the dynamic behaviour of the skin of fingers, skin of palm, fingers, etc. In addition, these models are very useful for simulating the performance of gloves even before their manufacture. For this purpose, by creating a lumped-mass model of the damping-material inside the glove and combining it with a model of the HAS, a complex model for simulating the dynamic behaviour of the hand-arm with the glove can be generated.

Generally, the vibration can have one or more directions. Figure 6-1 shows the three directions of vibration relevant to HAV. The focus of this study is on the one-directional vibration in the Z_h direction which is the most common direction of vibration in HAV analysis.

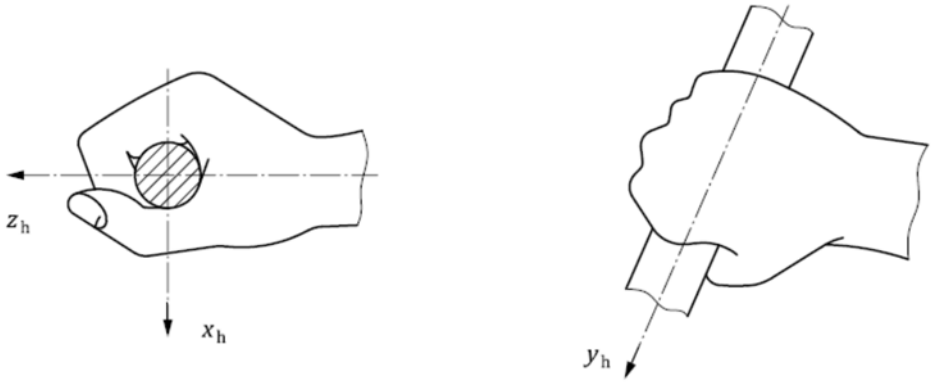

Figure 6-1 – Hand-arm vibration directions [30]

For a 1-DOF model which consists of a mass, a spring and a damper, the equation of motion can be written as,

$$m\ddot{x}(t) + c\dot{x}(t) + kx(t) = f(t), \quad \text{Eq. 6-1}$$

where m, c and k represent the mas, damping coefficient and stiffness respectively, $f(t)$ is output force and $\ddot{x}(t)$, $\dot{x}(t)$ and $x(t)$ are acceleration, velocity and displacement of the mass as function of time. For multi-DOF models, Eq. 6-1 can be written in matrix form,

$$[m]\{\ddot{x}(t)\} + [c]\{\dot{x}(t)\} + [k]\{x(t)\} = \{f(t)\}. \quad \text{Eq. 6-2}$$

By solving this equation, the response of the system for any arbitrary applied force can be calculated. Since this equation is essentially linear, State-Space methods can be used for solving the equation. For this purpose Eq. 6-2 can be written as,

$$\{\ddot{x}(t)\} = -[m]^{-1}[c]\{\dot{x}(t)\} - [m]^{-1}[k]\{x(t)\} = [m]^{-1}\{f(t)\}. \quad \text{Eq. 6-3}$$

Now by defining two new state variables,

$$v_1(t) = \{x(t)\}, \quad \text{Eq. 6-4}$$

$$v_2(t) = \{\dot{x}(t)\}. \quad \text{Eq. 6-5}$$

This will result in,

$$\dot{v}_2(t) = \{\ddot{x}\ (t)\}\,. \qquad \text{Eq. 6-6}$$

By substituting Eq. 6-4 to Eq. 6-6 in Eq. 6-3, the result becomes,

$$\dot{v}_2(t) = -\,[m]^{-1}[c]v_2(t) - [m]^{-1}[k]v_1\ (t) = [m]^{-1}f(t)\,, \qquad \text{Eq. 6-7}$$

or in matrix form,

$$\begin{Bmatrix}\dot{v}_1(t)\\ \dot{v}_2(t)\end{Bmatrix} = \begin{bmatrix}0 & I\\ -[m]^{-1}[k] & -[m]^{-1}[c]\end{bmatrix}\begin{Bmatrix}v_1(t)\\ v_2(t)\end{Bmatrix} + \begin{Bmatrix}0\\ [m]^{-1}\end{Bmatrix}f(t)\,, \qquad \text{Eq. 6-8}$$

where I is the identity matrix. By numerical integration of this equation, as a function of time, $v_1(t)$ and $v_2(t)$ will be known. As a result, the displacement, velocity and acceleration of each part of the system as function of time can be obtained.

6.1 Mechanical Impedance

The analytical model should be able to simulate the dynamic behaviour of the actual system; therefore the resultant MI of the analytical model should be compared with the MI of the actual system. For this purpose, by measuring the acceleration and applied force at the driving point during the vibration test, the MI can be calculated. By subsequent manipulation of the parameters of the model while minimising the differences between the model MI and the measured MI, the system parameters can be identified.

For finding the MI of the palm, the measurement of acceleration and force should be at the palm side of the handle and for the MI of the fingers, the measurement should be at the fingers' side. The measured MI while the operator is holding the handle, is the combination of the operator's MI and the handle's MI; therefore for finding the

MI of the operator, the MI of the handle is required. Dong [41] has shown that the MI of the hand can be derived from,

$$Z_{Hand}(\omega) = Z_{Total}(\omega) - Z_{Handle}(\omega)\ , \qquad \text{Eq. 6.9}$$

where Z_{Hand} is MI of the hand (palm or fingers), Z_{Handle} is MI of the handle and Z_{Total} is the total measured MI while the operator is holding the handle.

In this study, 10 males participated in the experiments. For the experiment with each participant, while the handle was vibrating according to the defined vibration level in ISO 10819 [21], accelerations and applied forces at the palm and finger sides were captured simultaneously for a duration of 60 seconds. The resultant MIs of each participants palm and fingers were then calculated individually. Although the maximum excitation frequency in these tests was $1600Hz$, since the handle has a natural frequency around $1400Hz$, the MI were only calculated up to $500Hz$ [54, 56].

Figure A.6.1 in the Appendix compares the average measured palm MI of these participants with the reported MI in ISO 10068 [30] and from Dong's study [50]. Figure A.6.2 in the Appendix compares the average measured finger MI with the previously reported finger MI. The results show that the average measured palm MI for these participants is higher than the previously reported palm MI while the average measured finger MI is lower than the reported finger MI.

The overall Hand MI can also be calculated as a summation of the palm and finger MI. Figure 6-2 compares the calculated hand MI in this study and from Dong's study [50] with the minimum and maximum reported MI values for the hand [30]. The result shows that for frequencies between $25Hz$ to $80Hz$, the magnitude of the

calculated hand MI is higher than the maximum reported MI; however, for the rest of the frequency range, the MI is within reported limits.

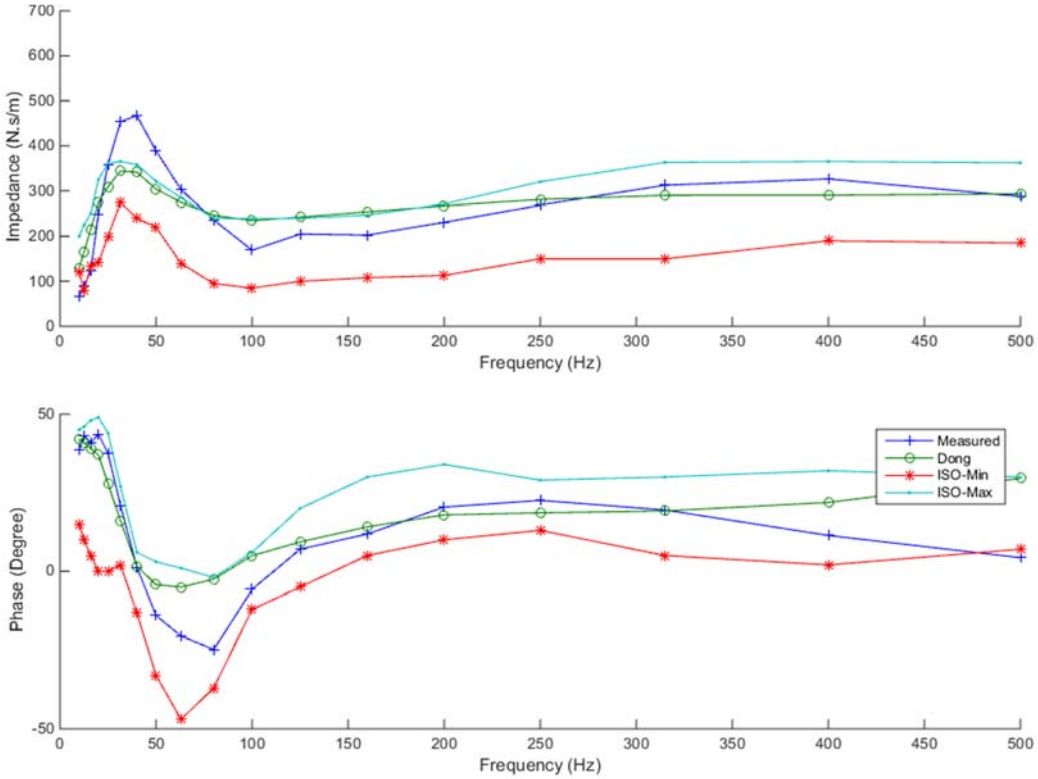

Figure 6-2 – Calculated hand's MI and Dong's result [50] in compare with minimum and maximum hand's MI in ISO 10068 [30]

6.2 2-DOF model of Hand-Arm

The 2-DOF model is the simplest model for simulating the HAS. It consists of only two parts which are connected together with spring and damper. In this model of the HAS, the upper body is assumed to be fixed while the palm and wrist are modelled together with one mass which is attached to the upper body with spring and damper. The skin of the hand is modelled as a mass which is attached to the palm with spring and damper. In addition, the skin is assumed to be in contact with the vibrating handle.

Figure 6-3Figure 4-1.a shows the parts of the model. In this model, m_1 represents the mass of the palm and wrist together, while m_2 is the mass of the skin of the hand and finally m_h represents the mass of the vibrating handle. Since the skin and handle are in contact, it is assumed that both of them move together and therefore there is no spring or damper between them (Figure 6-3Figure 4-1.b).

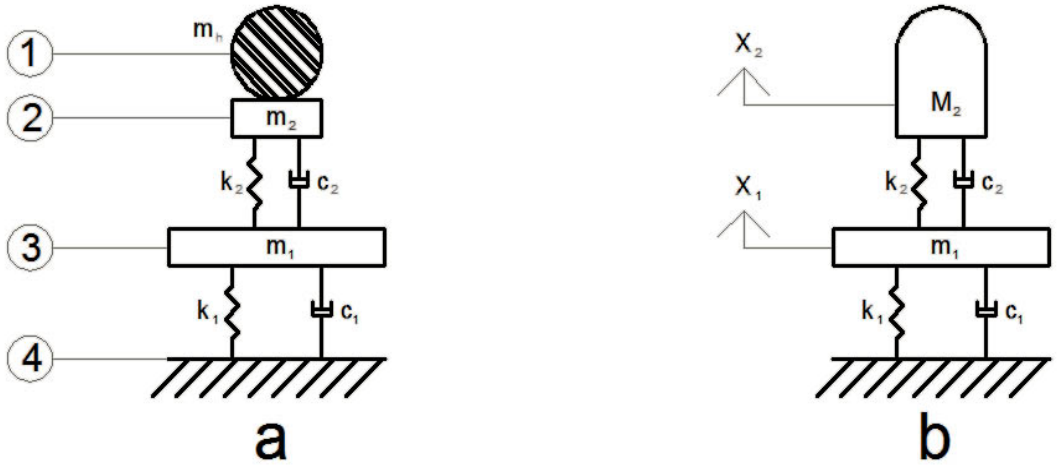

Figure 6-3 – Two-DOF model of hand-arm (a) [30] and resultant 2-DOF model with handle (b) (1.Handle, 2.Contact skin, 3.Palm and wrist & 4.Upper Body)

For this model, the displacement matrix in Eq. 6-2 Eq. 6-2, can be written as,

$$X(t) = \begin{Bmatrix} X_1 \\ X_2 \end{Bmatrix}, \qquad \text{Eq. 6-10}$$

where X_1 is the displacement of the palm and wrist while X_2 is the displacement of the handle and skin of the hand. The mass matrix of this model can be written as,

$$M = \begin{bmatrix} m_1 & 0 \\ 0 & m_2 + m_h \end{bmatrix}, \qquad \text{Eq. 6-11}$$

and the damping matrix as,

$$C = \begin{bmatrix} c_1 + c_2 & -c_2 \\ -c_2 & c_2 \end{bmatrix}, \qquad \text{Eq. 6-12}$$

where c_1 and c_2 are damping coefficients of the dampers between the upper body and the palm/wrist and between the palm/wrist and skin respectively. The stiffness matrix for this model is,

$$K = \begin{bmatrix} k_1 + k_2 & -k_2 \\ -k_2 & k_2 \end{bmatrix}, \qquad \text{Eq. 6-13}$$

where k_1 and k_2 are the stiffness's of the springs between the upper body and palm/wrist and between the palm/wrist and skin. By knowing the values of all of these parameters, the dynamic response of the model to any input force can be calculated. Therefore, for any arbitrary applied force to the system or for any arbitrary movement of the handle, the displacements, velocities and accelerations of all parts of the system can be calculated.

For identifying the parameter values, the measured MI of the hand can be used. By defining an error function equal to the measured hand's MI minus the resultant hand's MI of the model and by minimizing the error function, the parameter values can be identified. The MI of the hand for this model can be calculated from,

$$Z_{Hand} = \frac{(k_2 + j\omega C_2)(X_2 - X_1)}{j\omega X_2} + j\omega m_2 \ , \qquad \text{Eq. 6-14}$$

where X_1 and X_2 are displacements of the palm and handle in the frequency domain respectively, j is the square root of minus one and ω is the angular frequency.

Table 6.1 shows the values of parameters for this model according to ISO 10068 [30] and also the derived values for the measured hand MI in the z-direction. These values are not unique and for different body shapes and sizes or even for different postures will be altered. Figure A.6.3 in the Appendix compares the reported hand's MI by ISO10068 and the resultant MI from the 2-DOF model. The result shows that this 2-DOF model cannot simulate the behaviour of the HAS very accurately,

especially after 125Hz. Figure A.6.4 in the Appendix compares the measured hand MI values in this study and the resultant MI from the generated 2-DOF model based on the measured hand's MI. The result shows this model cannot simulate the phase of MI for most of the frequencies and also cannot simulate the magnitude of MI after 300Hz and around 80Hz.

Table 6.1 – Values for parameters in Two-DOF model of hand-arm

Parameter	Unit	Direction of vibration			
		x_h [30]	y_h [30]	z_h [30]	z_h (Generated model)
m_1	kg	0.5479	0.5374	1.2458	1.4580
m_2	kg	0.0391	0.0100	0.0742	0.0998
k_1	N/m	400	400	1,000	2,000
k_2	N/m	0	17,648	50,000	67,480
c_1	$N.s/m$	22.5	38.3	108.1	54.1
c_2	$N.s/m$	202.6	75.5	142.4	182.8

6.3 3-DOF model of Hand-Arm

For simulating the behaviour of the palm and fingers individually, a HAS model with at least Four-DOF is required. Figure 6-4.a shows the different parts for this model. Similar to the Two-DOF HAS model, for this model it can be assumed that the upper body is fixed. The palm and wrist are also lumped together and they are connected to the upper body by spring and damper. The skin of the hand, is separated into two parts, the skin of the palm and skin of the fingers. Both of these two parts are in contact with the vibrating handle and it can be assumed that they move together (Figure 6-4.b); therefore, the resultant hand-arm model with the handle acts as a 3-DOF model. In this model, the fingers are included with separate

mass to that from the palm and wrist; In addition it is assumed that the fingers are connected to the palm and also to the skin with separate springs and dampers.

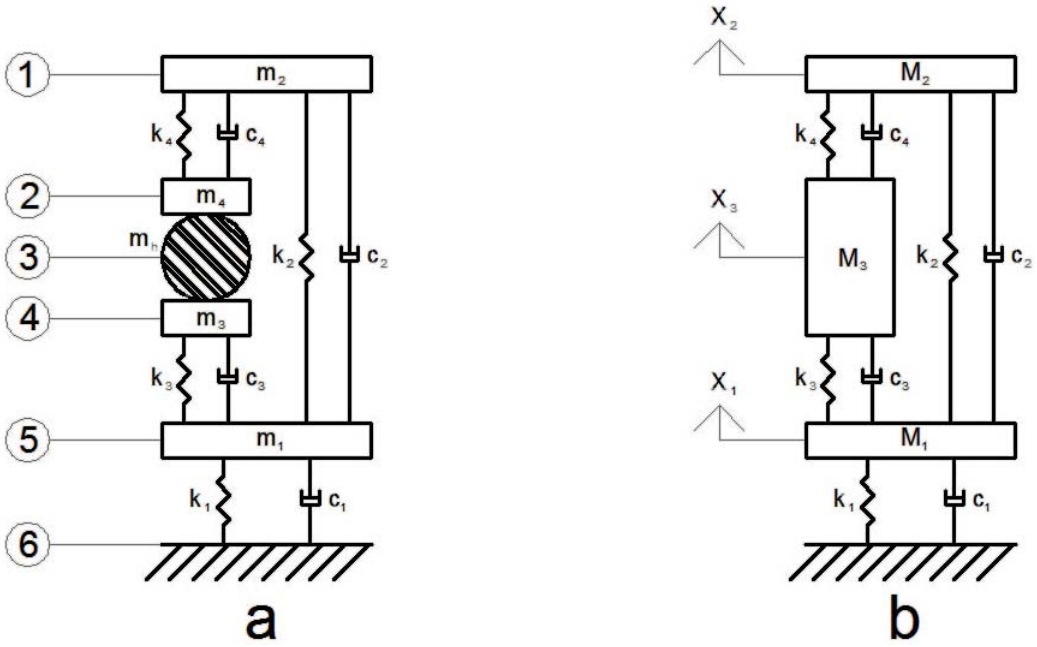

Figure 6-4 – Four-DOF model of hand-arm (a) [30] and resultant 3-DOF model with handle (b) (1.Fingers, 2.Contact skin of fingers, 3.Handle, 4.Contact skin of palm, 5.Palm and wrist & 6.Upper Body)

For this model, the displacement matrix in Eq. 6-2, can be written as,

$$X(t) = \begin{Bmatrix} X_1 \\ X_2 \\ X_3 \end{Bmatrix}, \qquad \text{Eq. 6-15}$$

where X_1 is the displacement of the palm and wrist, X_2 is the displacement of the fingers and X_3 is the displacement of the handle and skin of the palm and fingers. The mass matrix of this model is,

$$M = \begin{bmatrix} m_1 & 0 & 0 \\ 0 & m_2 & 0 \\ 0 & 0 & m_3 + m_4 + m_h \end{bmatrix}, \qquad \text{Eq. 6-16}$$

where m_1, m_2, m_3 and m_4 are the masses of the palm/wrist, fingers and skin at the palm side and skin at the finger side respectively. The damping matrix is given by,

$$C = \begin{bmatrix} c_1 + c_2 + c_3 & -c_2 & -c_3 \\ -c_2 & c_2 + c_4 & -c_4 \\ -c_3 & -c_4 & c_3 + c_4 \end{bmatrix}, \quad \text{Eq. 6-17}$$

where c_1, c_2, c_3 and c_4 are damping coefficients of dampers between the upper body and palm/wrist, between the palm/wrist and fingers, between the palm/wrist and skin and finally between the fingers and skin. The stiffness matrix becomes,

$$K = \begin{bmatrix} k_1 + k_2 + k_3 & -k_2 & -k_3 \\ -k_2 & k_2 + k_4 & -k_4 \\ -k_3 & -k_4 & k_3 + k_4 \end{bmatrix}, \quad \text{Eq. 6-18}$$

where k_1, k_2, k_3 and k_4 are stiffness's of springs between the upper body and palm/wrist, between the palm/wrist and fingers, between the palm/wrist and skin and finally between the fingers and skin. Table 6.2 shows the values of these parameters for the Four-DOF model of hand-arm according to ISO 10068 [30] and the derived values for the measured MIs for the palm and fingers in the z-direction.

Table 6.2 – Values for parameters in Four-DOF hand-arm model

Parameter	Unit	Direction of vibration			
		x_h [30]	y_h [30]	z_h [30]	z_h (Generated model)
m_1	kg	0.4129	0.7600	1.1252	1.5910
m_2	kg	0.0736	0.0521	0.0769	0.0385
m_3	kg	0.0163	0.0060	0.0200	0.0400
m_4	kg	0.0100	0.0028	0.0100	0.0050
k_1	N/m	400	500	1,100	2,000
k_2	N/m	200	100	12,000	12,850
k_3	N/m	4,000	4,907	43,635	45,480
k_4	N/m	8,000	17,943	174,542	174,500
c_1	$N.s/m$	20.0	28.1	111.5	55.8
c_2	$N.s/m$	100	39.7	39.3	19.7
c_3	$N.s/m$	144.6	50.7	86.8	173.6
c_4	$N.s/m$	79.9	14.3	121.0	242.0

For this model the MIs of palm and fingers can be derived from,

$$Z_{Palm} = \frac{(k_3 + j\omega C_3)(X_3 - X_1)}{j\omega X_3} + j\omega m_3 \ , \qquad \text{Eq. 6-19}$$

and,

$$Z_{Finger} = \frac{(k_4 + j\omega C_4)(X_3 - X_2)}{j\omega X_3} + j\omega m_4 \ , \qquad \text{Eq. 6-20}$$

where X_1, X_2 and X_3 are displacements of the palm/wrist, fingers and handle in the frequency domain respectively.

6.4 4-DOF model of Hand-Arm

In previous models, it was assumed that the whole upper body including the upper arm and shoulders were fixed. By adding one more DOF to the previous model and by modelling the movement of the upper arm and shoulder, the resultant model becomes more accurate. Figure 6-5.a shows a Five-DOF model of hand-arm where the upper arm and shoulder can also move. Figure 6-5.b shows the resultant 4-DOF hand-arm model with the handle. For this model, the displacement matrix in Eq. 6-2, can be written as,

$$X(t) = \begin{Bmatrix} X_0 \\ X_1 \\ X_2 \\ X_3 \end{Bmatrix} , \qquad \text{Eq. 6-21}$$

where X_0 represents the displacement of the added part for the upper arm and shoulder. For this model, the mass matrix can be written as,

$$M = \begin{bmatrix} m_0 & 0 & 0 & 0 \\ 0 & m_1 & 0 & 0 \\ 0 & 0 & m_2 & 0 \\ 0 & 0 & 0 & m_3 + m_4 + m_h \end{bmatrix} , \qquad \text{Eq. 6-22}$$

where m_0 is the mass of the upper arm.

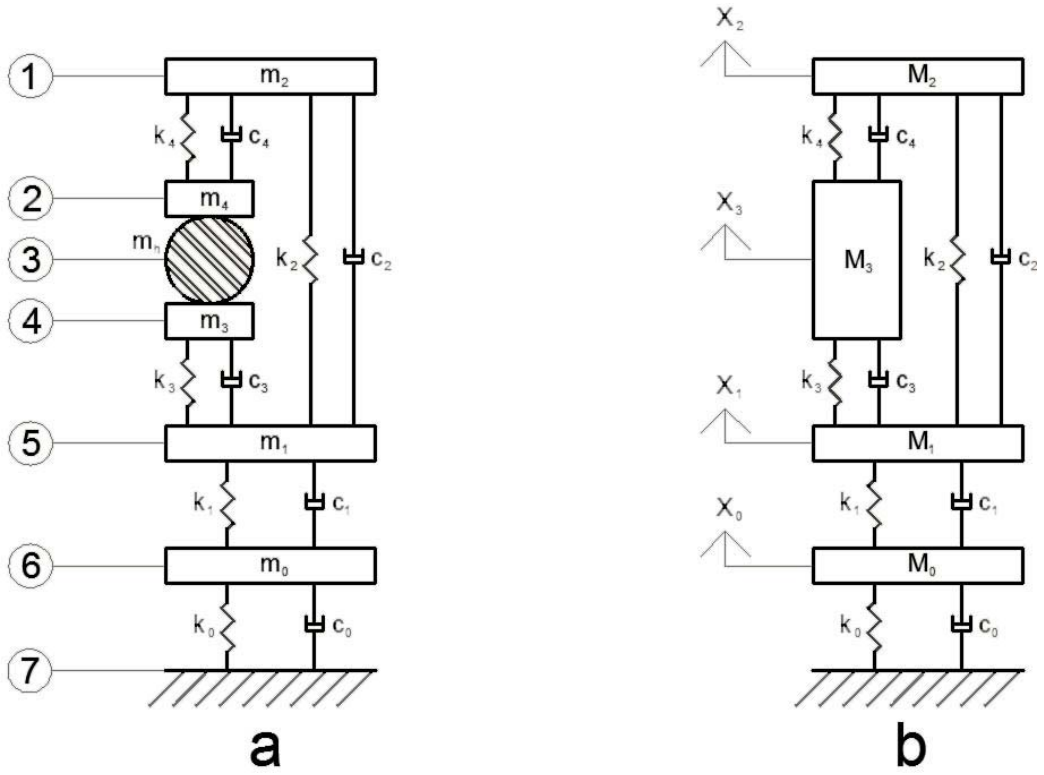

Figure 6-5 – Five-DOF model of hand-arm (a) [30] and resultant 4-DOF model with handle (b) (1.Fingers, 2.Contact skin of fingers, 3.Handle, 4.Contact skin of palm, 5.Palm and wrist, 6.Upper arm and shoulder & 7.Upper Body).

The damping matrix becomes,

$$C = \begin{bmatrix} c_0 + c_1 & -c_1 & 0 & 0 \\ -c_1 & c_1 + c_2 + c_3 & -c_2 & -c_3 \\ 0 & -c_2 & c_2 + c_4 & -c_4 \\ 0 & -c_3 & -c_4 & c_3 + c_4 \end{bmatrix}, \qquad \text{Eq. 6-23}$$

where c_0 is damping coefficient of damper between the upper arm and palm/wrist. The stiffness matrix for this model is,

$$K = \begin{bmatrix} k_0 + k_1 & -k_1 & 0 & 0 \\ -k_1 & k_1 + k_2 + k_3 & -k_2 & -k_3 \\ 0 & -k_2 & k_2 + k_4 & -k_4 \\ 0 & -k_3 & -k_4 & k_3 + k_4 \end{bmatrix}, \qquad \text{Eq. 6-24}$$

where k_0 is the stiffness between the upper arm and palm/wrist. Table 6.3 shows the values of these parameters for the Four-DOF model of hand-arm according to ISO

10068 [30] and also the derived values for measured MIs of palm and fingers in z-direction.

In this model by knowing displacements of the palm (X_3), fingers (X_4) and handle (X_5) in the frequency domain, the MI of the palm and fingers can be derived from,

$$Z_{Palm} = \frac{(k_3 + j\omega C_3)(X_3 - X_1)}{j\omega X_3} + j\omega m_3 \,, \qquad \text{Eq. 6-25}$$

and,

$$Z_{Finger} = \frac{(k_4 + j\omega C_4)(X_3 - X_2)}{j\omega X_2} + j\omega m_4 \,. \qquad \text{Eq. 6-26}$$

Table 6.3 – Values for parameters in Four-DOF model of hand-arm

Parameter	Unit	Direction of vibration			
		x_h [30]	y_h [30]	z_h [30]	z_h (Generated model)
m_0	kg	0.02360	0.3605	7.5000	3.7500
m_1	kg	0.3998	0.5515	1.0721	1.5170
m_2	kg	0.0576	0.0725	0.0760	0.0464
m_3	kg	0.0205	0.0050	0.0200	0.0371
m_4	kg	0.0100	0.003	0.0100	0.0062
k_0	N/m	1,000	1,000	8,059	8,061
k_1	N/m	6,972	1,000	1,891	1,901
k_2	N/m	100	100	12,000	12,010
k_3	N/m	4,000	5,443	44,220	44,230
k_4	N/m	65,844	15,170	176,880	176,900
c_0	$N.s/m$	21.8	40.5	93.1	186.2
c_1	$N.s/m$	22.1	95.7	112.1	56.1
c_2	$N.s/m$	69.8	37.6	39.7	19.9
c_3	$N.s/m$	128.6	51.5	83.9	167.8
c_4	$N.s/m$	81.5	11.4	116.7	101.0

Each of these resultant lumped-mass models has several natural frequencies and damping ratios. The number of natural frequencies depends on the number of DOF in the model. Table 6.4 shows the natural frequencies for these analytical models. The result of the 4-DOF model shows that the system has two natural frequencies below $10Hz$, one at about $55Hz$ and one at about $258Hz$. The other two models also show one natural frequency below $10Hz$ and one about $55Hz$.

Table 6.4 – Natural frequencies of the resultant hand-arm models with handle

		$\omega_n\ (Hz)$				ζ			
Model	Direction	1st	2nd	3rd	4th	1st	2nd	3rd	4th
2-DOF	x_h	0	3.0	-	-	-	0.55	-	-
	y_h	3.1	41.0	-	-	0.94	0.63	-	-
	z_h	7.7	56.4	-	-	1.00	0.55	-	-
3-DOF	x_h	3.1	10.7	415.4	-	1.00	1.00	0.49	-
	y_h	3.1	67.0	86.2	-	1.00	0.83	0.54	-
	z_h	1.7	59.5	262.8	-	1.00	0.47	0.69	-
4-DOF	x_h	4.3	31.3	109.3	361.6	1.00	0.91	0.51	0.28
	y_h	1.8	3.5	68.3	100.7	1.00	0.62	0.52	1.00
	z_h	4.6	9.2	54.1	258.9	0.21	1.00	0.53	0.68

Figure A.6.5 in the Appendix compares the resultant palm's MI for 3-DOF and 4-DOF models with the reported palm MI in the Z_h direction. Figure A.6.6 in the Appendix compares the resultant finger MI of these models with the reported finger MI in the Z_h direction. As these two figures show, both 3-DOF and 4-DOF models can simulate the MI of both palm and fingers with reasonable accuracy while the 4-DOF model simulates the MI with improved accuracy.

Figure A.6.7 and Figure A.6.8 in the Appendix compare the measured MIs with the resultant MI of the palm and fingers for the 3-DOF and 4-DOF models generated

from measured data in this study. The results show the generated models can only reproduce the MI for frequencies below $50Hz$ for the palm's MI.

6.5 6-DOF model of hand-arm with glove

For creating a model of the hand-arm with a glove, the glove should also be modelled as a lumped-mass system, as shown in Figure 6-6.a. In this model, the glove is modelled as two separated parts. One part represents the glove between the skin of the palm and handle and the other part between the skin of the fingers and handle. With the addition of these two parts, the resultant model becomes a 6-DOF system as shown in Figure 6-6.b.

In this model, it is assumed that the skin of the palm and surface of the glove at the palm side move together, the skin of the fingers and surface of the glove at the finger side move together and the other surfaces of the glove and handle move together. For this model, the resultant displacement matrix in Eq. 6-2, can be written as,

$$X(t) = \begin{Bmatrix} X_0 \\ X_1 \\ X_2 \\ X_3 \\ X_4 \\ X_5 \end{Bmatrix}, \qquad \text{Eq. 6-27}$$

where X_0, X_1 and X_2 are displacements of the upper arm/shoulder, palm/wrist and fingers similar to the original 4-DOF. X_3, X_4 and X_5 are displacements of the contact skin of the palm/glove, contact skin of the finger/glove and handle/glove respectively. The mass matrix of this model can be written as,

$$M = \begin{bmatrix} m_0 & 0 & 0 & 0 & 0 & 0 \\ 0 & m_1 & 0 & 0 & 0 & 0 \\ 0 & 0 & m_2 & 0 & 0 & 0 \\ 0 & 0 & 0 & m_3 + m_7 & 0 & 0 \\ 0 & 0 & 0 & 0 & m_4 + m_8 & 0 \\ 0 & 0 & 0 & 0 & 0 & m_5 + m_6 + m_h \end{bmatrix}, \quad \text{Eq. 6-28}$$

where m_5 and m_7 are the masses of the glove at the palm side. m_6 and m_8 are the masses of the glove at the finger side. The damping coefficient matrix for this model becomes,

$$C = \begin{bmatrix} c_0 + c_1 & -c_1 & 0 & 0 & 0 & 0 \\ -c_1 & c_1 + c_2 + c_3 & -c_2 & -c_3 & 0 & 0 \\ 0 & -c_2 & c_2 + c_4 & 0 & -c_4 & 0 \\ 0 & -c_3 & 0 & c_3 + c_5 & 0 & -c_5 \\ 0 & 0 & -c_4 & 0 & c_4 + c_6 & -c_6 \\ 0 & 0 & 0 & -c_5 & -c_6 & c_5 + c_6 \end{bmatrix}, \quad \text{Eq. 6-29}$$

where c_5 and c_6 are damping coefficients of the dampers in the glove model at the palm and finger side respectively. The stiffness matrix is,

$$K = \begin{bmatrix} k_0 + k_1 & -k_1 & 0 & 0 & 0 & 0 \\ -k_1 & k_1 + k_2 + k_3 & -k_2 & -k_3 & 0 & 0 \\ 0 & -k_2 & k_2 + k_4 & 0 & -k_4 & 0 \\ 0 & -k_3 & 0 & k_3 + k_5 & 0 & -k_5 \\ 0 & 0 & -k_4 & 0 & k_4 + k_6 & -k_6 \\ 0 & 0 & 0 & -k_5 & -k_6 & k_5 + k_6 \end{bmatrix}, \quad \text{Eq. 6-30}$$

where k_5 and k_6 are the stiffness's of springs in the glove model at the palm and finger side respectively.

In this model, the MIs of the glove at palm and fingers sides are,

$$Z_{Glove(Palm\ side)} = \frac{(k_5 + j\omega C_5)(X_5 - X_3)}{j\omega X_5} + j\omega m_5 , \quad \text{Eq. 6-31}$$

and,

$$Z_{Glove(Fingers\ side)} = \frac{(k_6 + j\omega C_6)(X_5 - X_4)}{j\omega X_5} + j\omega m_6 , \quad \text{Eq. 6-32}$$

where X_3, X_4 and X_5 are displacements of the skin of the palm, skin of fingers and handle in the frequency domain respectively.

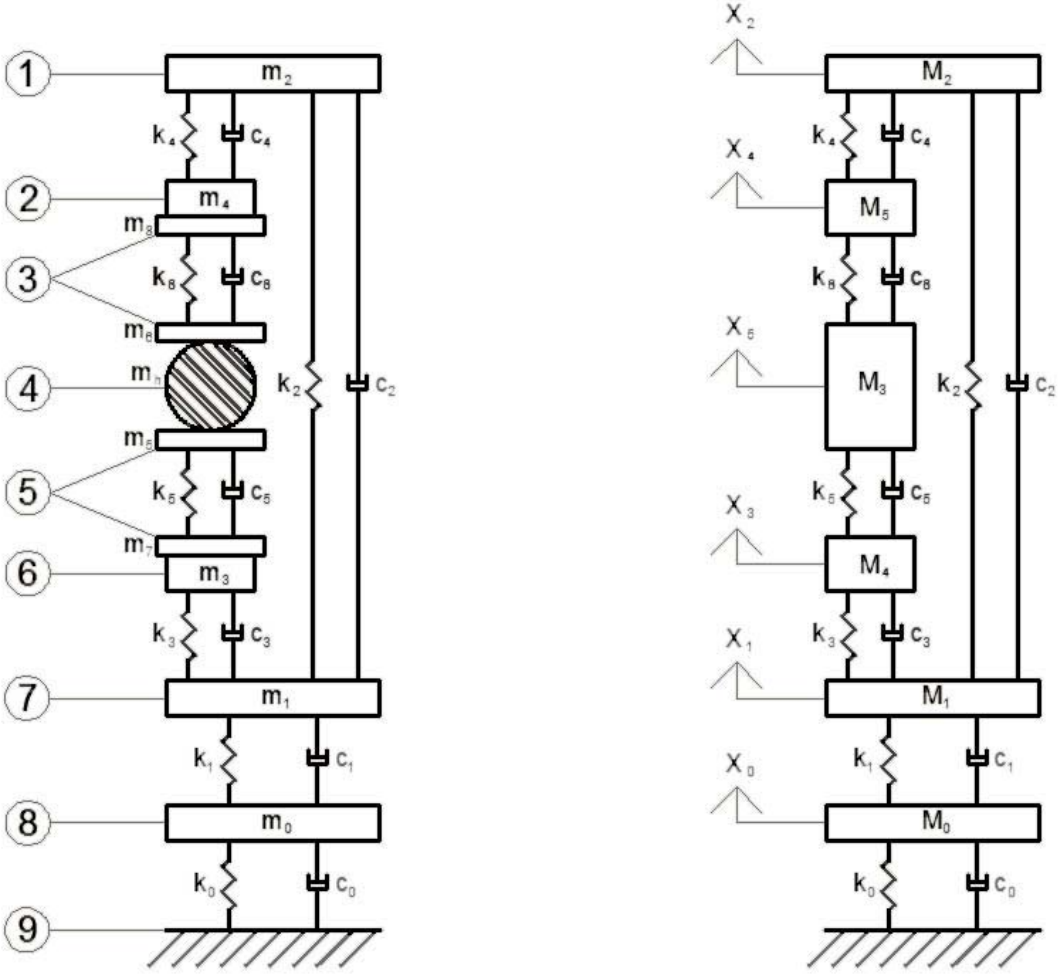

Figure 6-6 – Five-DOF model of hand-arm with two 2-DOF models for glove (a) [30] and resultant 6-DOF model (b)

(1.Fingers, 2.Contact skin of fingers, 3.Glove (finger side), 4.Handle, 5.Glove (palm side), 6.Contact skin of palm, 7.Palm and wrist,8.Upper arm and shoulder & 9.Upper Body)

6.6 Modified 6-DOF model of hand-arm with glove

The previous model of the hand-arm with the glove, only models the glove between the skin of the palm and handle and also between the skin of the fingers and handle. For increased accuracy of the model, the glove can also be modelled between the skin of the palm and the skin of the fingers, and also between the palm and fingers [84]. Figure 6-7.a shows this modified model and Figure 6-7.b shows the resultant 6-DOF model of the hand-arm with the glove and handle. This model has the same displacement matrix as the previous model (Eq. 6-27). The mass matrix of this model becomes,

$$M = \begin{bmatrix} m_0 & 0 & 0 & 0 & 0 & 0 \\ 0 & m_1 + m_9 & 0 & 0 & 0 & 0 \\ 0 & 0 & m_2 + m_{10} & 0 & 0 & 0 \\ 0 & 0 & 0 & m_3 + m_7 & 0 & 0 \\ 0 & 0 & 0 & 0 & m_4 + m_8 & 0 \\ 0 & 0 & 0 & 0 & 0 & m_5 + m_6 + m_h \end{bmatrix}, \quad \text{Eq. 6-33}$$

where m_8 and m_{10} are the masses of the glove between the palm and fingers. These two masses are assumed to move with the palm and fingers. The damping matrix is,

$$C = \begin{bmatrix} c_0 + c_1 & -c_1 & 0 & 0 & 0 & 0 \\ -c_1 & c_1 + c_2 + c_3 + c_8 & -c_2 - c_8 & -c_3 & 0 & 0 \\ 0 & -c_2 - c_8 & c_2 + c_4 + c_8 & 0 & -c_4 & 0 \\ 0 & -c_3 & 0 & c_3 + c_5 + c_7 & -c_7 & -c_5 \\ 0 & 0 & -c_4 & -c_7 & c_4 + c_6 + c_7 & -c_6 \\ 0 & 0 & 0 & -c_5 & -c_6 & c_5 + c_6 \end{bmatrix}. \quad \text{Eq. 6-34}$$

where c_7 is the damping coefficient of the damper in the glove model between the skin of the palm and the skin of the fingers, c_8 is the damping coefficient of the damper in the glove model between the palm and fingers. The stiffness matrix is,

$$K = \begin{bmatrix} k_0 + k_1 & -k_1 & 0 & 0 & 0 & 0 \\ -k_1 & k_1 + k_2 + k_3 + k_8 & -k_2 - k_8 & -k_3 & 0 & 0 \\ 0 & -k_2 - k_8 & k_2 + k_4 + k_6 & 0 & -k_4 & 0 \\ 0 & -k_3 & 0 & k_3 + k_5 + k_7 & -k_7 & -k_5 \\ 0 & 0 & -k_4 & -k_7 & k_4 + k_6 + k_7 & -k_6 \\ 0 & 0 & 0 & -k_5 & -k_6 & k_5 + k_6 \end{bmatrix}, \quad \text{Eq. 6-35}$$

where k_7 is the stiffness of the spring in the glove model between the skin of the palm and the skin of the fingers, k_8 is the stiffness of the spring in the glove model between the palm and fingers.

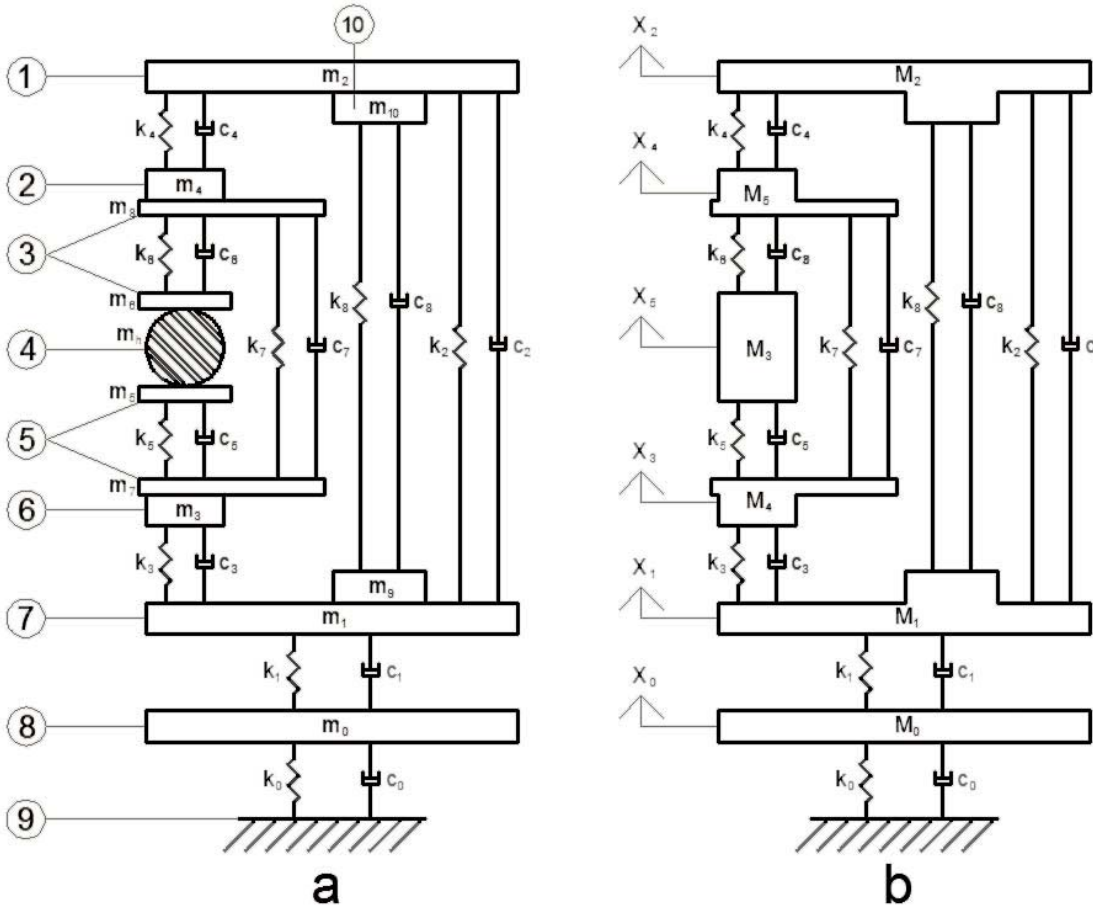

Figure 6-7 – Five-DOF model plus modified glove model (a) [84] resultant 6-DOF model (b) (1.Fingers, 2.Contact skin of fingers, 3.Glove (finger side), 4.Handle, 5.Glove (palm side), 6.Contact skin of palm, 7.Palm and wrist, 8.Upper arm and shoulder, 9.Upper Body & 10.Glove)

6.7 Glove Vibration Transmissibility

Anti-vibration gloves should attenuate the vibration amplitude and dampen the vibration; for this purpose they need damping materials to provide cushioning inside them. There are procedures to evaluate the performance of these products; however, there is no practical procedure for designing these gloves. This part of the study investigated the effect of coverage area of damping-material inside the glove on the resultant glove VT, by using analytical models.

This study used a 4-DOF model of hand-arm with handle. This model can simulate the response of the fingers, handle, palm and upper arm. Furthermore, by adding two more DOF to it, the resultant model can simulate the vibration behaviour of the hand-arm and the glove with the handle. One of these parts is in contact between the handle and palm and the other is in contact with the handle and finger. Figure 6-7.b shows the resultant 6-DOF model which is useful for estimating the VT of the glove for both palm and finger sides.

In Figure 6-7.a, m_5, c_5 and k_5 are the mass, coefficient of damping and stiffness of the glove at the palm side and m_6, c_6 and k_6 are the mass, coefficient of damping and stiffness of the glove at the finger side. The rest of the parameters are the mass, stiffness and coefficient of damping of the HAS. This study uses the same values for mass, coefficient of damping and stiffness that have been defined in ISO 10068 [30] for the z-direction. This study also assumes that the glove uses the same material for both palm and finger sides with constant thickness. For investigating the effect of coverage area of damping-material inside the glove, the properties for parts 5 and 6 can be defined as functions of area coverage of damping material at each side, which can be written as,

$$m_5 = A_1 m_m \,, \quad \text{Eq. 6-36}$$

$$c_5 = A_1 c_m \,, \quad \text{Eq. 6-37}$$

$$k_5 = A_1 k_m \,, \quad \text{Eq. 6-38}$$

$$m_6 = A_2 m_m \,, \quad \text{Eq. 6-39}$$

$$c_6 = A_2 c_m \,, \quad \text{Eq. 6-40}$$

$$k_6 = A_2 k_m \,, \quad \text{Eq. 6-41}$$

where m_m, c_m and k_m are the mass, coefficient of damping and stiffness of material per unit of area. A_1 is the area of the damping material at the palm side and A_2 is the area of the damping material at the finger side.

Three different specimens were tested according to ISO 13753 [113] and each specimen has been modelled as a lumped-mass with 1-DOF where both stiffness and damping coefficients were complex values. Firstly D3O-A, with 6 mm thickness and density of 915 kg/m^3, secondly D3O-B, with 4 mm thickness and density of 435 kg/m^3 and lastly GT6R with 6 mm thickness and density of 1050 kg/m^3. The properties of these samples have been used as properties of the glove in the 6-DOF model. Table 6.5 shows the values of c_m and k_m for these samples.

Table 6.5 – Material properties

Sample	c_m	k_m
	$N.s/m/_{m^2}$	$N/m/_{m^2}$
1	2.09E+05-1.54E+05i	4.99E+08+1.39E+08i
2	4.37E+02+7.77E+04i	5.12E+08+1.05E+08i
3	7.34E+04-1.43E+05i	3.75E+08+1.50E+08i

By assuming the diameter of the handle is 40mm and length of the handle is 110mm, and also by assuming the effective contact area for each of palm and fingers side in

the z-direction is about one quarter of the whole handle area, the maximum effective contact area will become about 3,455 mm^2 for each side. Figure 6-8 shows the effective contact area between the hand and handle in z-direction. In addition, the study assumes that the whole transmitted vibration from the handle to the hand goes through the damping-material and no point of the hand is in direct contact with the handle.

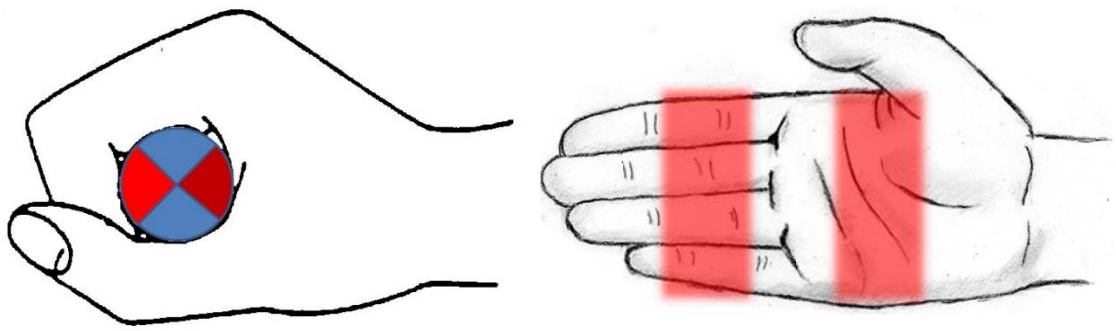

Figure 6-8 –Assumption for effective contact area in z-direction for palm and finger sides

ISO 10819 [21] defines the vibration level for each 1/3rd octave bands from 25Hz to 1600Hz. This study uses the same vibration levels and utilizes MATLAB developed code for simulation. The resulting VT of the glove with these models can be estimated. Simulating the response of the system for different coverage areas of damping material for the finger and palm sides provides the resulting VT of the glove as a function of these two coverage areas. Figure A.6.9, Figure A.6.11 and Figure A.6.13 in the Appendix show the resultant VT of the glove at the palm side in 1/3rd octave bands. As these figures show, by increasing coverage area at the palm side, the VT of the glove at the palm increases.

For the first and third samples and for coverage areas below 30% the VT decreases with increasing frequency and by increasing the coverage area the sensitivity of VT to frequency decreases; however for coverage areas above 30%, the response of VT

to frequency shows the completely opposite trend. As frequency increases, the VT decreases; while by increasing coverage area, the sensitivity of VT to frequency increases. For the second sample, by increasing the coverage area, the VT increases. For low coverage area, the VT is more sensitive in low frequencies and by increasing the coverage area, the sensitivity shifts to the higher frequencies. For low frequencies the third sample has lower VT and for high frequencies the second sample has lower VT.

Figure A.6.10, Figure A.6.12 and Figure A.6.14 in the Appendix show the resultant VT of the glove at the finger side in 1/3rd octave bands. These results show a minimum response around 50 Hz and one peak around 200Hz. For the frequencies around the peak, by increasing the coverage area, the VT decreases, while for other frequencies, by increasing the coverage area, the VT increases. The second sample, has the highest VT at the peak and the lowest VT for the high frequencies.

ISO 10819 [21] defines weighting factors for each of the 1/3rd octave bands (Table 3.1) which can be used for calculating the mean vibration transmissibility (MVT) of the glove at the palm side. This study assumes that the same weighting factors can be used for calculating the MVT at the finger side.

The frequency weighted vibration transmissibility (FWVT) can be calculated as,

$$T = \frac{\sqrt{\sum_{i=i_L}^{i_u}[a_h(f_i)W_{hi}]^2}}{\sqrt{\sum_{i=i_L}^{i_u}[a_H(f_i)W_{hi}]^2}}, \qquad \text{Eq. 6-42}$$

where $a_h(f_i)$ and $a_H(f_i)$ are the acceleration at the hand and at the handle respectively. The MVT is the ratio of the FWVT of the glove test over the FWVT of the bare hand test. In this study, it was assumed that for the bare hand test the whole

vibration was transmitted to the hand and that the resultant FWVT of the bare hand is one.

Using a series of simulations while the coverage area of the palm and finger sides are changing, the VT's of the glove have been estimated and in result the MVT's as function of coverage areas of damping material at palm and fingers sides have been calculated.

Figure A.6.15 to Figure A.6.18 in the Appendix show the result of the simulation for the MVT at the finger side and the palm side for medium and high frequency ranges as a function of coverage area of damping material at the finger and palm side.

Figure A.6.15 shows that when the coverage area of these damping materials at the finger side is less than 10% of the effective contact area, the MVT for the medium band at the finger side is a function of coverage area for both finger and palm sides; however when the coverage area at the fingers side goes above 10%, the MVT of the medium band becomes only a function of coverage area at the finger side.

Figure A.6.16 shows that the MVT for the high frequency range at the finger side is only a function of coverage area of the damping material at the finger side and not at the palm side. Figure A.6.17 and Figure A.6.18 show that the MVT's at the palm side for both medium and high frequency bands are only a function of coverage area of the damping material at the palm side. Therefore, for each side the MVT can be plotted as a function of coverage area of damping material at the same side.

Figure A.6.19 and Figure A.6.20 in the Appendix show the result of MVT at the finger side as a function of coverage area of damping material at the finger side and Figure A.6.21 and Figure A.6.22 in the Appendix show the result of MVT at the palm as a function of coverage area of damping material at the palm.

Anti-Vibration gloves should reduce the VT. This study shows that by covering the entire palm or finger side with any of these tested materials, proper vibration attenuation is not possible and almost the whole vibration will be transmitted through these materials. This means having a resultant MVT equal to one for gloves that use these materials as cushioning materials over the whole area.

The result shows that by decreasing the coverage area of these materials, the MVT of the glove also decreases. Table 6.6 and Table 6.7 show the maximum coverage area of each of these samples at the palm side for satisfying ISO 10819 criteria. By assuming that the practical contact area at palm side is about 3,455mm^2, Table 6.6 shows that by covering about 17% of the palm area with sample #1, the MVT for the medium frequency range can be below 0.9. This percentage for sample #2 and #3 is about 17% and 21% respectively. Table 6.7 shows that by covering about 9% of the palm area with sample #1, the MVT for the high frequency range can be below 0.6. The same value for sample #2 and #3 is about 11% and 21% respectively. Table 6.8 shows that for the finger side and for the medium frequency band, none of these materials can satisfy the required criteria. Table 6.9 shows that for the finger side and for the high frequency band, except sample #2 which can barely satisfy the criteria, the other two samples cannot at all.

Table 6.6 – MVT results in medium frequency band for palm side

Sample	Area	Length of Equivalent Square	TM
	mm^2	mm	
1	578	24	0.90
2	578	24	0.89
3	714	27	0.90

Table 6.7 – MVT results in high frequency band for palm side

Sample	Area	Length of Equivalent Square	TH
	mm^2	mm	
1	306	17	0.56
2	374	19	0.57
3	714	27	0.58

Table 6.8 - MVT results in medium frequency band for finger side

Sample	Area	Length of Equivalent Square	TM
	mm^2	mm	
1	170	13	0.98
2	3400	58	1.00
3	170	13	0.97

Table 6.9 - MVT results in high frequency band for finger side

Sample	Area	Length of Equivalent Square	TH
	mm^2	mm	
1	170	13	0.74
2	170	13	0.57
3	170	13	0.7

This study assumes the transmitted vibration from the handle to the hand only goes through the glove; however, when the whole area of the hand is not covered with damping material, the vibration can also be transmitted from parts of the glove which are not covered with damping material. This means there is practical limitation for the minimum coverage area at each side of the glove. In addition, proper design and orientation is required for avoiding transmitting vibration from any part of the glove except the parts that have damping material inside.

6.8 Summary

Lumped-mass models can be used for simulating the vibration behaviour of the HAS. The measured MI at the driving point can be used for deriving the relevant parameters of these models. The simplest model for simulating the hand-arm system has two degrees of freedom. By increasing the number of DOF, the accuracy of the model increases. In addition, by increasing the DOF, the behaviour of different parts of the HAS can be modelled.

Furthermore, by modelling the damping material inside the glove and by combining it with models of the HAS, a complex model of the HAS with the glove can be developed. These kinds of models are useful for investigating the performance of the gloves even before manufacturing them.

The lumped-mass models of three damping materials have been used for simulating the performance of the gloves which used these materials as cushioning materials. For different coverage areas at the palm and finger sides, the resultant VT of the glove at both palm and finger sides have been calculated. Later by applying weighting factors for each $1/3^{rd}$ octave bands, the MVT's of the glove have been estimated. The results show that by using proper amounts of the damping material at the palm side, the resultant gloves can satisfy the criteria of ISO 10819 for the palm side; however, for the finger side none of these samples were able to satisfy the criteria.

7 Discussion

7.1 Hand arm measurement

7.1.1 Resonance of the system

For hand-arm vibration tests, the ISO standard requests for a cylindrical handle with $40mm$ diameter and minimum length of $110mm$ which is attached to an exciter system. The test rig should not have any resonance in the frequency range of the test to avoid the interfering of high amplitude of vibration at resonance frequencies on the measured vibration transmissibility [21]. During hand-arm vibration tests, the operator should apply certain amounts of feed and grip forces, and these forces should be monitored for the operator in order to keep them in the defined criteria ranges. By equipping the handle with the sensors for measuring these forces, the flexibility of the handle increases and as a result the frequency of the resonance decreases.

The existing handle before this study, used strain gauges for the force measurement. This method of force measurement can decrease the complexity of the handle and in result increase the natural frequency; however, the first resonance of this handle was at about $500Hz$ which was in the middle of frequency test range for the HAV tests. In addition, the handle had several resonances in the test frequency range. For increasing the frequency of the resonance, the stiffness of the handle can be increased; however, this could lead to lower resolution of the measured strains and result in lower resolution for the calculated applied forces. For improving this issue, the geometry of the handle was modelled with SolidWorks and the vibration behaviour of the model was simulated with ANSYS. With the result of this simulation the effective parameters on the natural frequency and flexibility of the

handle at the measuring points were found. In general, the frequency of resonance depends on the mass and stiffness of the system. By decreasing the mass, the frequency of resonance will increase. Since, the main mass of this handle was the mass of the cylindrical part, by using a hollow cylindrical part, the mass of the system can be minimized. In addition, by reducing the mass of the handle, the shaker requires less energy to excite the system. Furthermore, the hollow handle provides enough space for mounting several accelerometers inside the handle. For instance, in this study three accelerometers were mounted inside the handle; two for measuring the accelerations of the front and back sides of the handle, and one for getting feedback from the handle for the vibration controller.

For measuring strain in the system, the structure should be flexible; therefore, at the measuring points, the thickness of the structure needed to be decreased, and for the rest it can be increased. This study used the ANSYS model, and through an optimization process and by manipulating the effective parameters and dimensions, the frequency of the first resonance was increased up to $1400Hz$ without reducing the resolution for the strain measurement. This handle consisted of a very robust base structure, and two hollow half cylindrical parts with two thin plates at the top and bottom (Figure 7-2). All the strain gauges mounted on the thin plates; therefore, the strain measurement was as close as possible to the cylindrical part of the handle. These plates were flexible enough to provide proper resolution for the force measurement while the rest of the structure was relativity stiff to avoid reduction of the natural frequency.

7.1.2 Force measurement

The existing handle before this study, utilized four sets of strain gauges for measuring feed and grip forces. Two sets of active-active strain gauges on the base plate for measuring the feed force, and two sets of active-dummy strain gauges at the two ends of the cylinder part for measuring the grip force (Figure 7-1). For the active-active configuration, both strain measurements were along the direction of elongation, while for the active-dummy configuration, only one of them was along the direction of elongation and the other one was perpendicular to it. In HAV, the applied forces are along the z-direction (direction of vibration); therefore, the applied forces cause elongation in only one direction. As a result, the active-active configuration has higher resolution in comparison with the active-dummy configuration. Furthermore, the temperature does not have any effect on the strain measurement with the active-active configuration.

For the existing handle due to shape and technical difficulty, the active-active configuration was not possible for the grip force measurement, while for the new design, the aim was to utilize active-active configuration for all sets of strain gauges to achieve higher measurement resolution and eliminate the effect of change of temperature on the measured result.

For MI measurement, by measuring the applied force at the closer point to the hand, the MI can be calculated to a higher frequency [54, 56]. Therefore, another criterial for the design of new handle was to put the strain gauges as close as possible to the cylindrical part of the handle which is the driving point (Figure 7-2).

The main part of the new handle consists of two half-cylindrical parts which have two thin plates on the top and bottom. Since these two parts mount onto a very stiff

structure, each of them can be modelled as a fixed beam. The strains at the two ends of each of these beams are functions of the applied load and position of the load. In general, the strain at the thin flat part is a function of a cubic equation of the load position; however, in this beam since the stiffness of the two flat ends in comparison with the stiffness of the half-cylindrical shape in the middle is significantly lower, the strain has almost linear relationship with the load position. Therefore, by knowing the difference of two strains at two ends of the beam, the position of the load can be calculated and then the applied load will be known.

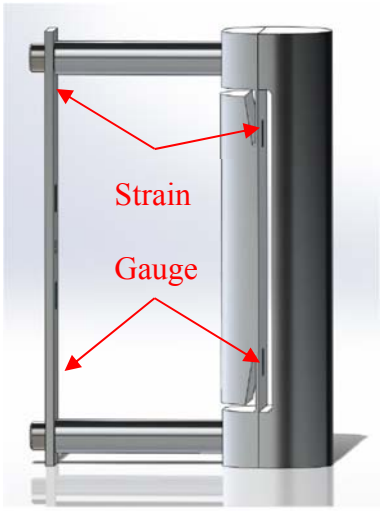

Figure 7-1 – Handle designed by T. Walkemeyer (2013)

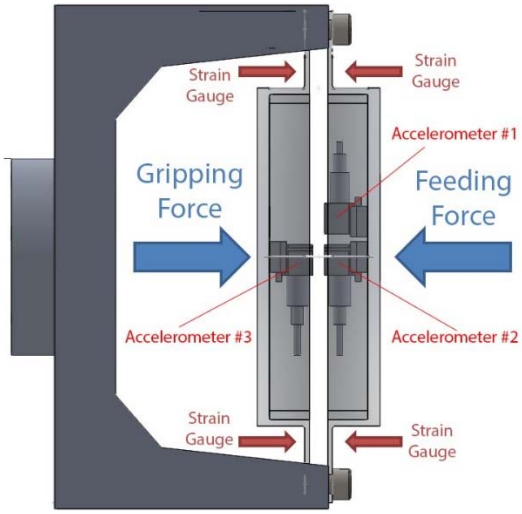

Figure 7-2 – The designed handle

In this handle, two sets of active-active strain gauges mount on thin flat plates at top and bottom of each of the half-cylindrical parts. With these strain gauges, the total applied force and direction of the force at each side of the handle are measureable. The ISO standard requests for monitoring the amount of applied forces and not the directions, while it requests for the forearm of the operator to be aligned with the direction of vibration [21]. Since the wrist of the operator can apply moments to the handle, the alignment of the forearm with the handle cannot guarantee that the applied forces will be aligned with the direction of vibration. Since the ISO standard requests for one-direction of vibration, any misalignment of the applied force with

the direction of vibration will lead to lower amplitude of the applied force in the direction of vibration. In addition, since the normal exciter cannot tolerate non-axial forces, applying any bending moment could cause damage to the exciter.

By monitoring the direction of the forces during the test, the operator can adjust his/her hand to be in the correct direction and avoid any possible damage to the system. For this purpose, the generated MATLAB's toolbox for this study, captures the strain data from the system, and calculates the relevant forces, and in real time, graphically shows the applied force at the top and bottom of each side, which includes the angle of the applied forces. Furthermore, by showing the limitation for each force, the operator can easily maintain the amount and direction of the force during the test.

7.1.3 Vibration direction(s)

The ISO standard for evaluating the performance of a glove suggests two ways for acceleration measurement:

- One directional
- Three orthogonal directional

While, according to this procedure the handle only needs to vibrate in the z-direction (Figure 2-5). Studies on different types of power tools show that the z-direction does not necessary have the highest level of vibration for all tools [28], and many of the tested tools vibrate in all three orthogonal directions [95, 108, 129]. Figure 7-3 shows example acceleration spectra of some of these tools which shows that the level of vibration in three orthogonal directions are comparable. Although common electro-magnetic exciters which are used for HAV test can generate non-axial

vibration due to their side-loads [29], the levels of vibration in the other two directions are not close to the level of vibration for their direction of excitation.

Comparison between the result of one-direction and three orthogonal directions vibration attenuation of the gloves shows the performance of a glove depends on the type of vibration [118]. Therefore, it is more logical to generate vibration in all directions simultaneously and also measure the vibration in all directions to accurately evaluate a glove.

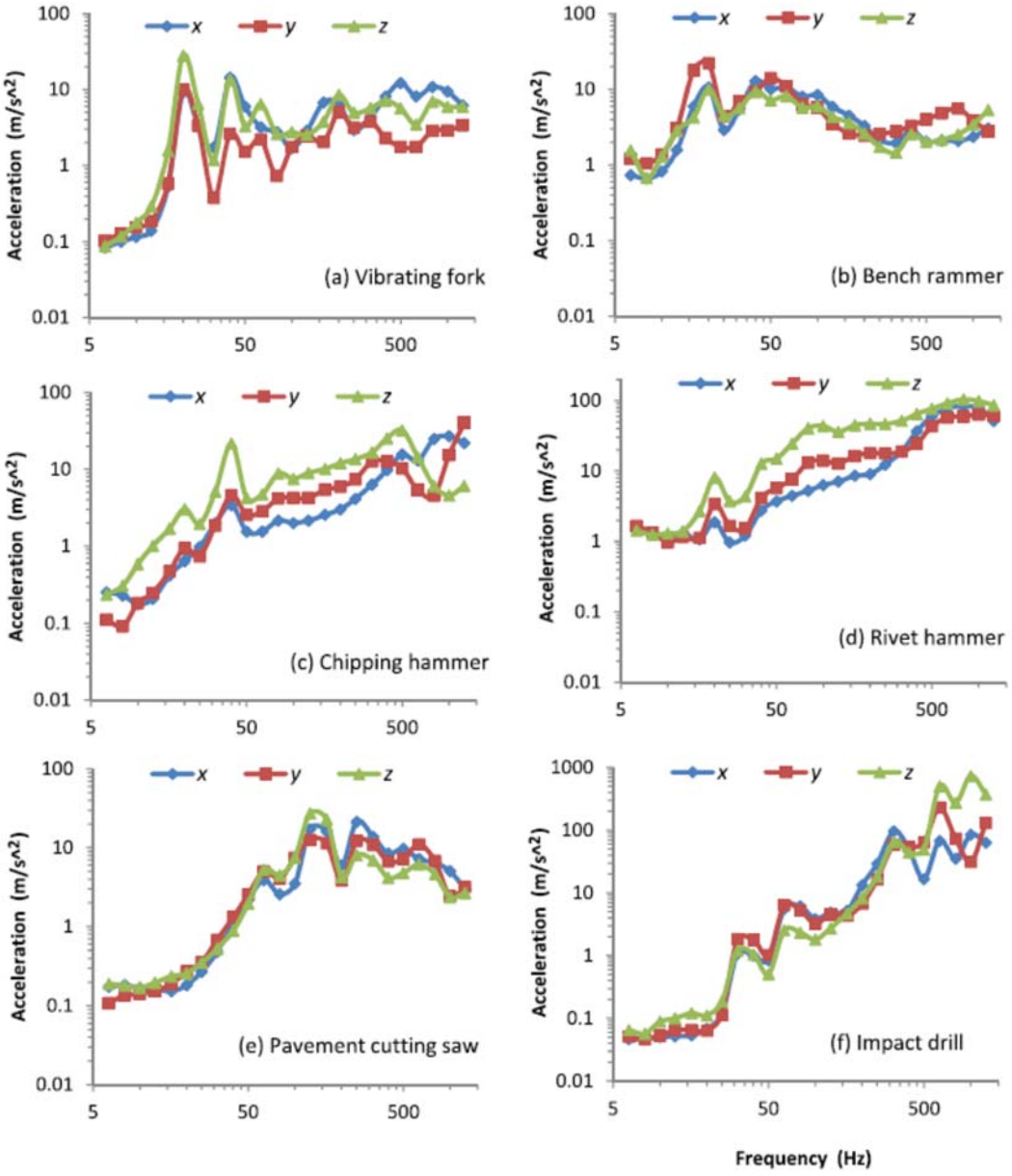

Figure 7-3 – Acceleration spectra of different power tools handle [108]

7.1.4 Accuracy of the measurement

The ISO standards for evaluating the accuracy of the measurement, requests for measuring the VT from the handle to the adaptor while the adaptor is attached to the handle with contact force of $80\pm10N$. Studies show that different shapes of the adaptor can pass this test; however, they do not agree on the vibration transmissibility [40]. This procedure only investigates the VT from the handle to the adaptor without involving the characteristics of the operator. The result of this measurement can only show the agreement between the two accelerometers inside the handle and inside the adaptor, and it cannot prove that the adaptor can measure the vibration at the palm of the hand.

The adaptor in this study passed the accuracy test according to the ISO standard (Figure 5-1); however, the result of bare hand tests show that the adaptor cannot show any of the resonances of the hand-arm system for frequencies below $50Hz$. While, the result of the bare hand test from the strap method shows high amplitude of vibration at low frequencies which represents the resonances of the hand-arm system.

Therefore, despite the ISO standard evaluation, having the VT equal to one while the adaptor is attached to the handle is not enough to prove the accuracy of the system. Furthermore, for evaluating the measurement of the device, the VT from the handle to the hand while the operator holds the handle should be investigated. In this test, the result should be able to show the resonance of the hand-arm system, otherwise the measuring device at the hand is unable to measure the vibration behaviour of the hand-arm system.

7.1.5 Alignment

During the hand-arm vibration test, the accelerometer at the palm side should be aligned with the accelerometer inside the handle. For the adaptor measurement, since the adaptor should be inside the glove and the position and orientation of the adaptor is not visible, the standard suggests to put a slit in the seam for monitoring the adaptor [21, 44]; however, this only helps for monitoring the yaw angle and the adaptor can still have a miss-alignment in the Y-Z plane (Figure 2-10).

The strap on the other hand only needs to be aligned with the handle while the operator is not wearing the glove, and the position of the strap will not change by wearing the glove. Therefore, the accelerometers on the strap can easily maintain their original positions and remain aligned with the handle.

The adaptor has a solid structure; therefore, it cannot adjust itself with either the surface of the palm or the glove. The ISO suggests a symmetric shape adaptor, while the palm of the hand is not symmetric. Since the design of the glove is based on the shape of the hand and not the shape of the adaptor, by putting the adaptor inside the glove, the adaptor can easily deform the glove. This not only causes discomfort for the operator, but can also lead to misalignment of the adaptor with the handle.

The strap is flexible and each of the accelerometers in the strap can adjust themself with the surface of the palm; therefore, the strap does not change the configuration of the glove and adapts itself to the shape of the hand.

7.1.6 Vibration at the palm side

Studies show that the pressure distribution at the hand is a function of applied forces to the handle and the movement of the handle [60, 68]. Figure 2-7 shows the

pressure distribution at the palm when the hand is in direct contact with the vibrating handle. By using the adaptor, points #1 to #4 will be covered with the adaptor. As the figure shows for these points without using any adaptor the pressure increases as the point gets closer to the thumb. As a result due to the variation of the contact forces between the hand and the handle, the VT to different parts of the palm cannot be the same. The stiffness of the adaptor compared to the skin is relatively high, therefore it can be assumed to be solid. As a result, the adaptor can only measure the average of the VT for the whole contact surface and not the VT for any arbitrary point on the hand. On the other hand, the strap on the hand is flexible and each of the accelerometers in the strap can measure the vibration behaviour at its location.

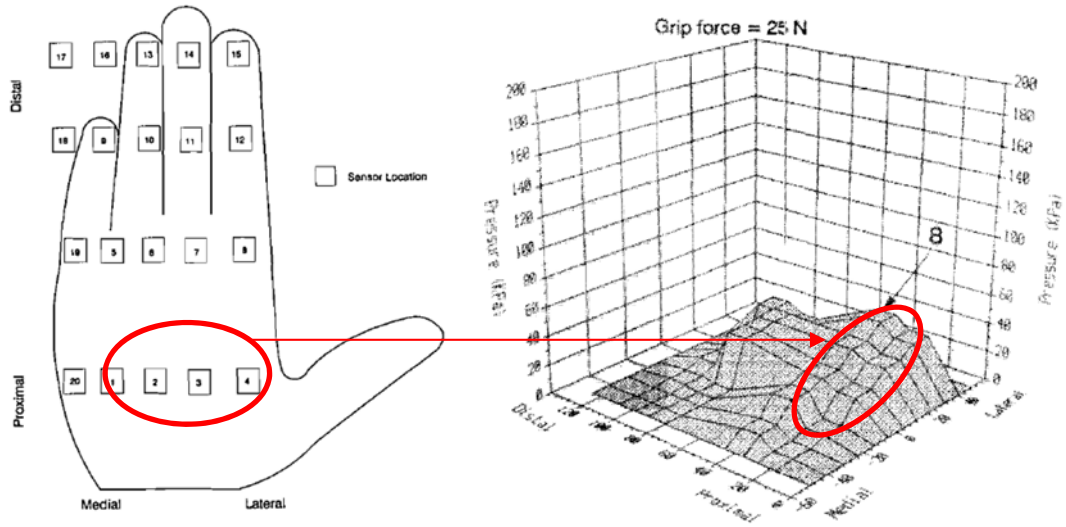

Figure 7-4 – Pressure distribution on vibrating handle [60]

The curvature of the solid adaptor is close to the curvature of the handle [21, 40], and by pushing the adaptor toward the handle, the distribution of pressure between the adaptor and the handle or between the adaptor and the glove will be spread evenly. Since the contact pressure between the hand and handle without any adaptor is not even, the stiffness of the adaptor effects on the applied pressure on the glove, and in result it affects the vibration behaviour of the glove. Therefore, the measured

vibration transmissibility with the adaptor cannot be accurate for the normal condition of using the glove.

7.1.7 Vibration at the fingers side

The ISO standard evaluates the glove based on the VT from the handle to the palm, and it neglects the VT to the fingers. It only requests the use of the same damping material for both palm and finger sides, while this cannot guarantee the proper vibration attenuation at the fingers side [47]. In this study, both front and back sides of the handle were equipped with the accelerometers; therefore, the vibrations of both front and back sides of the handle are measureable. This not only helps for MI measurement at the front and back sides of the handle, but also helps for measuring the VT to the fingers. For this purpose by using similar method on the fingers side, and by using miniature accelerometers, the VT from the handle to each finger is measureable.

7.1.8 Glove thickness

For evaluating a glove, the ISO standard requests the result from a bare hand test and a glove test with the same system. According to this standard, an anti-vibration glove should not have thickness greater than $8mm$ [21]. During HAV test, the operator should wear the glove and hold the handle. As a result, for the glove test, the hand of the operator could see a handle with total diameter up to $56mm$ which includes the diameter of the cylindrical handle and the thickness of damping material inside the glove which is wrapped around the handle.

Studies show that the highest comfort for the male operator comes by the use of a handle with diameter of $40mm$ and for the female operator a handle with diameter of

35mm. In general, the optimal diameter for the handle should be 19.7% of the operator hand length to achieve the maximum comfort [73]. In addition, by increasing the diameter due to thickness of the damping material inside the glove, the dexterity of the hand and TTS of vibrotactile perception decreases [71]. Therefore, it is more practical to define the maximum allowable thickness of the glove based on the diameter of the handle.

Furthermore many parameters of the hand-arm system such as the MI, the contact force and even the absorbed power of the hand-arm are functions of the diameter of the handle [35, 58, 68, 82]; therefore, the palm' MI of the same operator in the bare hand test and in the glove test cannot be the same due to different effective diameters of the handle in the bare hand and the glove test. Figure 7-5 shows coefficient of variation for the MI of the hand, for three different diameters of the handle. Since the VT of a glove is a function of MI of the hand-arm system and the MI of the damping material inside the glove (Eq. 2-13), any change in the MI of the hand-arm system leads to changes of the VT in the glove test. In addition, as Figure 7-6 shows, by increasing the diameter of the handle, the contact forces decrease [68].

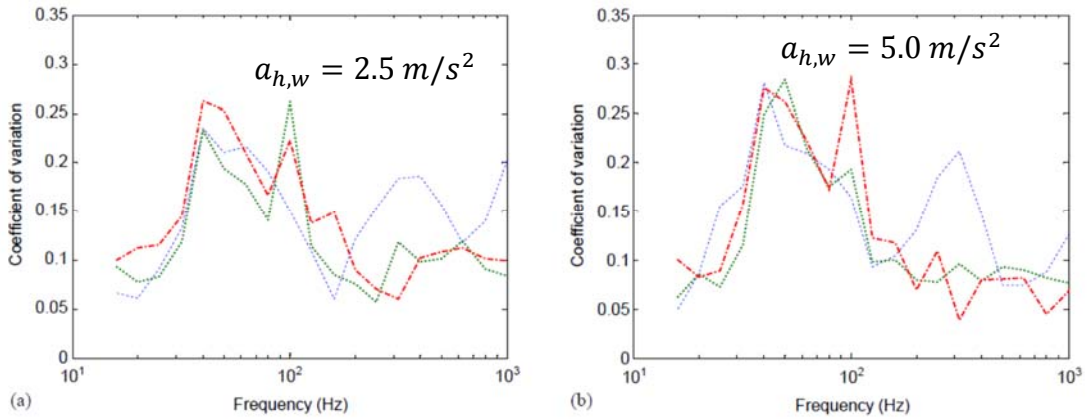

Figure 7-5 – Coefficient of variation of the mean MI for different handle diameters (30mm handle: - - - - -; 40mm handle: . . . . . , 50mm handle: - . - . - ,) [69]

The ISO standard defines the VT of the glove as the ratio of two weighted VT from the bare hand test and the glove test, while by introducing the glove to the system, due to the change of effective diameter of the handle, the characteristics of the hand-arm system will also change. Therefore, the change of VT in these two tests is the combination of vibration attenuation of the glove and the change of contact force and MI of the hand due to change of diameter. As a result, it is not accurate to define the VT of the glove based on the result of these two tests.

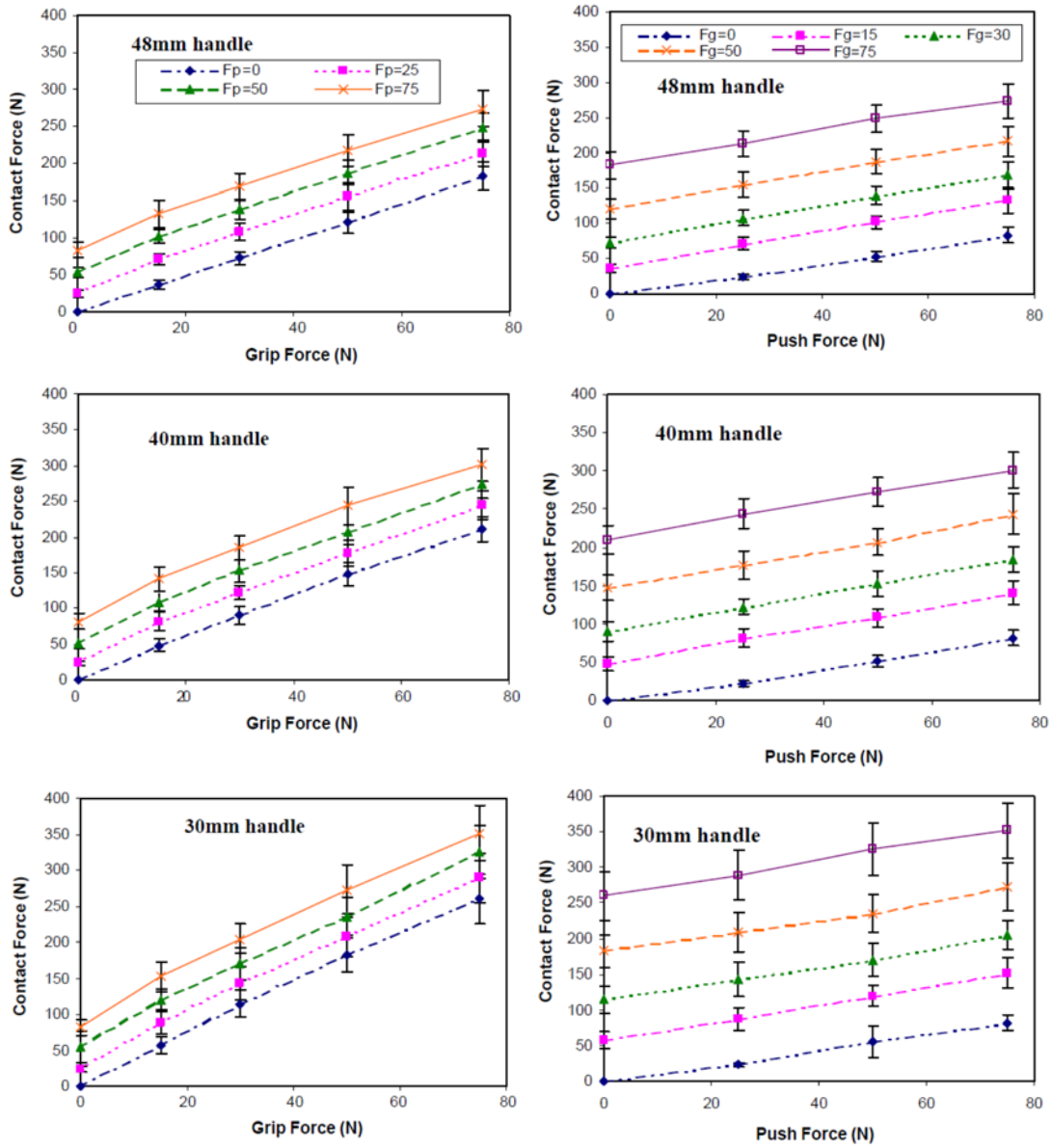

Figure 7-6 – Variation of contact force for different handle diameters [68]

7.2 Damping material

7.2.1 Vibration transmissibility

Any anti-vibration glove needs damping material to provide cushioning. For measuring the VT of the damping material, the ISO standard requests to put a circular disk with $90mm$ diameter of the material on top of a flat plate which is mounted to an exciter, and it requests to put a $2.5kg$ mass with the same diameter on top of the sample [113]. In this procedure, the ratio of the two measured accelerations from the top mass and the flat plate during the vibration test, defines the VT of the material; however, this study shows that this ratio determines the VT of the specific size of the material. By changing the coverage area of the sample while the thickness is constant, the VT changes. Therefore, defining the VT of a specific size of a sample as the VT of the sample is not correct.

This research shows that the tested materials can be modelled as one DOF lumped-mass model while both stiffness and damping coefficient are complex values. The stiffness and damping coefficient for these models can be derived from results of the VT tests with different coverage areas of the sample. These properties have linear relationship with the coverage area, while the VT has non-linear relationship with the coverage area. As a result, the generated lumped-mass model for the unit of area can be used to calculate the VT of the sample as a function of coverage area.

The VT spectra of the tested samples in this study show there is at least one resonance for each VT spectra in the test frequency range. The frequency of this resonance for coverage area less than 30% of the whole area of a disk with $90mm$ diameter has a linear relationship with the coverage area of the sample. Since after any resonances, the amplitude of vibration decreases dramatically, by decreasing the

frequency of the resonance, the overall VT will be decreased. In other words, for increasing vibration attenuation for a constant load, the coverage area of the damping material should be decreased.

7.2.2 Loading mass

Studies show that the damping materials inside the glove have non-linear dynamic behaviour, and as a result the performance of the resultant glove depends on the applied feed and grip forces [38, 39, 47, 110]. Therefore, the mechanical properties and vibration behaviour of the damping material should be defined as functions of the applied load.

The ISO standard requests for a $2.5Kg$ load for simulating the applied forces in the HAV tests [113]. The circular sample in this test has $90mm$ diameter and by applying $24.5N$ load on it, the pressure become almost $3885Pa$. The handle in the HAV test has $40mm$ diameter and $110mm$ height; therefore, by using the same size of the sample inside the glove, the sample covers the entire area of the palm. In the HAV tests, the push force is $50\pm8N$ and the grip force is $30\pm5N$; therefore, even for a uniform pressure distribution at the palm side, the magnitude of pressure on the damping material is about $7860Pa$. This pressure is almost twice the pressure which the ISO requests to apply during VT testing of the damping material.

Furthermore, the handle has cylindrical shape, and the palm of the hand does not have uniform surface. As Figure 2-7 shows the pressure distribution on the hand is highly dependent on the position. These facts show that the maximum pressure that applies to the damping material in the HAV tests, is several times higher than the pressure applied to the material during the VT test. Therefore, the result of this

measurement cannot be used directly for predicting the resultant glove VT in the HAV test.

In this study, the VT of the samples for various coverage areas was measured while the top load remained the same. The change of area of the sample while the applied load was constant, can be interpreted as the change of pressure on the sample. Table 7.1 shows the equivalent pressure for each of the tested coverage area. The VT results reveal that by decreasing the coverage area for any of these tested materials, the overall VT decreases as well. Therefore, for these materials by increasing the load, better vibration attenuation is achievable.

Table 7.1 – Equivalent pressure on the material

Coverage Area	Pressure
%	N/m^2 (Pa)
3	128,456
5	77,102
10	38,559
15	25,748
20	19,272
25	15,420
30	12,795
40	9,714
50	7,718
100	3,851

7.3 Analytical modelling of the Hand-arm system

Analytical models and simulations help in understanding the behaviour of the dynamics and vibration behaviour of the system. Unlike the common HAV tests

which are usually involved with various kinds of human errors, the results from analytical simulation can be free from these errors and have high repeatability.

There are several different types of lumped-mass models with different degrees of freedom for simulating the vibration behaviour of hand-arm system. Some of these models only simulate the hand-arm system [30, 31, 49, 66, 83, 123, 126] while the others also simulate the behaviour of the glove [30, 46, 84]. These models are used for simulating the existing hand-arm system with or without the glove. The mechanical properties in these models are usually derived from the measured MI of the system at the driving point. The gloves in these models can be modelled as one element or more, and the mechanical properties of these elements can be derived from the tests on existing gloves [84].

This study uses the measured VT from different coverage area and derives mechanical properties of the samples as functions of area. These materials could potentially be used as cushioning components inside the glove; therefore, the mechanical properties of them have been used as mechanical properties of the different parts of the glove in the lumped-mass model of hand-arm system with the glove. Since the mechanical properties of these materials are functions of area, by generating individual models for each coverage area, the proper amount of the damping material can be identified for achieving the required vibration attenuation in the resultant glove.

7.3.1 Vibration attenuation at the palm side

Simulation results show the VT to the palm is highly dependent on the coverage area of the damping material between the skin of the palm and the handle. Since the ISO

standard requests for only one VT measurement at the palm of the hand, it also requests to cover the entire palm area with the same damping material [21].

Simulations show that by covering the entire area of the palm with any of the tested damping materials, almost the entire vibration will be transmitted to the hand. Results show that for frequencies below $50Hz$ there could be also vibration amplification and at some frequencies there could be minor vibration attenuation that would result in the overall MVT of the resultant glove to be almost one. However, by partially covering the palm area with these damping materials, the proper vibration attenuation is achievable, and the MVT of both the medium and high frequency bands for certain coverage areas of these materials could be below the standard's criteria range. Therefore, all of these damping materials can be used for developing anti-vibration gloves; however, careful design is required to use correct amounts of damping material at the proper locations.

7.3.2 Vibration attenuation at the fingers side

Analytical simulation results show that the VT to the fingers also highly depends on the amount of the damping material. For coverage area less than 10% of the entire area of the fingers side, the VT to the fingers is dependent on the amount of damping material on both finger and palm sides, while for the coverage area of more than 10%, the VT is only a function of coverage area of the damping material at the fingers side.

The standard for evaluating a glove as an anti-vibration glove requests the use of the same damping material for both palm and finger sides. This procedure only requests the VT measurement at the palm side; however, the research shows that some of the

gloves that are evaluated as anti-vibration gloves, do not necessary reduce the VT at the fingers side [47].

Since there is no criteria for vibration attenuation at the finger side, this study assumes the same criteria that applies for the palm side can be applied to the finger side. Results of analytical simulations for the three tested materials show that although there is a minor vibration attenuation for the medium frequency band for the fingers side, none of the coverage areas of these materials would lead to proper vibration attenuation to satisfy the criteria. For the high frequency band only sample #2 can barely satisfy the criteria. Therefore, none of these damping materials can reduce the VT to the fingers the same as they could for the palm side. These results agree with the results of previous studies on VT to the fingers [47].

Studies show that the current weighting factor is not suitable for the fingers and the VPA in the fingers is more correlated with the unweighted acceleration [98]. Therefore, if this criteria applies for the fingers side, the MVT for both medium and high bands drop. In this case all of the materials can satisfy the criteria for the high band, but not for the medium band.

7.4 Vibration transmissibility reduction

Any anti-vibration glove requires the use of appropriate damping material. The VT of the damping material also depends on the applied load on it. Therefore, this study suggests that for designing an anti-vibration glove, first the VT of damping material under different pressures should be measured. Then, analytical models of the material should be generated from the result of these tests. Since the vibration characteristics of a glove mainly depends on the vibration characteristic of the

damping material inside it, this model can represent the analytical model of the glove as well. Later, the combined analytical model of the hand-arm system with the glove can be used to evaluate the performance of the material inside the glove. Furthermore, the analytical simulation can identify the proper size of the damping material to be used for both the palm and finger sides.

For the tested damping materials, by increasing the applied pressure, the overall VT decreased. Since for an anti-vibration glove, the applied pressure on the material depends on the applied feed and grip forces, the only way for increasing the pressure on the damping material is by reducing the coverage area of material inside the glove. This means that not all the surface area of the glove should be covered with damping material. It should also allow for hollow space between different parts of the damping material inside the glove. Therefore, careful design for the damping material is required to guarantee that the hand will only be in contact with the damping material, and that no point of the hand will have direct contact with the handle. This guarantees that all vibration transmissibility goes through the damping material, and not the space between them. Studies showed that contact pressure between the hand and handle does not distribute evenly. The distribution pattern of contact pressure can be used to properly locate the position of damping material inside the glove.

The other alternative way for reducing VT is by wrapping damping material around the handle of the power tool, and not by putting it inside the glove. Either way of using the damping material, the overall diameter of the handle increases which decreases the comfort of the operator. Therefore, this study suggests that the existing handle of the power tool be replaced with handles which have smaller diameter. This not only controls the overall diameter of the handle, but also helps for increasing the

thickness of damping material between the hand and handle without decreasing the comfort of the operator. Therefore, higher vibration attenuation should be possible.

8 Conclusions

This study shows that for measurement of the hand-arm vibration transmissibility, using several accelerometers at different parts of the palm leads to having a clearer picture of the vibration transmissibility at the palm. This helps in the design process of anti-vibration gloves. Furthermore, for choosing proper damping material inside the glove, the vibration transmissibility of the candidate materials should be measured under various load pressures.

8.1 Handle

In HAV tests both feed and grip forces should be measured, and by putting the measuring sensors as close as possible to the hand, a better picture of HAV is achievable. For improved accuracy of the measurement, the system should not have any resonance to interfere with the measured accelerations; therefore, the first resonance of the system should be higher than the highest frequency in this test. This research has shown that with careful design and optimization, the resonance of the handle can be increased while the flexibility of the handle at the measuring points remains the same.

Since the wrist of the hand can easily apply bending moments to the handle, by just aligning the forearm with the handle, the alignment of the applied forces with the handle cannot be guaranteed. By measuring forces at the top and bottom of each side of the handle, the angles of the applied forces are measureable. By monitoring these angles for the operator during the test, the applied forces can be aligned with the direction of vibration. This not only improve the accuracy of the result, but also protected the exciter system from any undesired applied torque.

8.2 Adaptor

The suggested palm adaptor in the ISO standard has a solid structure and it is much stiffer than the skin of the palm. There are many issues with this adaptor, such as:

- The adaptor results cannot show the resonance of the hand-arm system in the bare hand test and therefore underestimates the vibration of the palm for frequencies below $50Hz$; therefore, the ratio of the two weighted VT from the bare hand test and the glove test cannot show the VT of the glove.
- Due to the solid structure of the adaptor, it cannot adjust its shape with the non-uniform shape of the palm; therefore, it cannot have proper contact with the palm of the hand. Furthermore, by putting the adaptor inside the glove since the adaptor and the palm do not have same curvature and shape, the shape of the glove will not remain the same as it was before introducing the adaptor for the measurement.
- The adaptor only provides one measure of the palm vibration behaviour, and it cannot measure vibrations at different parts of the palm. The measured vibration with this type of adaptor is the average vibration over the entire contact area of the adaptor with either the handle or the glove and not the palm. As the result of the bare hand test shows, it measures the vibration of the handle and not the vibration of the hand. Therefore the solid structure adaptor may be useful in the field test for measuring the vibration of the handle and not the hand.
- Measured contact force on the handle showed that the contact force between the hand and handle is not evenly distributed. Therefore, the hand does not apply an even contact force to either the handle or the glove. However, the adaptor is solid and distributes the force evenly over the contact surface. Since the VT of the material inside the glove is a function of the applied force, by introducing

the adaptor to the system, the VT of the glove will not remain the same. As a result, the measured VT with the adaptor cannot show the actual VT of the glove when there is no adaptor.

- The curvature of the adaptor should be close to that of the handle to increase the accuracy of the vibration measurement. It was also found that the size of the adaptor should also depend on the size of the operator's hand. Since all the power tools do not have same handle's diameter, and in addition, all the operators do not have same hand size, different shapes and sizes of the adaptor should be used for the HAV tests to remove this effect.
- It is difficult to align the adaptor with the direction of vibration. In the glove test, when the glove is in between the adaptor and the handle, even putting a slit in the seam of the glove only helps to monitor one of the misalignment angles with the handle and not all (Figure 2-10).

8.3 Strap

In this study, a strap with three miniature accelerometers has been used. Since this strap is flexible, the accelerometers in it can easily adjust themselves with the surface of their contact points. As a result, they can easily measure the vibration of the palm at their locations. The result of the bare hand tests show that all of these accelerometers can see the resonance of the hand-arm system at low frequency, while the adaptor fails to see it. For the rest of the frequencies, they have a proper agreement with the adaptor and the handle. Therefore, the miniature accelerometers actually represent the vibration behaviour of different parts of the palm with more accuracy than the adaptor.

8.4 Material vibration transmissibility

The VT of a material is a function of many parameters such as the applied force and the amount of the material; therefore, the VT of a specific shape and size of the material under a specific load cannot define the VT of the material. This study suggests to use various sizes of the sample with constant load for measuring the VT of the sample for various coverage areas. The result of these measurements can also be used as the VT of constant size of the sample under various loads.

The mechanical properties such as mass, stiffness and damping coefficient of the tested materials have linear relationship with the size of the samples. Therefore, for each of these samples a 1-DOF lumped-mass model can represent the vibration behaviour of the sample. For these tested materials, both stiffness and damping coefficients of the model should be complex values. The value of these parameters can be derived by using the measured VT of different sizes of the sample under constant load, and by minimizing the error between the measured VT and calculated VT from the model. With this generated model, the VT for any arbitrary size of the sample, can be derived from simulation.

All the measured VT spectra of the tested samples show at least one resonance in the test frequency range. The frequency of this resonance for different sizes of the sample has linear relationship with the size of the sample. Therefore, by decreasing the size of the material, the frequency of the resonance decreases and as a result the overall vibration attenuation increases.

8.5 Future work / Recommendations

In the last few decades many researchers have studied hand-arm vibration; however, there are still many aspects that need to be further investigated.

8.5.1 Vibration spectra and directions

The performance of a glove depends on many parameters such as direction(s) of vibration and the applied forces. Since many of the power tools generate vibration in more than one direction, generating vibration in only one direction is not sufficient for evaluating a glove. In addition, since the defined vibration spectra in the standard does not cover vibration spectra of all power tools, it should not be used for evaluating a glove for all power tools. The glove should be evaluated individually for different groups of power tools. Therefore, by measuring the generated vibration in all three orthogonal directions for each group of power tools, and regenerating the same vibration during HAV tests, the glove can be evaluated for that group of power tools.

8.5.2 Vibration transmissibility at the fingers

The designed handle in this study can measure the vibration at both front and back sides of the handle. The accelerometer in the back half-cylindrical part can be used to calculate the VT to the fingers. For this purpose, miniature accelerometers can be used at the fingers side. These accelerometers can be mounted on a thin glove to maintain their positions. The weight of this type of accelerometer is 0.2 gram and average weight of fingers in the analytical model is assumed to be 7.6 gram (Table 6.3); therefore, they should not have a significant effect on the vibration behaviour of the fingers.

8.5.3 Field test

The strap method can be used to measure the VT of a glove in the field test. For this purpose, by using two straps, one inside the glove and one outside the glove, the VT of the glove is measureable. The standard suggests to put a slit in the seam of the glove for aligning the adaptor. This slit can also be used to lock the two straps together which helps to align the two straps. By mounting same numbers of accelerometer with the same locations on both of the straps, the VT at those locations become measureable. With the adaptor method only the average VT is measureable, while, with this method a clearer picture of the VT for a certain glove in the field test will be generated.

8.5.4 Material vibration transmissibility

For measuring the VT of material, the gripping force was simulated with a $2.5kg$ mass. The change of the grip force leads to the change of VT of the glove [108]; therefore, for measuring mechanical behaviour of the material, different masses with different weights should be used to simulate different gripping forces on the whole disk of the sample. The other alternative is to measure VT while the top mass remains the same and the amount of the sample under the weight changes.

8.5.5 Comparison with an anti-Vibration glove

The tested glove in this study does not have uniform damping material at the palm side. The result shows that for this glove the VT at different parts of the glove is not the same; therefore, the measurement with the adaptor is not accurate. Although, the ISO requests for a glove with uniform damping material, the pressure on different parts of the glove is not uniform and as a result the VT at different parts cannot be

the same. Further investigation on other commercial gloves and also anti-vibration gloves may prove the outcome of this research and show that the strap method is more reliable and gives a better picture for VT of the glove.

References

1. *The minimum health and safety requirements regarding the exposure of workers to the risks arising from physical agents*, E.A.f.s.a. health, Editor. 2002.
2. *Health and Safety Executive*. [cited 2016 12/02/2016]; Available from: http://www.hse.gov.uk/vibration/hav/advicetoemployers/responsibilities.htm.
3. Vergara, M., J.n.-L. Sancho, P. Rodrı´guez, and A.P.r.-G. lez, *Hand-transmitted vibration in power tools: Accomplishment of standards and users' perception.* international Journal of Industrial Ergonomics, 2008. **38**(9-10): p. 652-660.
4. Griffin, M.J., H.V.C. Howarth, P.M. Pitts, S. Fischer, U. Kaulbars, P.M. Donati, and P.F. Bereton *Guide to good practice on Hand-Arm Vibration* HAV Good practice Guide, 2006.
5. Peterson, D.R., A.J. Brammer, and M.G. Cherniack, *Exposure monitoring system for day-long vibration and palm force measurements.* International Journal of Industrial Ergonomics, 2008. **38**(9-10): p. 676-686.
6. Edwards, D.J. and G.D. Holt, *Hand-Arm vibration exposure from construction tools: results of a field study.* Construction Management and Economics, 2006. **24**(2): p. 209-217.
7. ISO, *5349-Mechanical vibration - Measurement and evaluation of human exposure to hand-transmitted vibration*, in *5349*. 2001.
8. Hewitt, S. and H. Mason, *A critical review of evidence related to hand-arm vibration syndrome and the extent of exposure to vibration*, in *Health and Safety Executive*. 2015.
9. Sampson, E. and J.L. Niekerk, *Literature Survey on Anti-Vibration Gloves*. 2003, SIMRAC Health 806.
10. Wasserman, D.E. *Hand-Arm Vibration Standards: The New ANSI S2.70 Standard*. 2006; Available from: http://www.chaseergo.com/index.htm.
11. Dong, R.G., D.E. Welcome, T.W. McDowell, X.S. Xu, K. Krajnak, and J.Z. ZU, *A Proposed Theory on Biodynamic Frequency Weighting for Hand-Transmitted Vibration Exposure.* Industrial Health, 2012. **50**: p. 412-424.
12. Dong, R.G., D.E. Welcome, T.W. McDowell, J.Z. J.Z Wu, and A.W. Schopper, *Frequency weighting derived from power absorption of fingers-hand-arm system under z(h)-axis vibration.* J Biomech, 2006. **39**(12): p. 2311-2324.
13. Griffin, M.J., *Measurement, evaluation and assessment of occupational exposures to hand-transmitted vibration.* Occupational Enviromental Medicine, 1996(54): p. 73-89.
14. Mahbub, H., K. Yokoyama, S. Laskar, M. Inoue, Y. Takahashi, S. Yamamoto, and N. Harda, *Assessing the Influence of Antivibration Glove on Digital Vascular Responses to Acute Hand-arm Vibration.* Occup Health, 2007(49): p. 165-171.

15. Terada, K., N. Miyai, Y. Maejima, S. SakaGuchi, T. Tomura, K. Yoshimasu, I. Morioka, and K. Miyashita, *Laser Doppler Imaging of Skin Blood Flow for Assessing Peripheral Vascular Impairment in Hand-Arm Vibration Syndrome* Industrial Health, 2006(45): p. 309-317.

16. Cederlund, R., A. Isacsson, and G. Lundborg, *Hand Function in Workers with Hand-Arm Vibration Syndrome.* Journal of Hand Therapy, 1999(12): p. 16-24.

17. Necking, L.E., R. Lundstrom, L.B. Dahlin, G. Lundborg, L.-E. Thornell, and J. Frden, *Tissue Displacement is a Causative Factor in Vibration-Induced Muscle Injury.* Journal of Hand Surgery, 1996. **6**: p. 753-757.

18. Ainsa, I., D. Gonzalez, M. Lizaranzu, and C. Bernad, *Experimental evaluation of uncertainty in hand–arm vibration measurements.* International Journal of Industrial Ergonomics, 2011. **41**(2): p. 167-179.

19. Tarabini, M., B. Saggin, D. Scaccabarozzi, and G. Moschioni, *The potential of micro-electro-mechanical accelerometers in human vibration measurements.* Journal of Sound and Vibration, 2012. **331**(2): p. 487-499.

20. ISO, *10819-Mechanical vibration and shock - Hand-arm vibration - Method for the measurement and evaluation of the vibration transmissibility of gloves at the palm of the hand*, in *10819*. 1996.

21. ISO, *10819-Mechanical vibration and shock - Hand-arm vibration - Measurement and evaluation of the vibration transmissibility of gloves at the palm of the hand*, in *10819*. 2013.

22. Welcome, D.E., R.G. Dong, X.S. Xu, C. Warren, T.W. McDowell, and J.Z. Wu, *An examination of the vibration transmissibility of the hand-arm system in three orthogonal directions.* International Journal of Industrial Ergonomics, 2014. **45**: p. 21-34.

23. Xiao, J. and F. Zheng, *Measurement and evaluation of attenuation effectiveness of antivibration gloves*, in *Eighth International Conference on Hand-Arm Vibration*. 1998.

24. Kihlberg, S., *Biodynamic response of the hand-arm system to vibration from an impact hammer and a grinder.* International Journal of Industrial Ergonomics, 1994(16): p. 1-8.

25. Hewitt, S., *Triaxial measurements of the performance of anti-vibration gloves*. 2010, Health and Safety Laboratory.

26. Griffin, M.J., *Evaluating the effectiveness of gloves in reducing the hazards of hand-transmitted vibration.* International Journal of Industrial Ergonomics, 1998(55): p. 340-348.

27. Radwin, R.G., T.J. Armstrong, and E. Vanbergeijk, *Vibration Exposure for selected power hand tools used in automobile assembly.* American Industrial Hygiene Association, 1990(51(9)): p. 510-518.

28. Dewangan, K.N. and V.K. Tewari, *Characteristics of hand-transmitted vibration of a hand tractor used in three operational modes.* International Journal of Industrial Ergonomics, 2009. **39**(1): p. 239-245.

29. Dong, R.G., S. Rakheja, W.P. Smutz, A. Schopper, D. Welcome, and J.Z. Wu, *Effectiveness of a new method (TEAT) to assess vibration transmissibility of gloves.* International Journal of Industrial Ergonomics, 2002(30): p. 33-48.

30. ISO, *10068-Mechanical vibration and shock - Mechanical impedance of the human hand-arm system at the driving point*, in *10068*. 2012.

31. Reynolds, D.D. and R.J. Falkenberg, *A study of hand vibration on chipping and grinding operators, part II- Four-degree-of-freedom lumped parameter model of the vibration response of the human hand.* Journal of Sound and Vibration, 1984. **95**(4): p. 499-514.

32. Burstrom, L., *Measurements of the impedance of the hand and arm.* Occupational Enviromental Health, 1990(62): p. 431-439.

33. Reynolds, D.D. and J.K. Stein, *Design and evaluation of an inexpensive test fixture for conducting glove vibration test per ISO standard 10819*, in *8th International Conference on Hand-Arm Vibration*. 1998: Umea, Sweden.

34. Oddoa, R., T. Loyaub, P.E. Boileauc, and Y. Champoux, *Design of a suspended handle to attenuate rockdrill hand-arm vibration: model development and validation.* Journal of Sound and Vibration, 2004. **275**(3-5): p. 623-640.

35. Aldien, Y., D. Welcome, S. Rakheja, R. Dong, and P.E. Boileau, *Contact pressure distribution at hand–handle interface: role of hand forces and handle size.* International Journal of Industrial Ergonomics, 2005. **35**(3): p. 267-286.

36. Besa, A.J., F.J. Valero, J.L. Suner, and J. Carballeira, *Characterisation of the mechanical impedance of the human hand–arm system: The influence of vibration direction, hand–arm posture and muscle tension.* International Journal of Industrial Ergonomics, 2007. **37**(3): p. 225-231.

37. Tarabini, M., B. Saggin, D. Scaccabarozzi, and G. Moschioni, *Hand-Arm mechanical impedance in presence of unknown vibration direction.* International Journal of Industrial Ergonomics, 2013. **43**(1): p. 52-61.

38. Rakheja, S., R. Dong, D. Welcome, and A.W. Schopper, *Estimation of tool-specific isolation performance of anti-vibration gloves.* International Journal of Industrial Ergonomics, 2002(30): p. 71-87.

39. Dong, R.G., T.W. McDowell, D. Welcome, J. Barkley, C. Warren, and B. Washington, *Effects of Hand-Tool Coupling Conditions on the Isolation Effectiveness of Air Bladder Anti-Vibration Gloves.* Journal of low frequency noise, vibration and active control, 2004: p. 231-248.

40. Reynolds, D.D. and E. Wolf, *Evaluation of Antivibration Glove Test Protocols Associated with the Revision of ISO 10819.* Industrial Health, 2005(43): p. 556-565.

41. Dong, R.G., D.E. Welcome, T.W. McDowell, and J.Z. Wu, *Measurement of biodynamic response of human hand–arm system.* journal of Sound and Vibration, 2006. **294**(4-5): p. 807-827.

42. Xu, X.S., D.E. Welcome, T.W. McDowell, C. Warren, and R.G. Dong, *An investigation on characteristics of the vibration transmitted to wrist and elbow in the operation of impact wrenches.* International Journal of Industrial Ergonomics, 2009. **39**(1): p. 174-184.

43. Dong, R.G., D.E. Welcome, X. S.Xu, C. Warren, T. W.McDowell, J.Z. Wua, and S.R. b, *Mechanical impedances distributed at the fingers and palm of the human hand in three orthogonal directions.* Journal of Sound and Vibration, 2011. **331**(5): p. 1191-1206.

44. Welcome, D.E., R.G. Dong, X.S. Xu, C. Warren, and T.W. McDowell, *An evaluation of the proposed revision of the anti-vibration glove test method defined in ISO 10819.* International Journal of Industrial Ergonomics, 2011. **42**(1): p. 143-155.

45. Xu, X.S., D.E. Welcome, C. Warren, T.W. McDowell, and R.G. Dong, *Examination of the adaptor approach for the measurement of Hand-Transmitted Vibration Exposure.* 2011. **39 No.2**: p. 32-33.

46. Dong, R.G., D.E. Welcome, T.W. McDowell, and J.Z. Wu, *Modeling of the biodynamic responses distributed at the fingers and palm of the hand in three orthogonal directions.* Journal of Sound and Vibration, 2012. **332**(4): p. 1125-1140.

47. Welcome, D.E., R.G. Dong, X.S. Xu, C. Warren, and T.W. McDowell, *The effects of vibration-reducing gloves on finger vibration.* International Journal of Industrial Ergonomics, 2014. **44**(1): p. 45-59.

48. Xu, X.S., R.G. Dong, D.E. Welcome, C. Warren, and T.W. McDowell, *An examination of the handheld adapter approach for measuring hand-transmitted vibration exposure.* Measurement, 2014. **47**: p. 64-77.

49. Reynolds, D.D. and R.H. Keith, *Hand-Arm vibration, Part I-Analytical model of the vibration response characteristics of the hand.* Journal of Sound and Vibration, 1976(51): p. 237-253.

50. Dong, R.G., J.H. Dong, J.Z. Wu, and S. Rakheja, *Modeling of biodynamic responses distributed at the fingers and the palm of the human hand–arm system.* Journal of Biomechanics, 2006. **40**(10): p. 2335-2340.

51. Oka, H. and T. Yammaoto, *Measurement of Biomechanical Impedance -Its device and measuring conditions*, in *Memoirs of the Faculty of Engineering*. 1988, Okayama.

52. Gurram, R., S. Rakheja, and G.K. Gouw, *Mechanical impedance of the human hand-arm system subject to sinusoidal and stochastic excitations.* International Journal of Industrial Ergonomics, 1994(16): p. 135-145.

53. Aldien, Y., P. Marcotte, S. Rakheja, and P.E. Boilea, *Influence of hand–arm posture on biodynamic response of the human hand–arm exposed to zh-axis vibration.* International Journal of Industrial Ergonomics, 2005. **36**(1): p. 45-59.

54. Adewusi, S.A., S. Rakheja, P. Marcotte, and P.E. Boileau, *On the discrepancies in the reported human hand–arm impedance at higher frequencies.* International Journal of Industrial Ergonomics, 2008. **38**(9-10): p. 703-714.

55. Knez, L., J. Slavič, and M. Boltežar, *A Multi-Axis Biodynamic Measuring Handle for a Human Hand-Arm System.* Journal of Mechanical Engineering, 2012. **59**(2): p. 71-80.

56. Dong, R.G., D.E. Welcome, T.W. McDowell, and J.Z. Wu, *Analysis of handle dynamics-induced errors in hand biodynamic measurements.* Journal of Sound and Vibration, 2008. **318**(4-5): p. 1313-1333.

57. Wimer, B., R.G. Dong, D.E. Welcome, C. Warren, and T.W. McDowell, *Development of a new dynamometer for measuring grip strength applied on a cylindrical handle.* Medical Engieering & Physics, 2009. **31**(6): p. 695-704.

58. Lee, J.W. and K. Rim, *Measurement of finger joint angles and maximum finger forces during cylinder grip activity.* Scientific and Technical Record, 1990.

59. Burstrom, L., *The influence of biodynamic factors on the mechanical impedance of the hand and arm.* Int Arch Occp Environ Health, 1997(69): p. 437-446.

60. Gurram, R., S. Rakheja, and G.J. Gouw, *A study of hand grip pressure distribution and EMG of finger flexor muscles under dynamic loads.* Ergonomics, 1995. **38**(4): p. 684-699.

61. Wimer, B., T.W. McDowell, X.S. Xu, D.E. Welcome, C. Warren, and R.G. Dong, *Effects of gloves on the total grip strength applied to cylindrical handles.* International Journal of Industrial Ergonomics, 2010. **40**(5): p. 574-583.

62. Paddan, G.S. and M.J. Griffin, *Measurement of glove and hand dynamics using knuckle vibration*, in *9th International Conference on Hand-Arm Vibration*. 2001.

63. Vigouroux, L., J. Rossi, M. Foissac, L. Grelot, and E. Berton, *Finger force sharing during an adapted power grip task.* Neurosci Lett, 2011. **504**(3): p. 290-294.

64. Pyykkö, I., M. Färkkilä, J. Toivanen, O. Korhonen, and J. Hyvärinen, *Transmission of vibration in the hand-arm system with special reference to changes in compression force and acceleration.* Scandinavian Journal of Work, Environment & Health, 1976. **2**(2): p. 87-95.

65. Aatola, S., *Transmission of vibration to the wrist and comparison of frequency response function estimators.* Journal of Sound and Vibration, 1989. **131**(3): p. 497-507.

66. Gurram, R., S. Rakheja, and G.J. Gouw, *Vibration transmission characteristics of the human hand-arm and gloves.* International Journal of Industrial Ergonomics, 1994. **13**: p. 217-234.

67. Cherian, T., S. Rakheja, and R.B. Bhat, *An analytical investigation of an energy flow divider to attenuate hand-transmitted vibration.* International Journal of Industrial Ergonomics, 1995. **17**: p. 455-467.

68. Welcome, D., S. Rakheja, R. Dong, J.Z. Wu, and A.W. Schopper, *An investigation on the relationship between grip, push and contact forces*

applied to a tool handle. International Journal of Industrial Ergonomics, 2004. **34**(6): p. 507-518.

69. Marcotte, P., Y. Aldien, P.E. Boileau, S. Rakheja, and J. Boutin, *Effect of handle size and hand–handle contact force on the biodynamic response of the hand–arm system under zh-axis vibration.* Journal of Sound and Vibration, 2005. **283**(3-5): p. 1071-1091.

70. Scalise, L., F. Rossetti, and N. Paone, *Non-contact measurement of local transmissibility.* Int Arch Occup Environ Health, 2007(81): p. 31-40.

71. Shibata, N. and S. Maeda, *Effect of tool handle diameter on temporary threshold shift (TTS) of vibrotactile perception.* International Journal of Industrial Ergonomics, 2008. **38**(9-10): p. 697-702.

72. Kong, Y.-K. and B.D. Lowe, *Evaluation of handle diameters and orientations in a maximum torque task.* International Journal of Industrial Ergonomics, 2005. **35**(12): p. 1073-1084.

73. Kong, Y.-K. and B.D. Lowe, *Optimal cylindrical handle diameter for grip force tasks.* International Journal of Industrial Ergonomics, 2004. **35**(6): p. 495-507.

74. Hewitt, S., *Assessing the Performance of Antivibration Gloves.* 1996. **42**(4): p. 245-252.

75. Concettoni, E. and M. Griffin, *The apparent mass and mechanical impedance of the hand and the transmission of vibration to the fingers,hand,and arm.* Journal of Sound and Vibration, 2009. **325**(3): p. 664-678.

76. Xu, X.S., D.E. Welcome, T.W. McDowell, J.Z. Wu, B. Wimer, C. Warren, and R.G. Dong, *The vibration transmissibility and driving-point biodynamic response of the hand exposed to vibration normal to the palm.* International Journal of Industrial Ergonomics, 2011. **41**(5): p. 418-427.

77. Xu, X.S., R.G. Dong, D.E. Welcome, C. Warren, and T.W. McDowell, *An examination of an adapter method for measuring the vibration transmitted to the human arms.* Measurement, 2015. **73**: p. 318-334.

78. Rossi, G.L. and E.P. Tomasini, *Hand-Arm vibration measurement by a laser scanning vibrometer.* Measurement, 1995(16): p. 113-124.

79. Smutz, W.P., R.G. Dong, B. Han, A.W. Schopper, D.E. Welcome, and M.L. Kashon, *A Method for Reducing Adaptor Misalignment when Testing Gloves Using ISO 10819.* Annals of Occupational Hygiene, 2002. **46**(3): p. 309-315.

80. Dong, R.G., T.W. McDowell, D.E. Welcome, W.P. Smutz, A.W. Schopper, C. Warren, J.Z. Wu, and S. Rakheja, *On-the-hand measurement methods for assessing effectiveness of anti-vibration gloves.* International Journal of Industrial Ergonomics, 2003. **32**(4): p. 283-298.

81. Dong, R.G., S. Rakheja, T.W. McDowell, D.E. Welcome, and J.Z. Wu, *Estimation of the Biodynamic Responses Distributed at Fingers and Palm Based on the Total Response of the Hand-Arm System.* International Journal of Industrial Ergonomics, 2010. **40**(4): p. 425-436.

82. Aldien, Y., P. Marcotte, S. Rakheja, and P.-É. Boileau, *Mechanical Impedance and Absorbed Power of Hand-Arm under xh–Axis Vibration and Role of Hand Forces and Posture.* Industrial Health, 2005(43): p. 495-508.

83. Adewusi, S., S. Rakheja, and P. Marcotte, *Biomechanical models of the human hand-arm to simulate distributed biodynamic responses for different postures.* International Journal of Industrial Ergonomics, 2012. **42**(2): p. 249-260.

84. Dong, R.G., T.W. McDowell, D.E. Welcome, C. Warren, J.Z. Wu, and S. Rakheja, *Analysis of anti-vibration gloves mechanism and evaluation methods.* Journal of Sound and Vibration, 2009. **321**(1-2): p. 435-453.

85. Adewusi, S.A., S. Rakheja, P. Marcotte, and J. Boutin, *Vibration transmissibility characteristics of the human hand–arm system under different postures, hand forces and excitation levels.* Journal of Sound and Vibration, 2010. **329**(14): p. 2953-2971.

86. Moschioni, G., B. Saggin, and M. Tarabini, *Prediction of data variability in hand-arm vibration measurements.* Measurement, 2011. **44**(9): p. 1679-1690.

87. Bylund, S.H. and L. Burstrom, *The influence of gender, handle size, anthropometric measures, and vibration on the performance of a precision task.* International Journal of Industrial Ergonomics, 2006. **36**(10): p. 907-917.

88. Dong, R.G., D. E.Welcome, T.W. McDowell, and J.Z. Wu, *Methods for deriving a representative biodynamic response of the hand–arm system to vibration.* Journal of Sound and Vibration, 2009. **325**(4-5): p. 1047-1061.

89. Dong, R.G., T.W. McDowell, and D.E. Welcome, *Biodynamic Response at the Palm of the Human Hand Subjected to a Random Vibration.* Industrial Health, 2004(43): p. 241-255.

90. McDowell, T.W., S.F. Wiker, R.G. Dong, and D.E. Welcome, *Effects of vibration on grip and push force-recall performance.* International Journal of Industrial Ergonomics, 2007. **37**(3): p. 257-266.

91. Dong, R.G., D.E. Welcome, and J.Z. WU, *Estimation of Biodynamic Forces Distributed on the Fingers and the Palm Exposed to Vibration.* Industrial Health, 2005(43): p. 485-494.

92. Dong, R.G., J.Z. Wu, T.W. McDowell, D.E. Welcome, and A.W. Schopper, *Distribution of mechanical impedance at the fingers and the palm of the human hand.* Journal of Biomechanics, 2005. **38**(5): p. 1165-1175.

93. Dong, R.G., J.Z. Wu, D.E. Welcome, and T.W. McDowell, *Estimation of Vibration Power Absorption Density in Human Fingers.* Journal of Biomechanical Engineering, 2005. **127**(5): p. 849-856.

94. Dong, R.G., D.E. Welcome, T.W. McDowell, and J.Z. Wu, *Biodynamic Response of Human Fingers in a Power Grip Subjected to a Random Vibration.* Journal of Biomechanical Engineering, 2004. **126**(4): p. 447.

95. Dewangan, K.N. and V.K. Tewari, *Vibration energy absorption in the hand–arm system of hand tractor operator.* Biosystems Engineering, 2009. **103**(4): p. 445-454.

96. Marcotte, P., *Comments on ''A discussion on comparing alternative measures with frequency-weighted accelerations defined in ISO Standards'' [R.G. Dong, J.Z. Wu, D.E. Welcome, T.W. McDowell, Journal of Sound and Vibration]*. Journal of Sound and Vibration, 2008. **317**(3-5): p. 1051-1056.

97. Aldien, Y., P. Marcotte, S. Rakheja, and P.E. Boileau, *Influence of hand forces and handle size on power absorption of the human hand–arm exposed to zh-axis vibration.* Journal of Sound and Vibration, 2006. **290**(3-5): p. 1015-1039.

98. Dong, J.H., R.G. Dong, S. Rakheja, D.E. Welcome, T.W. McDowell, and J.Z. Wu, *A method for analyzing absorbed power distribution in the hand and arm substructures when operating vibrating tools.* Journal of Sound and Vibration, 2008. **311**(3-5): p. 1286-1304.

99. Dong, R.G., A.W. Schopper, T.W. McDowell, D.E. Welcome, J.Z. Wu, W.P. Smutz, C. Warren, and S. Rakheja, *Vibration energy absorption (VEA) in human fingers-hand-arm system.* Medical Engineering & Physics, 2004. **26**(6): p. 483-492.

100. Dong, R.G., J.Z. WU, and D.E. Welcome, *Recent Advances in Biodynamics of Human Hand-Arm System.* Industrial Health, 2005(43): p. 449-471.

101. Thomas, M. and Y. Beauchamp, *Development of a new frequency weighting filter for the assessment of grinder exposure to wrist-transmitted vibration.* Computers ind. Engng, 1998. **35**: p. 651-654.

102. Z.Wu, J., R.G. Dong, D.E. Welcome, and X.S. Xu, *A method for analyzing vibration power absorption density in human fingertip.* Journal of Sound and Vibration, 2010. **329**(26): p. 5600-5614.

103. Tudor, A.H., *Hand-Arm Vibration: Product Design Principles.* Journal of Safety Research, 1996. **27**: p. 157-162.

104. Saggin, B., D. Scaccabarozzi, and MarcoTarabini, *Optimized design of suspension systems for hand–arm transmitted vibration reduction.* journal of Sound and Vibration, 2012. **331**(11): p. 2671-2684.

105. Mallick, Z., *Optimization of operating parameters for a back-pack type grass trimmer.* International Journal of Industrial Ergonomics, 2008. **38**(1): p. 101-110.

106. Singh, J. and A.A. Khan, *Effect of coating over the handle of a drill machine on vibration transmissibility.* Applied Ergonomics, 2014. **45**(2): p. 239-246.

107. O'Boyle, M. and M.J. Griffin, *Inter-subject variability in the measurement of the vibration transmissibility of gloves according to current standards*, in *9th International Conference on Hand-Arm vibration*. 2001: Nancy (F).

108. Hewitt, S., R.G. Dong, D.E. Welcome, and T.W. McDowell, *Anti-vibration gloves?* Ann Occup Hyg, 2015. **59**(2): p. 127-41.

109. Dong, R.G., S. Rakhejab, T.W. McDowell, D.E. Welcome, J.Z. Wu, C. Warren, J. Barkley, B. Washington, and A.W. Schopper, *A method for assessing the effectiveness of anti-vibration gloves using biodynamic*

responses of the hand–arm system. Journal of Sound and Vibration, 2005. **282**(3-5): p. 1101-1118.

110. Dong, R.G., T.W. McDowell, D.E. Welcome, and W.P. Smutz, *Correlations between biodynamic characteristics of human hand–arm system and the isolation effectiveness of anti-vibration gloves.* International Journal of Industrial Ergonomics, 2005. **35**(3): p. 205-216.

111. Scarpa, F., J.A. Giacomin, A. Bezazi, and W.A. Bullough, *Dynamic behavior and damping capacity of auxetic foam pads*. 2006.

112. ISO, *13753-Mechanical vibration and shock - Hand-arm vibration - Method for measuring the vibration transmissibility of resilient materials when loaded by the hand-arm system*, in *13753*. 1998.

113. ISO, *13753-Mechanical vibration and shock - Hand-arm vibration - Method for measuring the vibration transmissibility of resilient materials when loaded by the hand-arm system*, in *13753*. 2008.

114. Koton, J., P. Kowalski, and J. Szopa, *An attempt to construct antivibration gloves on the basis of information on the vibration transmissibility of materials*, in *Eighth International Conference on Hand-Arm Vibration*. 1998.

115. Scarpa, F., J. Giacomin, Y. Zhang, and P. Pastorino, *Mechanical Performance of Auxetic Polyurethane Foam for Antivibration Glove Applications*, in *Cellular Polymers*. 2005.

116. Kaulbars, U., *Main parameters influencing damping performance of resilient materials.* Eighth International Conference on Hand-Arm Vibration, 1998.

117. Welcome, R.G.D.D.E., T.W. McDowell, and S. Rakheja, *Estimation of the transmissibility of anti-vibration gloves when used with specific tools*. 2005, Transmissibility of Anti-Vibration Gloves.

118. Dong, R.G., D.E. Welcome, D.R. Peterson, X.S. Xu, T.W. McDowell, C. Warren, T. Asaki, S. Kudernatsch, and A. Brammer, *Tool-specific performance of vibration-reducing gloves for attenuating palm-transmitted vibrations in three orthogonal directions.* International Journal of Industrial Ergonomics, 2014. **44**(6): p. 827-839.

119. Pinto, I., N. Stacchini, M. Bovenzi, G.S. Paddan, and M.J. Griffin, *Protection effectiveness of anti-vibration gloves - field evaluation and laboratory performance assessment*. 2001, Vibration Injury Network.

120. Cabeças, J.M. and R.J. Milho, *The efforts in the forearm during the use of anti-vibration gloves in simulated work tasks.* International Journal of Industrial Ergonomics, 2011. **41**(3): p. 289-297.

121. Dong, R.G., T.W. McDowell, D.E. Welcome, S. Rakheja, S.A. Caporali, A.W. Schopper, and A.I. Schoppe, *Effectiveness of a transfer function method for evaluating vibration isolation performance of gloves when used with chipping hammers.* Journal of low frequency noise, vibration and active control, 2002: p. 141-156.

122. Shibata, N. and S. Maeda, *Vibration-isolating Performance of Cotton Work Gloves Based on Newly Issued JIS T8114.* Industrial Health, 2008(46): p. 477-483.

123. Rakheja, S., R. Gurram, and G.J. Gouw, *Development of Linear and nonlinear hand-arm vibration models using optimization and linearization techniques*. Vol. 26. 1992.

124. Rakheja, S., J.Z. WU, R.G. Dong, and A.W. Schopper, *A comparison of biodynamic models of the human hand-arm system for applications to hand-held power tools.* Journal of Sound and Vibration, 2002. **249**(1): p. 55-82.

125. Marcotte, P., J. Boutin, and J. Jasinski, *Development of a hand–arm mechanical analogue for evaluating chipping hammer vibration emission values.* Journal of Sound and Vibration, 2010. **329**(10): p. 1968-1980.

126. Dobry, M.W. and T. Hermann, *A comparison of human physical models based on the distribution of power in a dynamic structure in the case of hand-arm vibrations.* Journal of Theoretical and applied mechanics, 2015(53): p. 3-13.

127. *Guide to adhesively mounting accelerometers*, MEGGITT and s.e.f.e. enviroments, Editors.

128. Sim, S. and K.J. Kim, *A Method to determine the complex modulus and Poisson's ratio of viscoelastic materials for FEM applications.* Journal of Sound and Vibration, 1989(141(1)): p. 71-82.

129. Kattel, B.P. and J.E. Fernandez, *The effects of rivet guns on hand-arm vibration.* International Journal of Industrial Ergonomics, 1999. **23**: p. 595-608.

Appendix

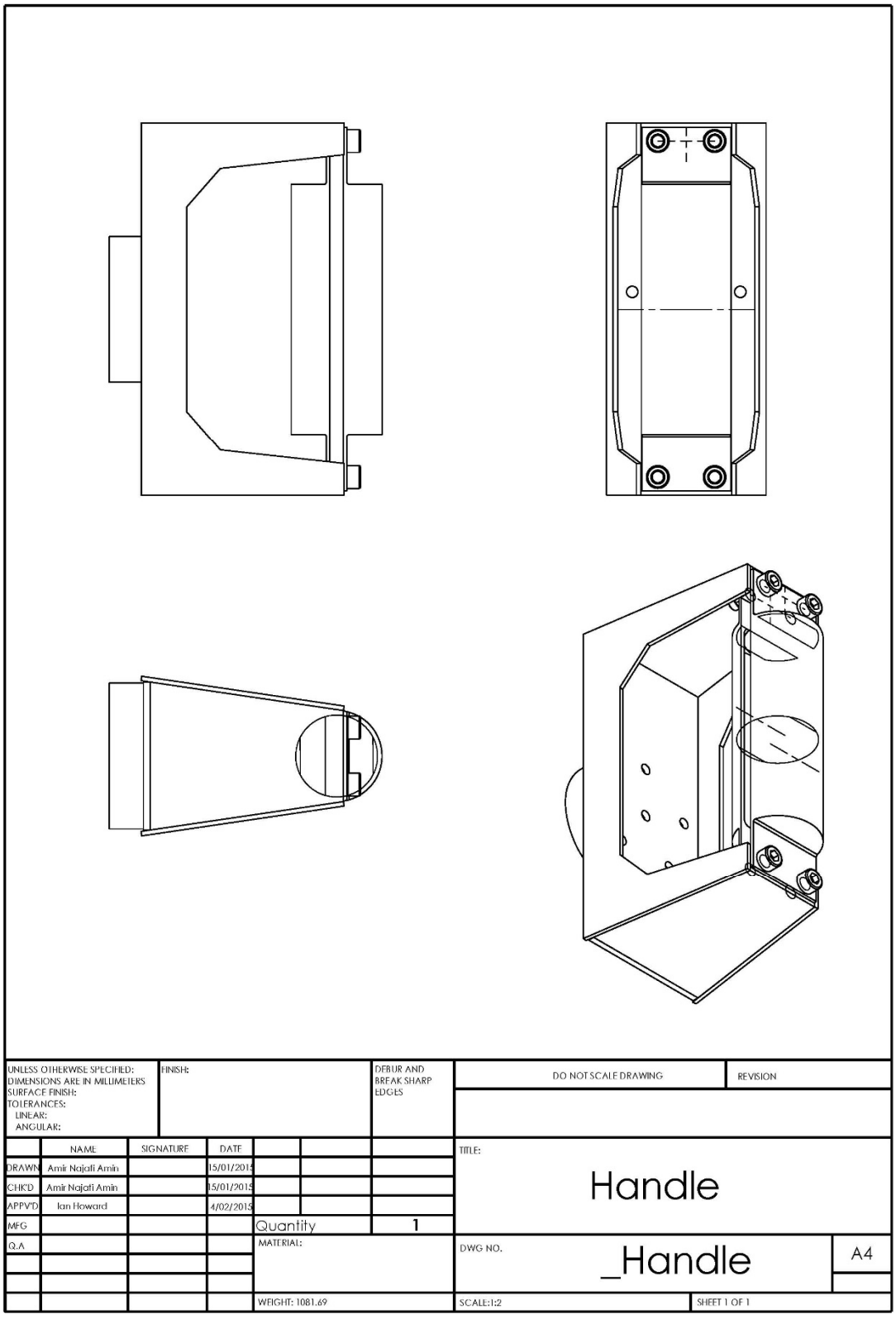

Figure A.3. 1 – Drawing of the handle assembly

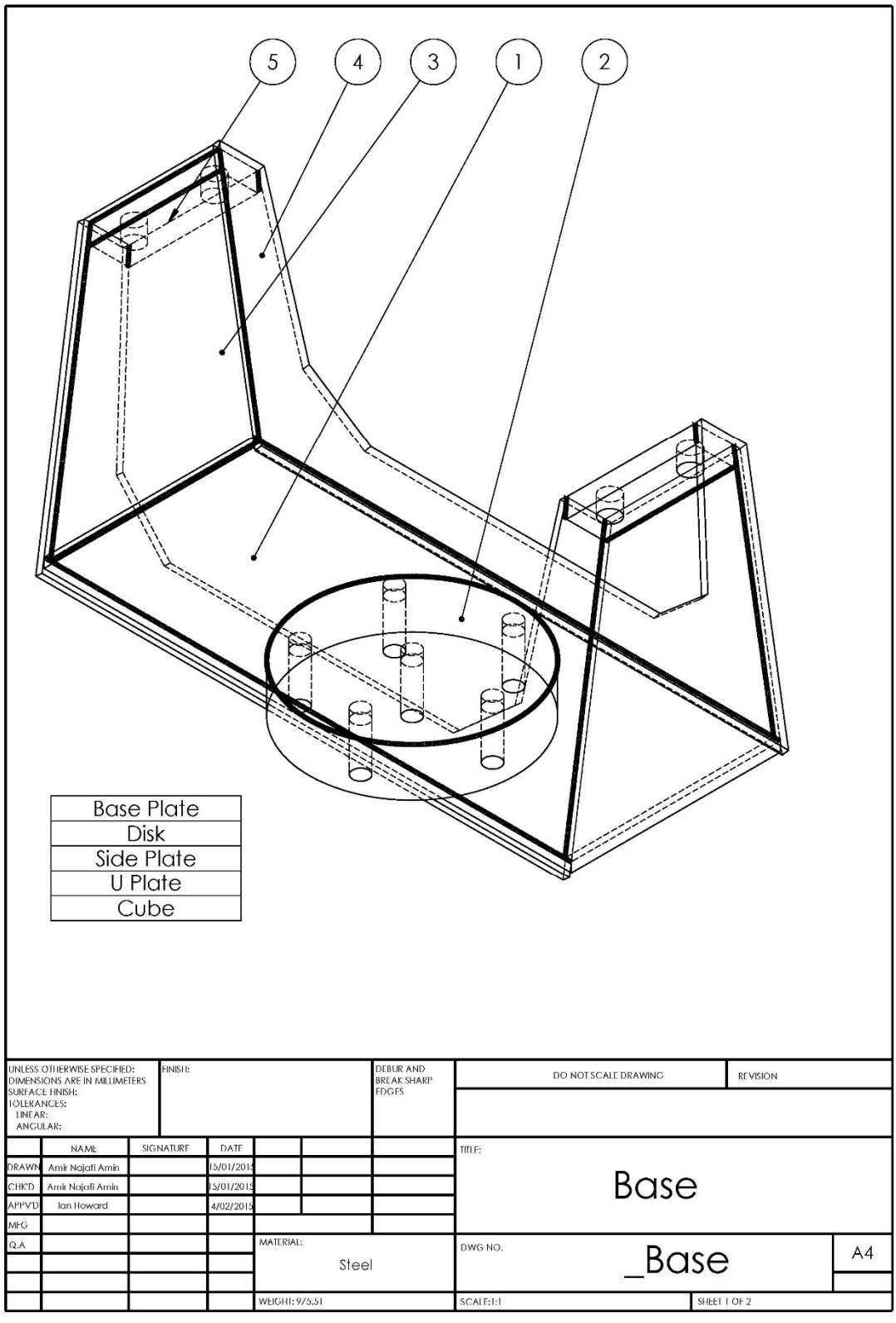

Figure A.3. 2 – Drawing of the base 1/2

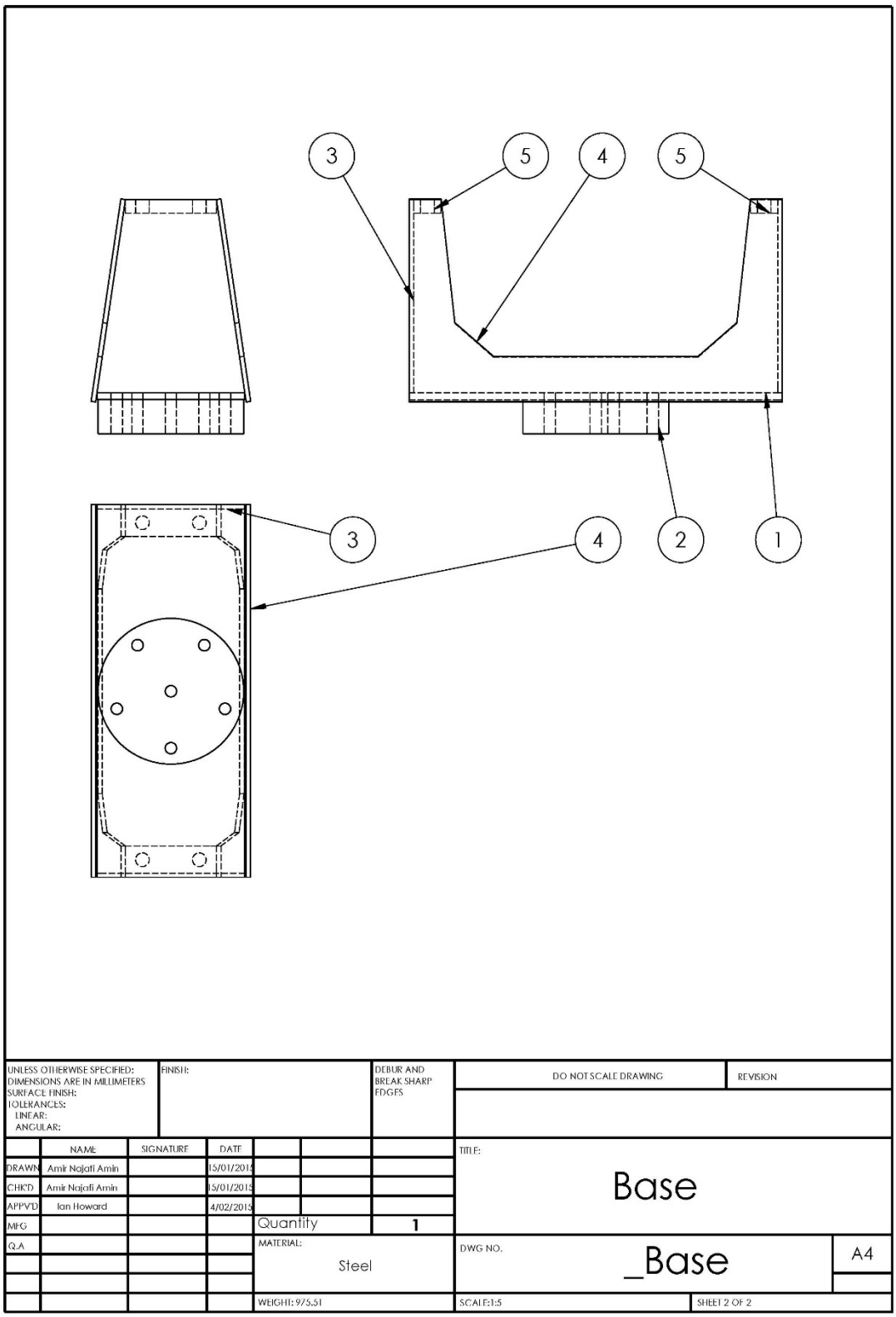

Figure A.3. 3 – Drawing of the base 2/2

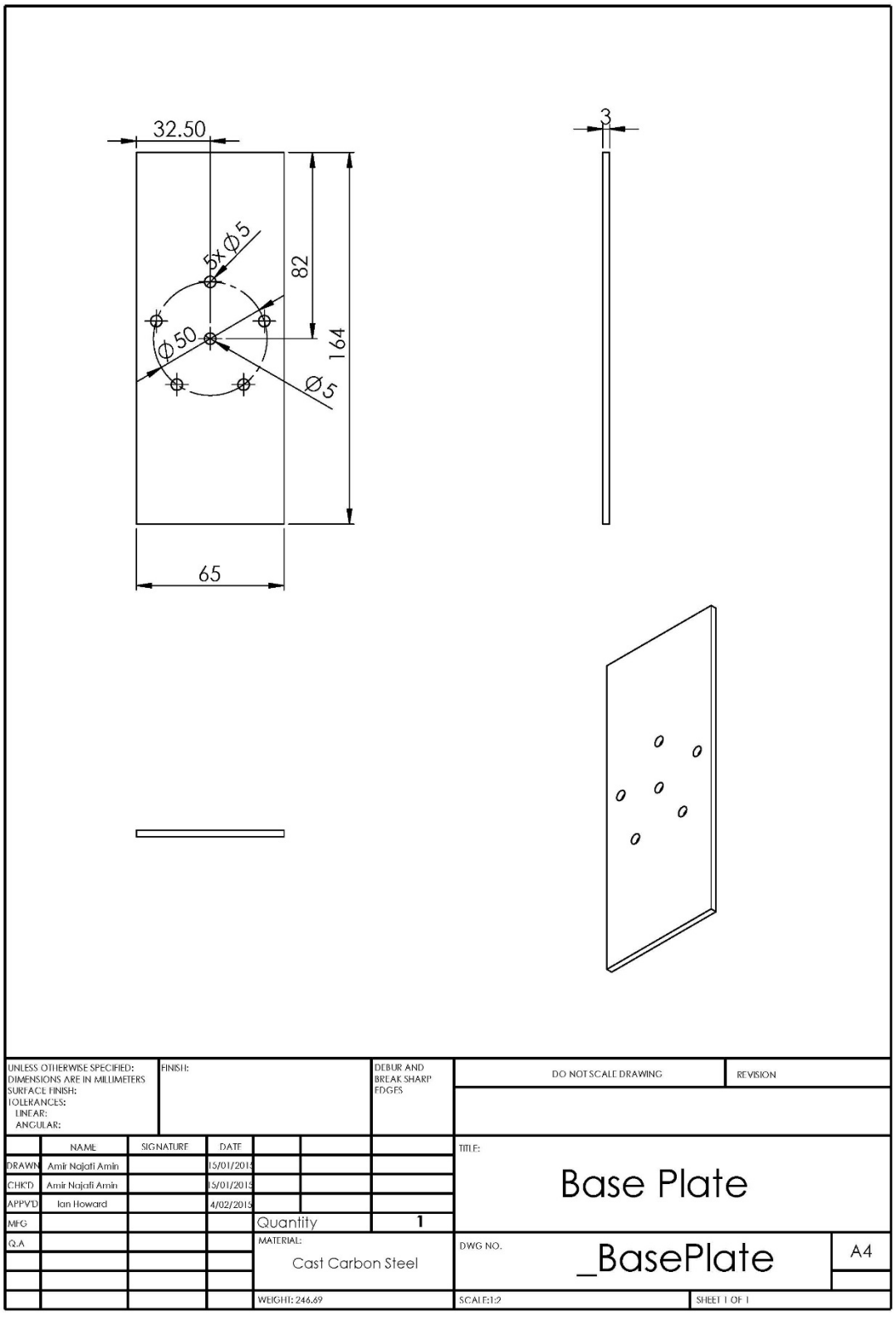

Figure A.3. 4 – Drawing of the base plate

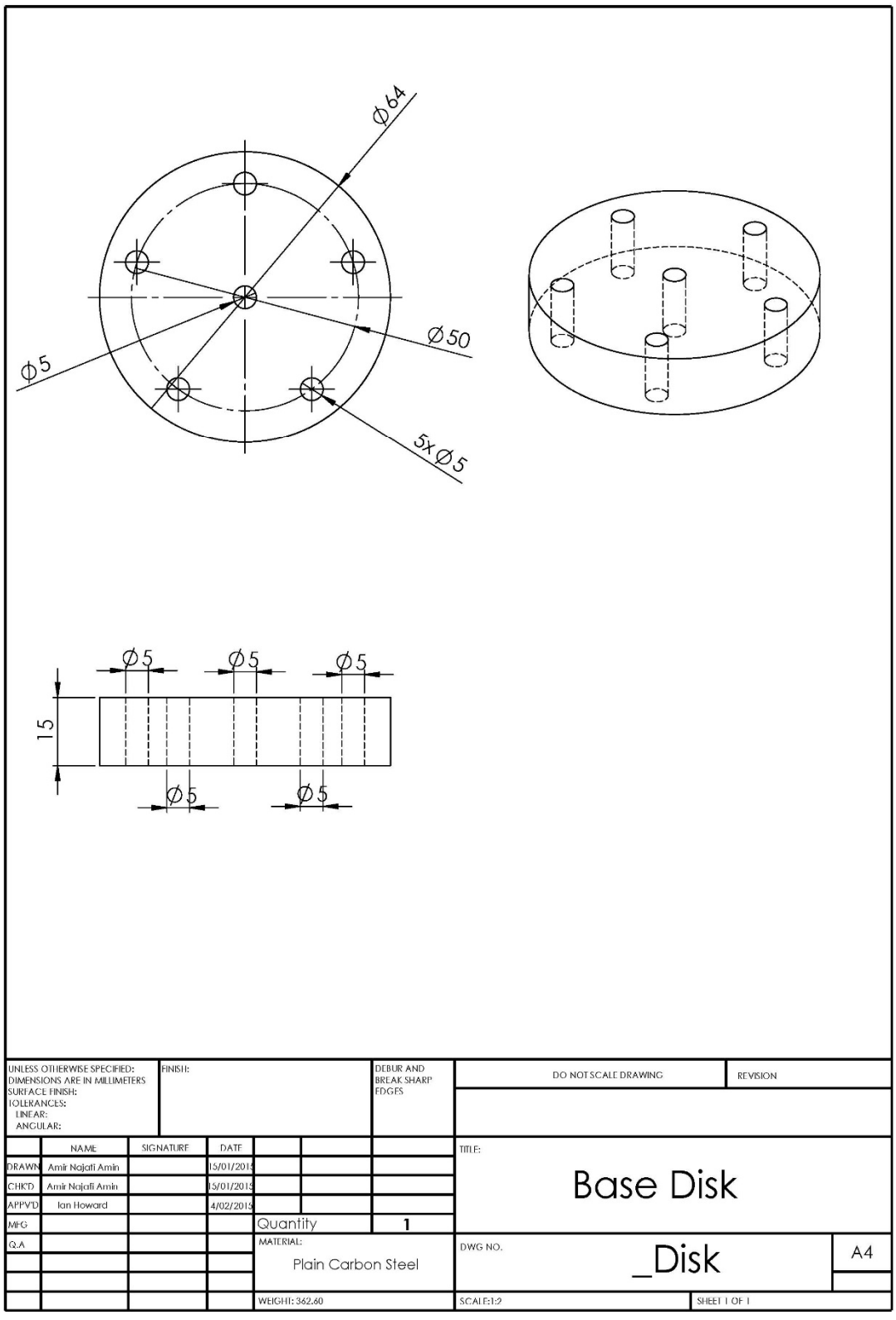

Figure A.3. 5 – Drawing of the base disk

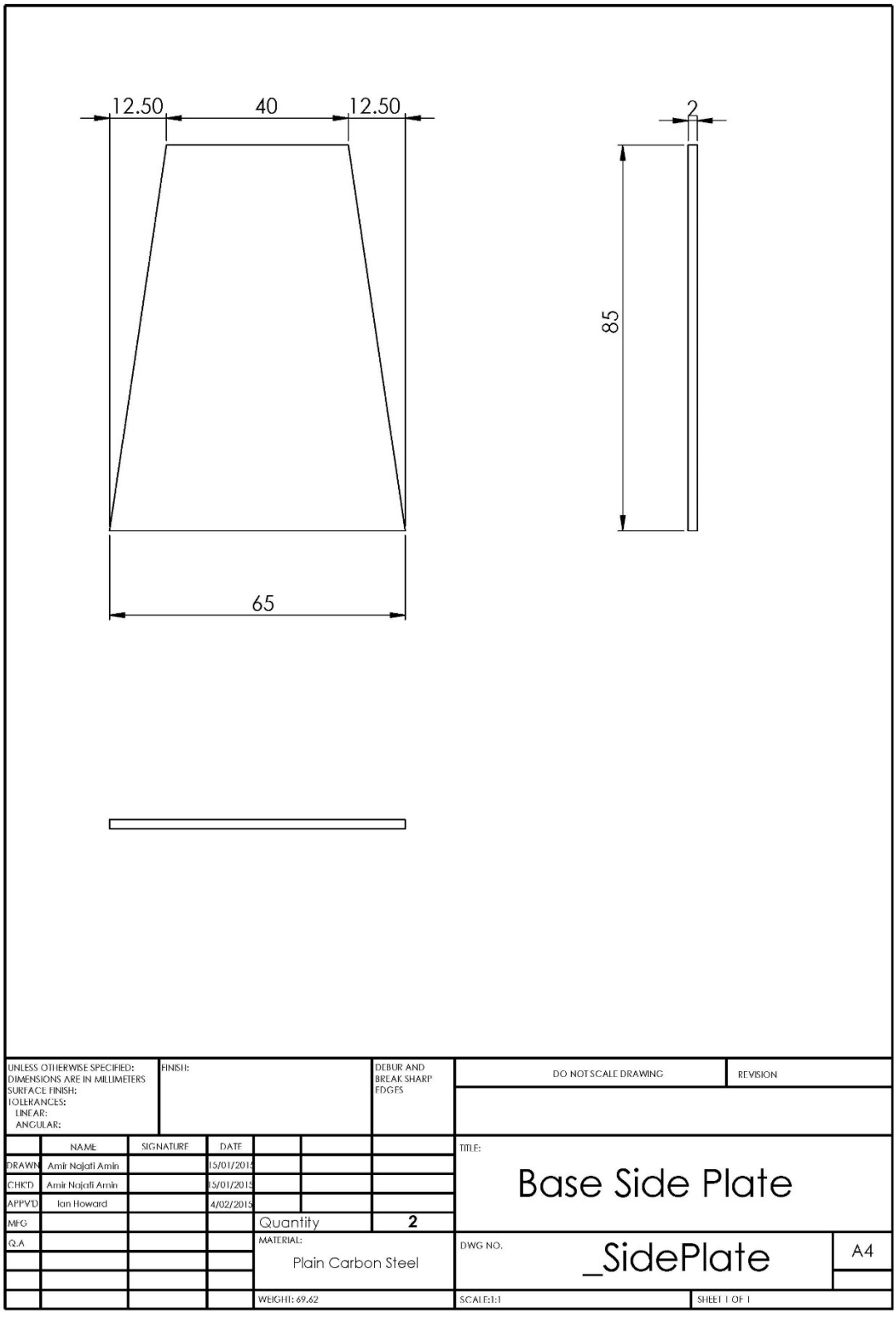

Figure A.3. 6 – Drawing of the base side plate

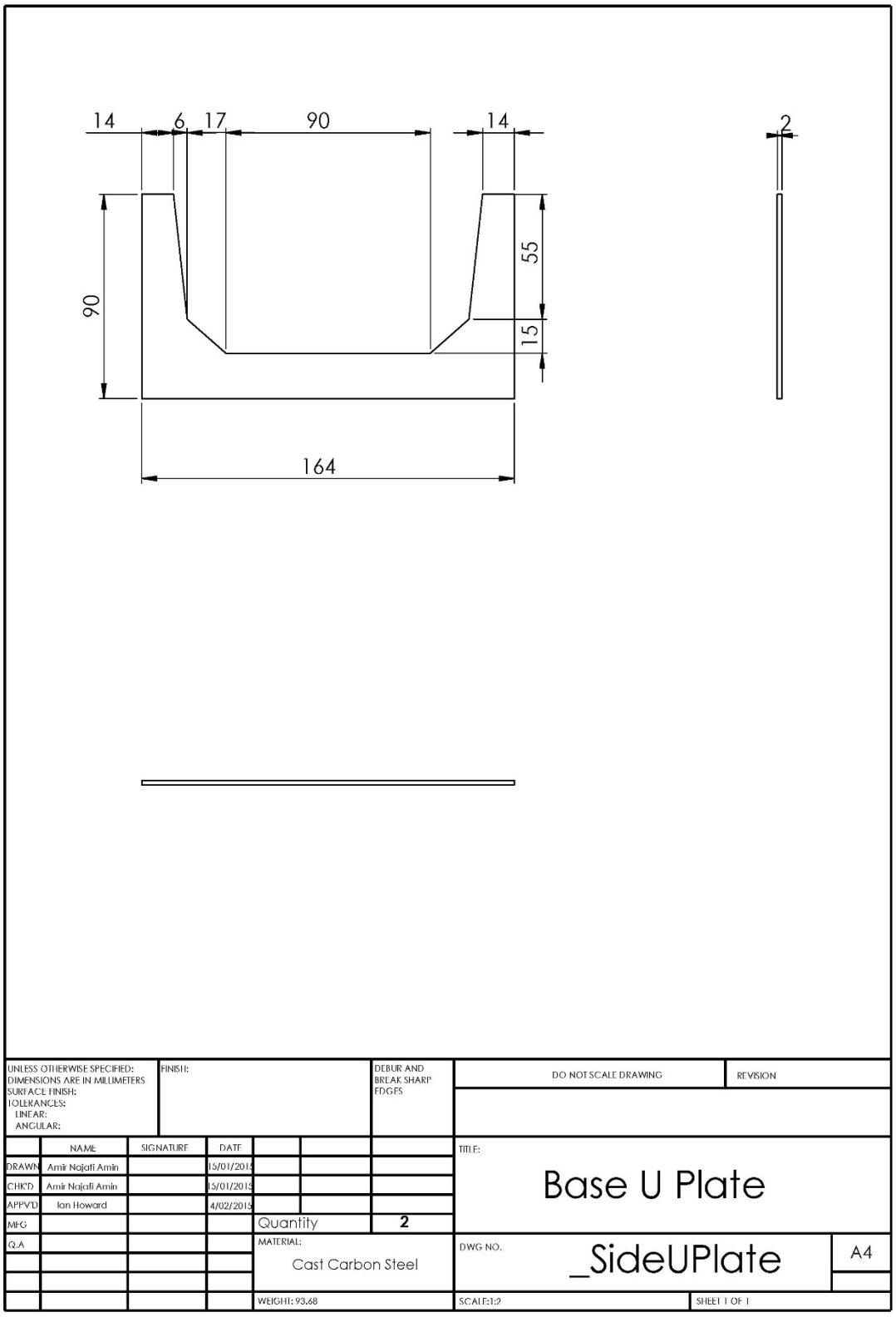

Figure A.3. 7 – Drawing of the base U plate

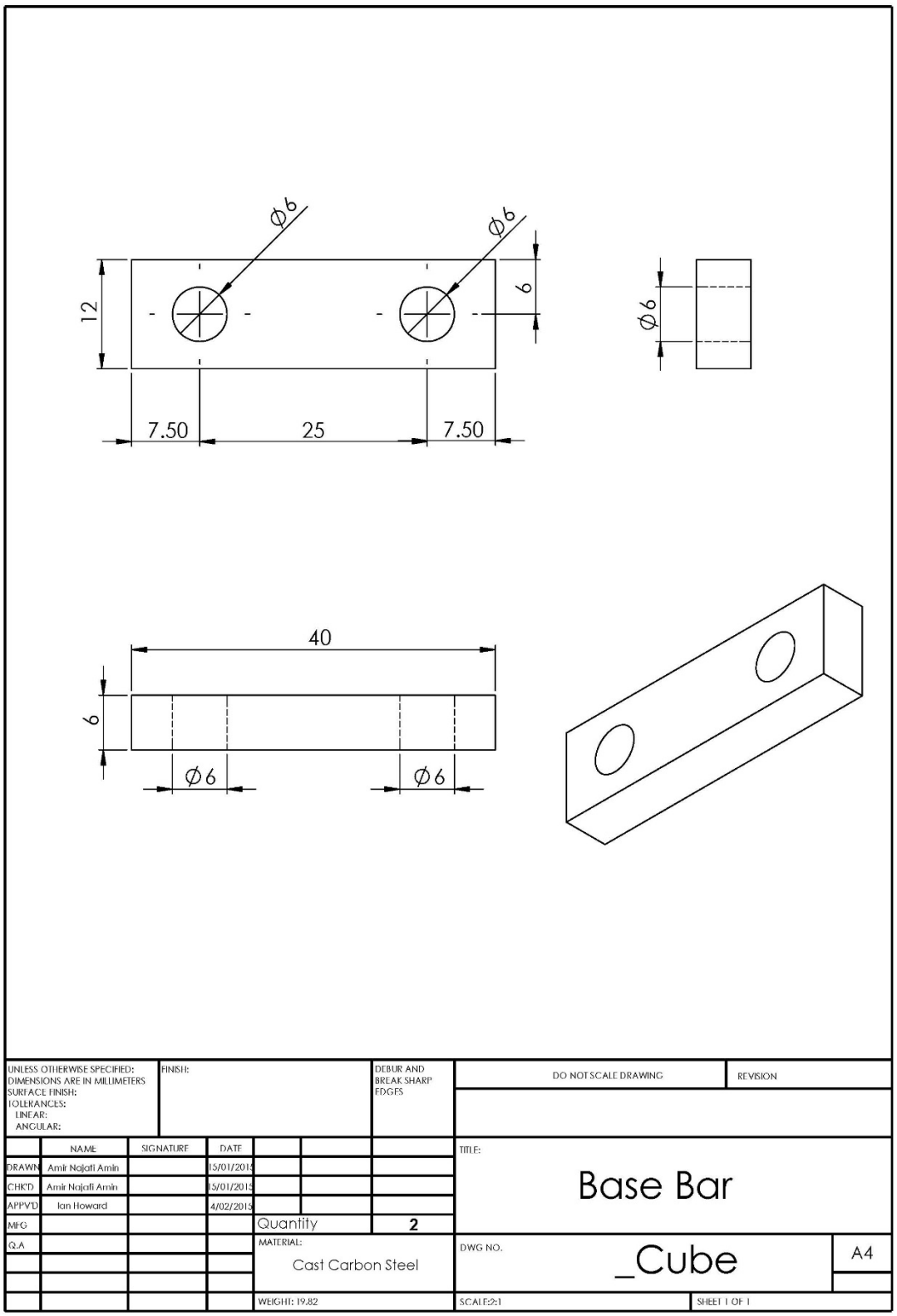

UNLESS OTHERWISE SPECIFIED: DIMENSIONS ARE IN MILLIMETERS SURFACE FINISH: TOLERANCES: LINEAR: ANGULAR:		FINISH:			DEBUR AND BREAK SHARP EDGES	DO NOT SCALE DRAWING	REVISION
	NAME	SIGNATURE	DATE			TITLE: Base Bar	
DRAWN	Amir Najafi Amin		15/01/2015				
CHK'D	Amir Najafi Amin		15/01/2015				
APPV'D	Ian Howard		4/02/2015				
MFG				Quantity	2		
Q.A				MATERIAL: Cast Carbon Steel		DWG NO. _Cube	A4
				WEIGHT: 19.82		SCALE:2:1	SHEET 1 OF 1

Figure A.3. 8 – Drawing of the base bar

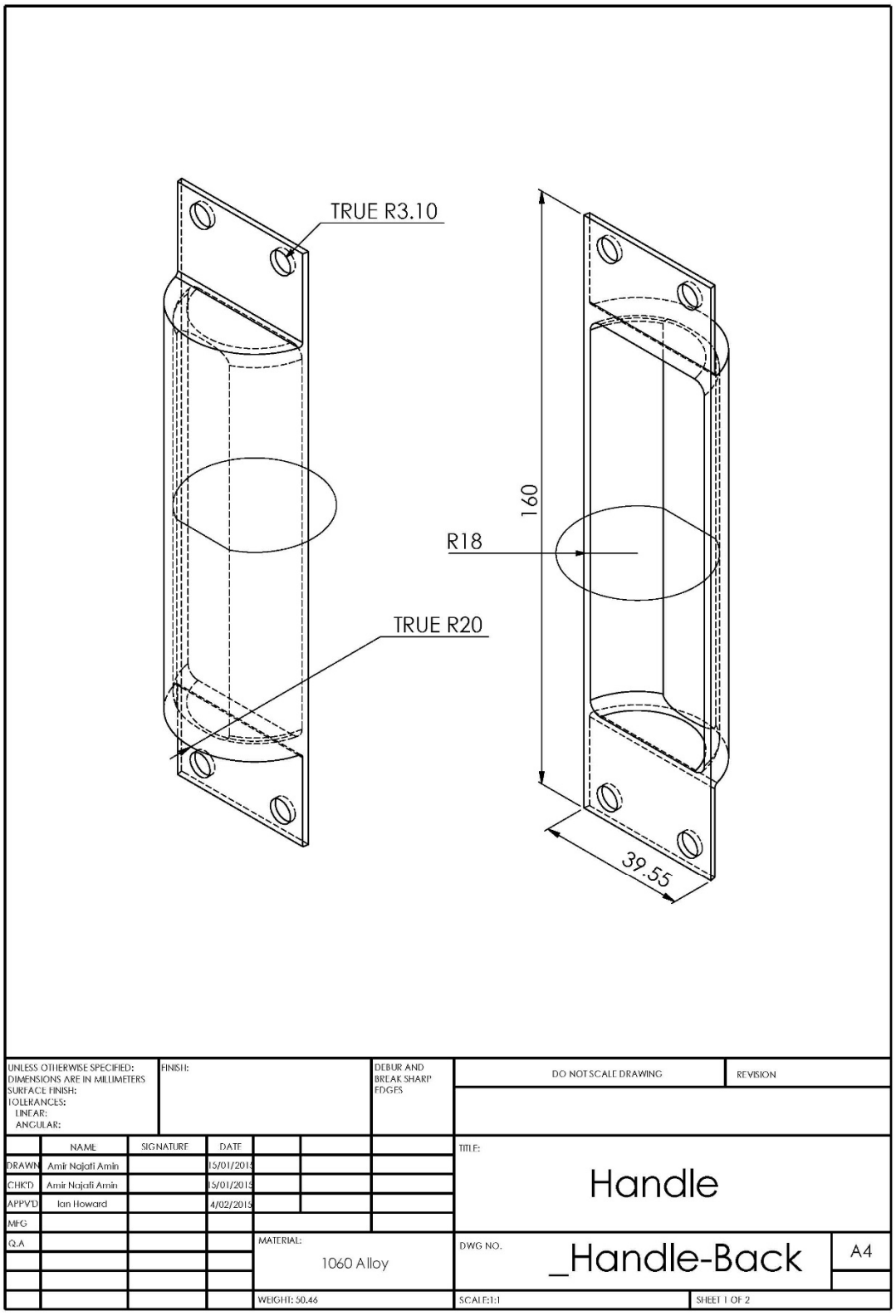

Figure A.3. 9 – Drawing of the handle 1/2

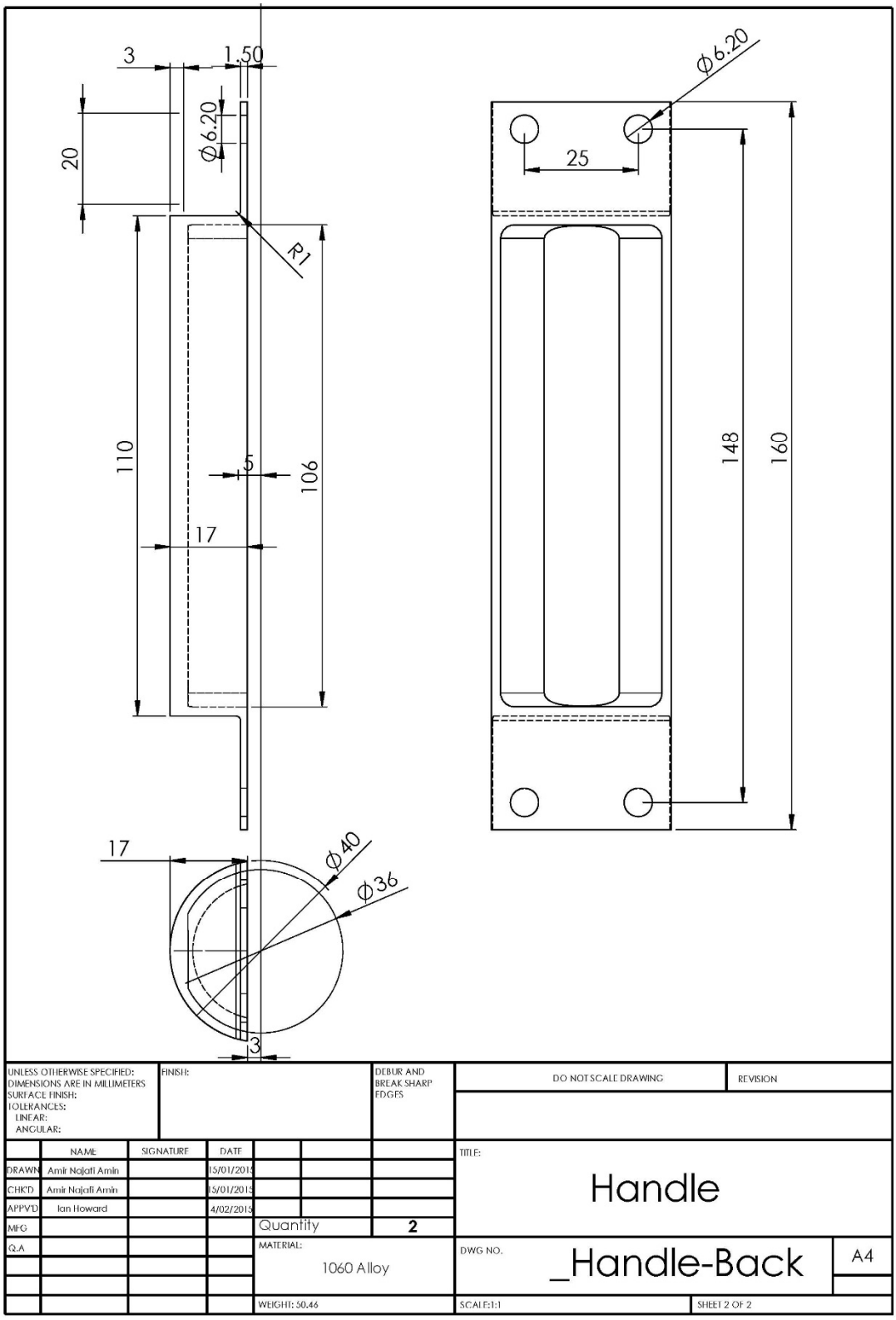

Figure A.3. 10 – Drawing of the handle 2/2

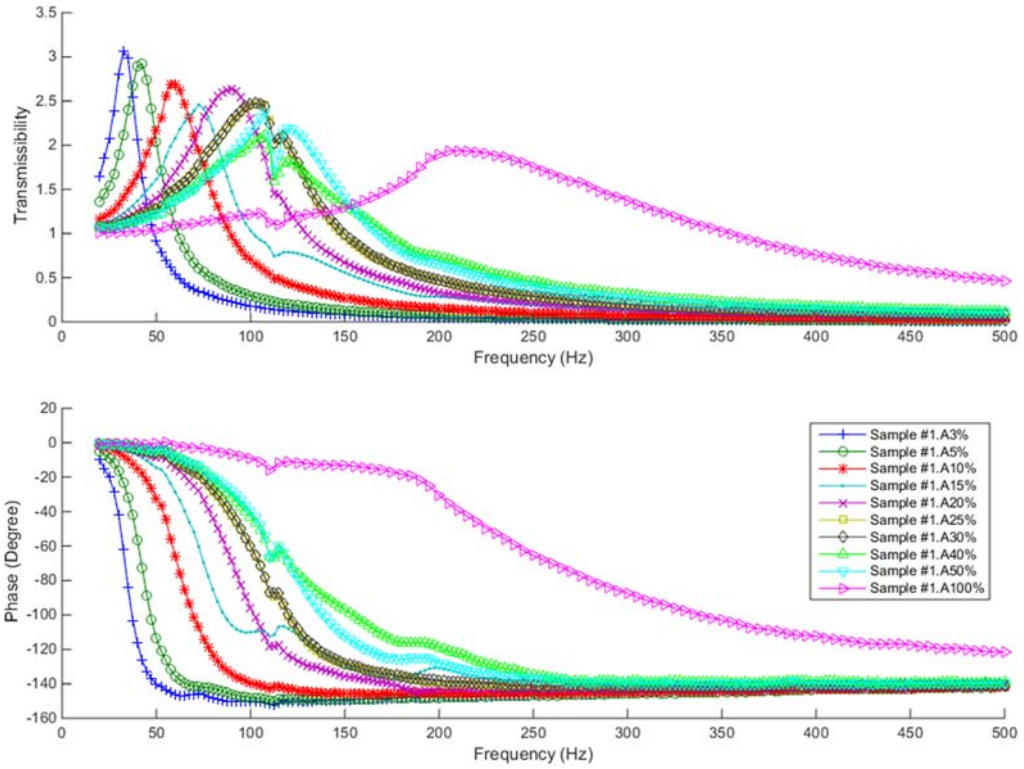

Figure A.4.1 – Vibration Transmissibility of sample #1 (3% to 100% of area)

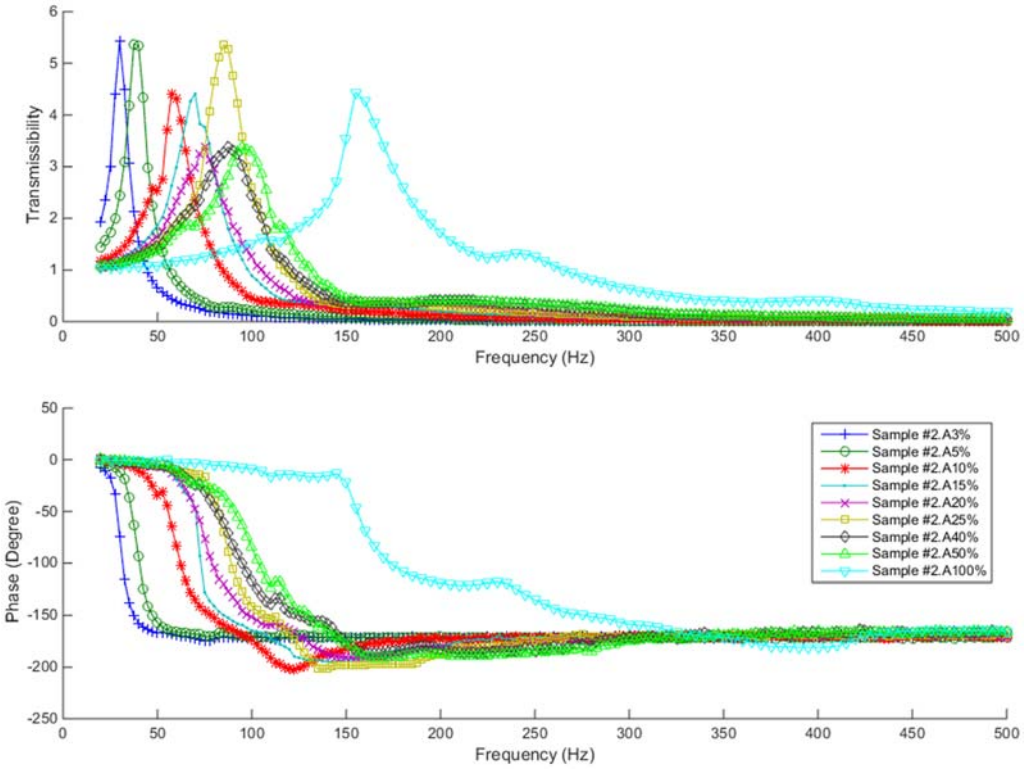

Figure A.4.2 – Vibration Transmissibility of sample #2 (3% to 100% of area)

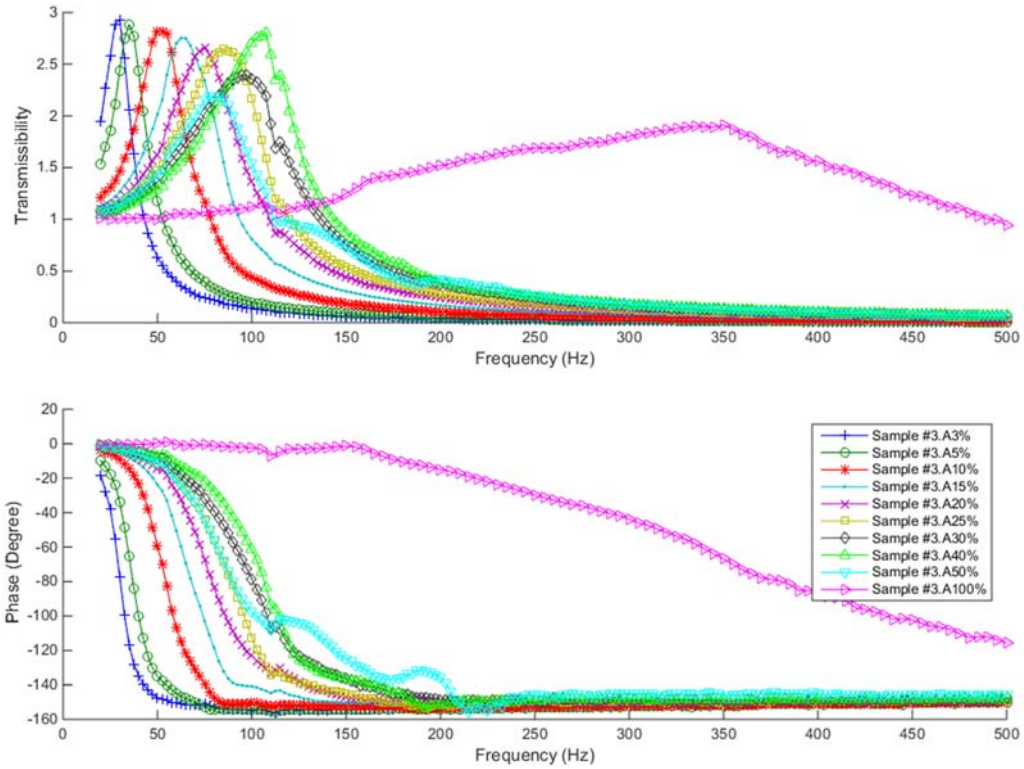

Figure A.4.3 – Vibration Transmissibility of sample #3 (3% to 100% of area)

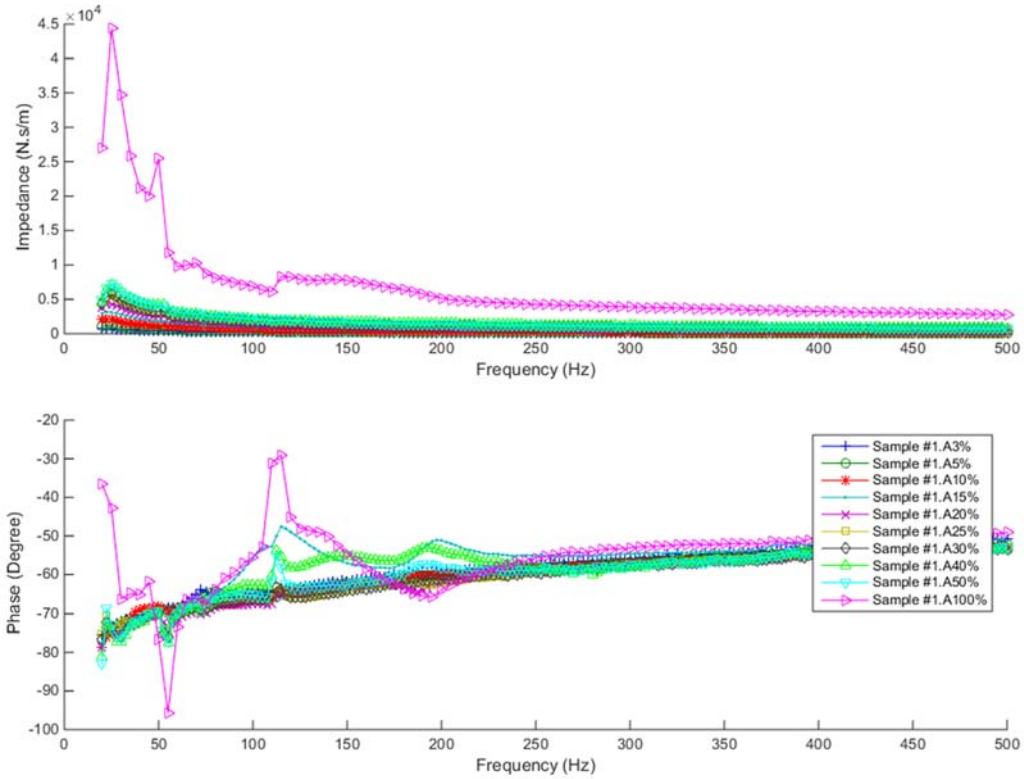

Figure A.4.4 - Mechanical Impedance of sample #1 (3% to 100% of area)

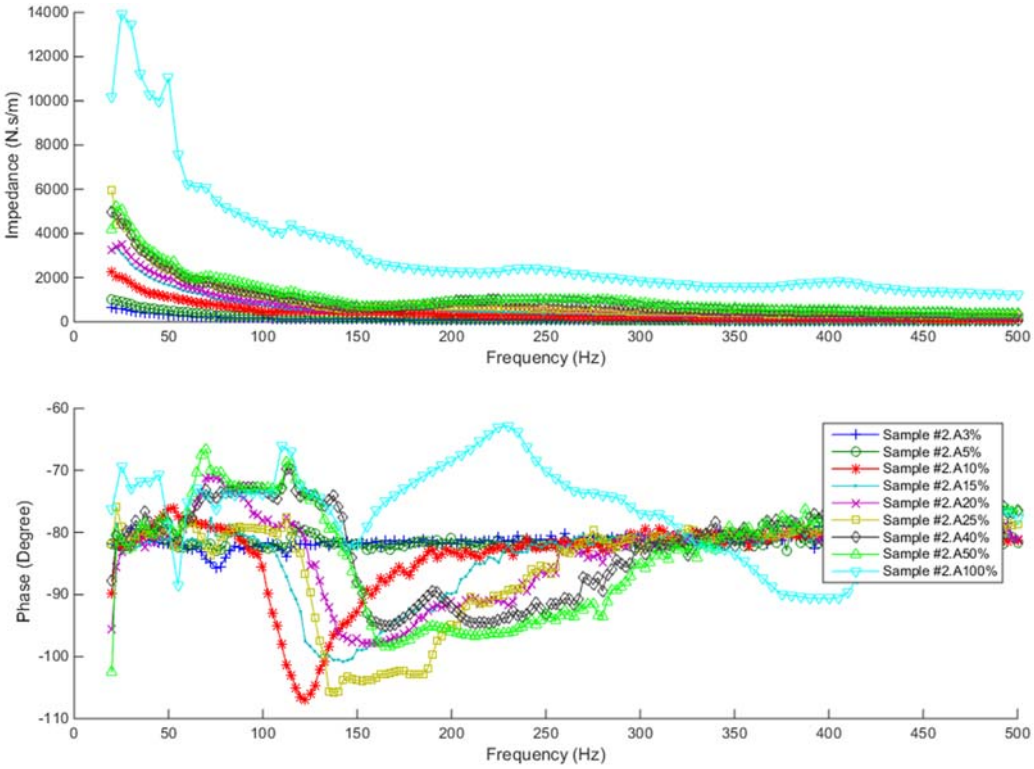

Figure A.4.5 - Mechanical Impedance of sample #2 (3% to 100% of area)

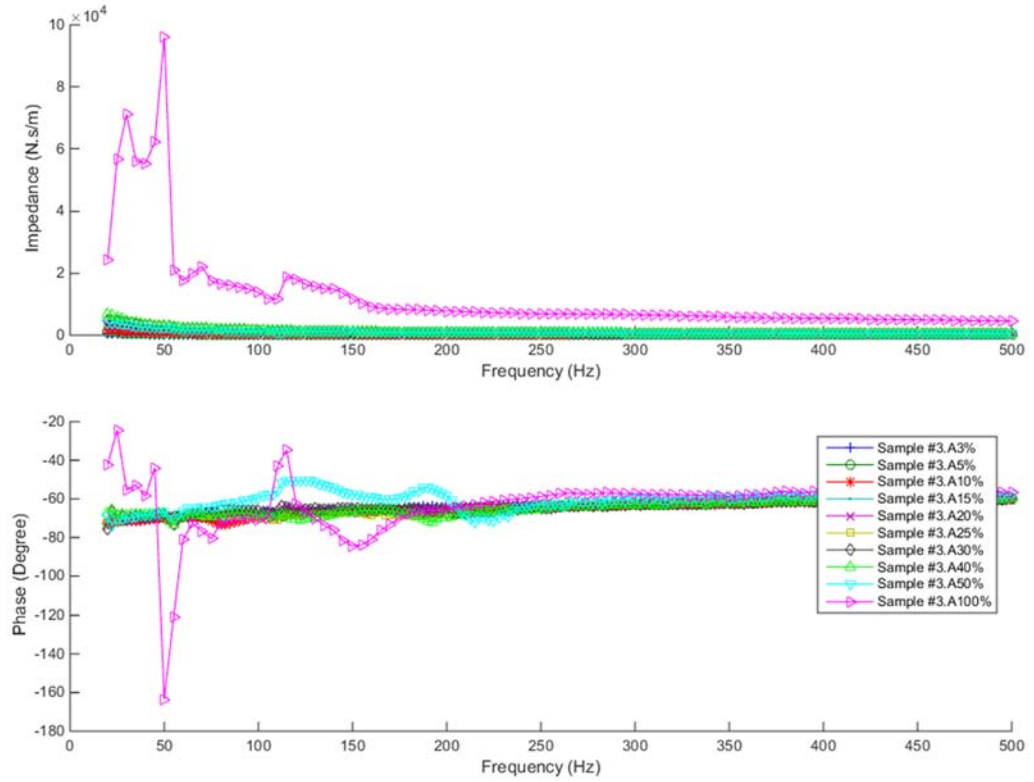

Figure A.4.6 - Mechanical Impedance of sample #3 (3% to 100% of area)

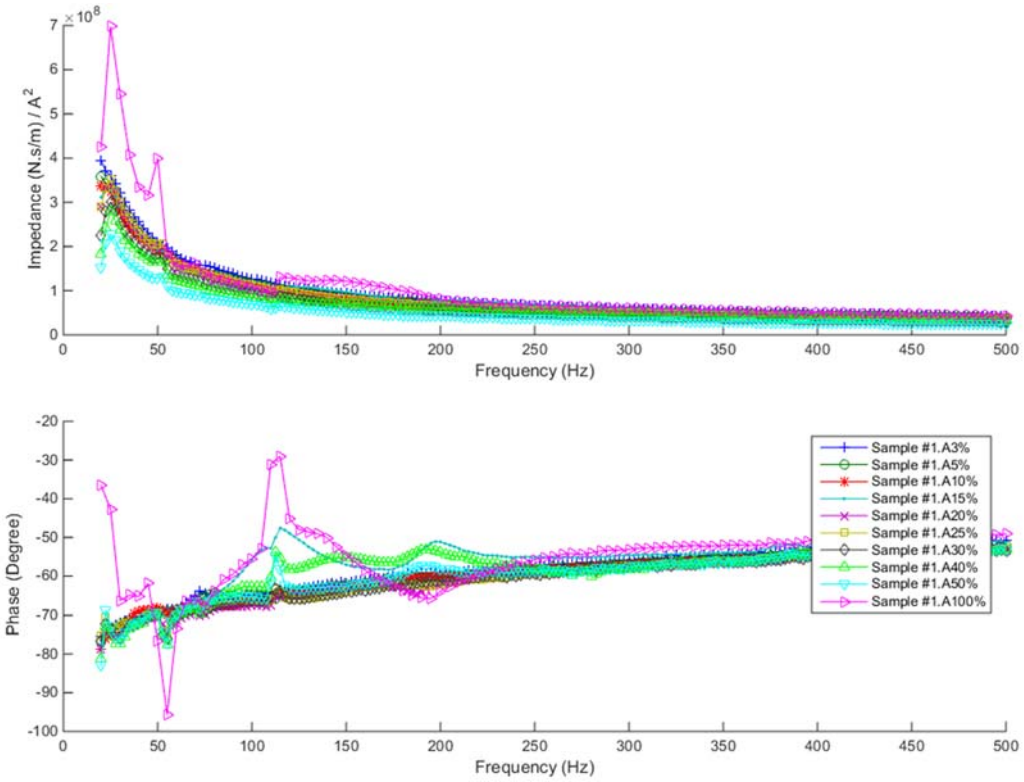

Figure A.4.7 – Normalized Mechanical Impedance by unit of area of sample #1

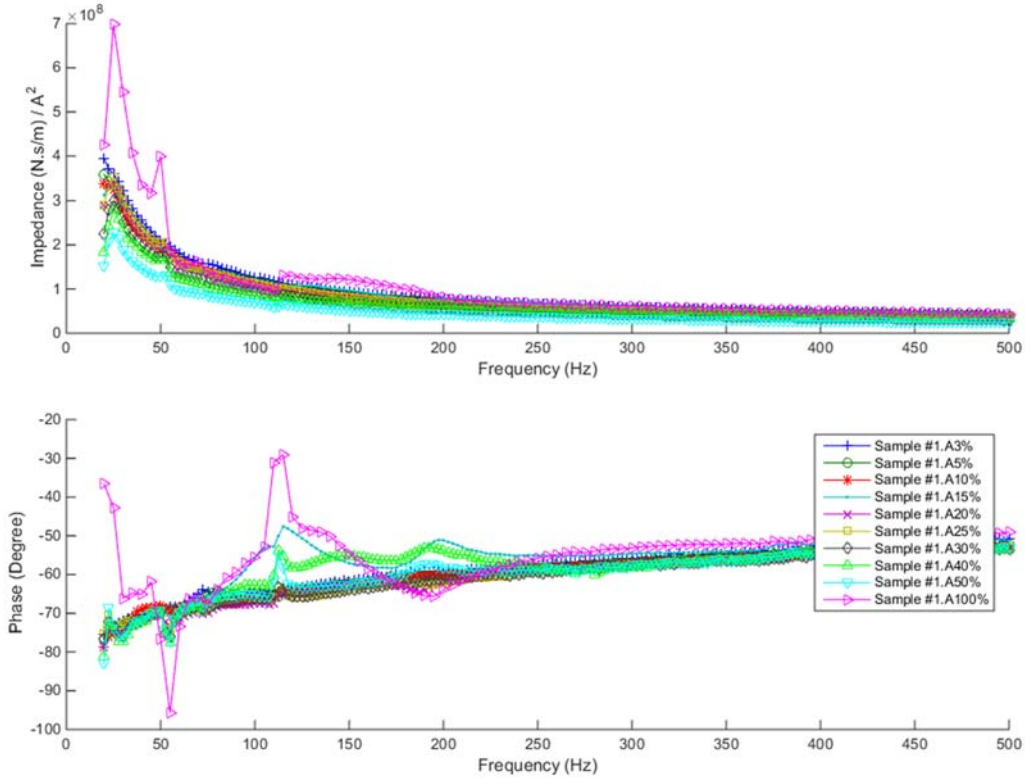

Figure A.4.8 - Normalized Mechanical Impedance by unit of area of sample #2

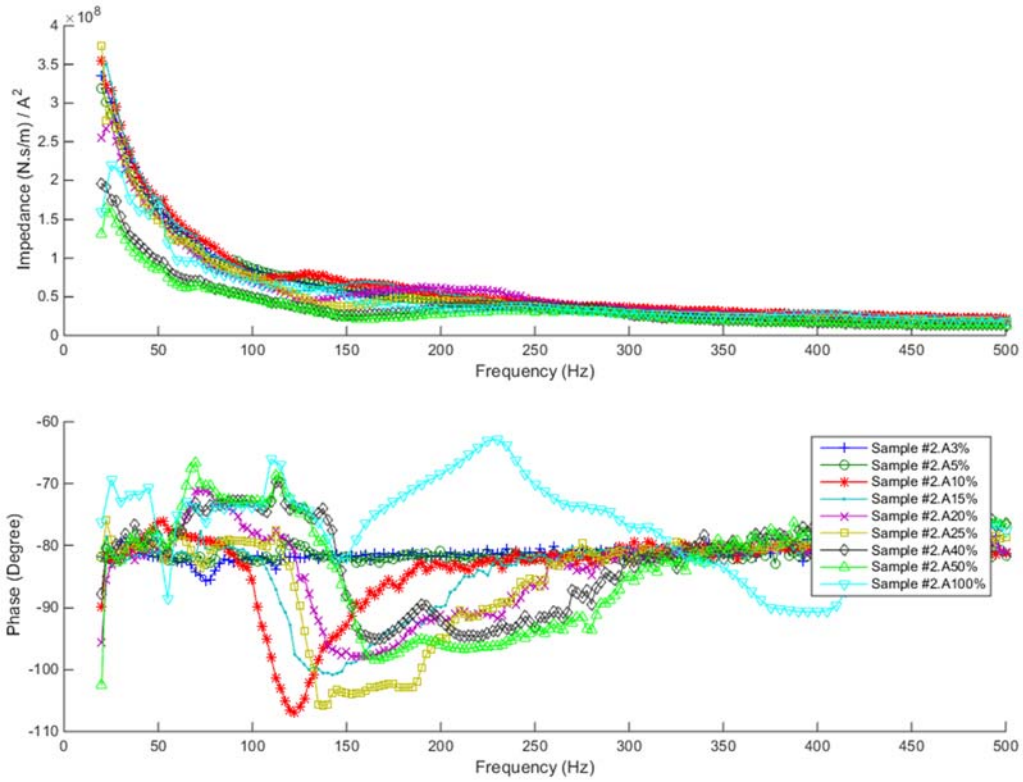

Figure A.4.9 – Normalized Mechanical Impedance by unit of area of sample #3

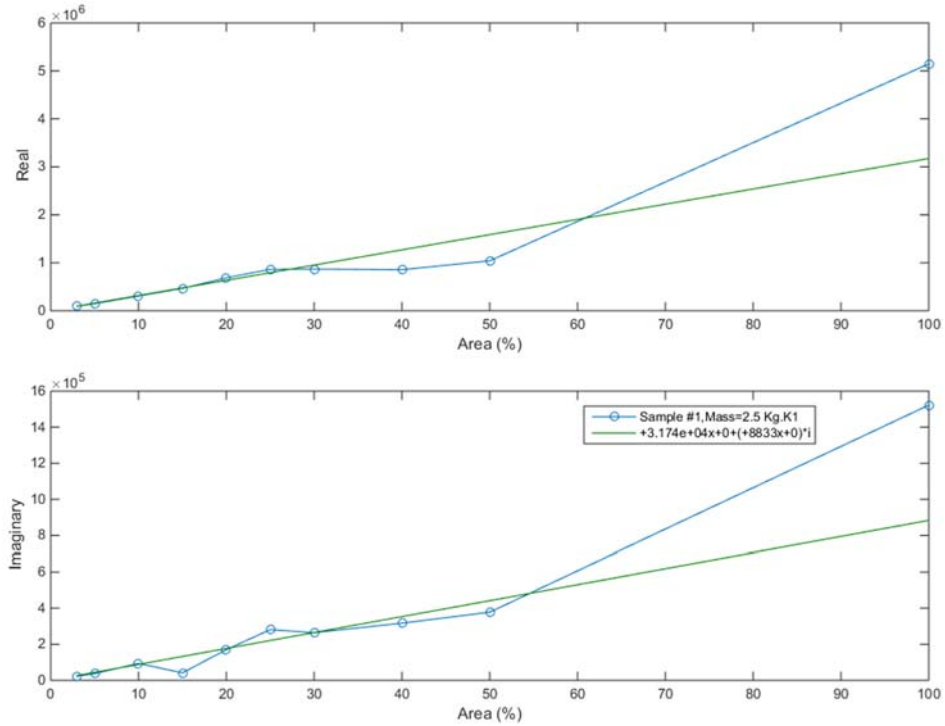

Figure A.4.10 - Stiffness for one DOF model of sample #1

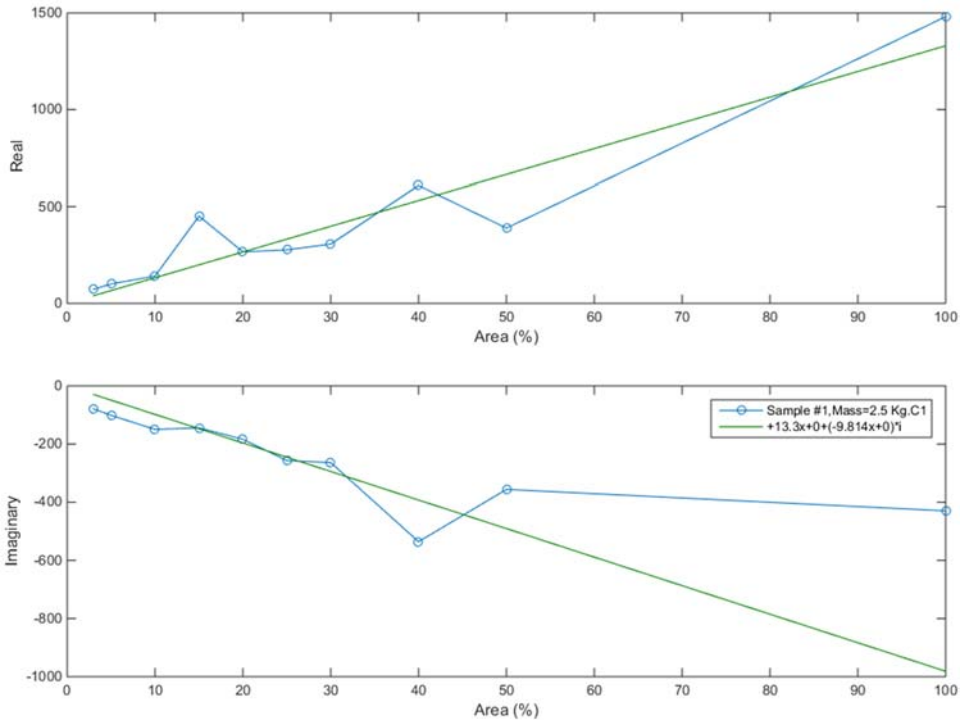

Figure A.4.11 - Damping for one DOF model of sample #1

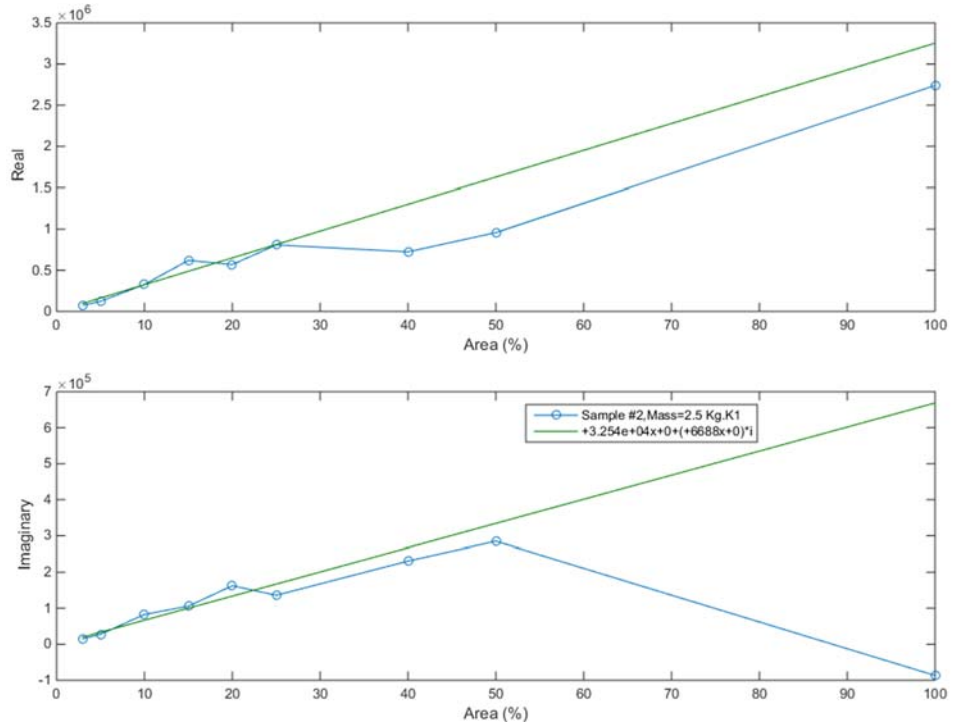

Figure A.4.12 - Stiffness for one DOF model of sample #2

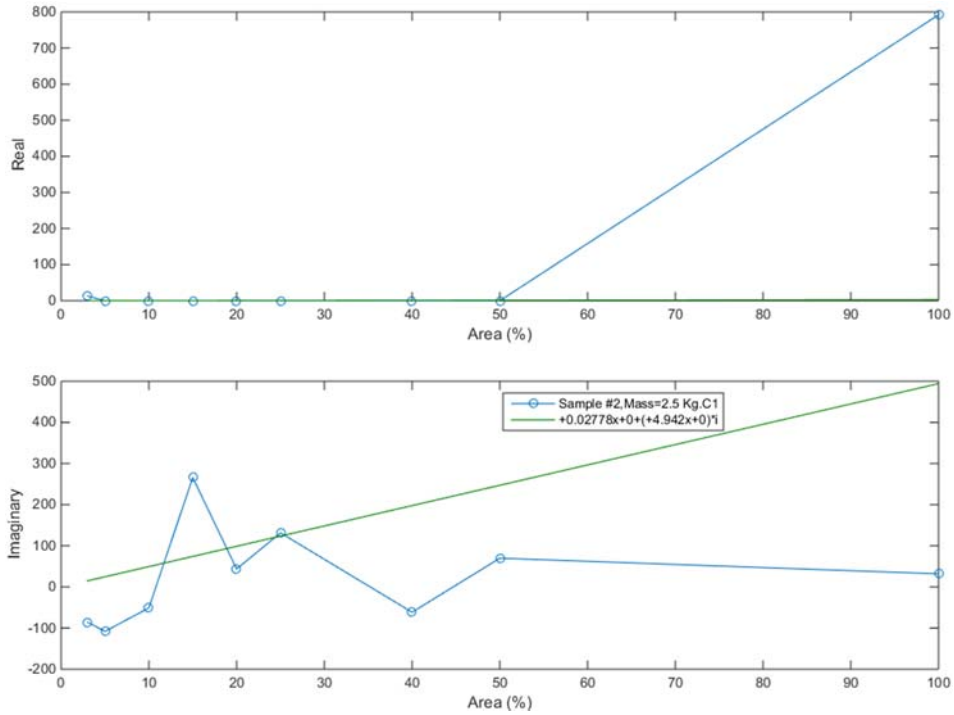

Figure A.4.13 - Damping for one DOF model of sample #2

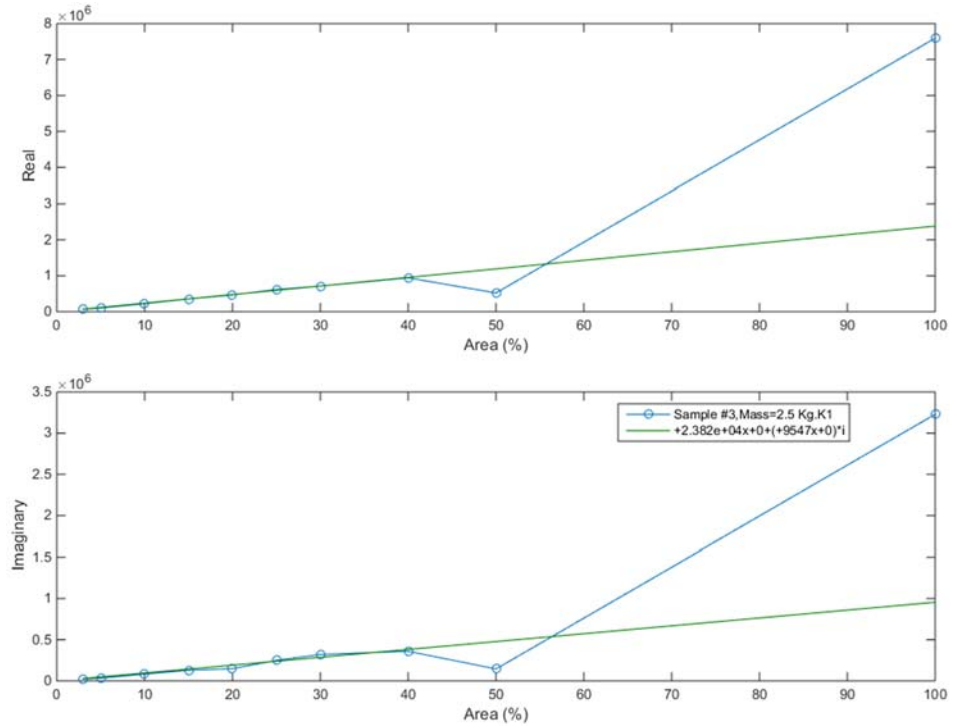

Figure A.4.14 - Stiffness for one DOF model of sample #3

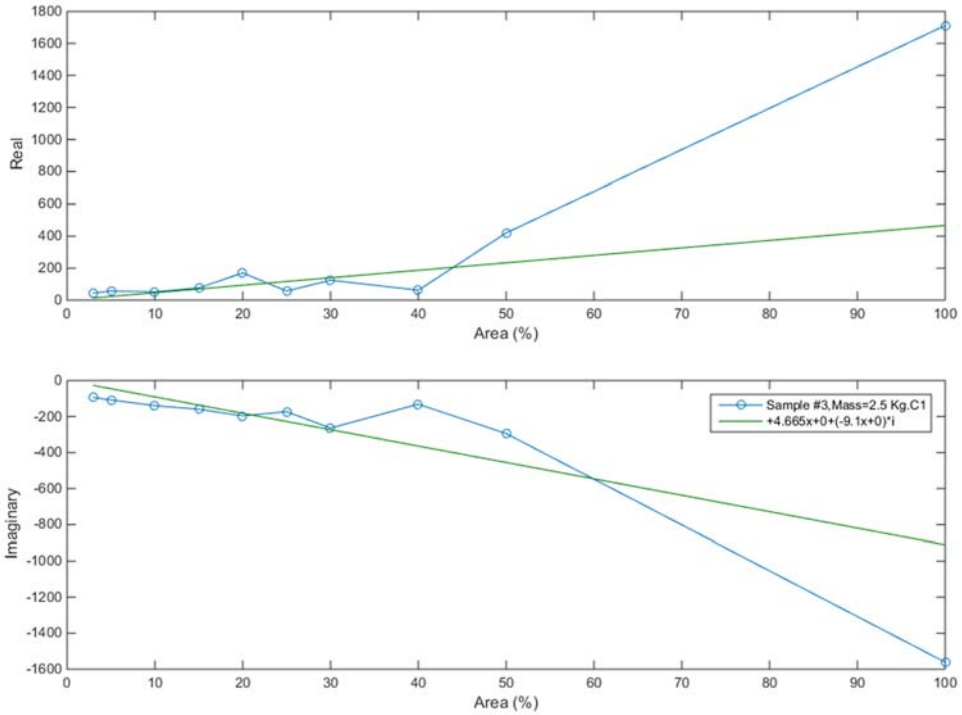

Figure A.4.15 - Damping for one DOF model of sample #3

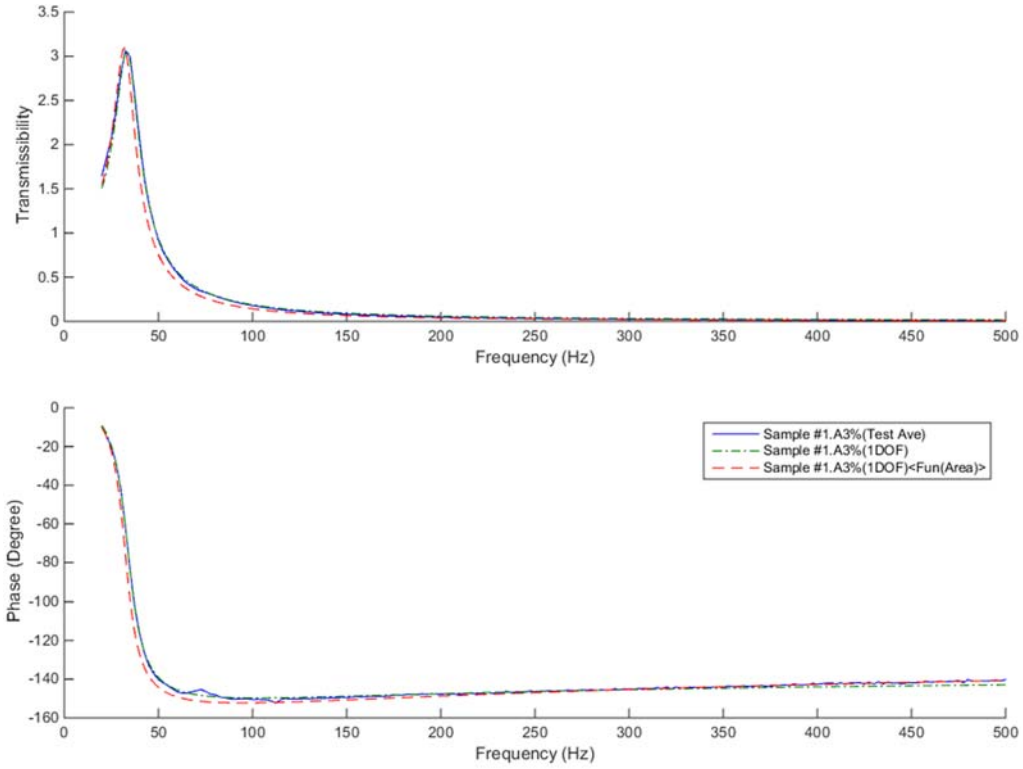

Figure A.4.16 - VT of sample #1 for 3% of area

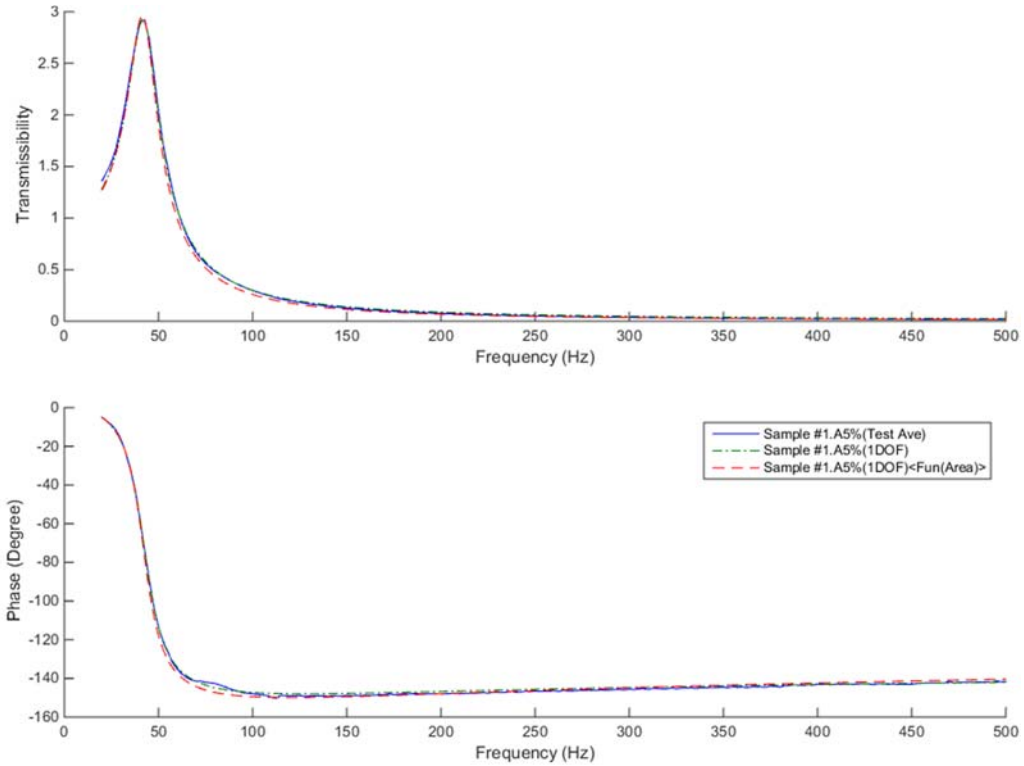

Figure A.4.17 - VT of sample #1 for 5% of area

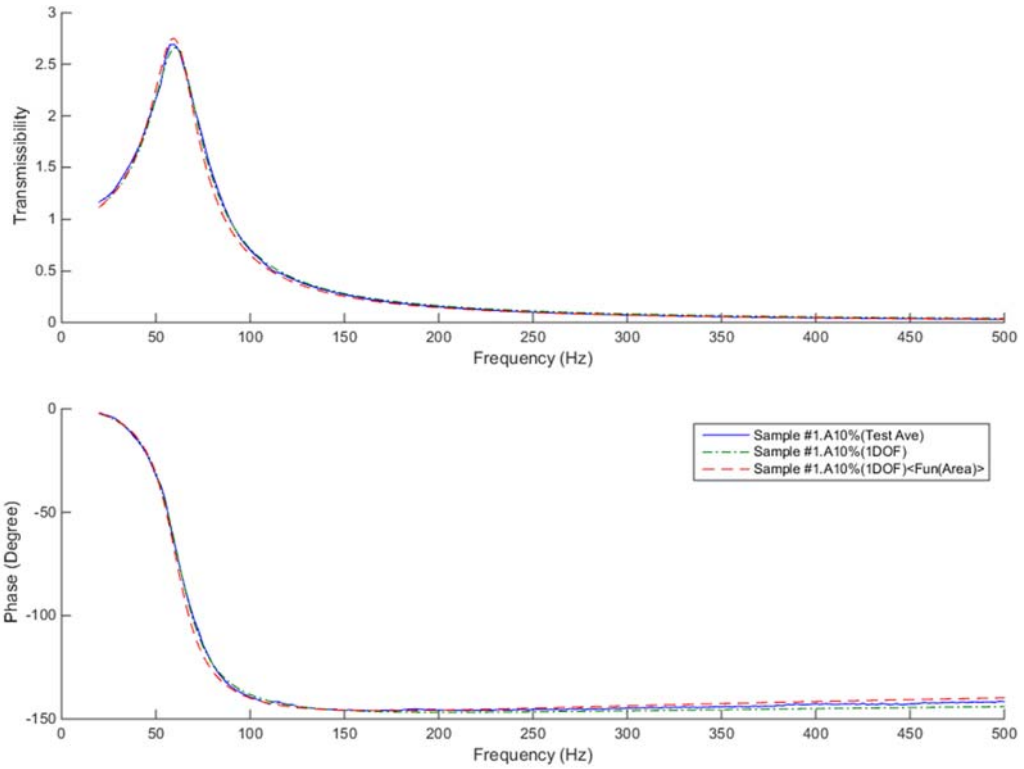

Figure A.4.18 - VT of sample #1 for 10% of area

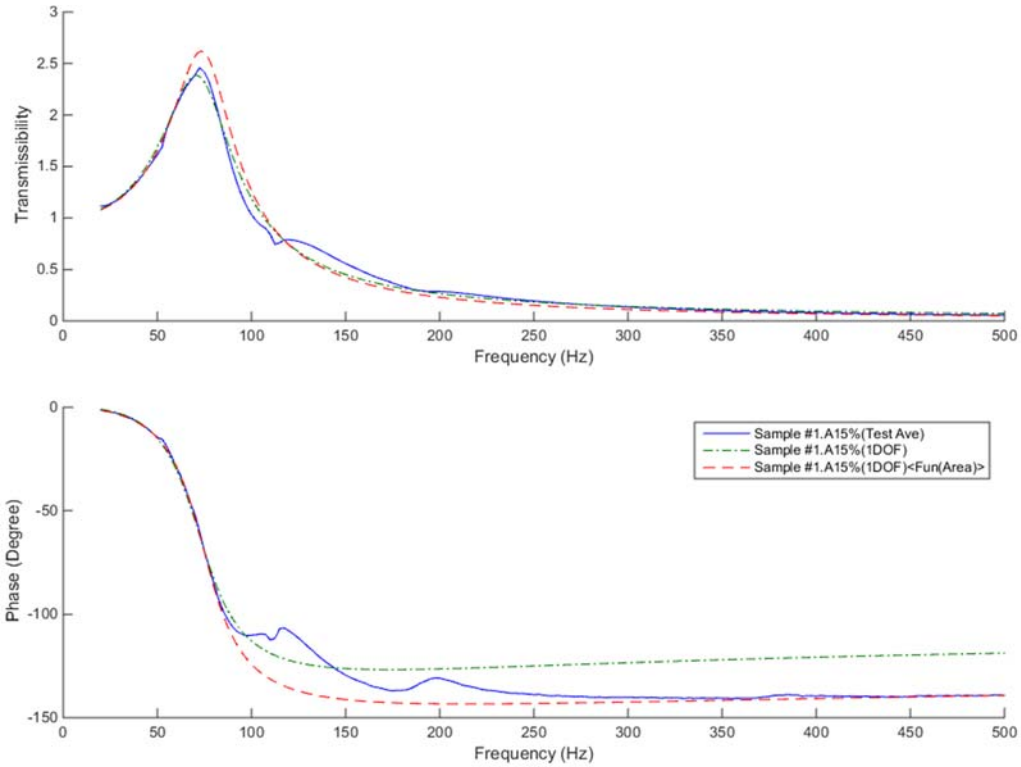

Figure A.4.19 - VT of sample #1 for 15% of area

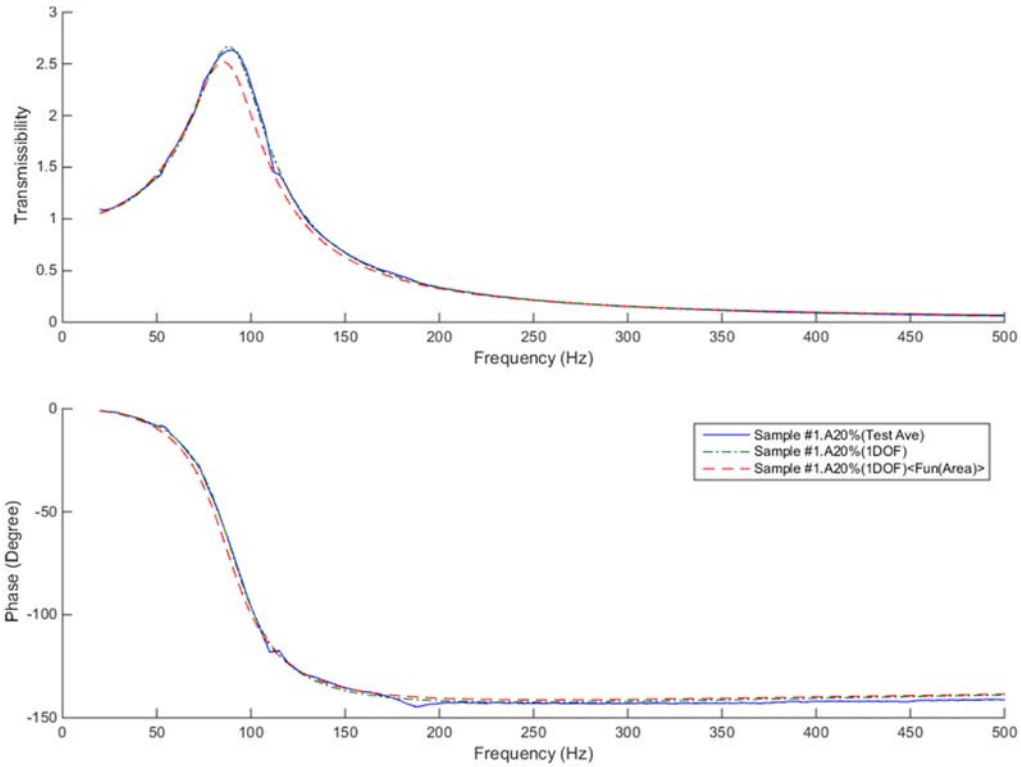

Figure A.4.20 - VT of sample #1 for 20% of area

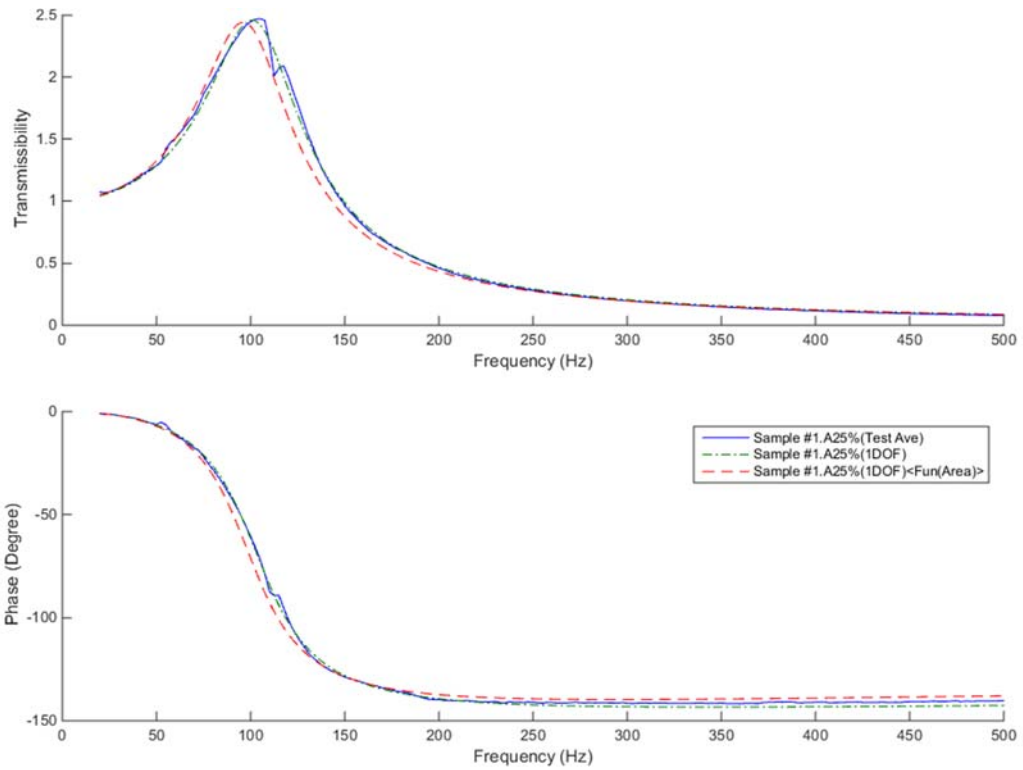

Figure A.4.21 - VT of sample #1 for 25% of area

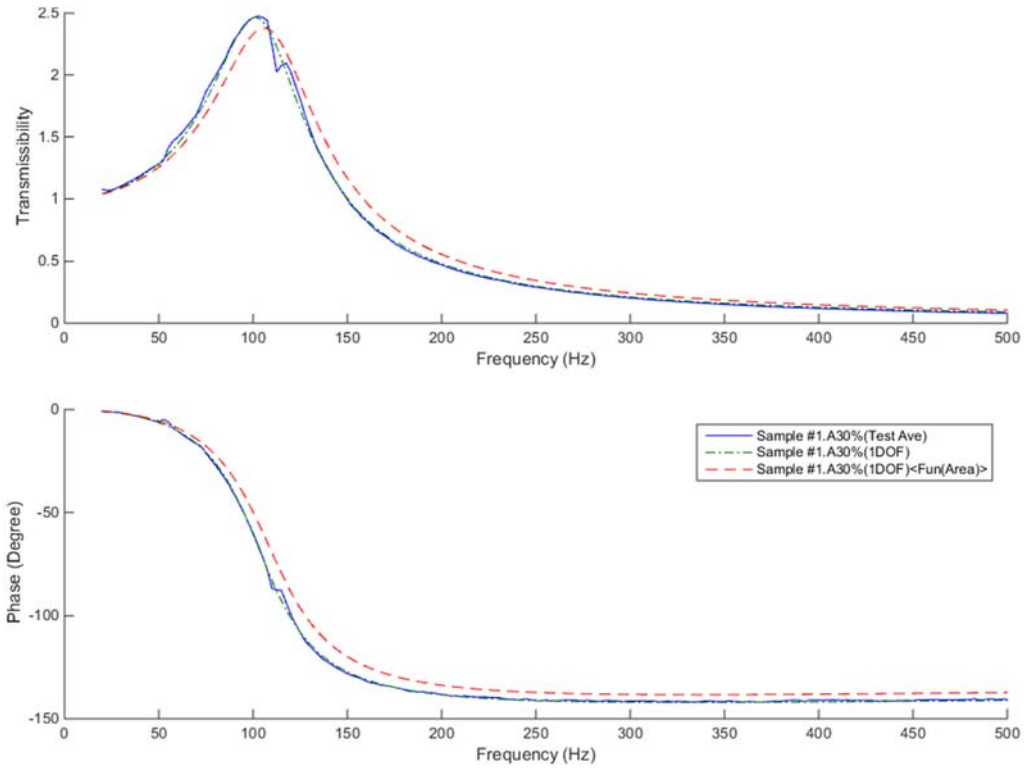

Figure A.4.22 - VT of sample #1 for 30% of area

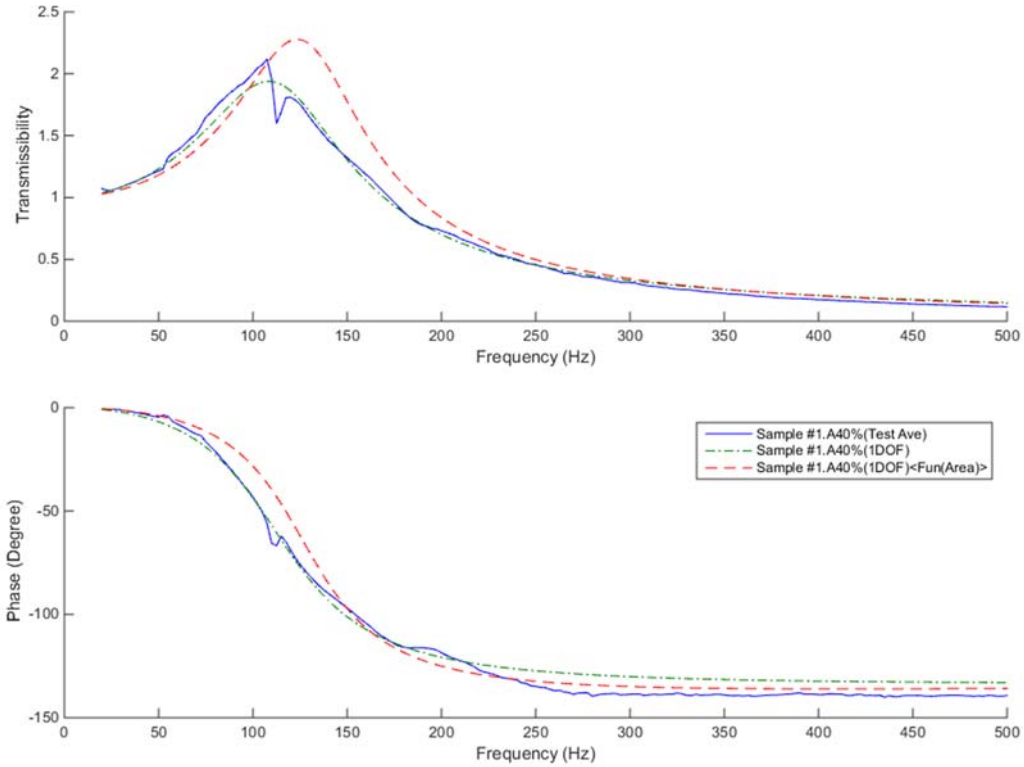

Figure A.4.23 - VT of sample #1 for 40% of area

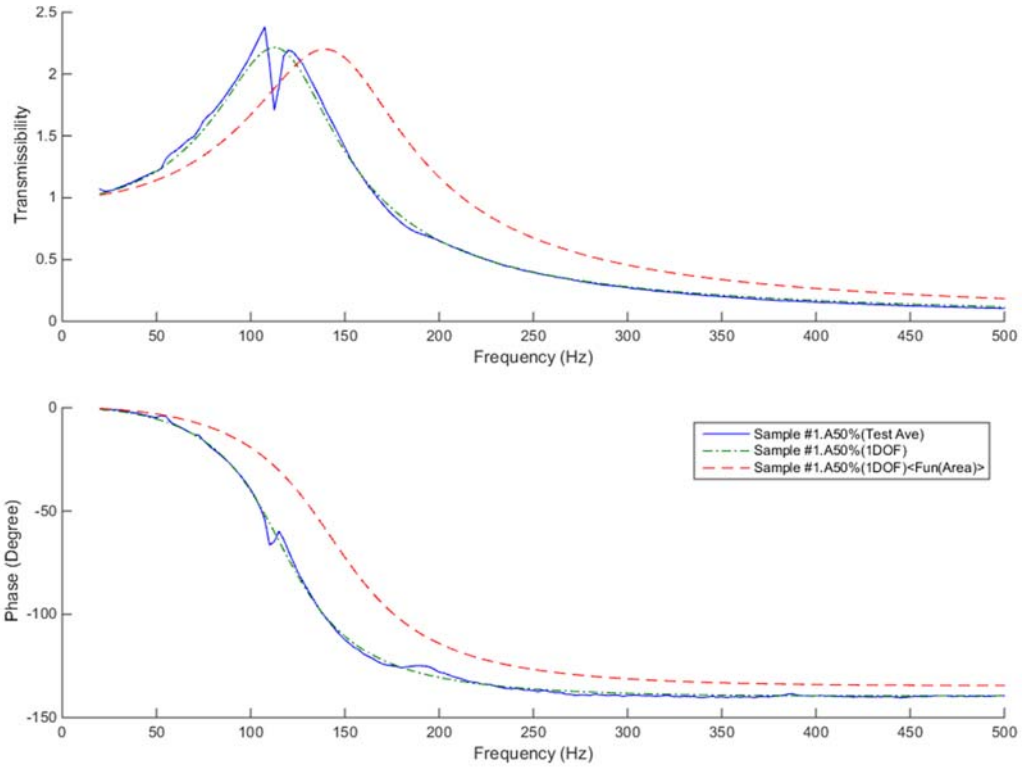

Figure A.4.24 - VT of sample #1 for 50% of area

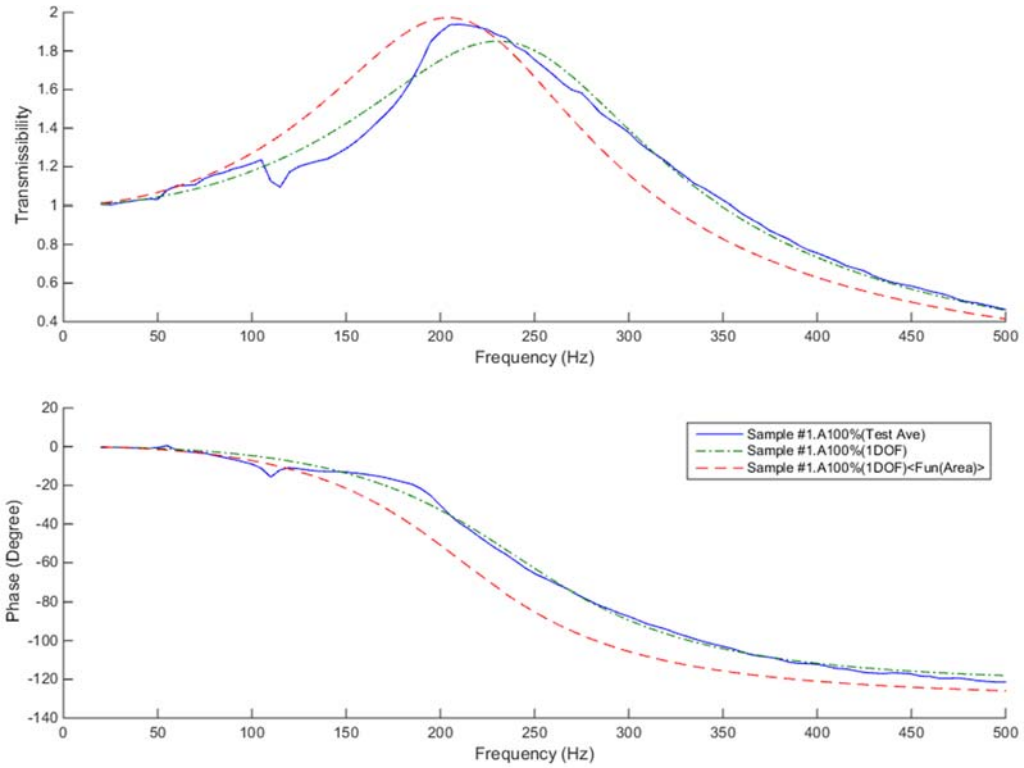

Figure A.4.25 - VT of sample #1 for 100% of area

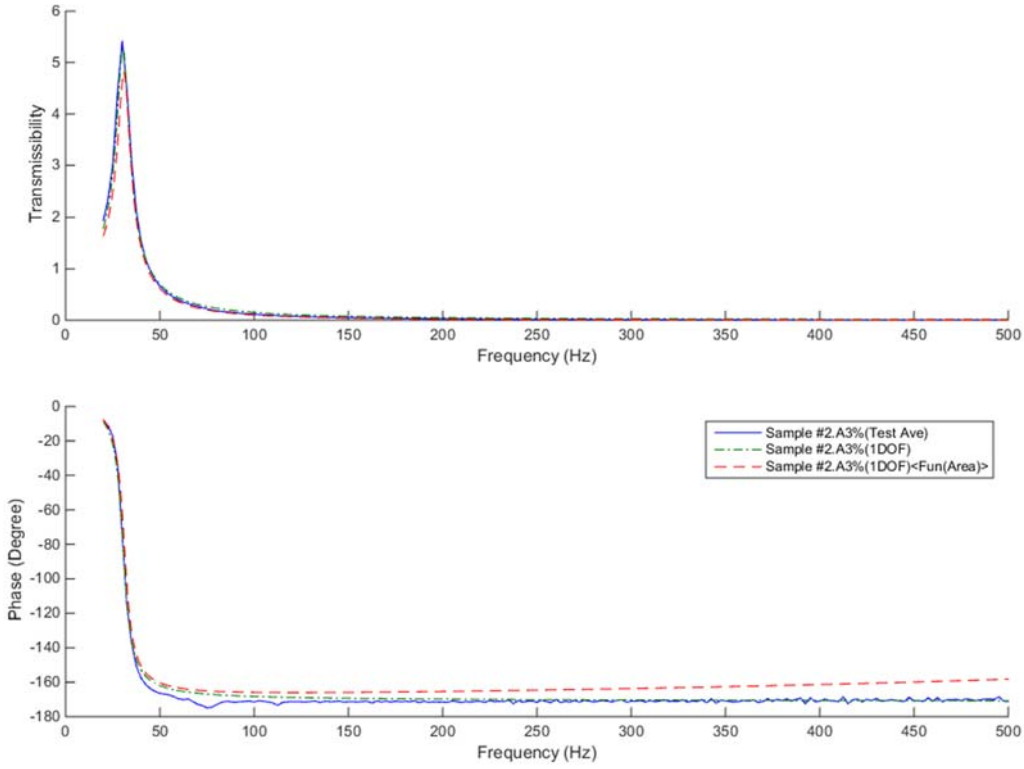

Figure A.4.26 - VT of sample #2 for 3% of area

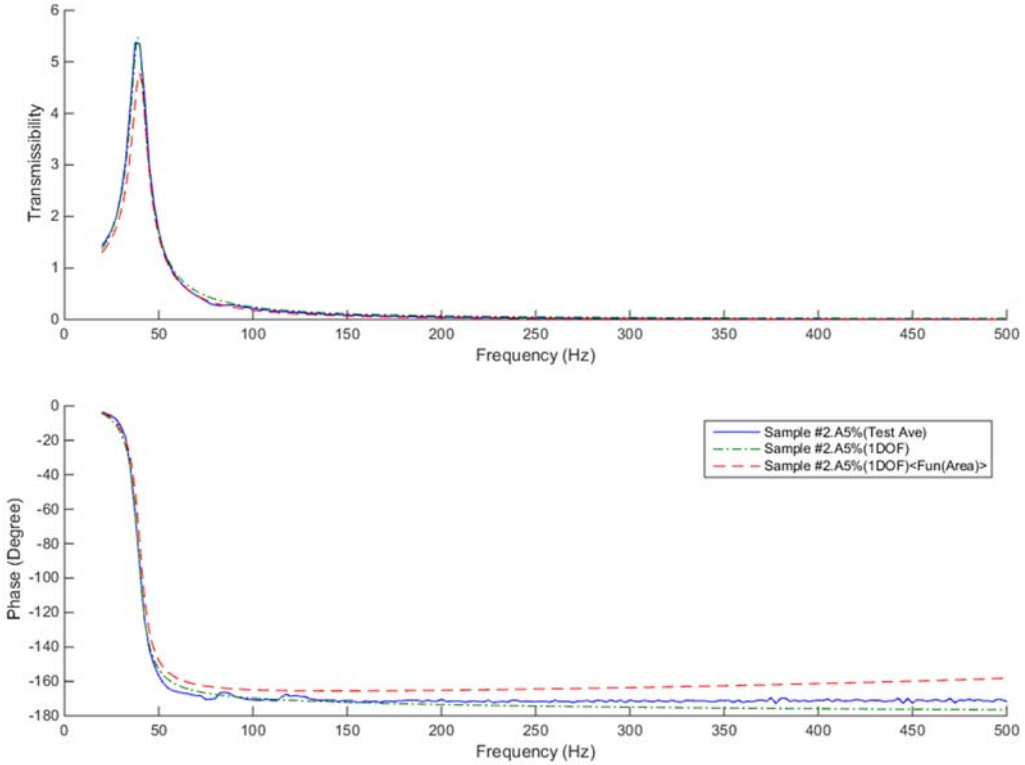

Figure A.4.27 - VT of sample #2 for 5% of area

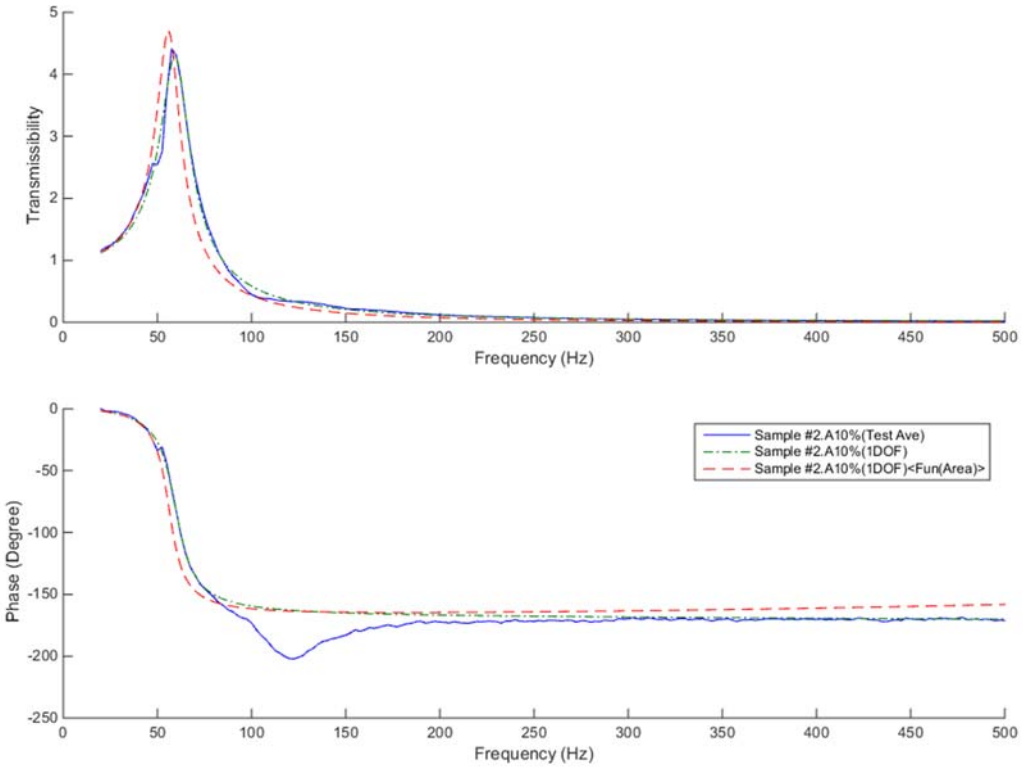

Figure A.4.28 - VT of sample #2 for 10% of area

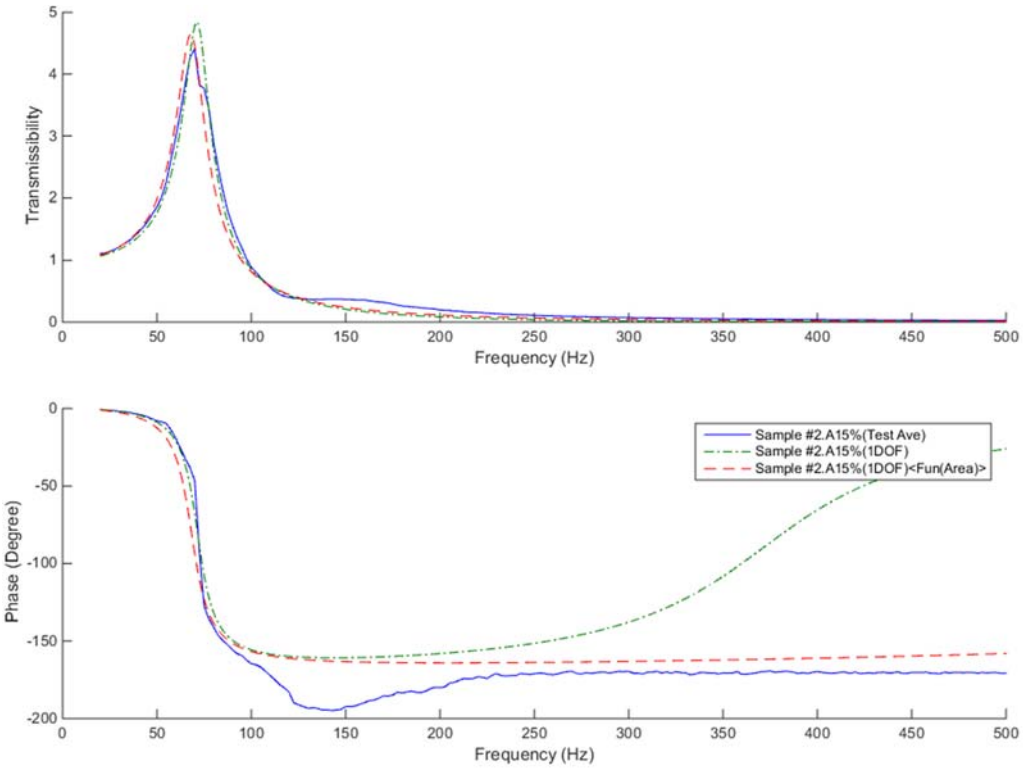

Figure A.4.29 - VT of sample #2 for 15% of area

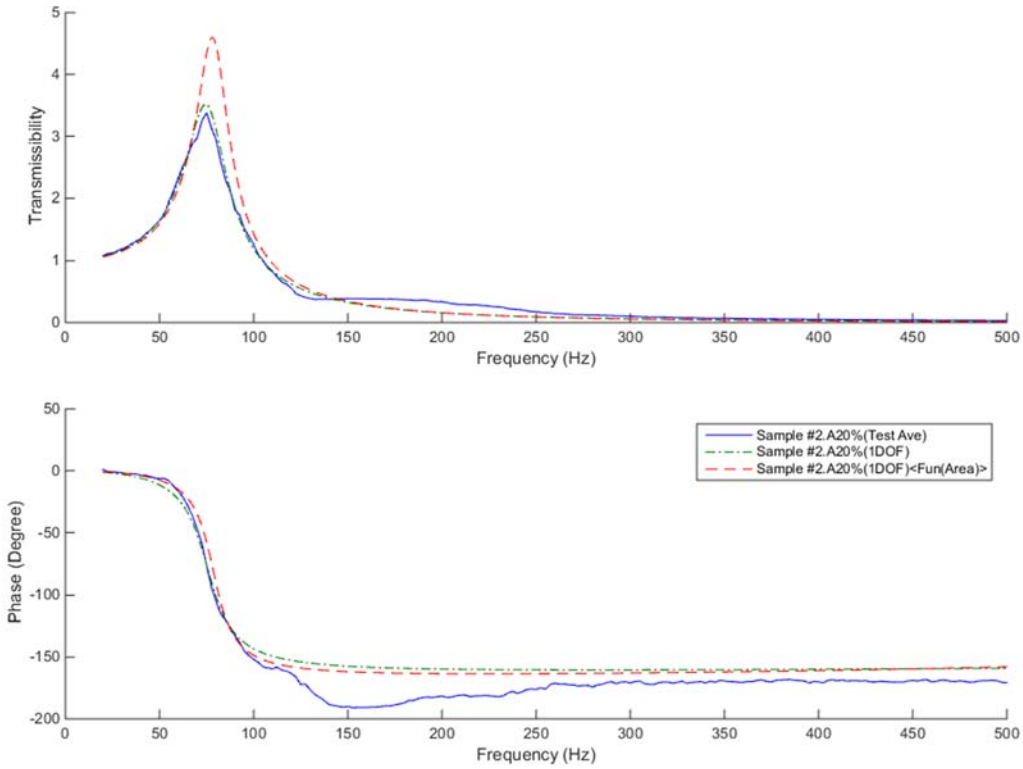

Figure A.4.30 - VT of sample #2 for 20% of area

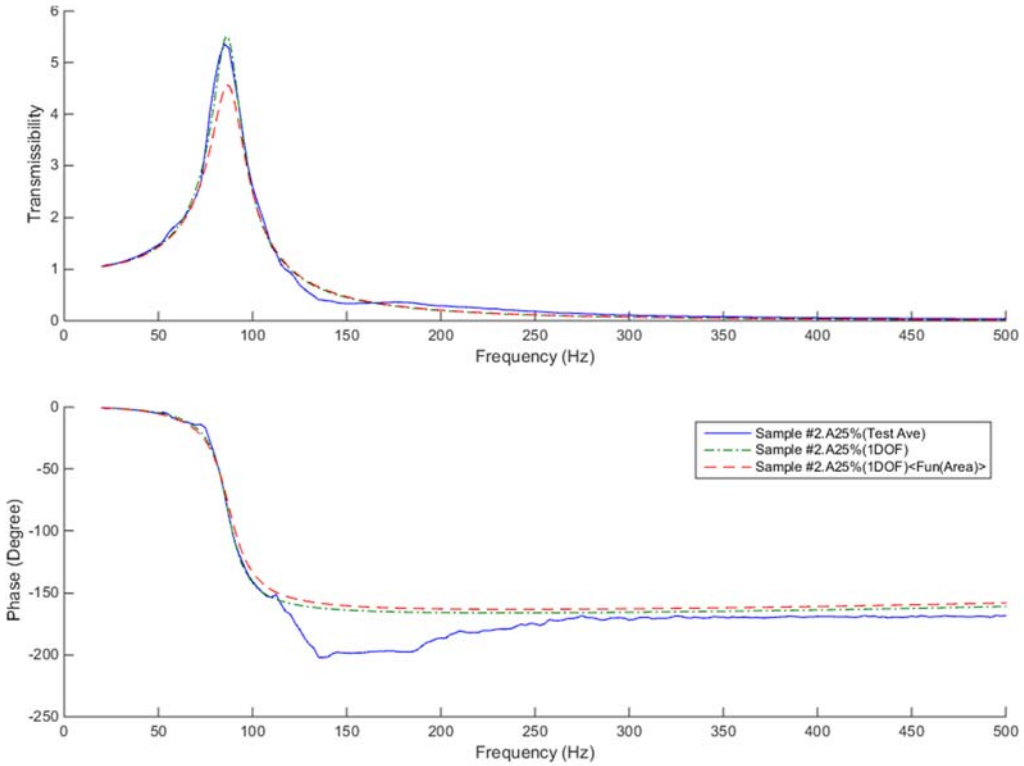

Figure A.4.31 - VT of sample #2 for 25% of area

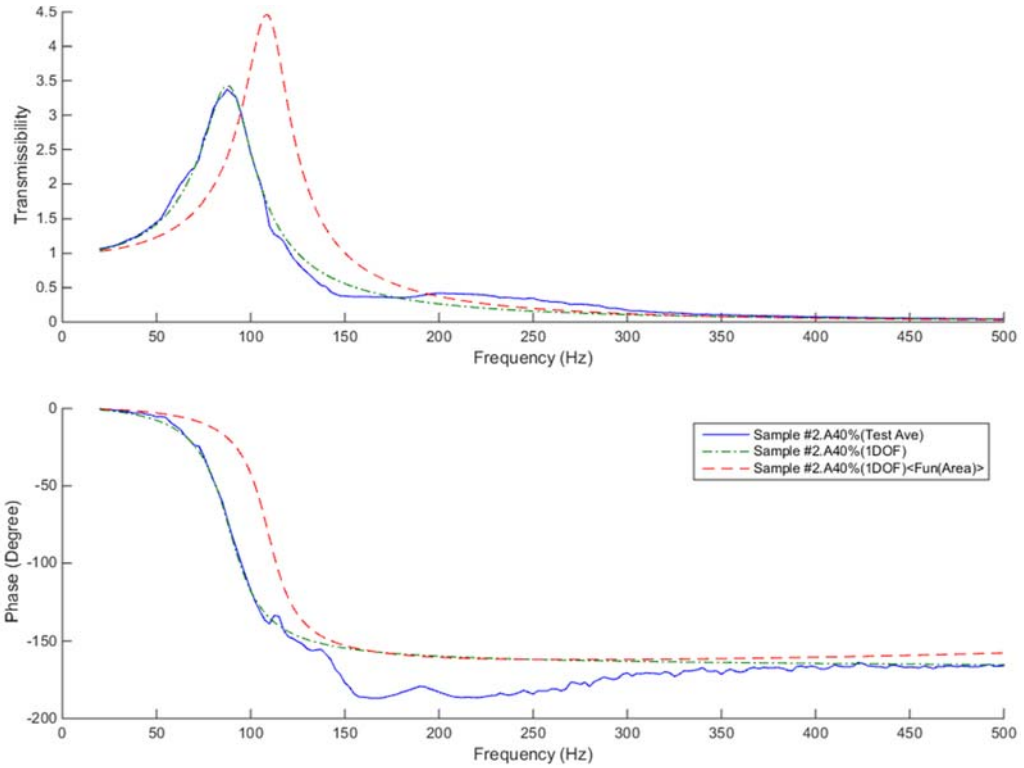

Figure A.4.32 - VT of sample #2 for 40% of area

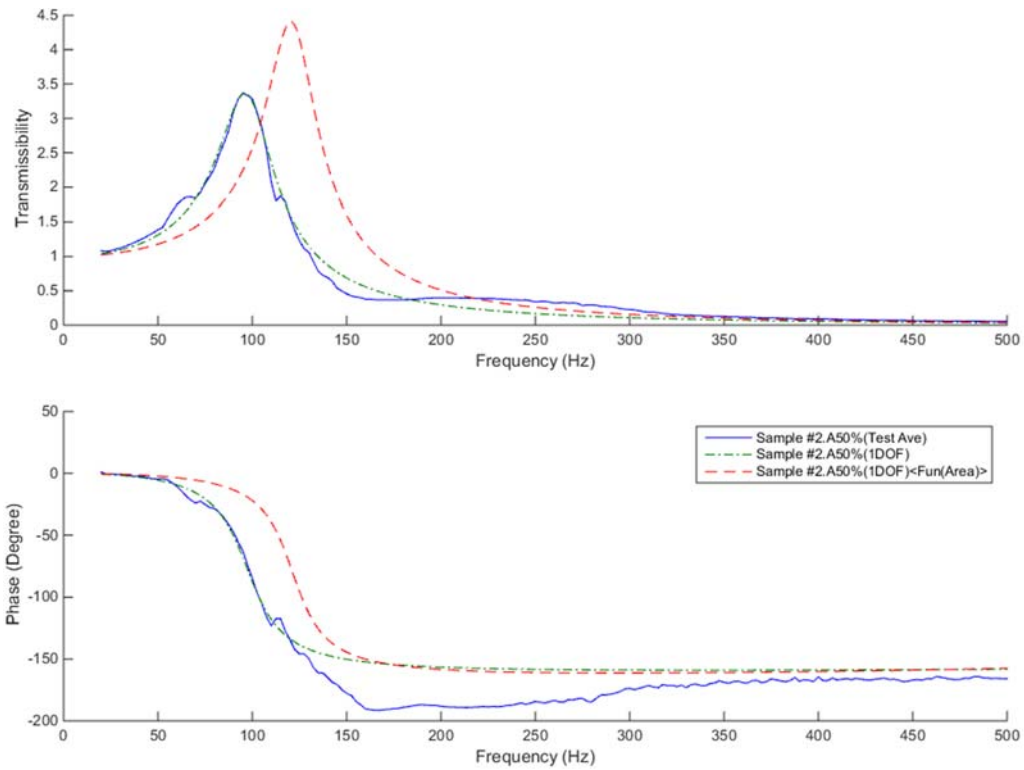

Figure A.4.33 - VT of sample #2 for 50% of area

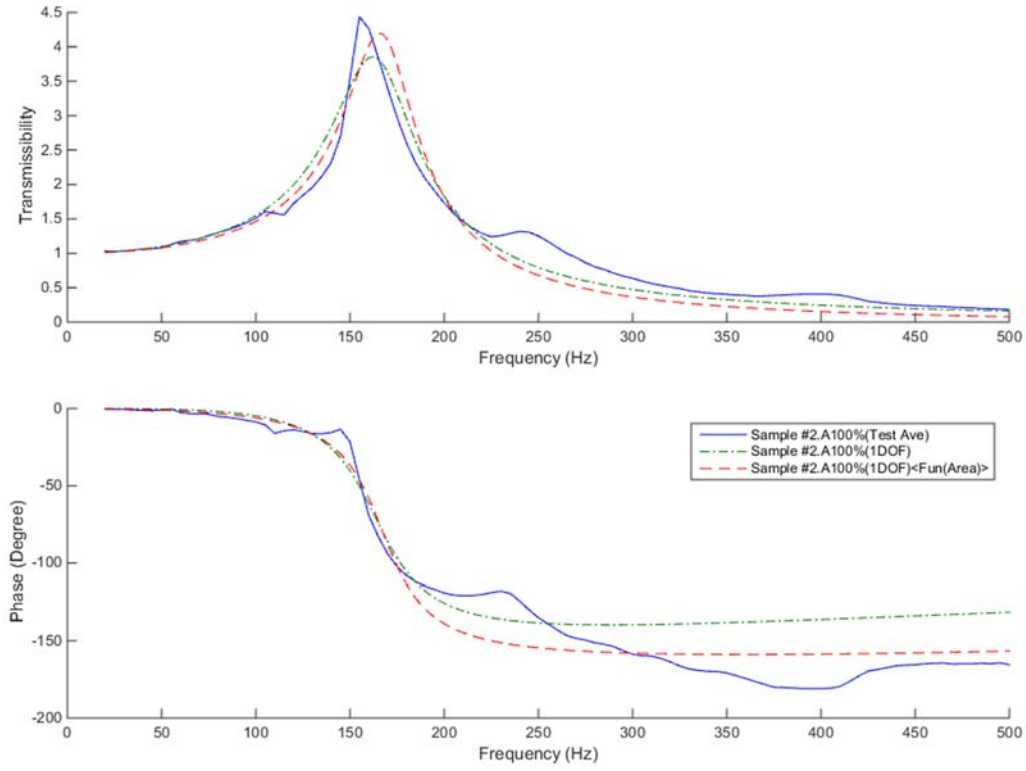

Figure A.4.34 - VT of sample #2 for 100% of area

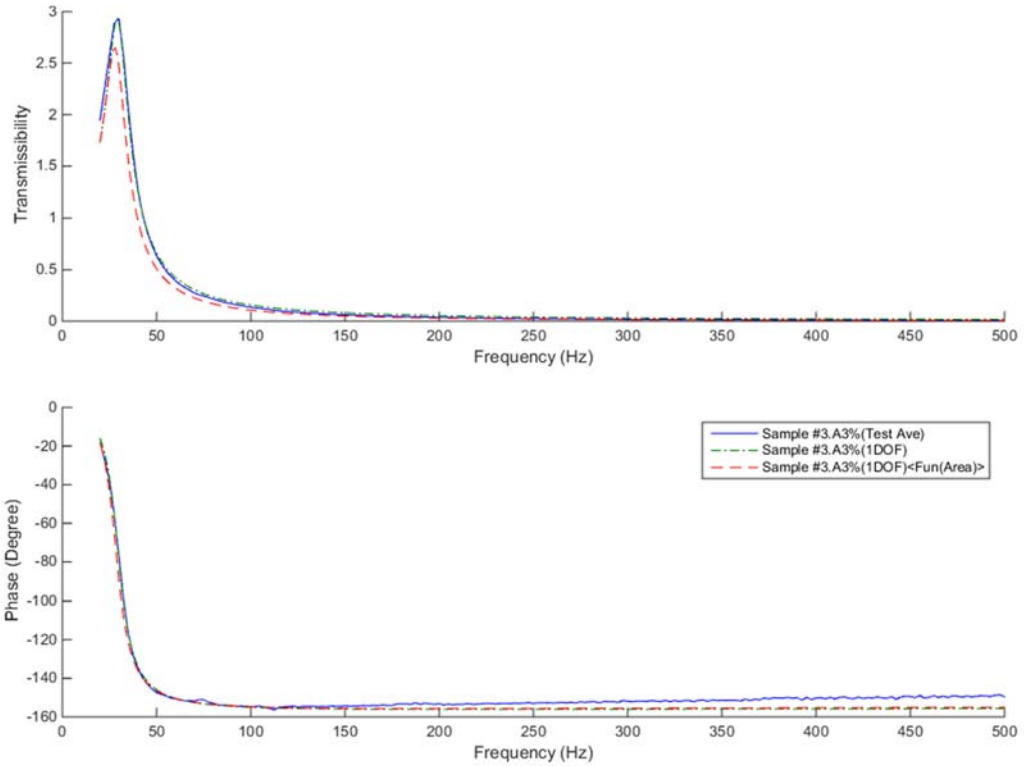

Figure A.4.35 - VT of sample #3 for 3% of area

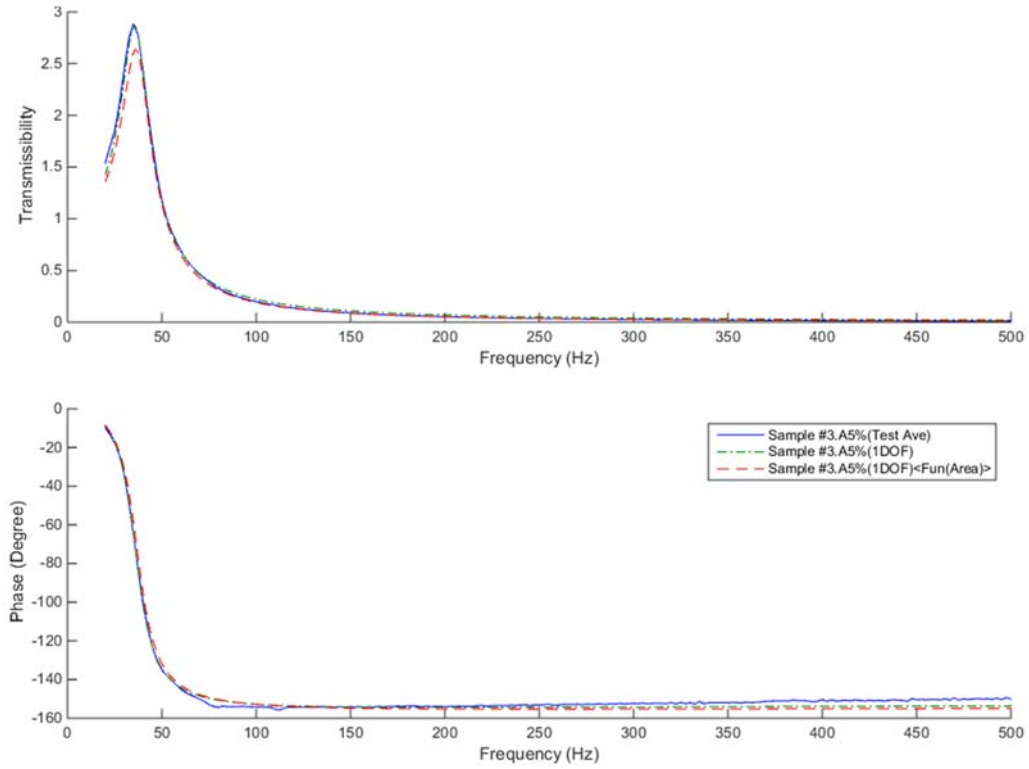

Figure A.4.36 - VT of sample #3 for 5% of area

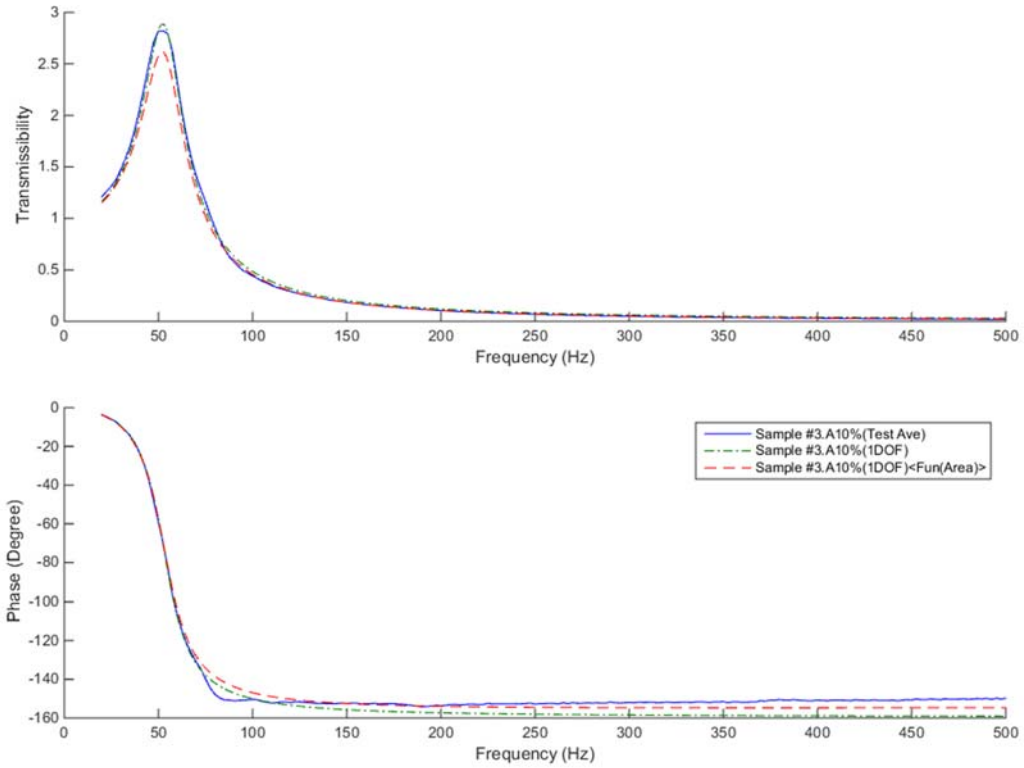

Figure A.4.37 - VT of sample #3 for 10% of area

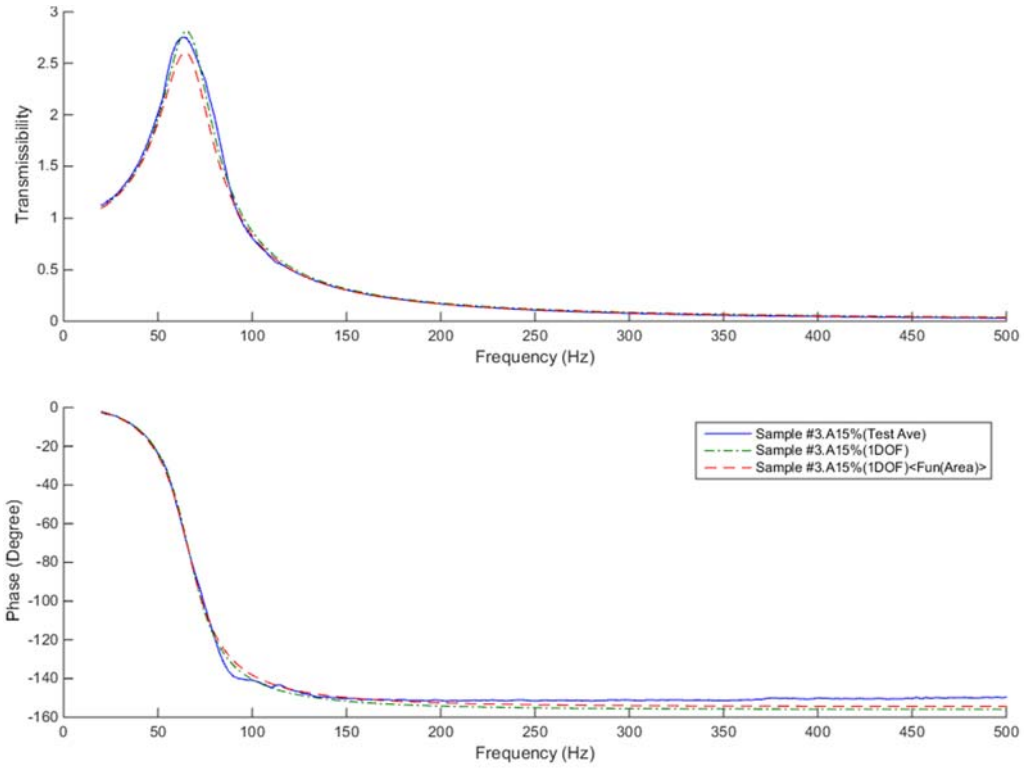

Figure A.4.38 - VT of sample #3 for 15% of area

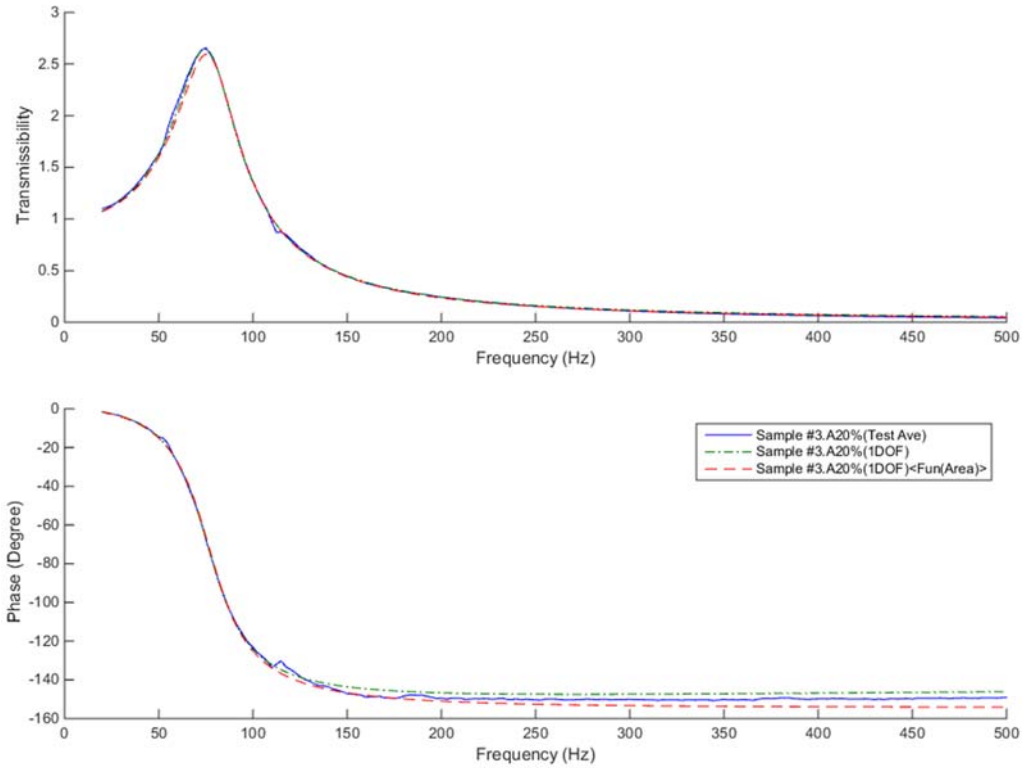

Figure A.4.39 - VT of sample #3 for 20% of area

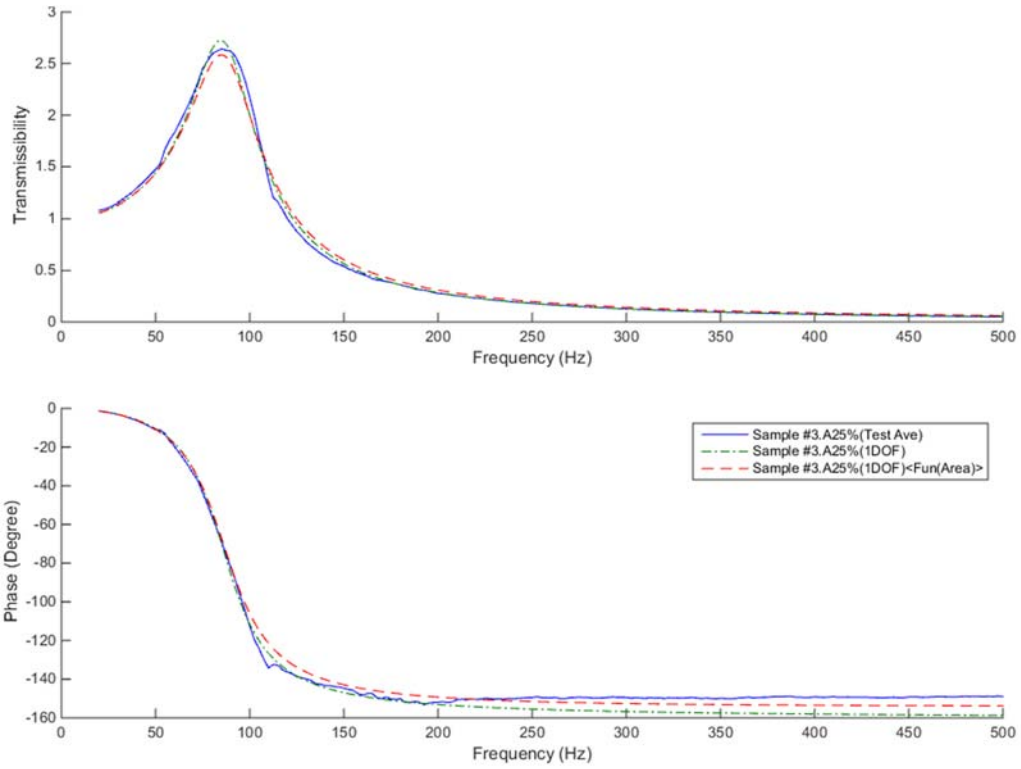

Figure A.4.40 - VT of sample #3 for 25% of area

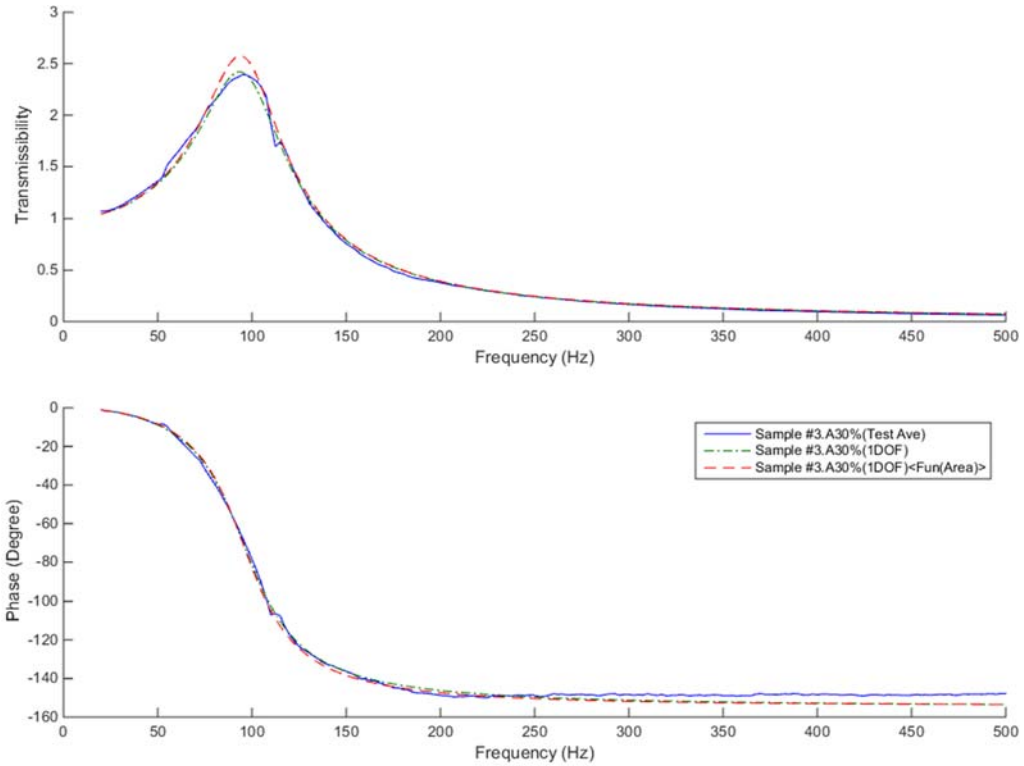

Figure A.4.41 - VT of sample #3 for 30% of area

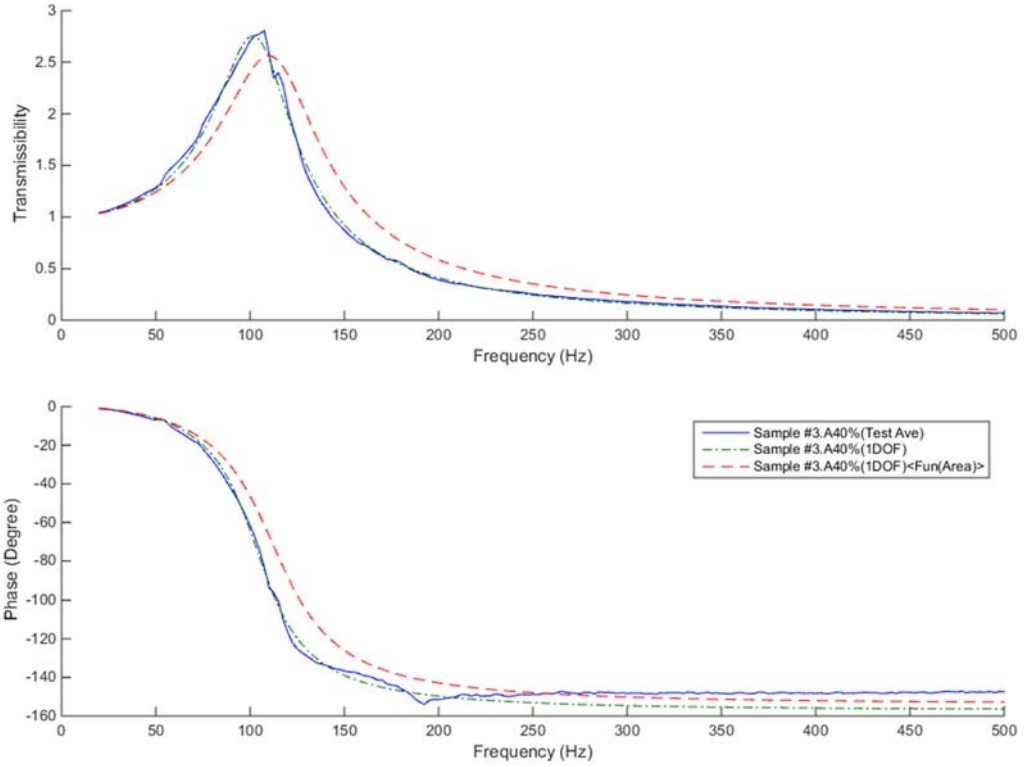

Figure A.4.42 - VT of sample #3 for 40% of area

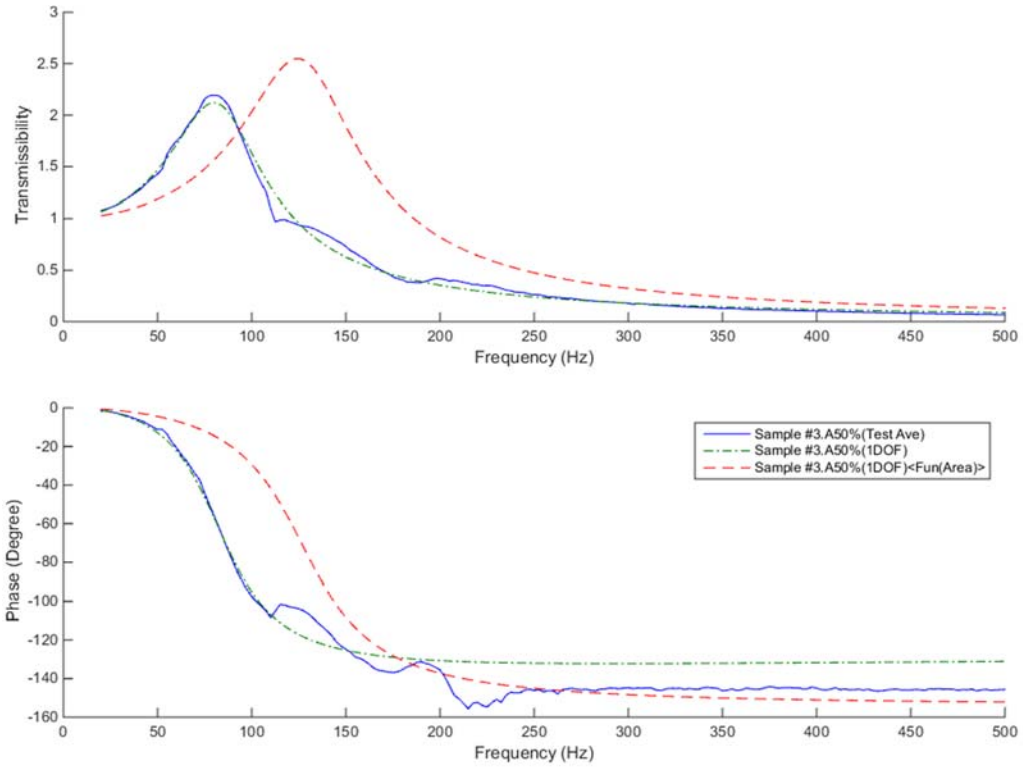

Figure A.4.43 - VT of sample #3 for 50% of area

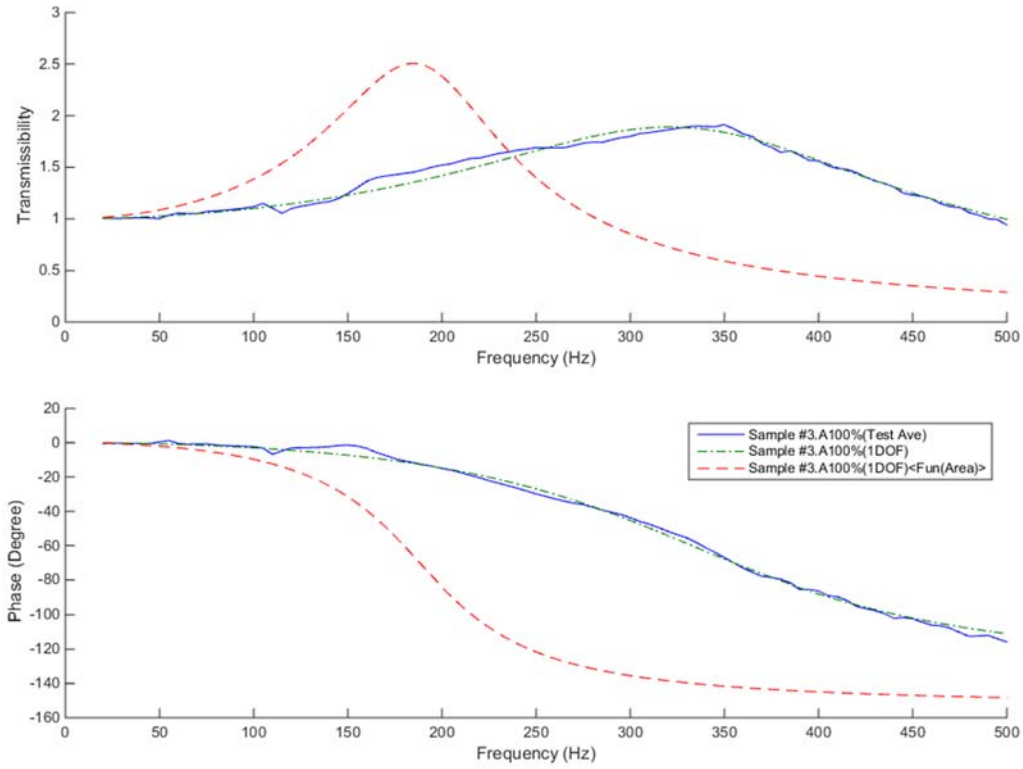

Figure A.4.44 - VT of sample #3 for 100% of area

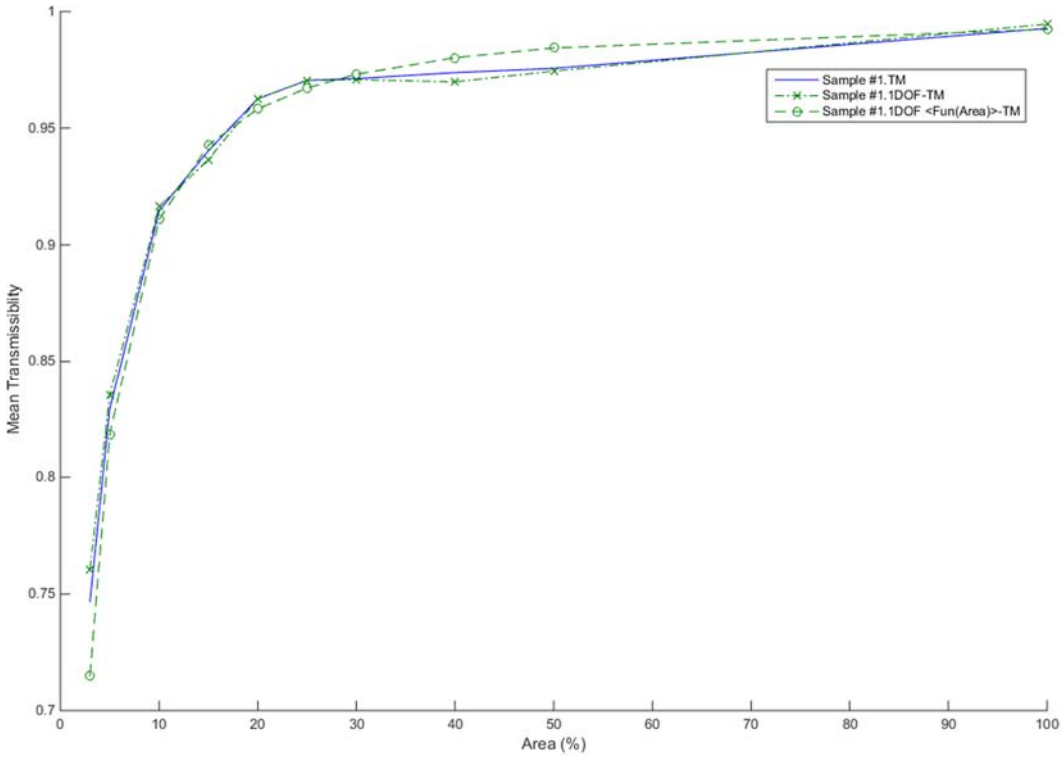

Figure A.4.45 - MVT (medium frequency) of sample #1

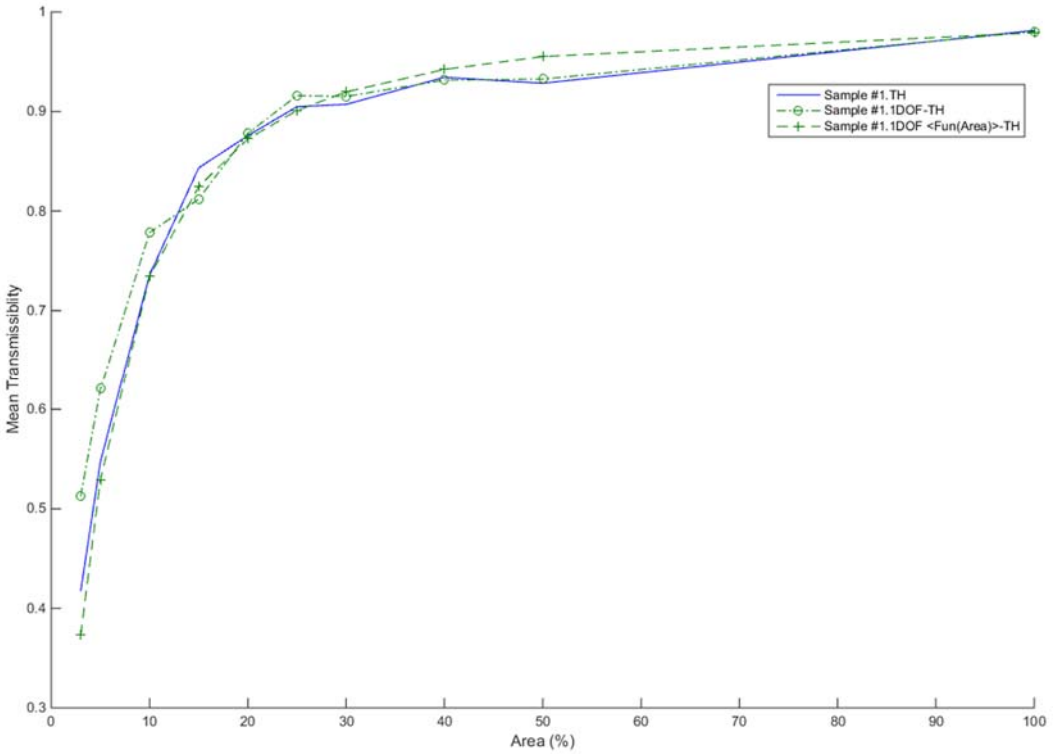

Figure A.4.46 - MVT (high frequency) of sample #1

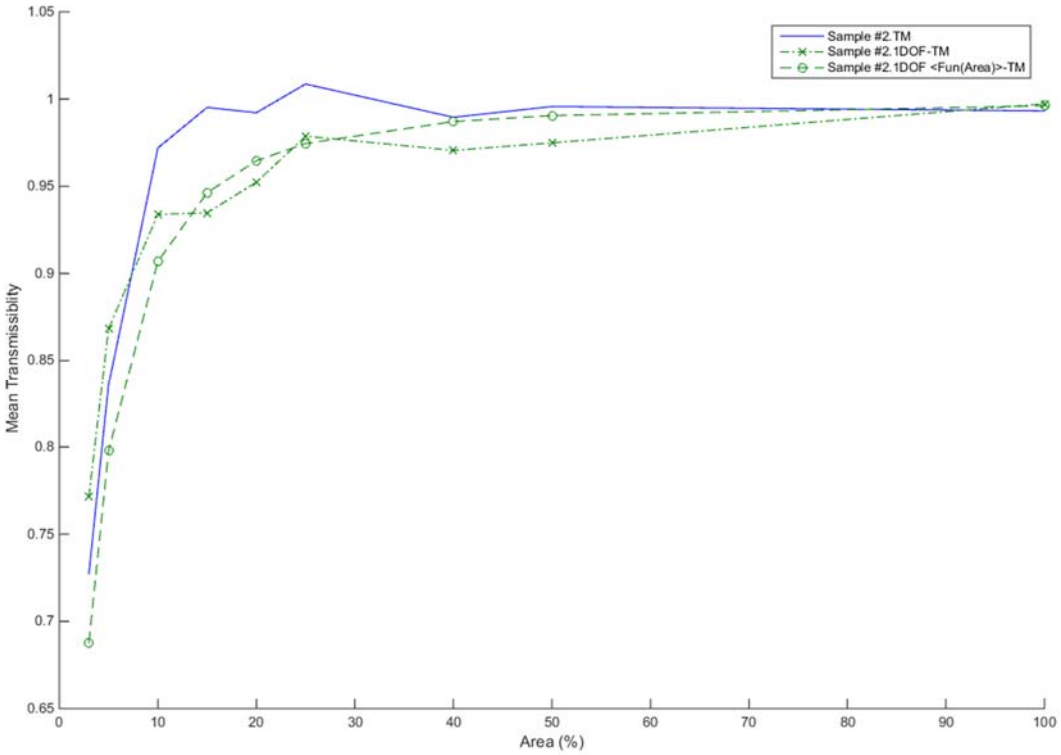

Figure A.4.47 - MVT (medium frequency) of sample #2

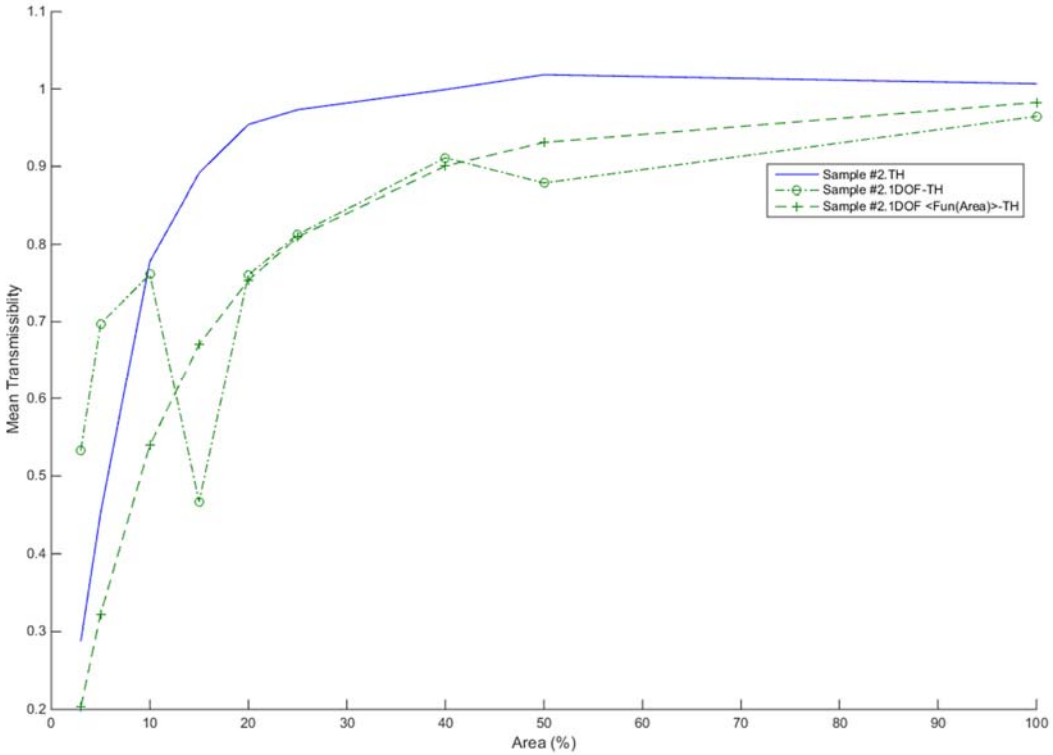

Figure A.4.48 - MVT (high frequency) of sample #2

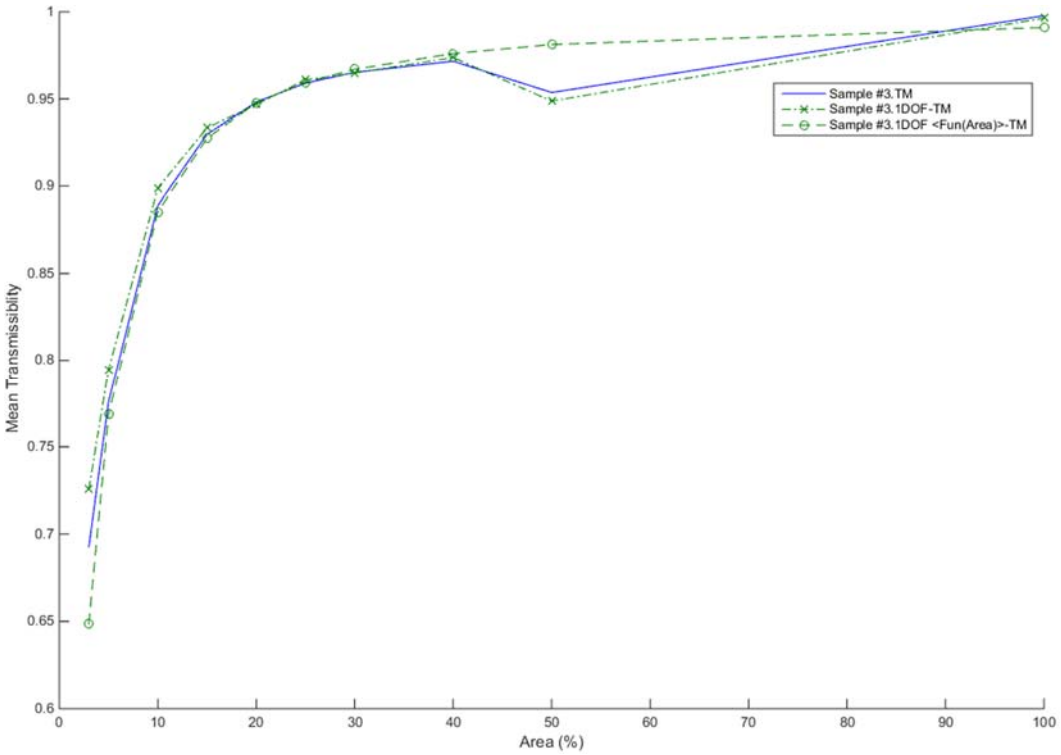

Figure A.4.49 - MVT (medium frequency) of sample #3

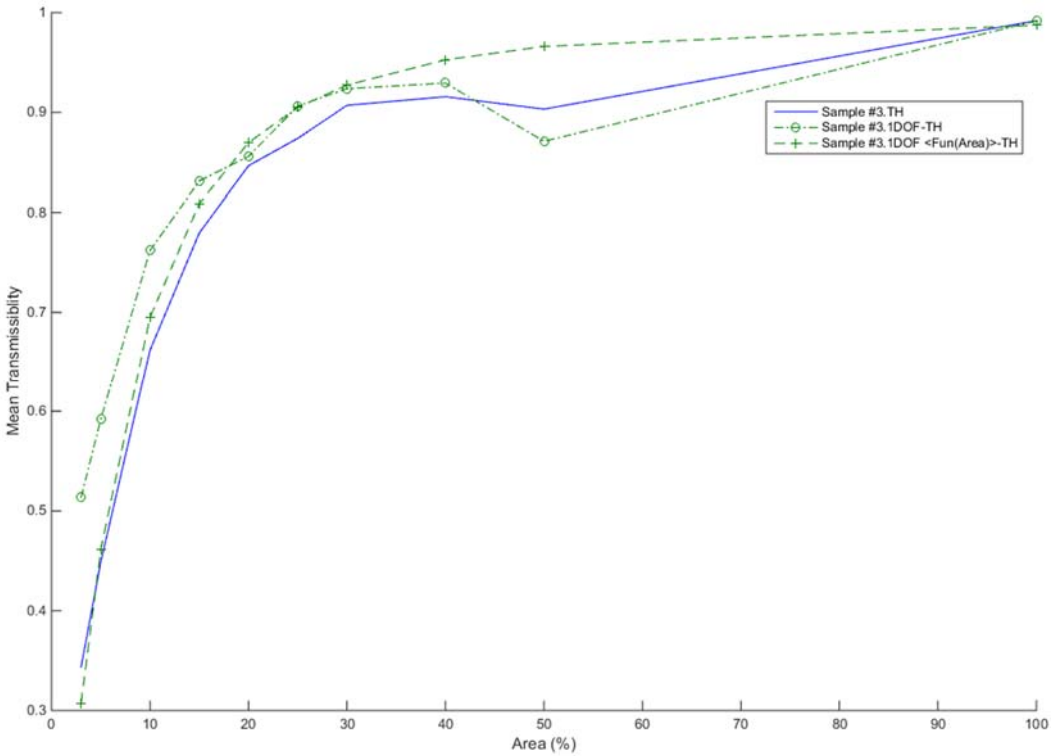

Figure A.4.50 - MVT (high frequency) of sample #3

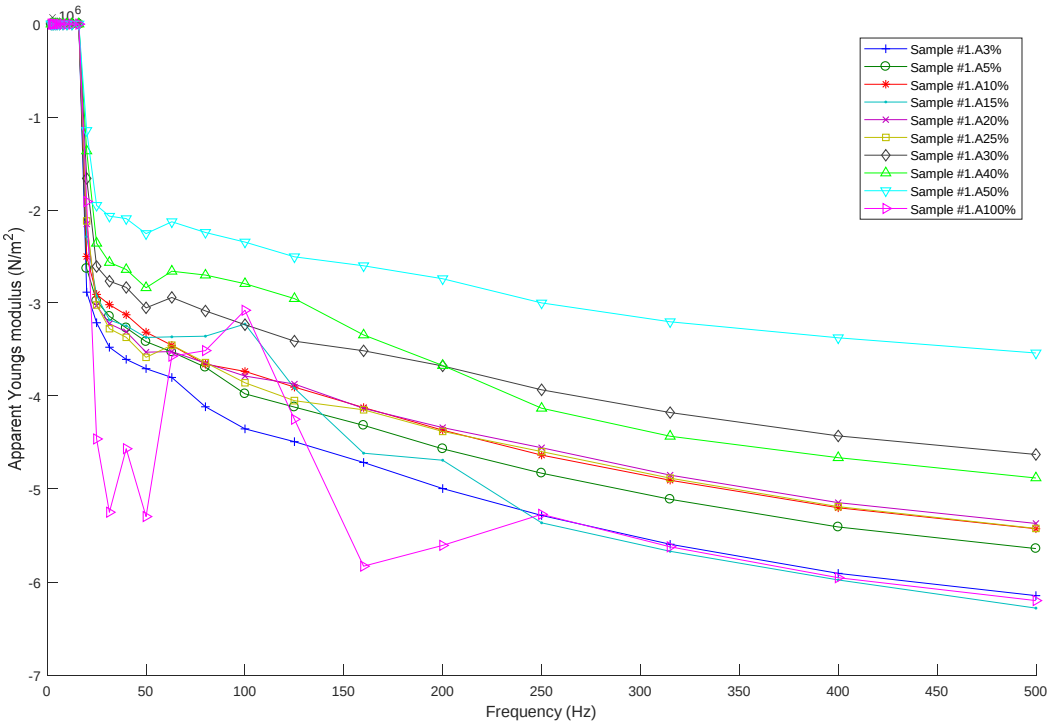

Figure A.4.51 - Apparent Young's modulus of sample #1

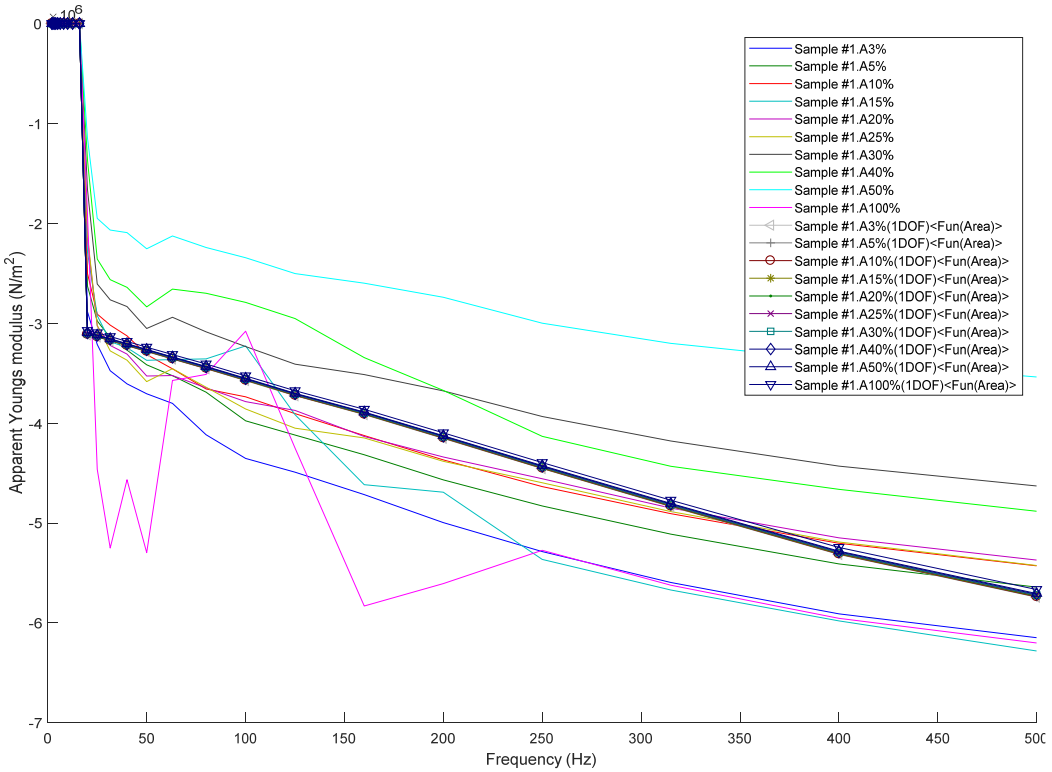

Figure A.4.52 - Apparent Young's modulus of sample #1 (Measured vs. Model)

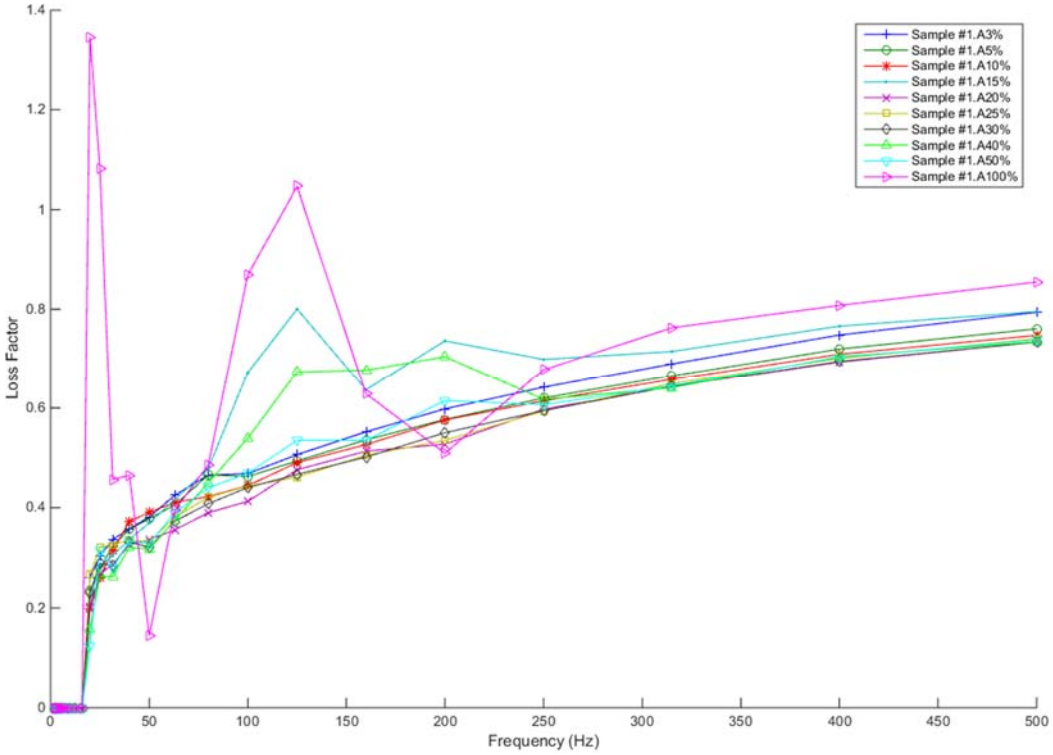

Figure A.4.53 - Loss Factor of sample #1

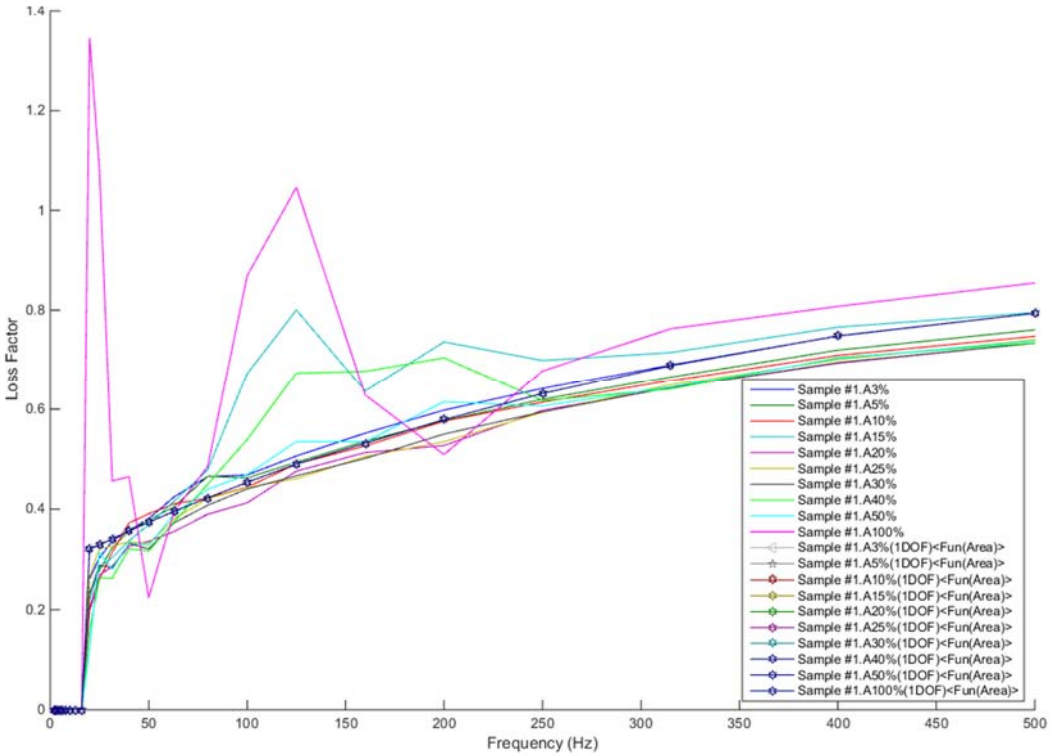

Figure A.4.54 - Loss Factor of sample #1 (Measured vs. Model)

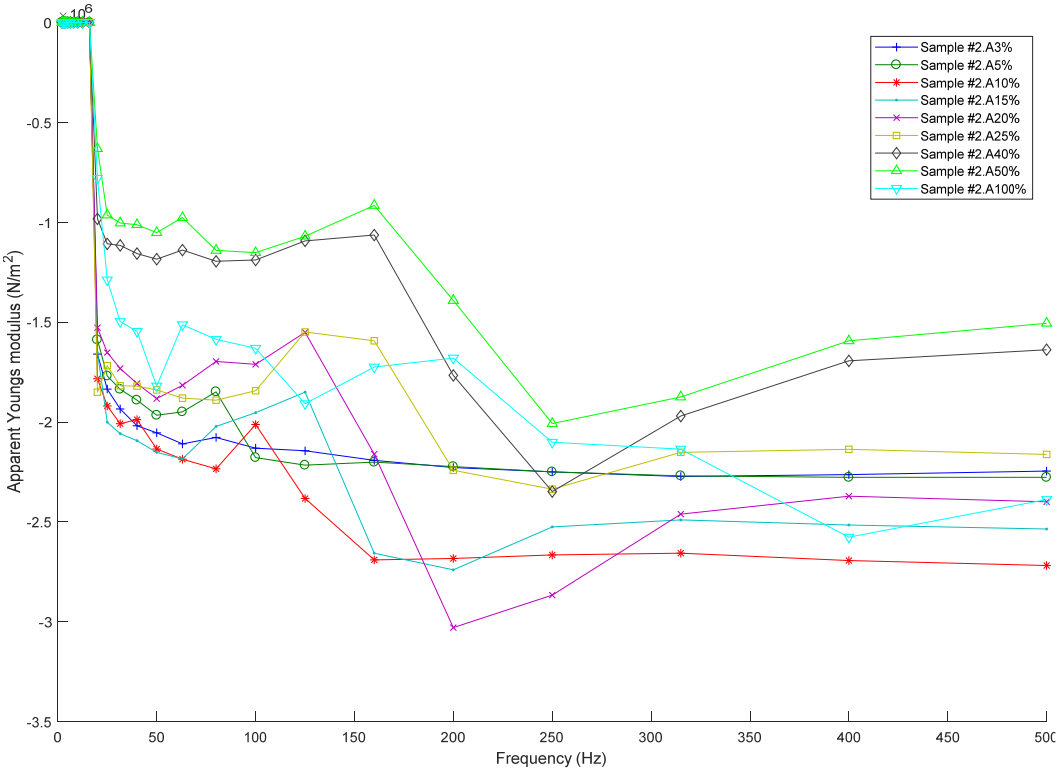

Figure A.4.55 - Apparent Young's modulus of sample #2

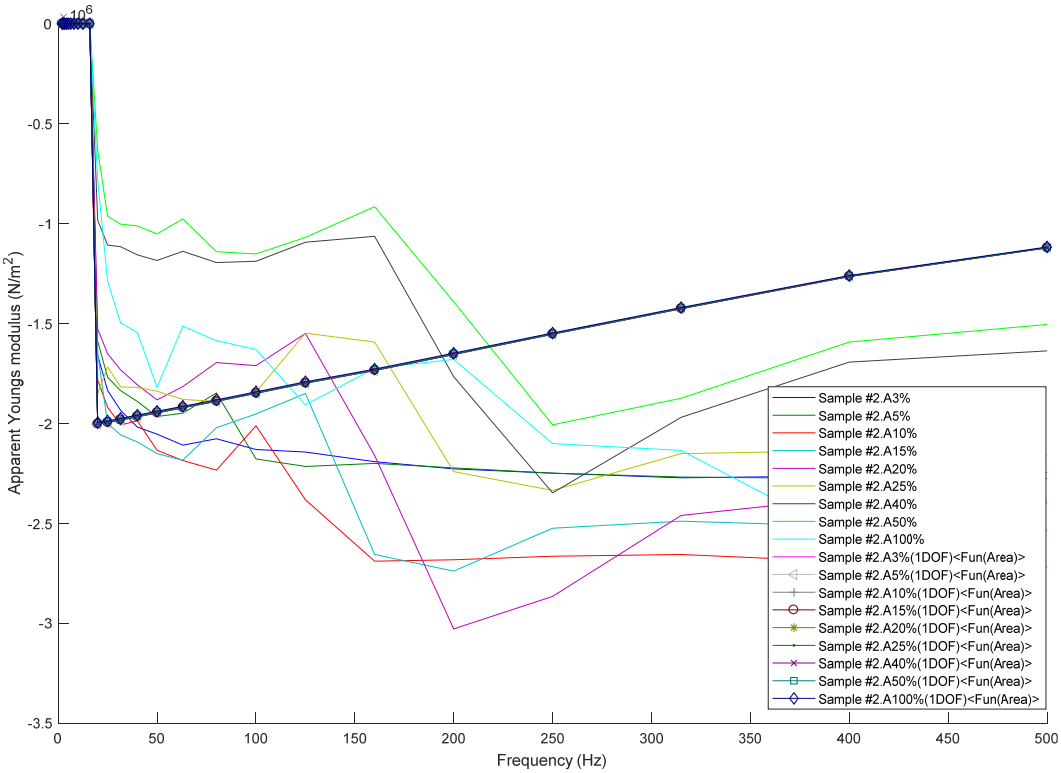

Figure A.4.56 - Apparent Young's modulus of sample #2 (Measured vs. Model)

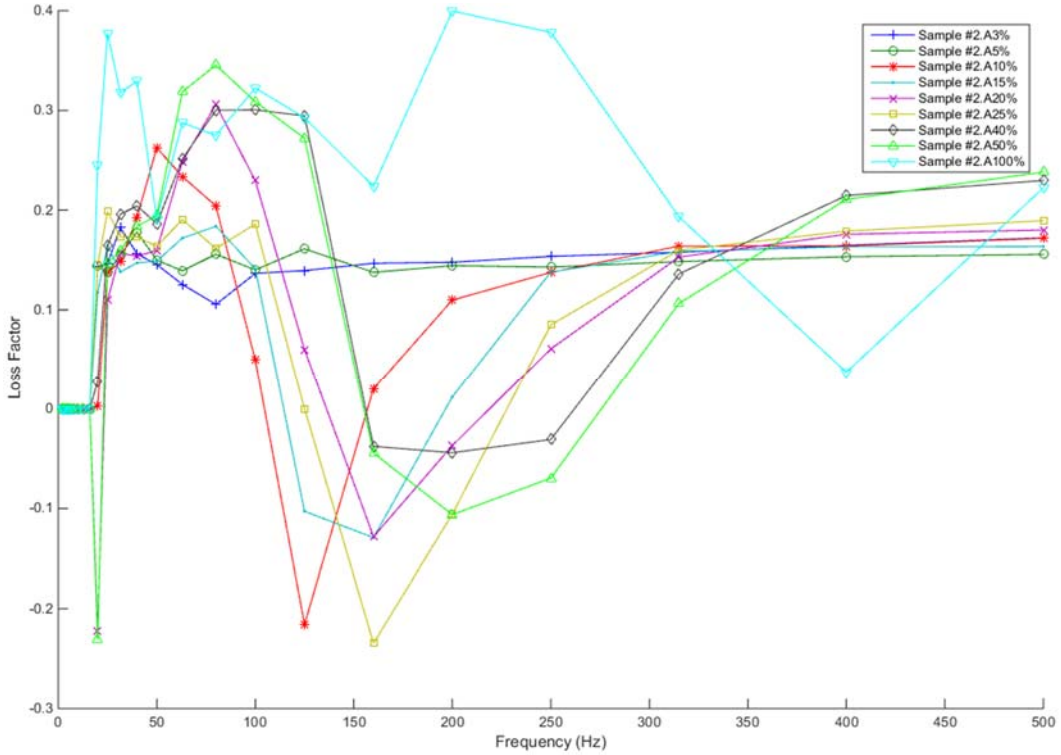

Figure A.4.57 - Loss Factor of sample #2

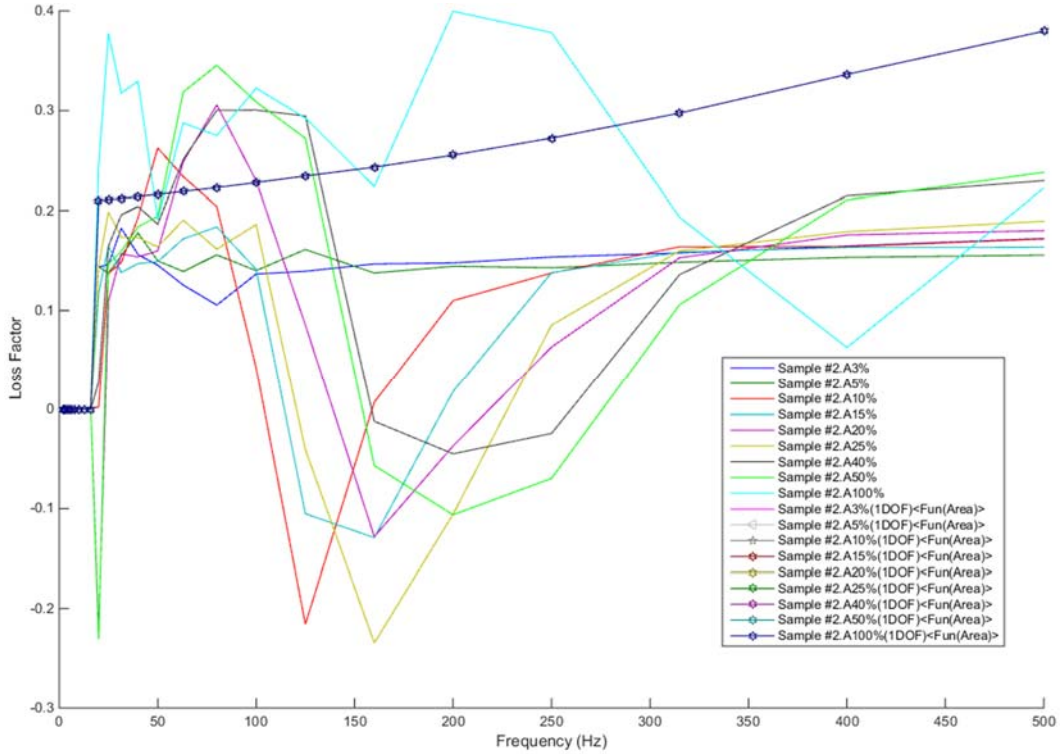

Figure A.4.58 - Loss Factor of sample #2 (Measured vs. Model)

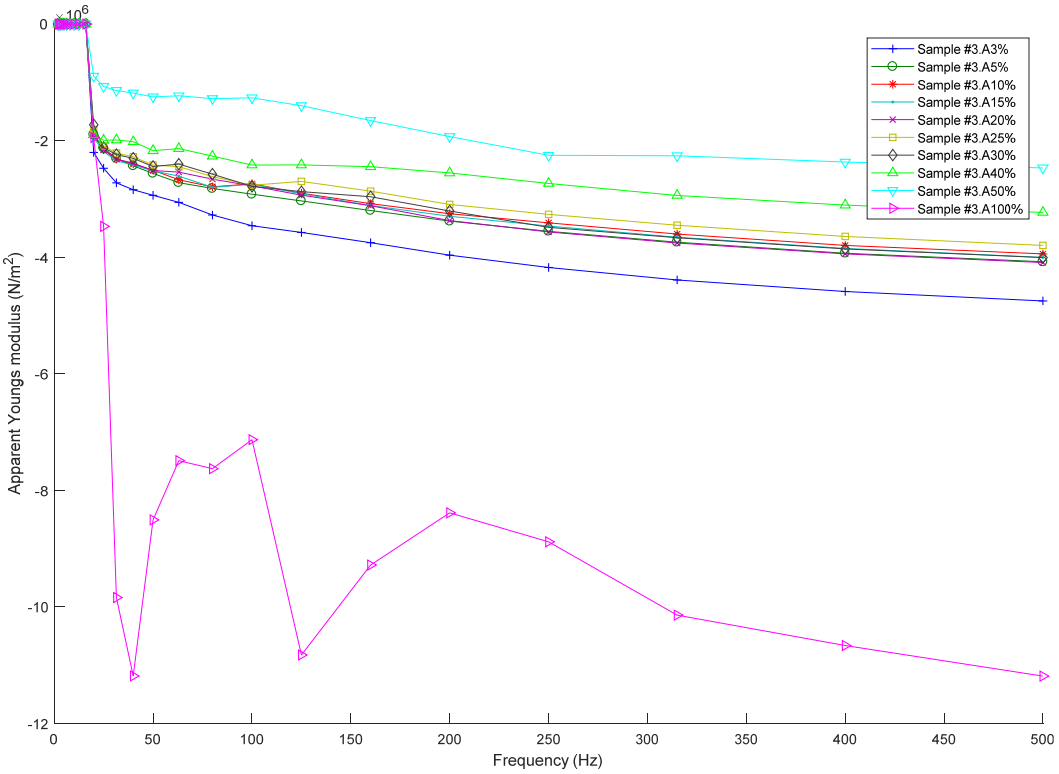

Figure A.4.59 - Apparent Young's modulus of sample #3

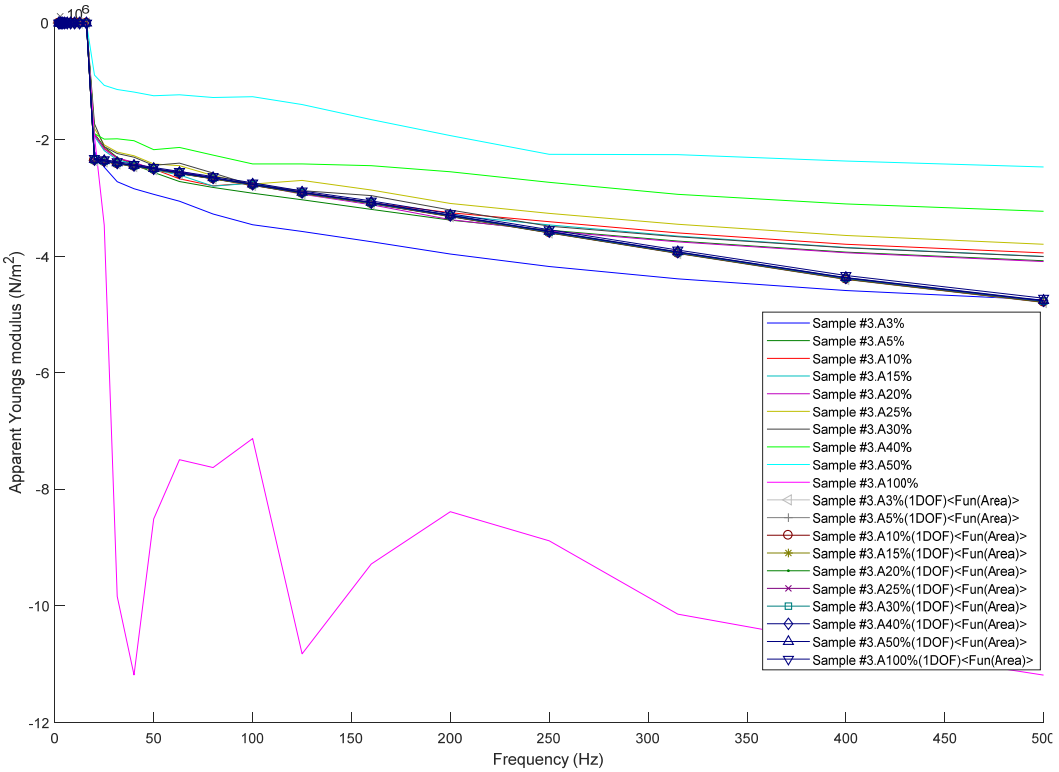

Figure A.4.60 - Apparent Young's modulus of sample #3 (Measured vs. Model)

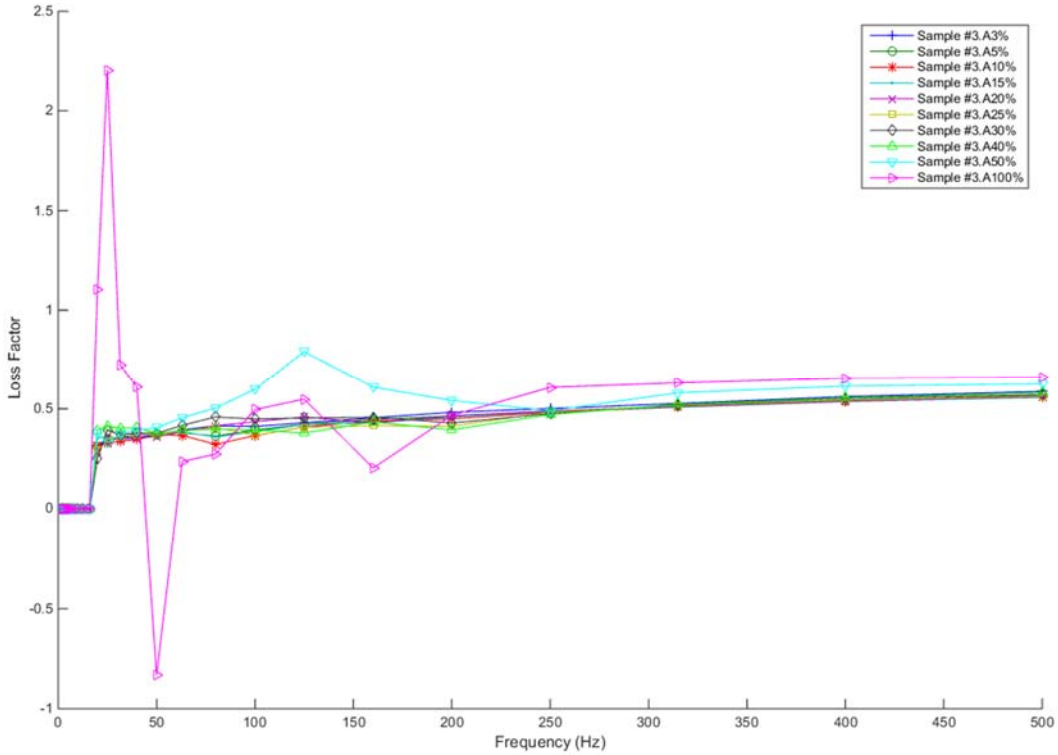

Figure A.4.61 - Loss Factor of sample #3

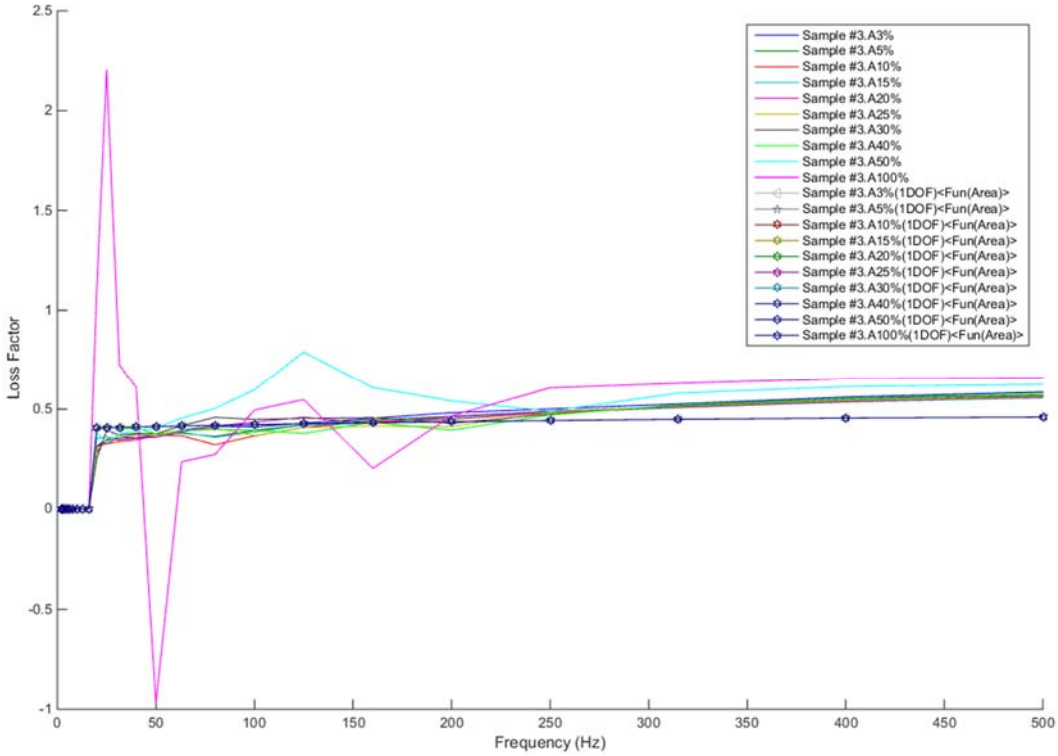

Figure A.4.62 - Loss Factor of sample #3 (Measured vs. Model)

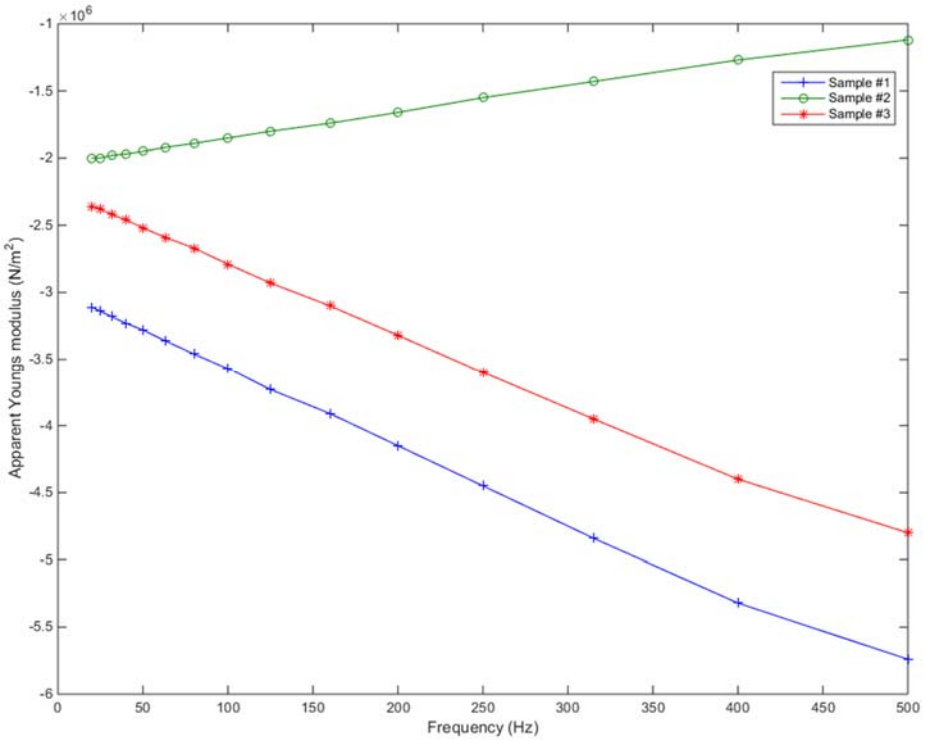

Figure A.4.63 - Apparent Young's modulus of samples' 1-DOF models

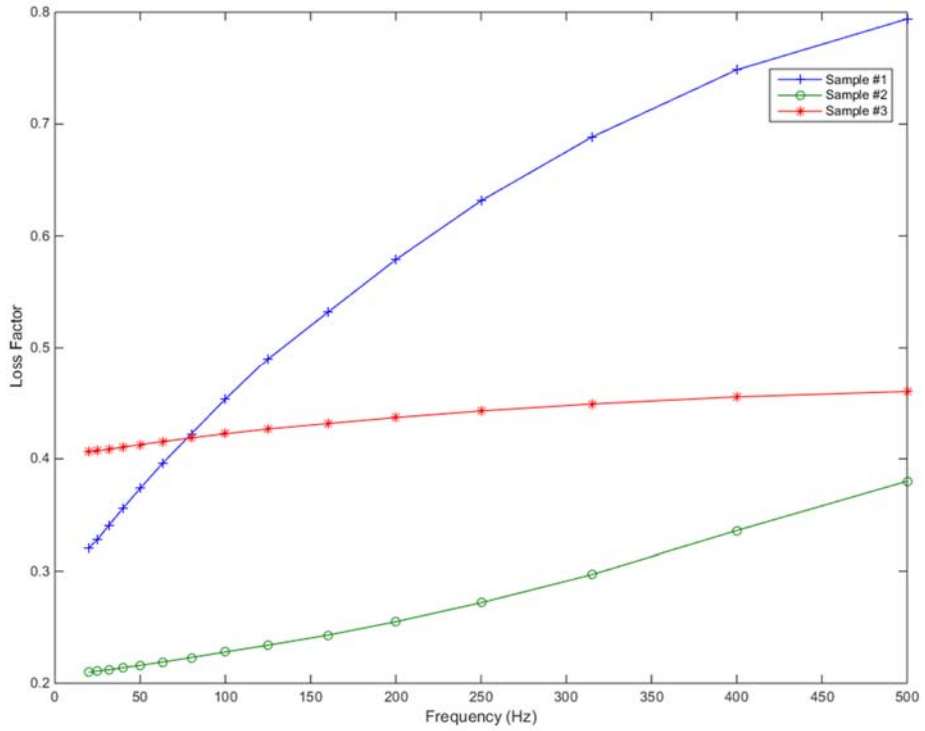

Figure A.4.64 - Loss Factor of samples' 1-DOF models

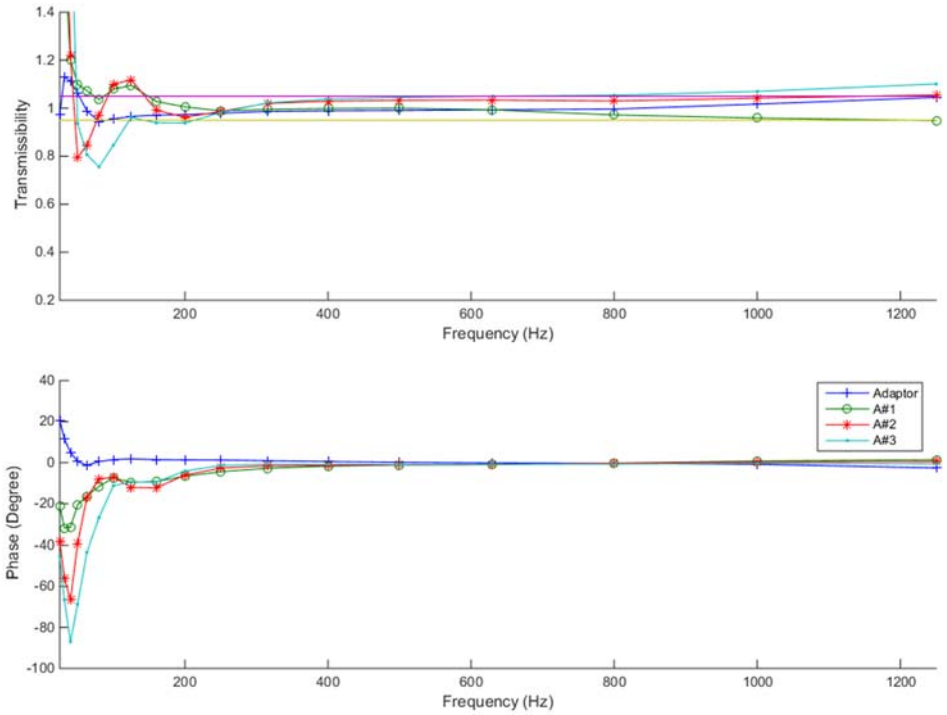

Figure A.5. 1 - VT of the bare hand test for participant #1

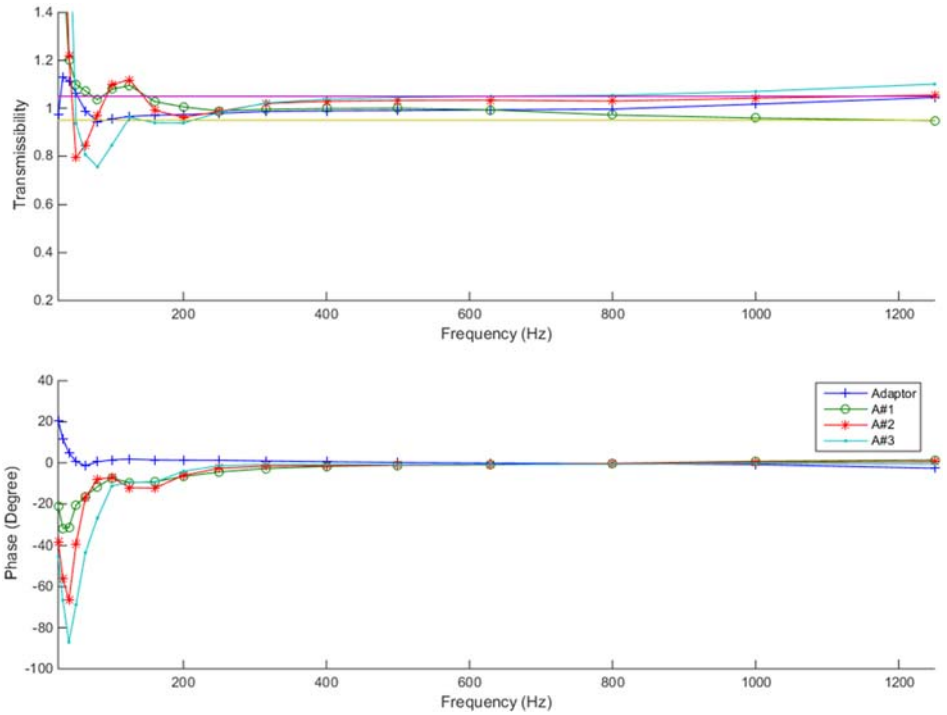

Figure A.5. 2 - VT of the bare hand test for participant #2

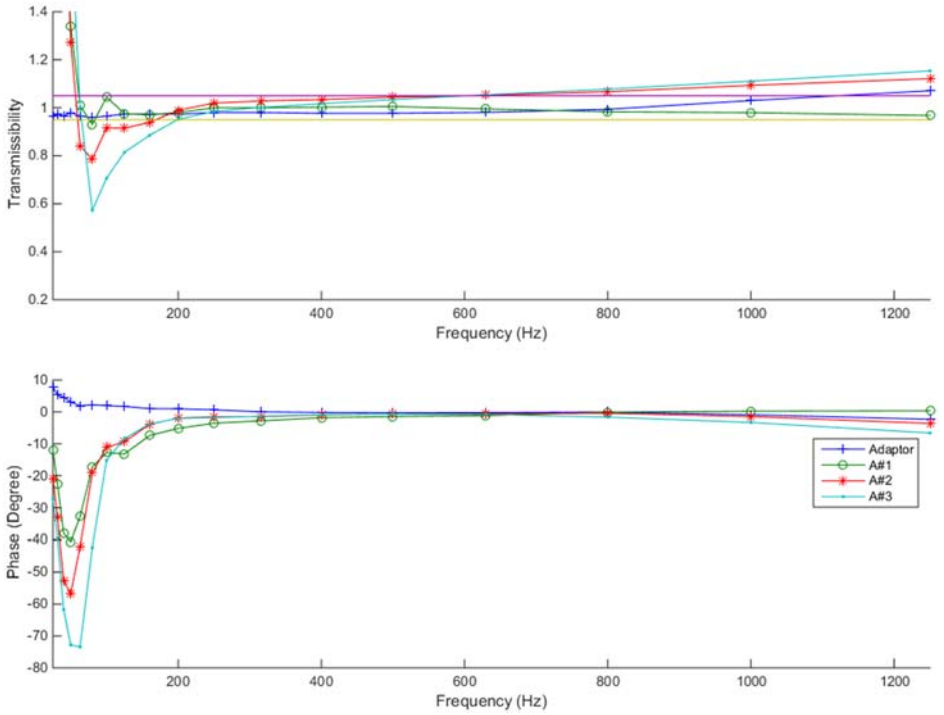

Figure A.5. 3 - VT of the bare hand test for participant #3

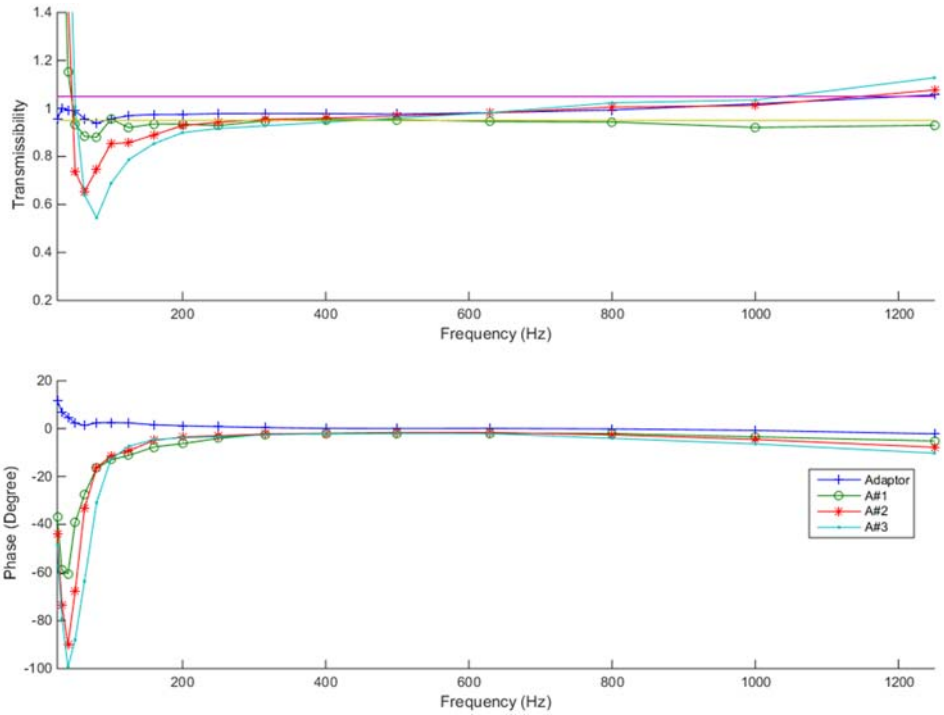

Figure A.5. 4 - VT of the bare hand test for participant #4

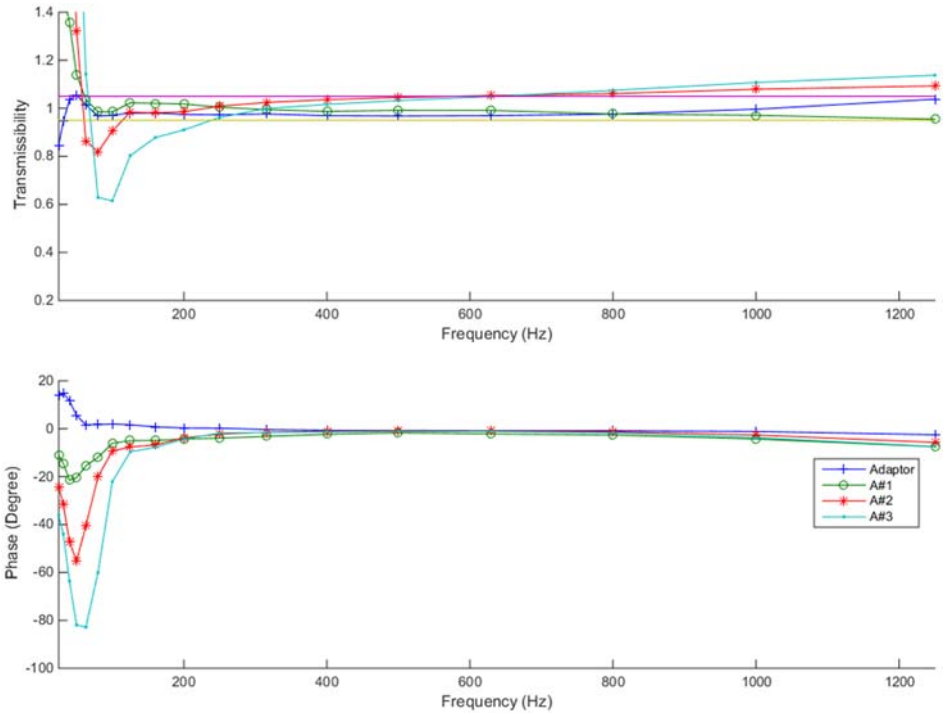

Figure A.5. 5 VT of the bare hand test for participant #5

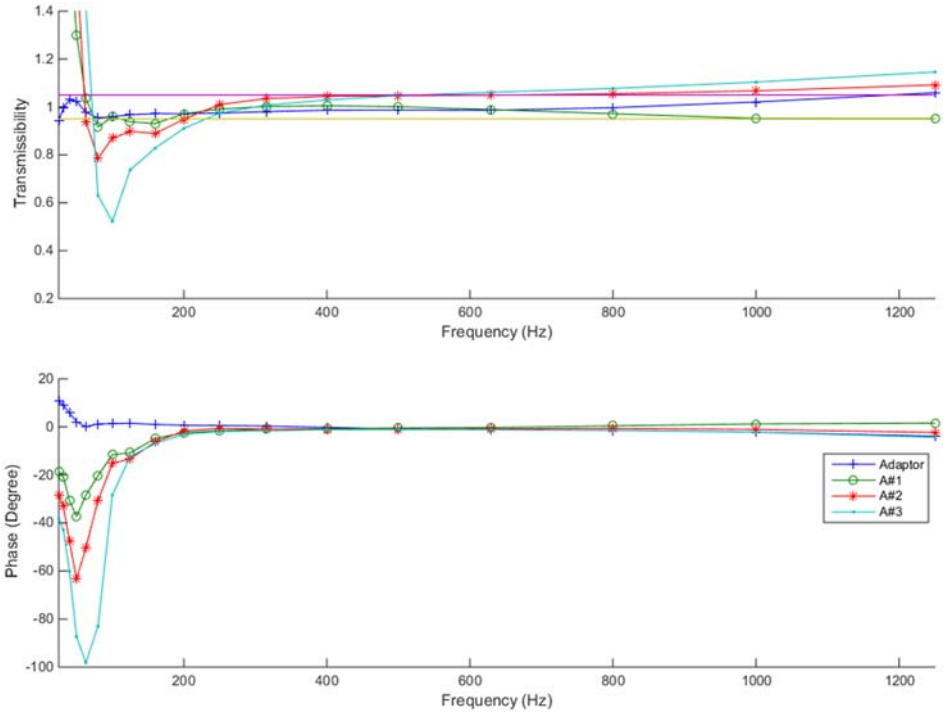

Figure A.5. 6 - VT of the bare hand test for participant #6

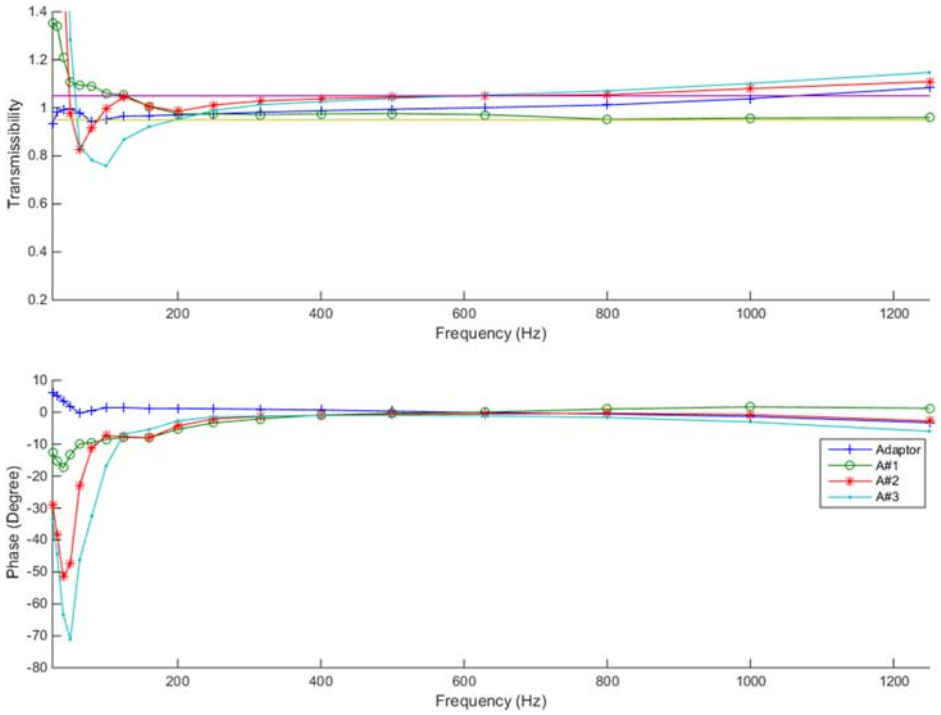

Figure A.5. 7 - VT of the bare hand test for participant #7

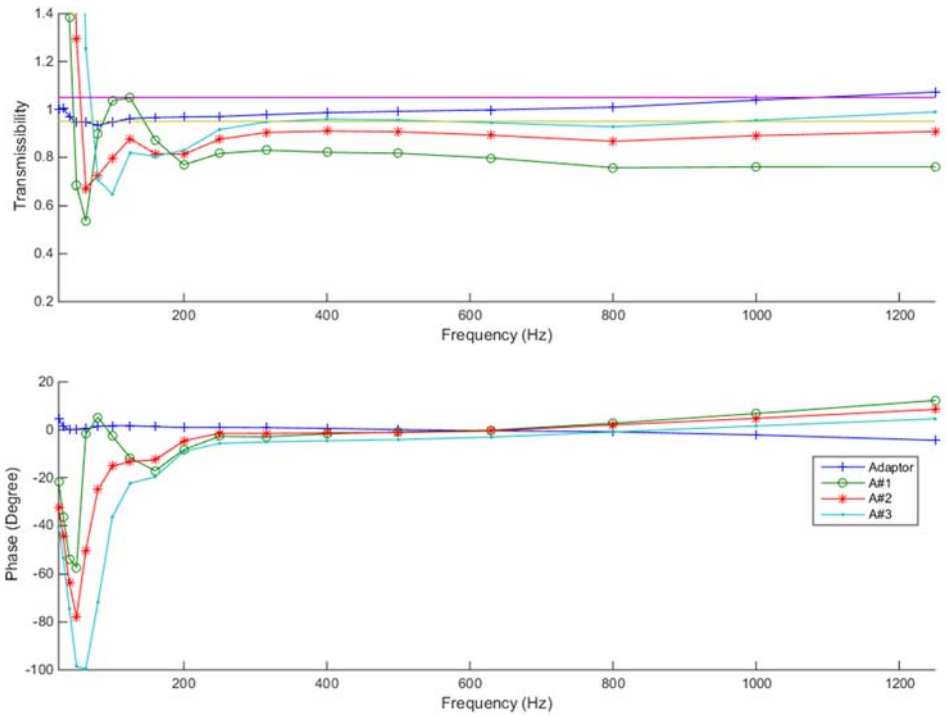

Figure A.5. 8 - VT of the bare hand test for participant #8

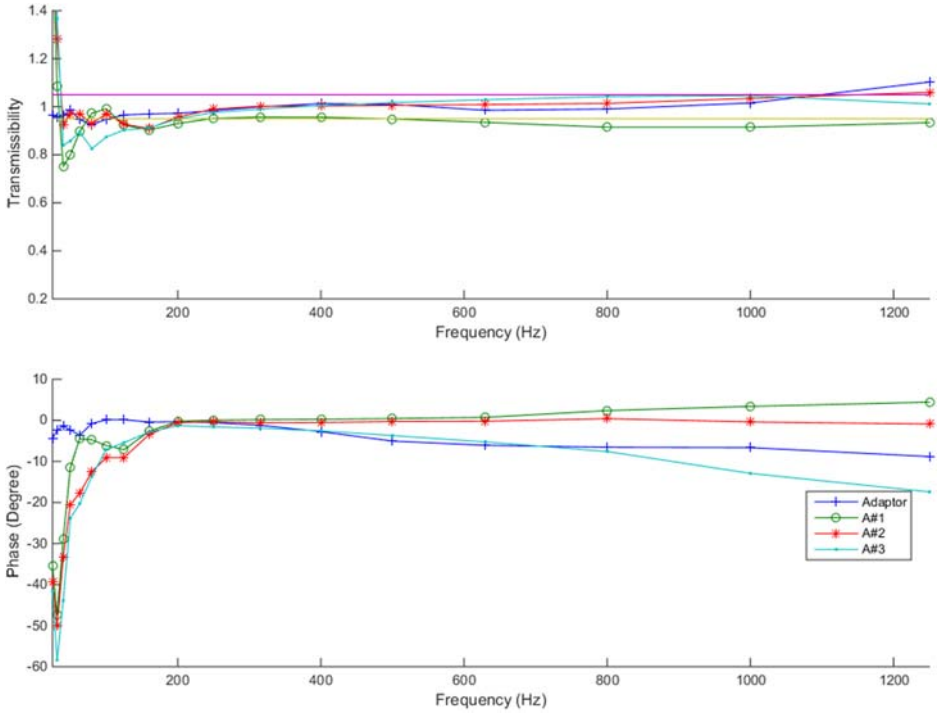

Figure A.5. 9 - VT of the bare hand test for participant #9

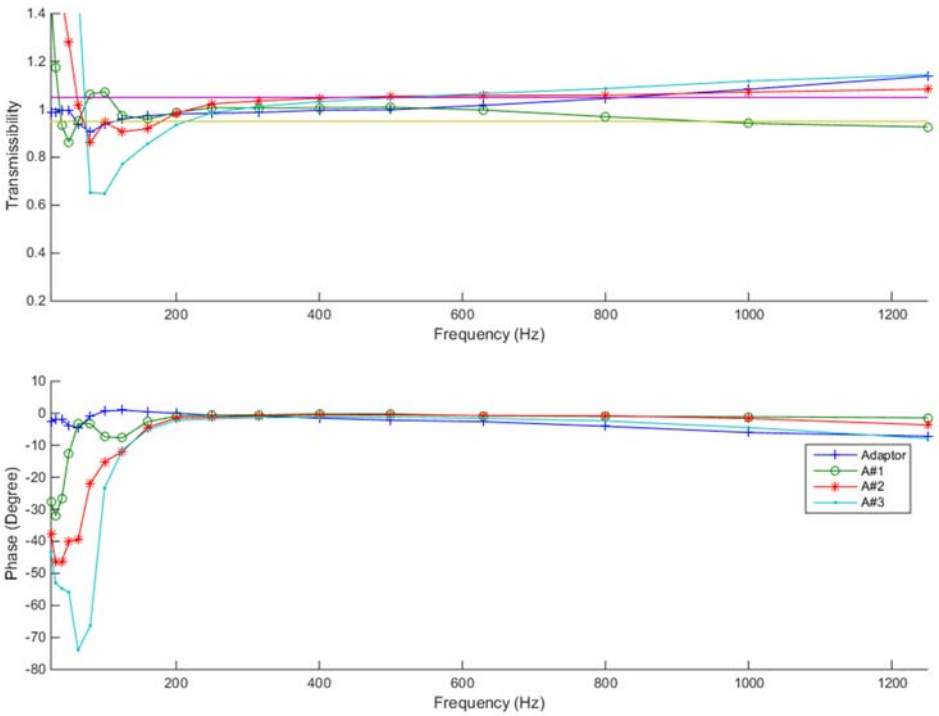

Figure A.5. 10 - VT of the bare hand test for participant #10

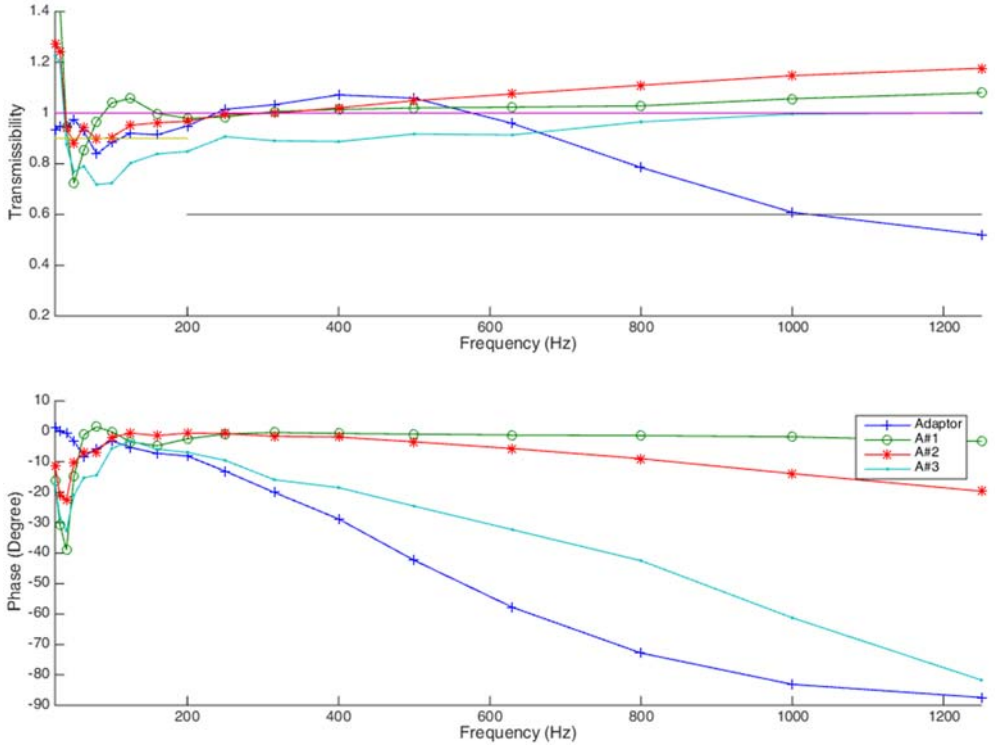

Figure A.5. 11 - VT of the glove test for participant #1

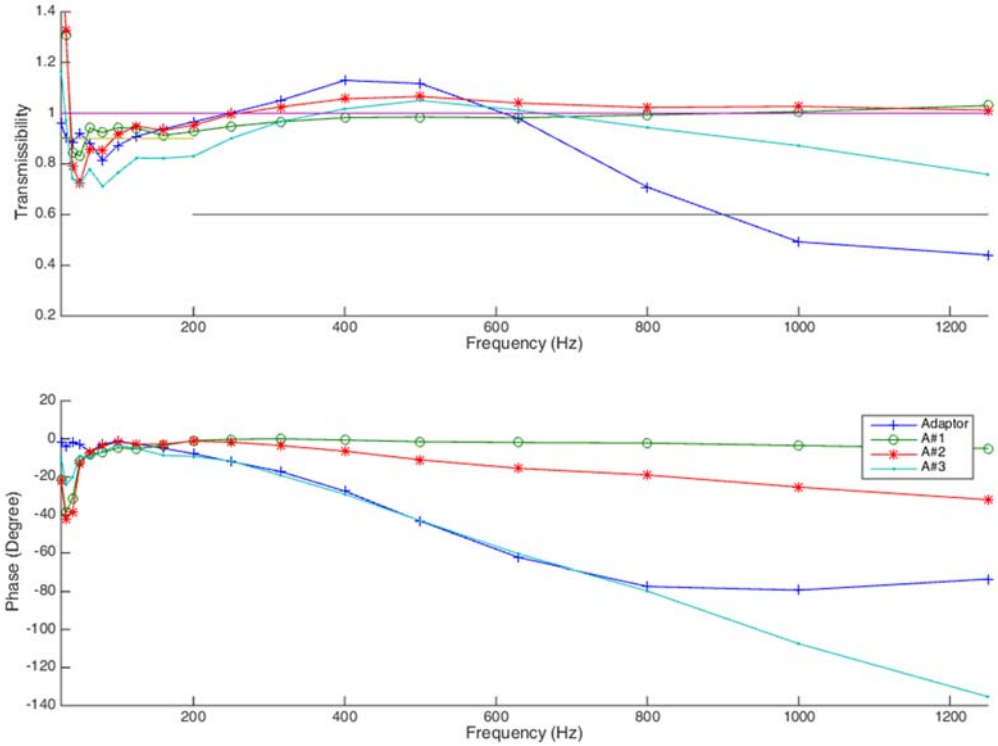

Figure A.5. 12 - VT of the glove test for participant #2

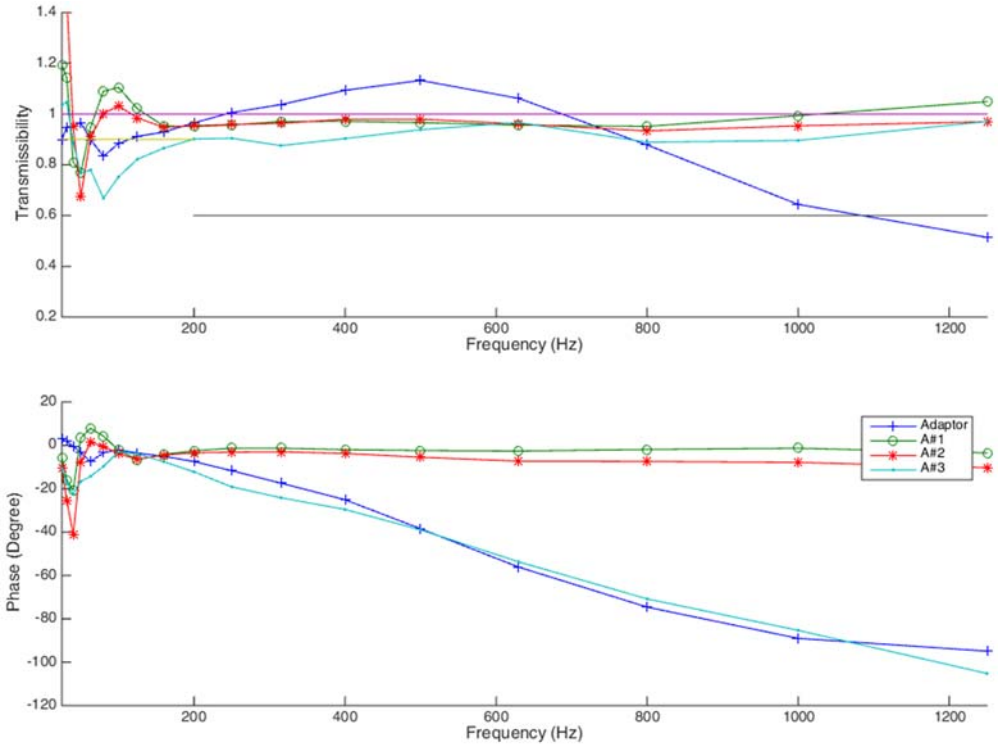

Figure A.5. 13 - VT of the glove test for participant #3

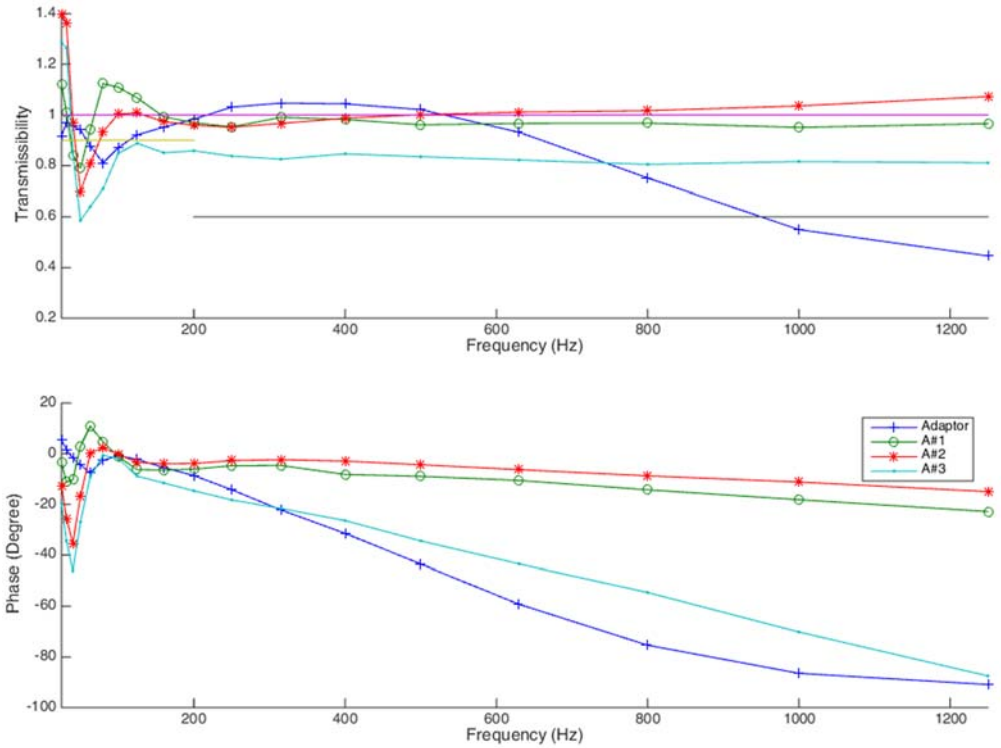

Figure A.5. 14 - VT of the glove test for participant #4

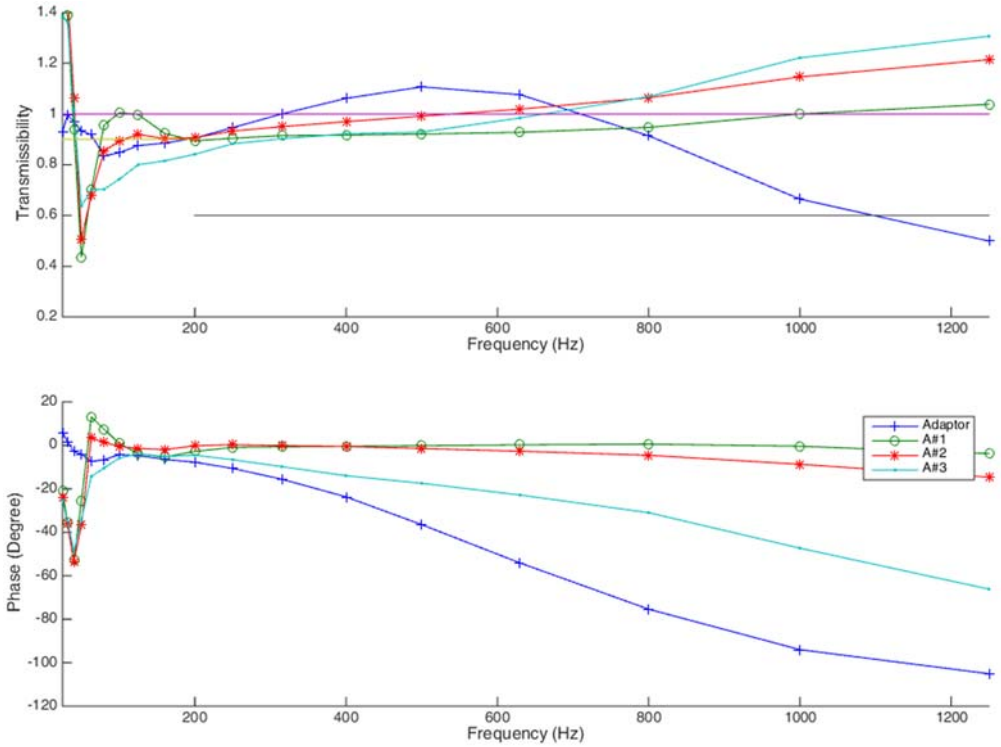

Figure A.5. 15 - VT of the glove test for participant #5

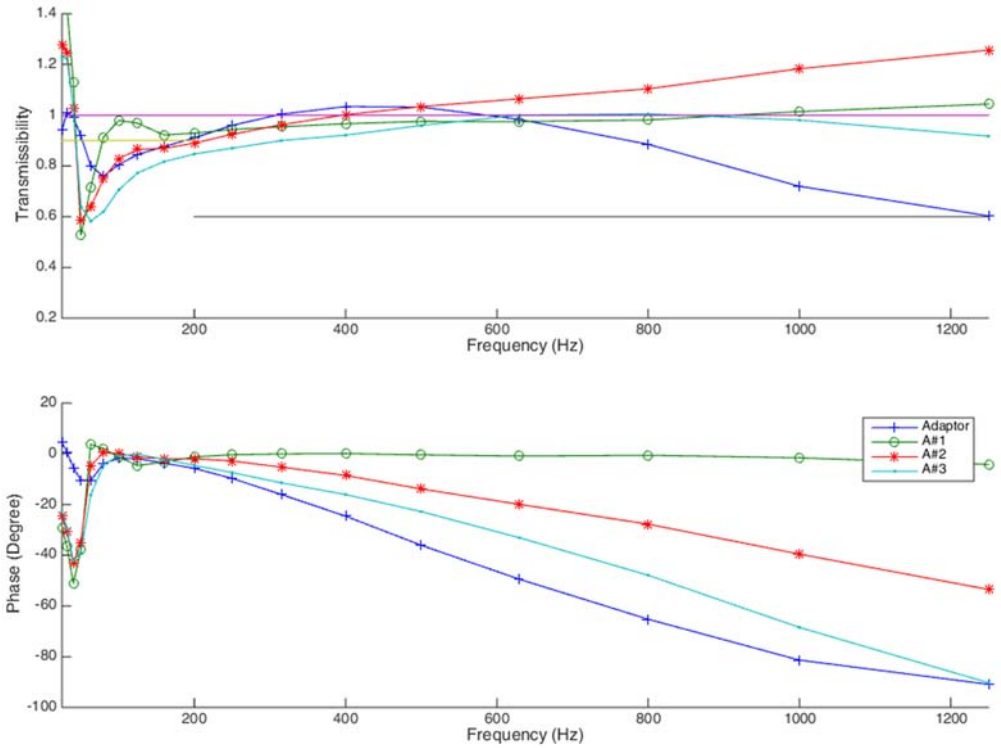

Figure A.5. 16 - VT of the glove test for participant #6

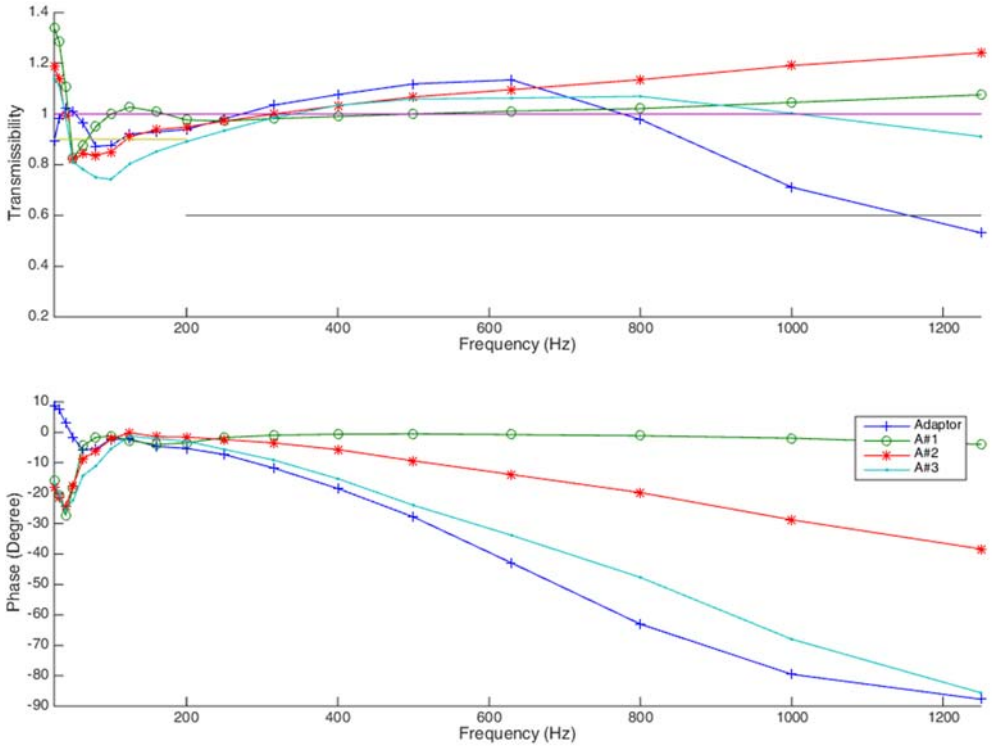

Figure A.5. 17 - VT of the glove test for participant #7

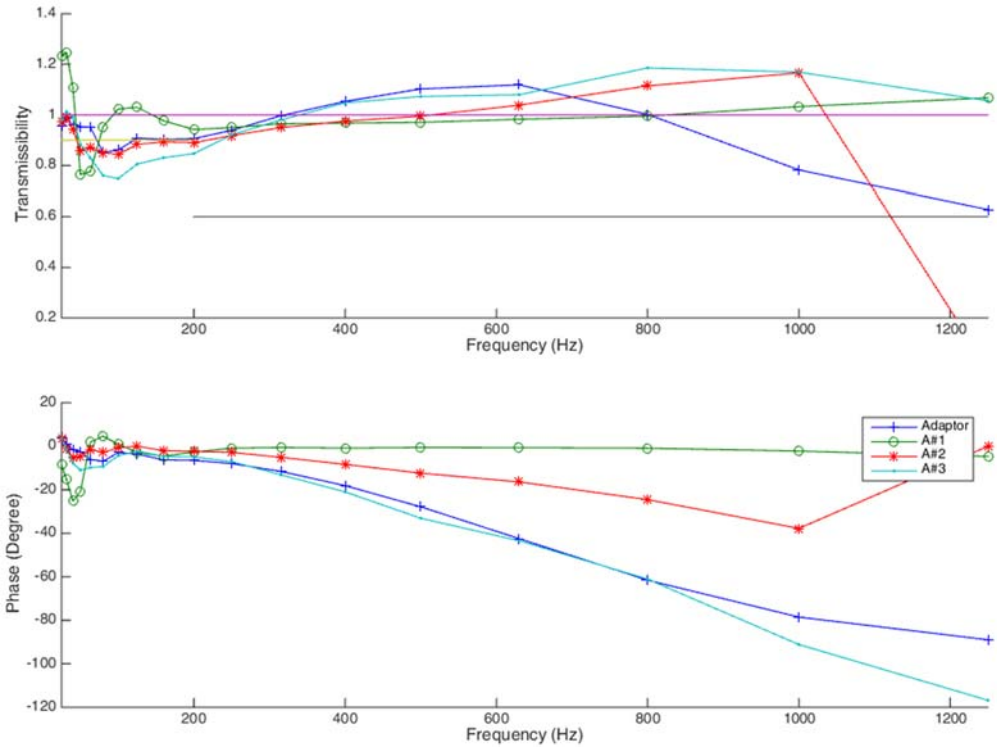

Figure A.5. 18 - VT of the glove test for participant #8

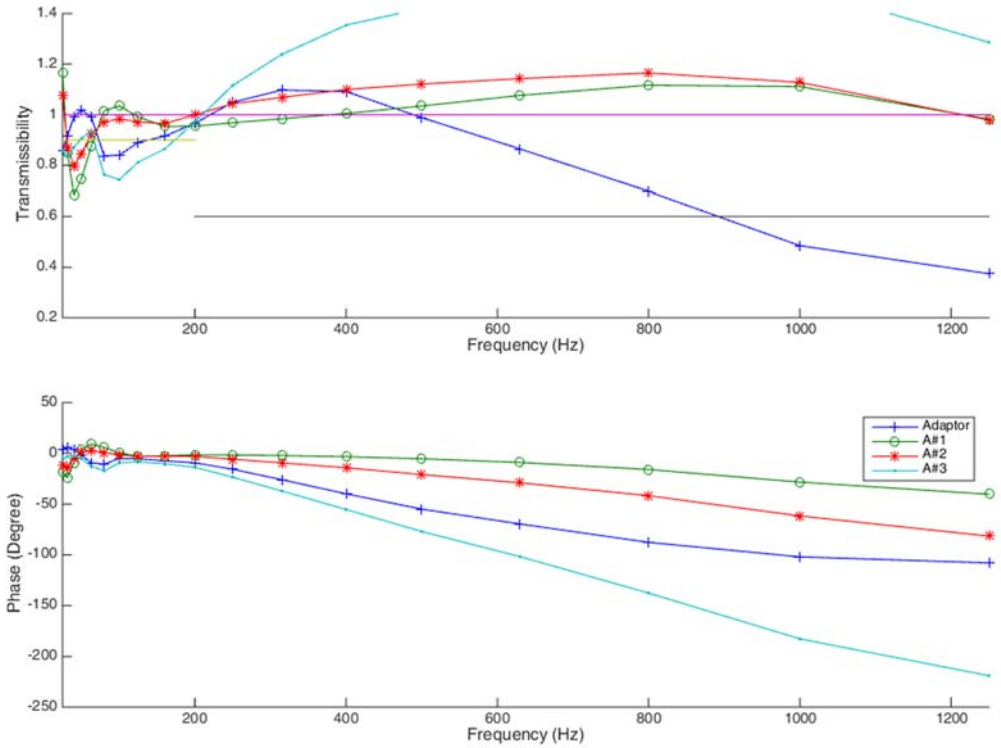

Figure A.5. 19 - VT of the glove test for participant #9

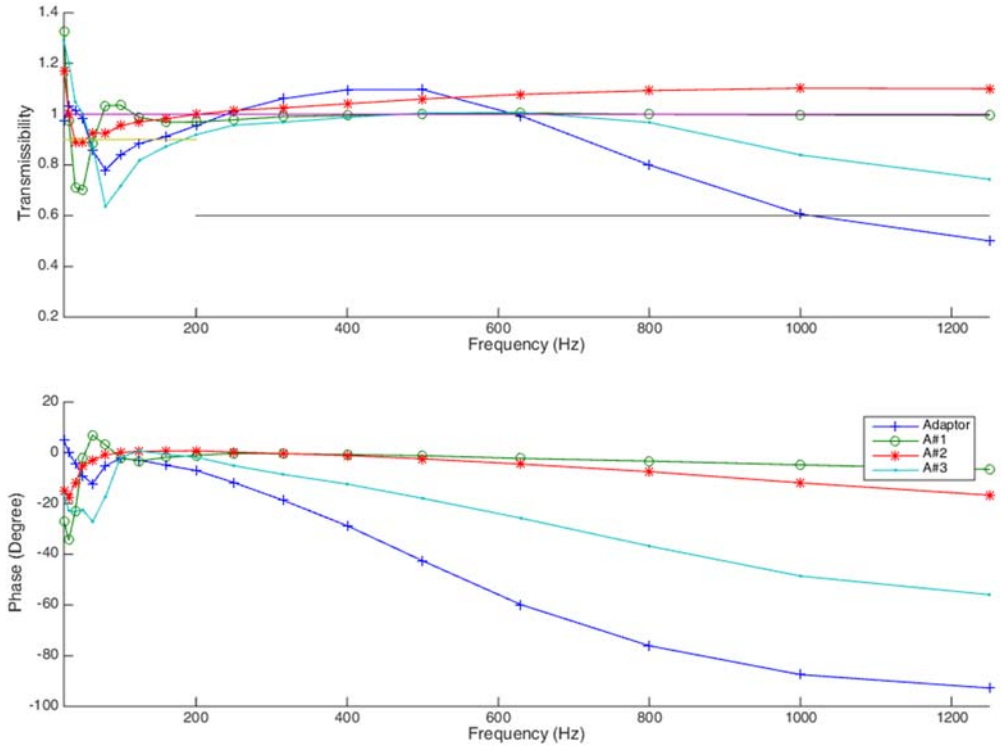

Figure A.5. 20 - VT of the glove test for participant #10

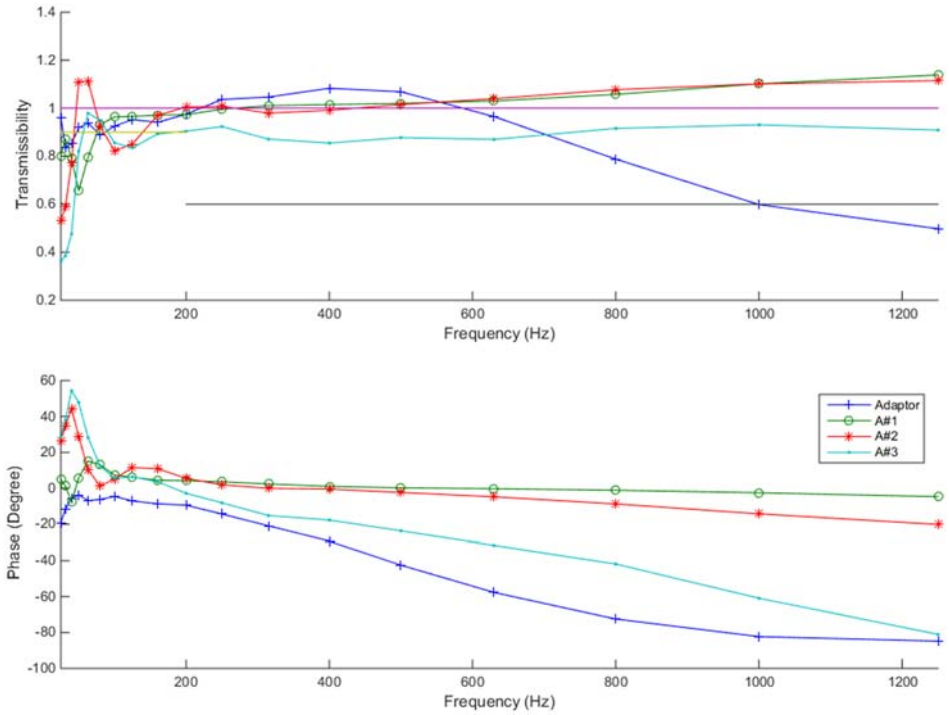

Figure A.5. 21 - VT of the glove for participant #1 (Adaptor vs individual accelerometers on strap)

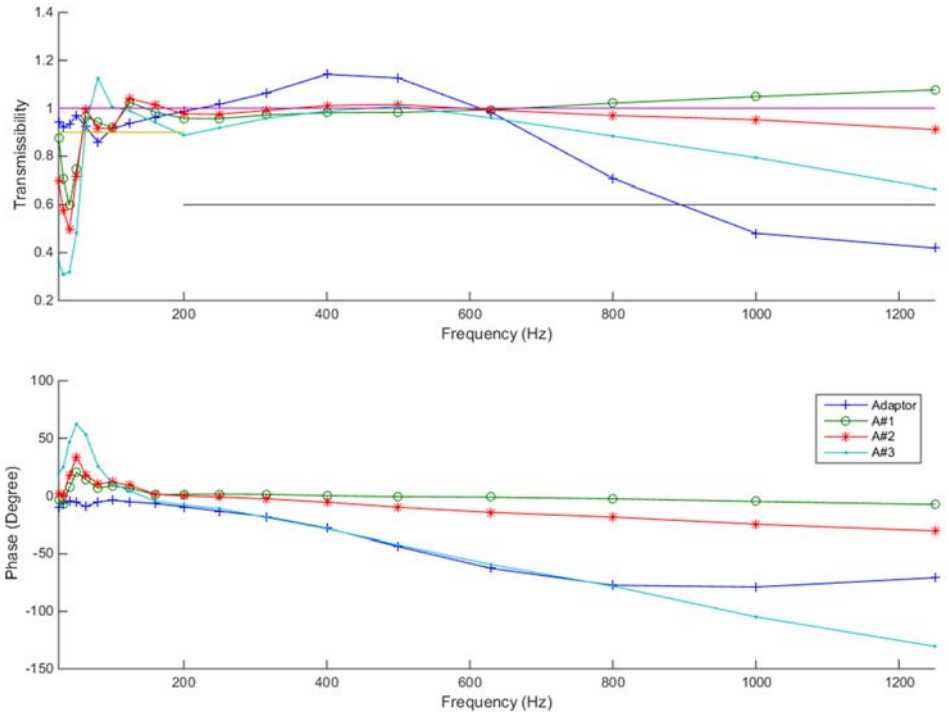

Figure A.5. 22 - VT of the glove for participant #2 (Adaptor vs individual accelerometers on strap)

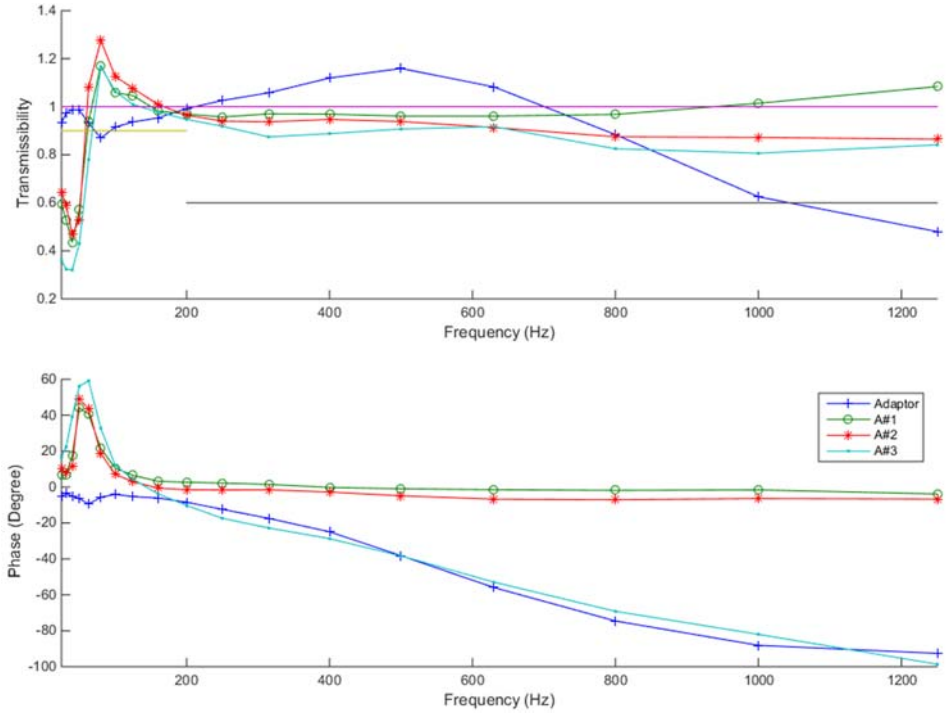

Figure A.5. 23 - VT of the glove for participant #3 (Adaptor vs individual accelerometers on strap)

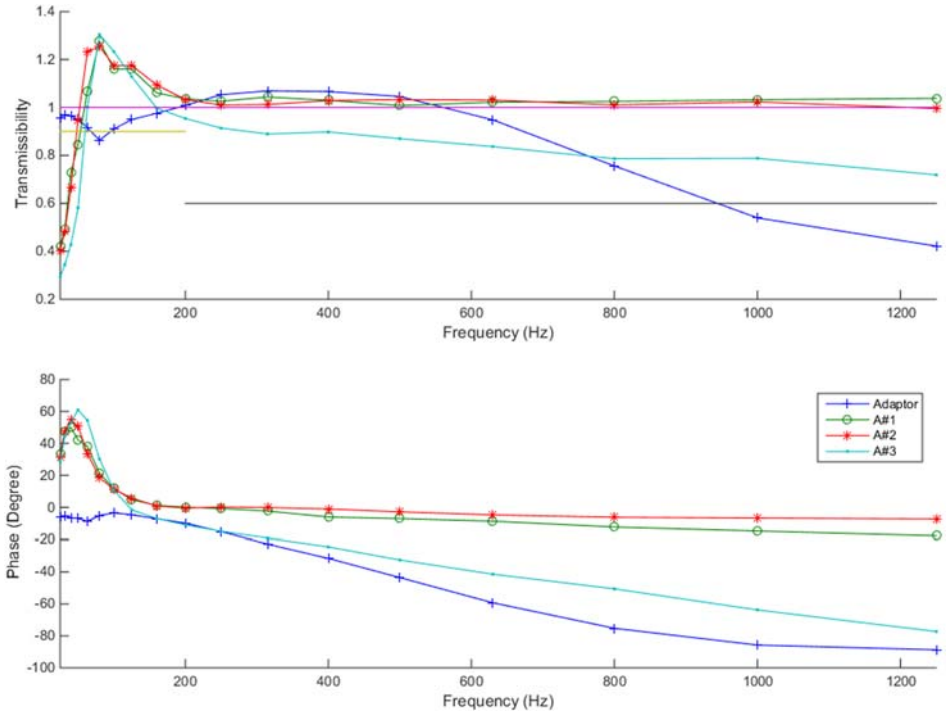

Figure A.5. 24 - VT of the glove for participant #4 (Adaptor vs individual accelerometers on strap)

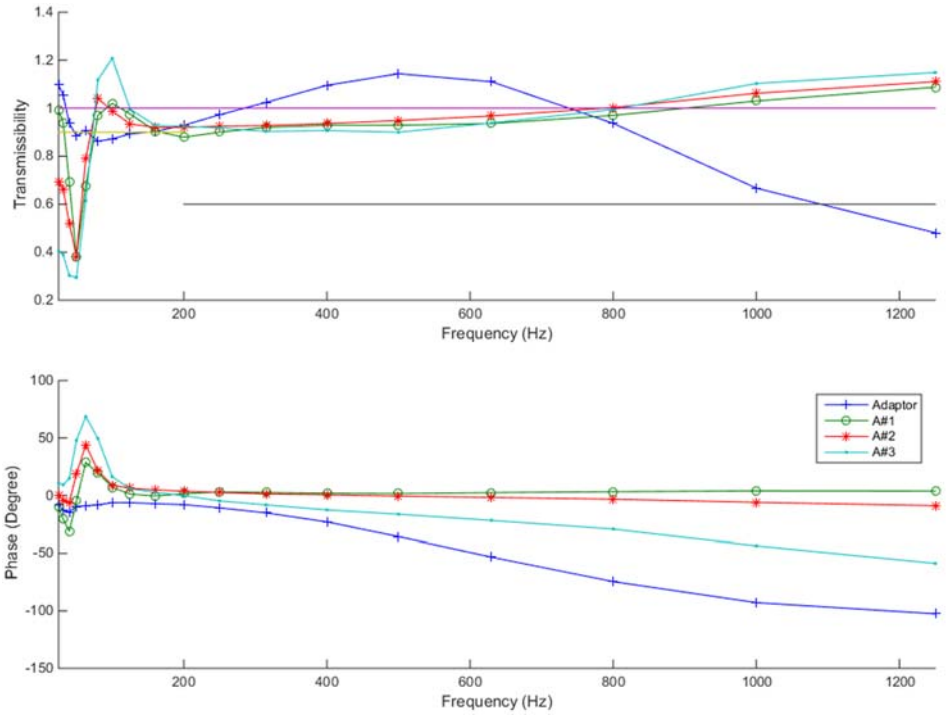

Figure A.5. 25 - VT of the glove for participant #5 (Adaptor vs individual accelerometers on strap)

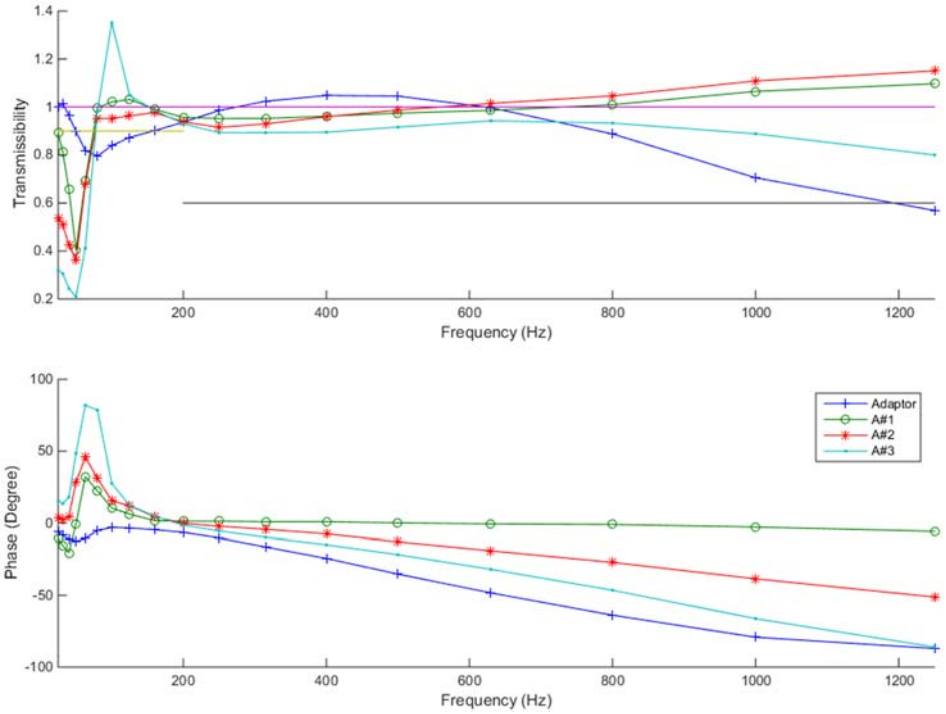

Figure A.5. 26 - VT of the glove for participant #6 (Adaptor vs individual accelerometers on strap)

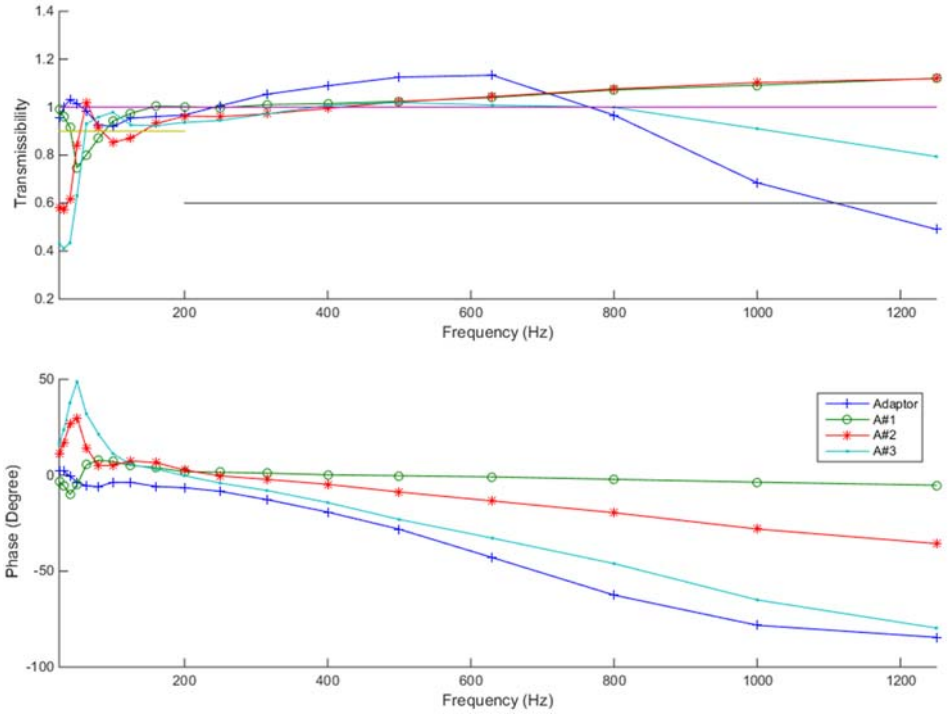

Figure A.5. 27 - VT of the glove for participant #7 (Adaptor vs individual accelerometers on strap)

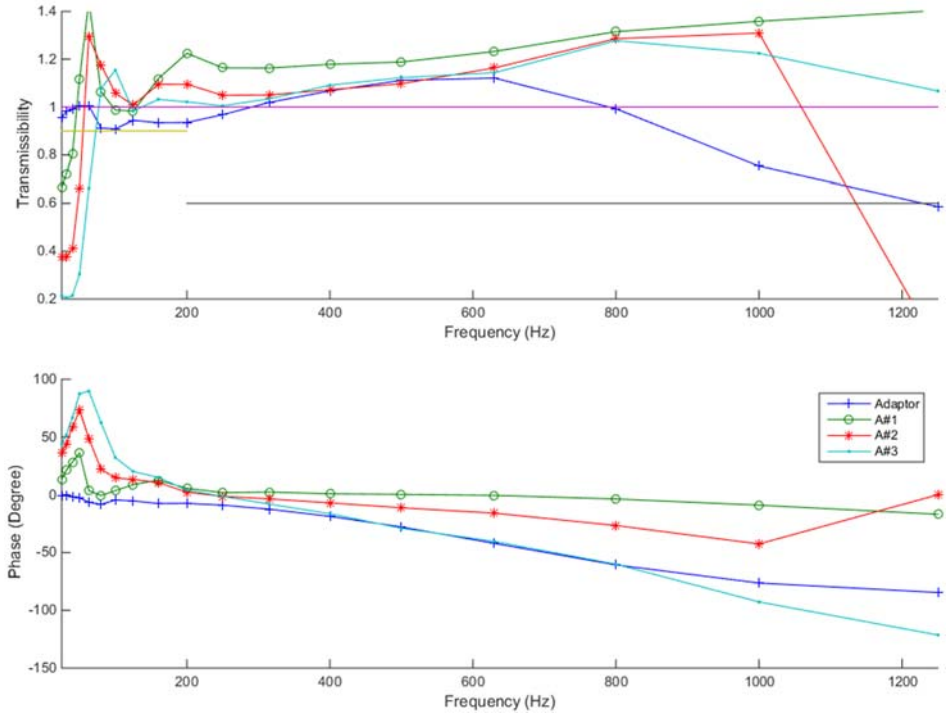

Figure A.5. 28 - VT of the glove for participant #8 (Adaptor vs individual accelerometers on strap)

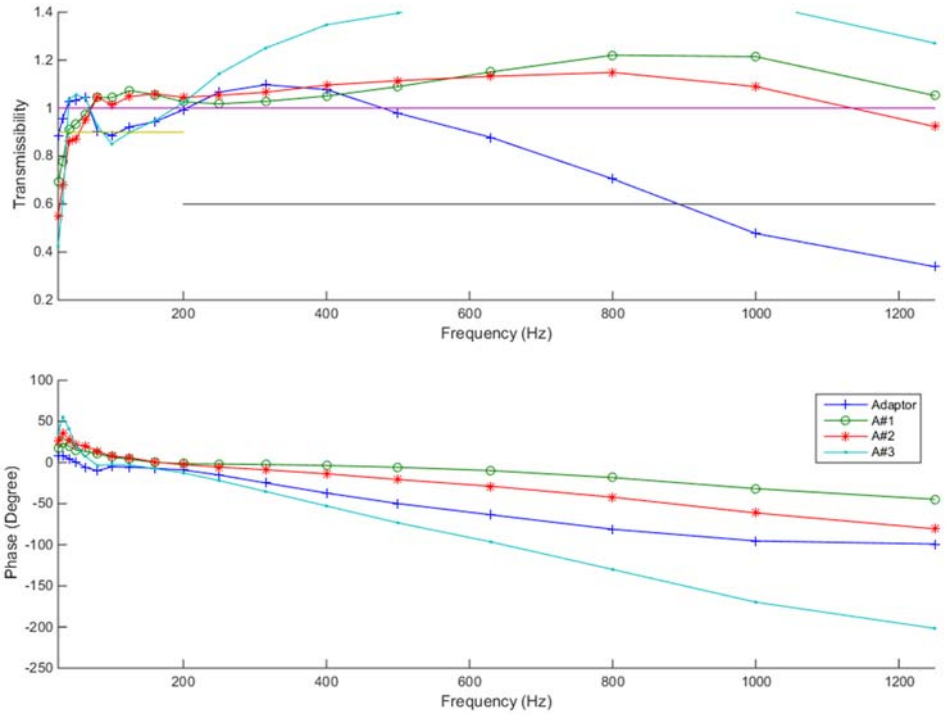

Figure A.5. 29 - VT of the glove for participant #9 (Adaptor vs individual accelerometers on strap)

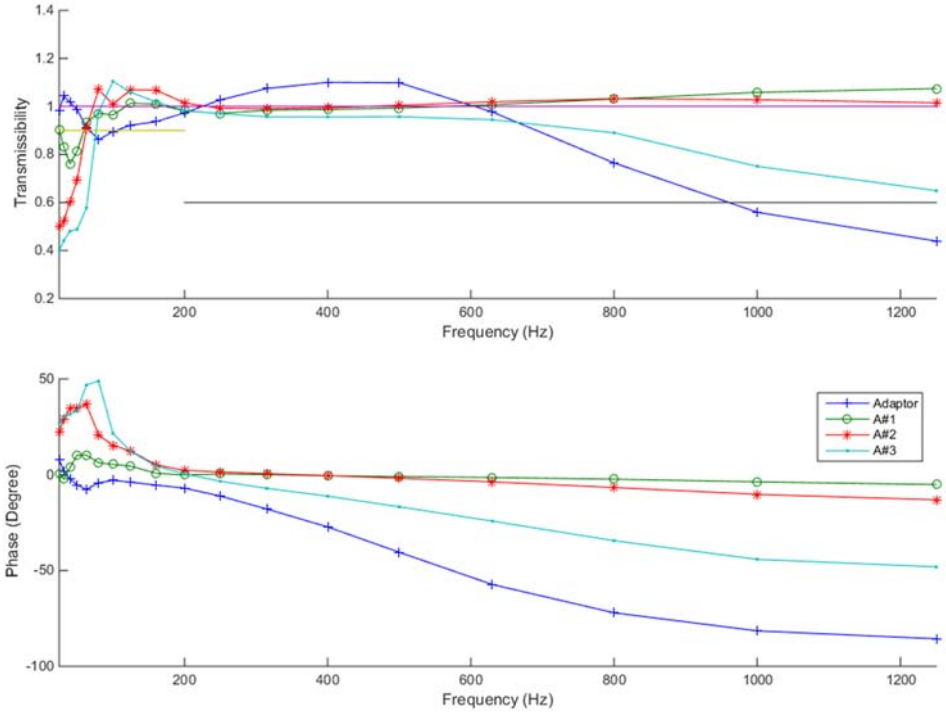

Figure A.5. 30 - VT of the glove for participant #10 (Adaptor vs individual accelerometers on strap)

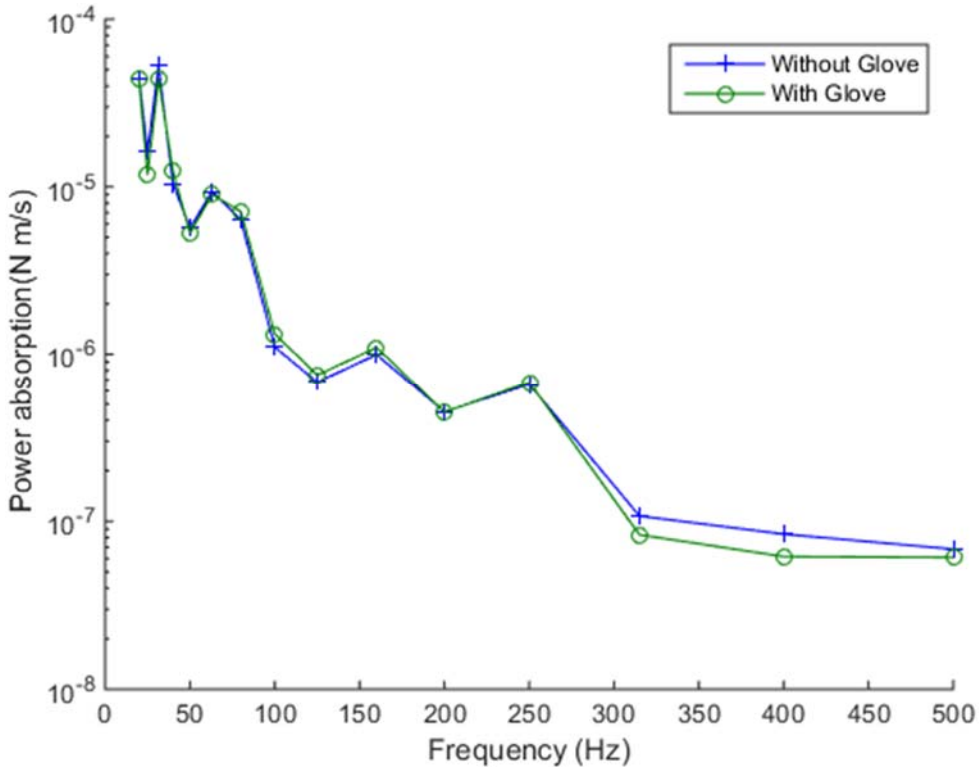

Figure A.5. 31 - Measured power absorption with the adaptor

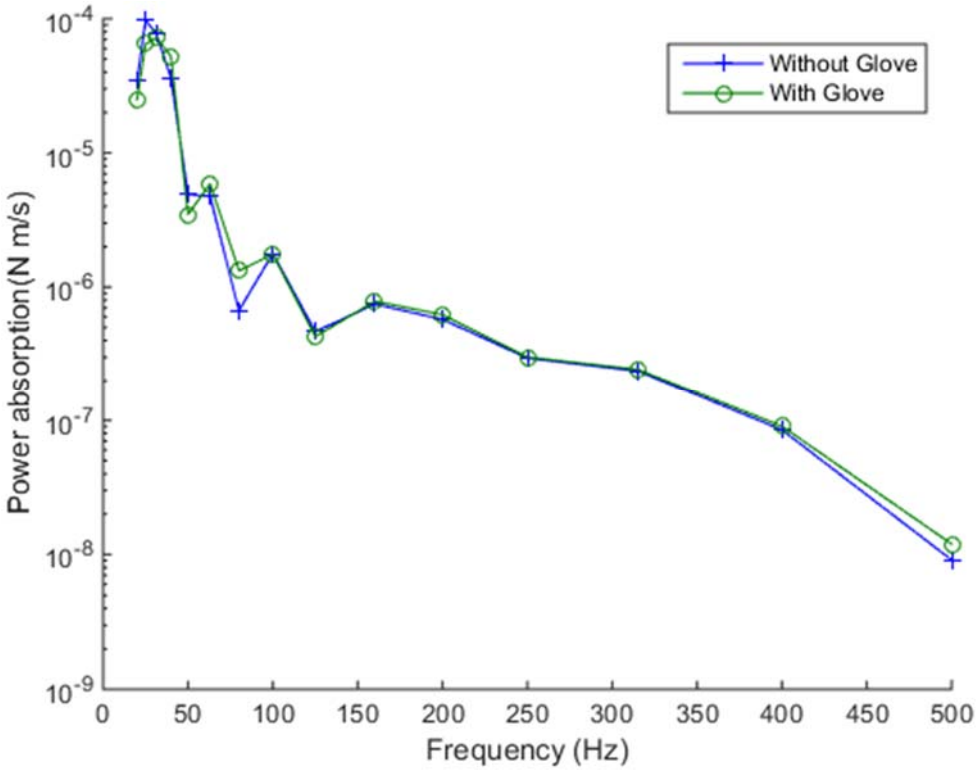

Figure A.5. 32 - Measured power absorption with the strap (A#1)

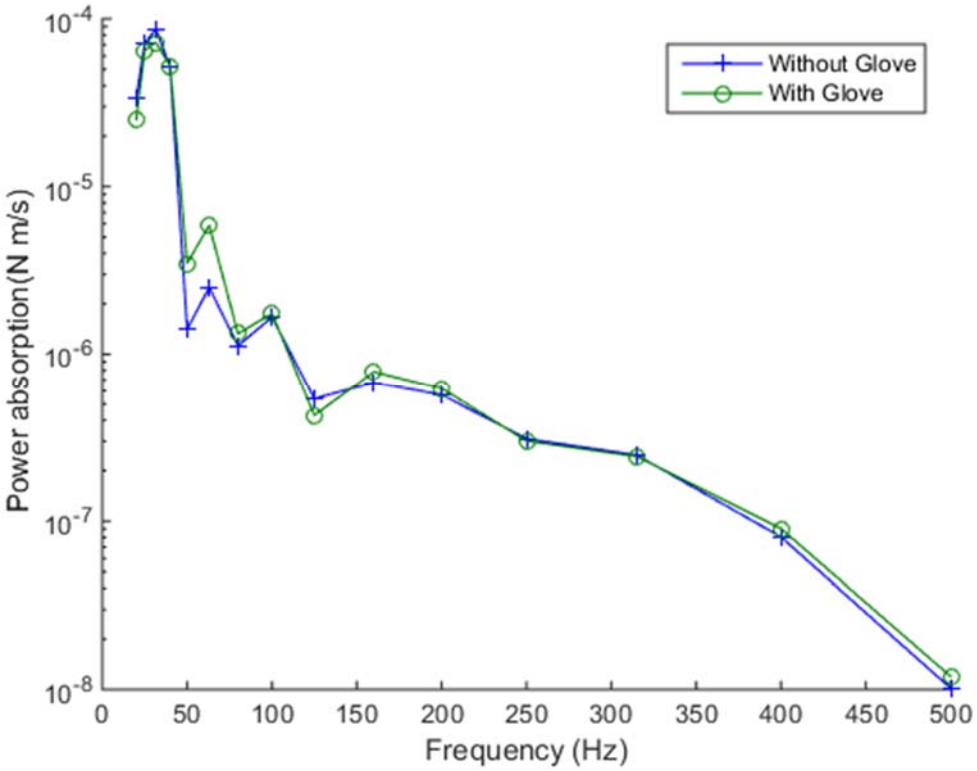

Figure A.5. 33 - Measured power absorption with the strap (A#2)

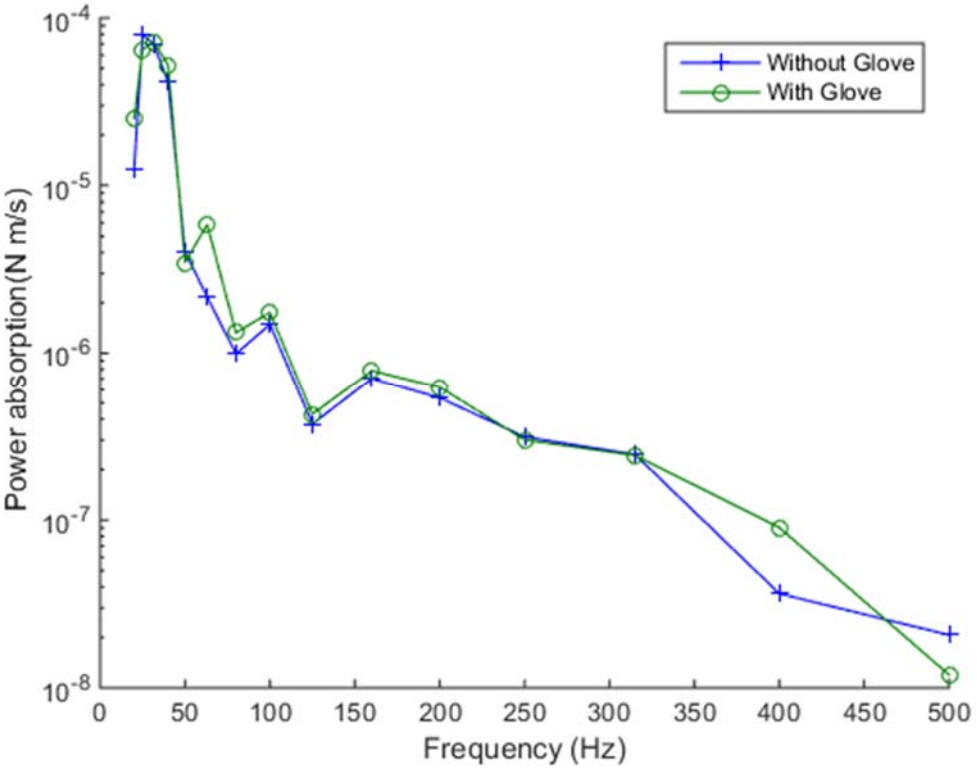

Figure A.5. 34 - Measured power absorption with the strap (A#3)

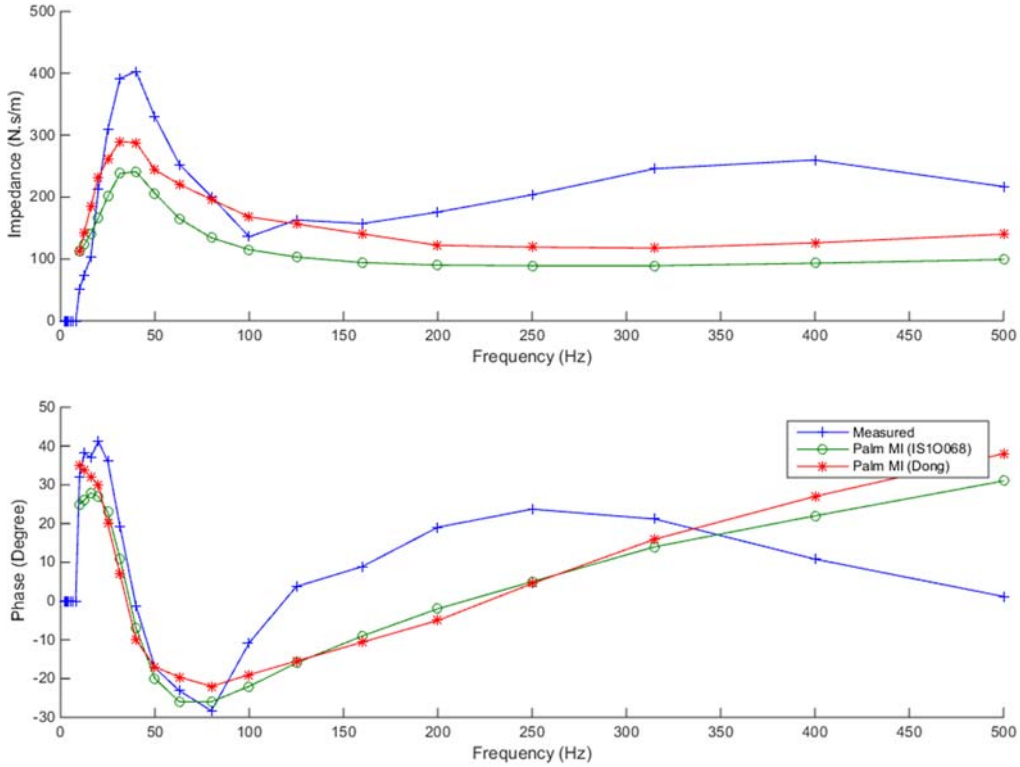

Figure A.6.1 – Measured Palm MI vs ISO 10068 [30] and Dong's result [50]

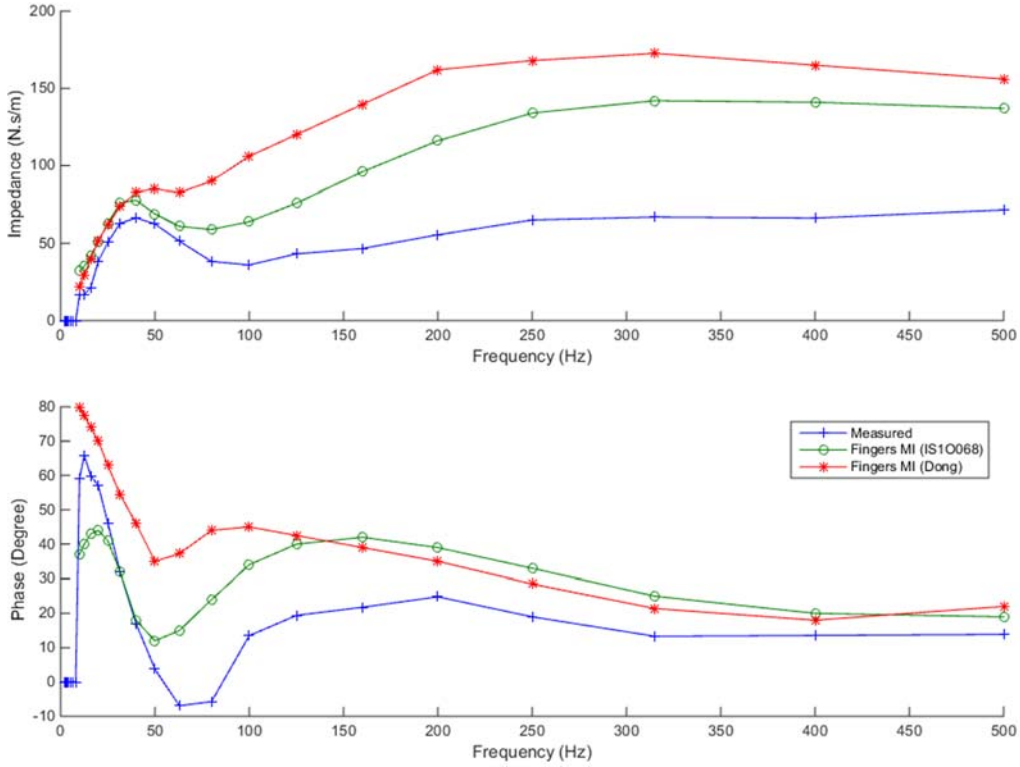

Figure A.6.2 – Measured Fingers MI vs ISO 10068 [30] and Dong's result [50]

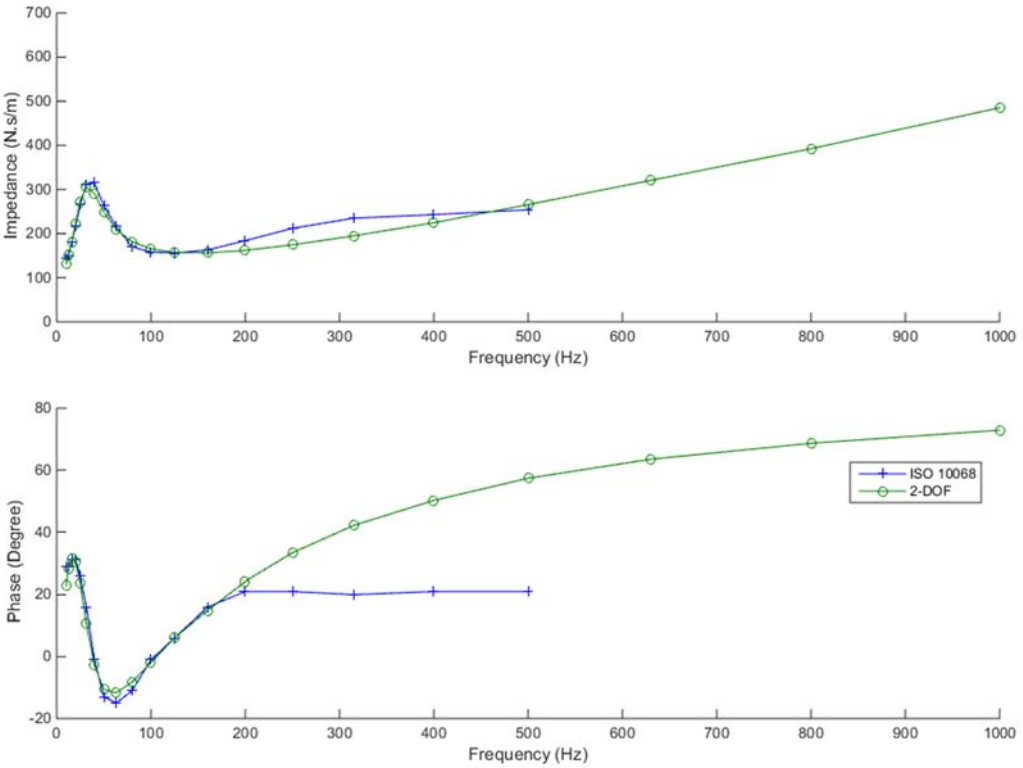

Figure A.6.3 – Reported hand's MI by ISO10068 vs simulation of ISO10068 2-DOF model

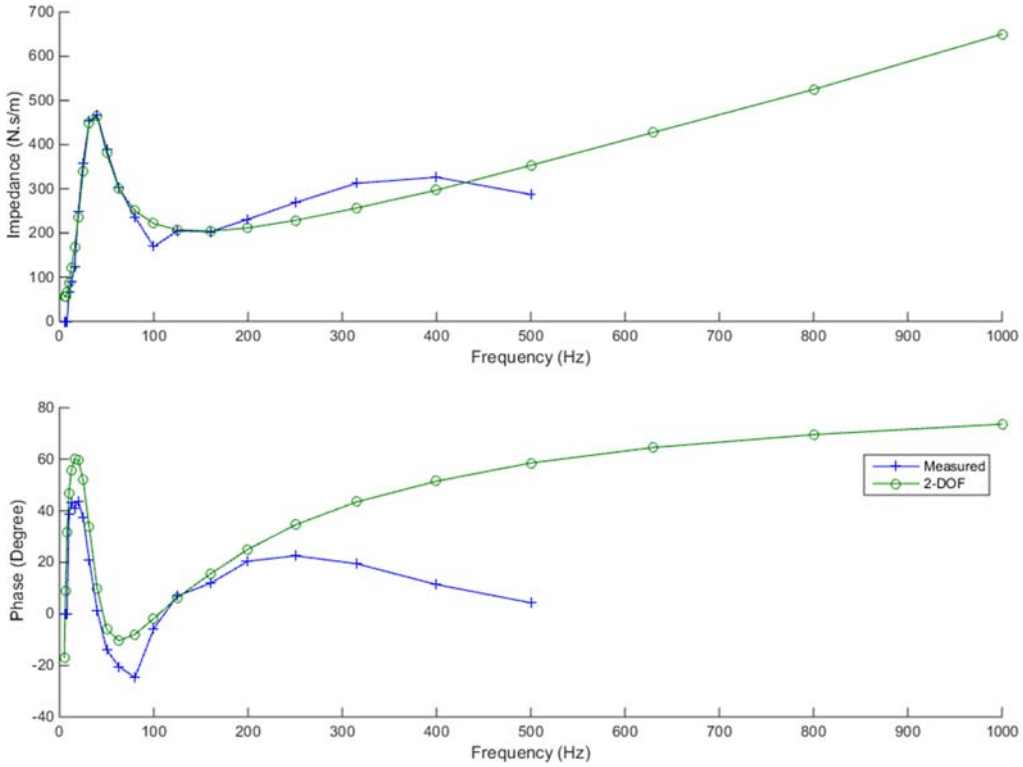

Figure A.6.4 – Measured hand's MI vs simulation of generated 2-DOF model

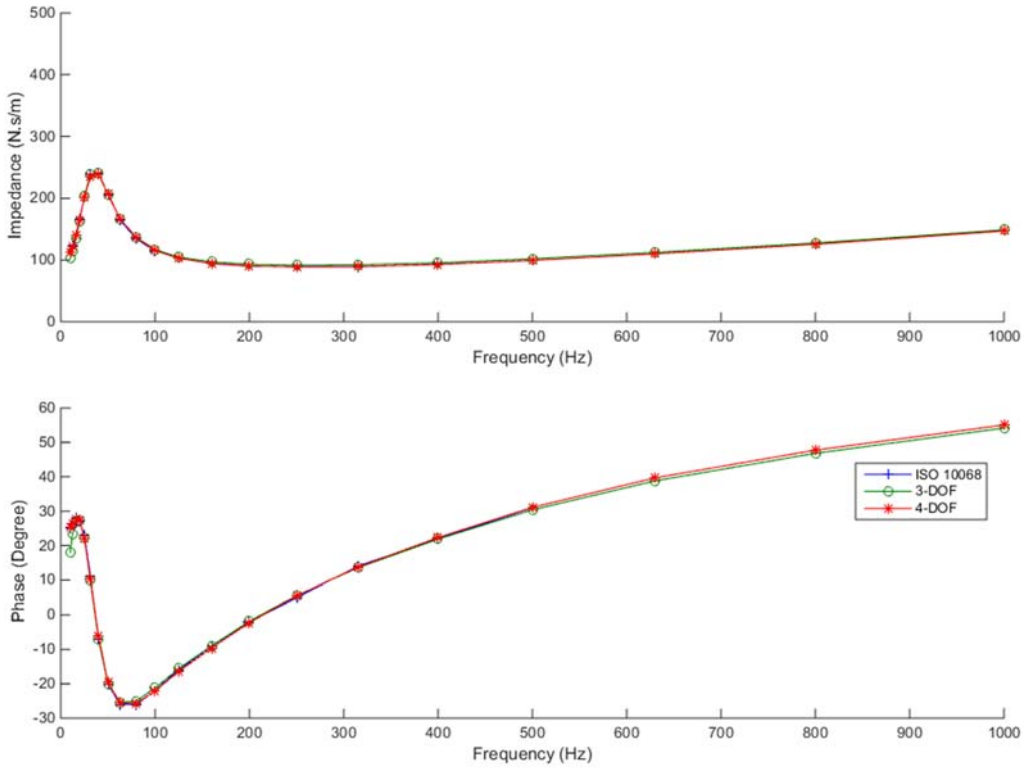

Figure A.6.5 – Reported palm's MI by ISO10068 vs simulation of ISO10068 3-DOF & 4-DOF models

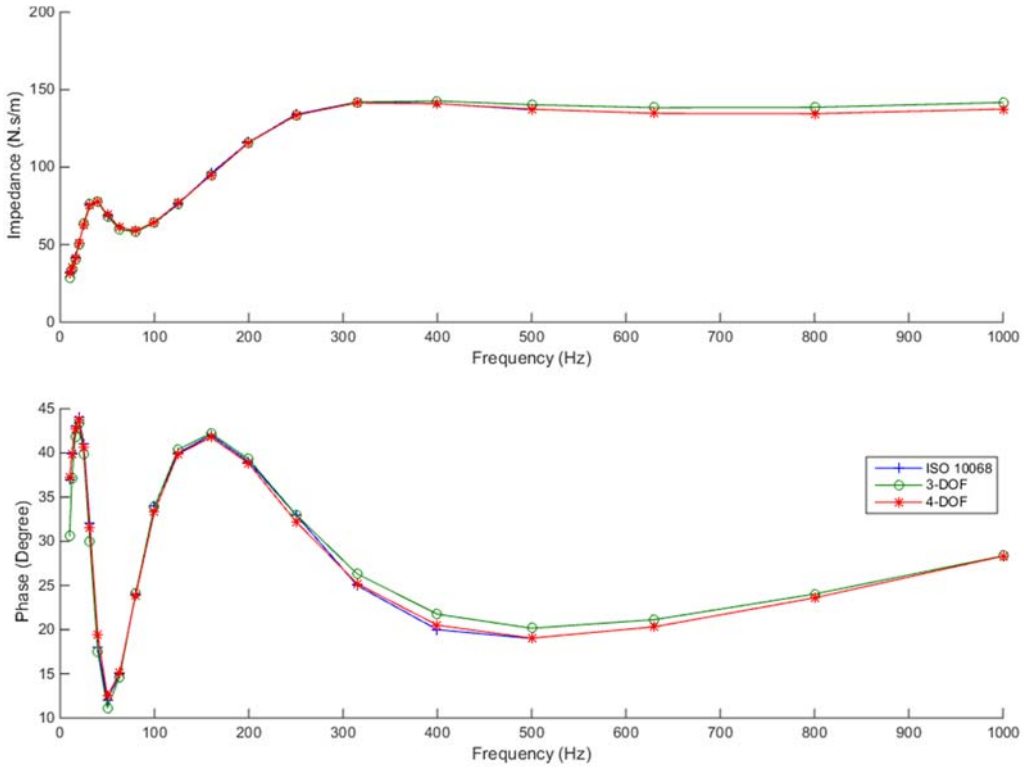

Figure A.6.6 – Reported fingers' MI by ISO10068 vs simulation of ISO10068 3-DOF & 4-DOF models

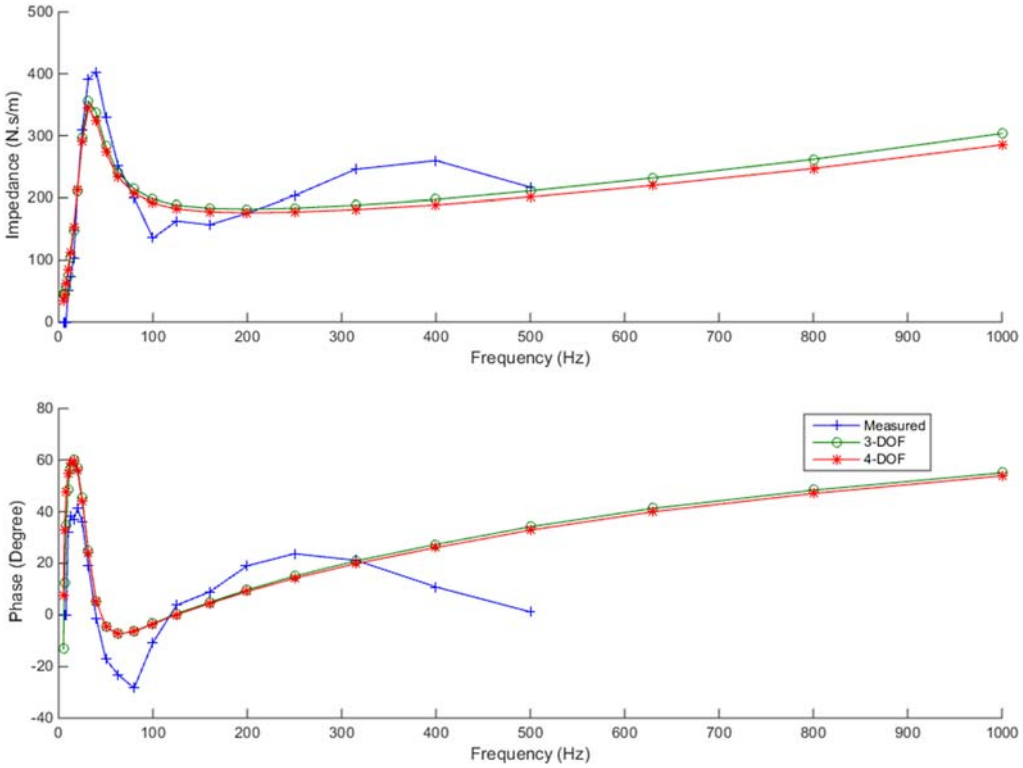

Figure A.6.7 – Measured palm's MI vs simulation of generated 3-DOF & 4-DOF models

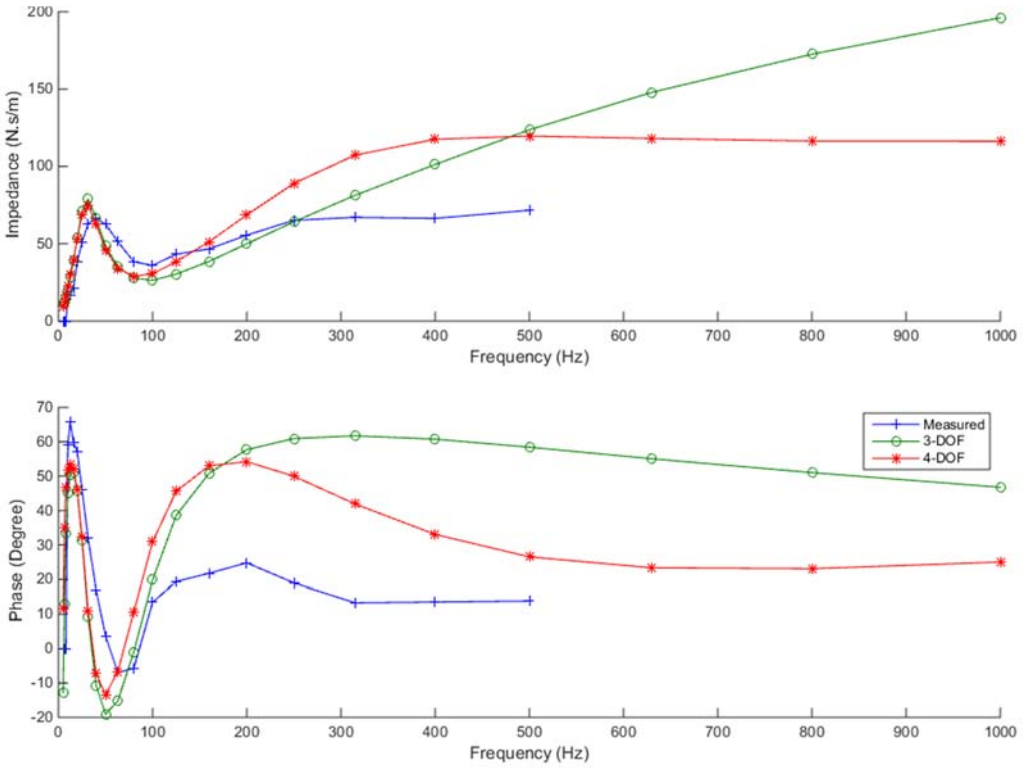

Figure A.6.8 – Measured fingers' MI vs simulation of generated 3-DOF & 4-DOF models

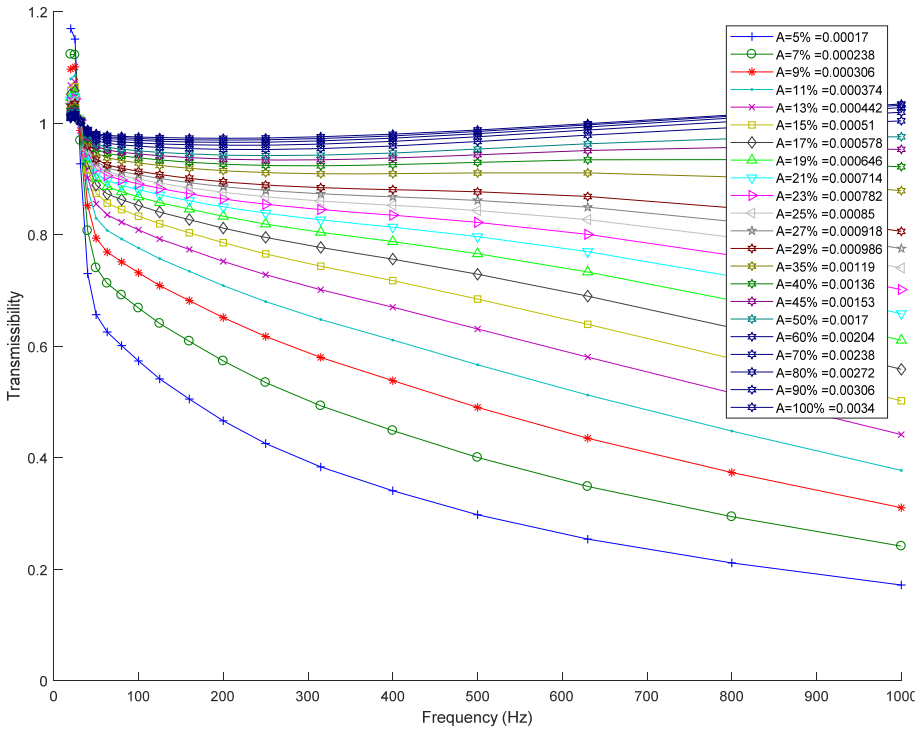

Figure A.6.9 - VT of glove at palm side uses sample #1 vs area of resilient material at palm side

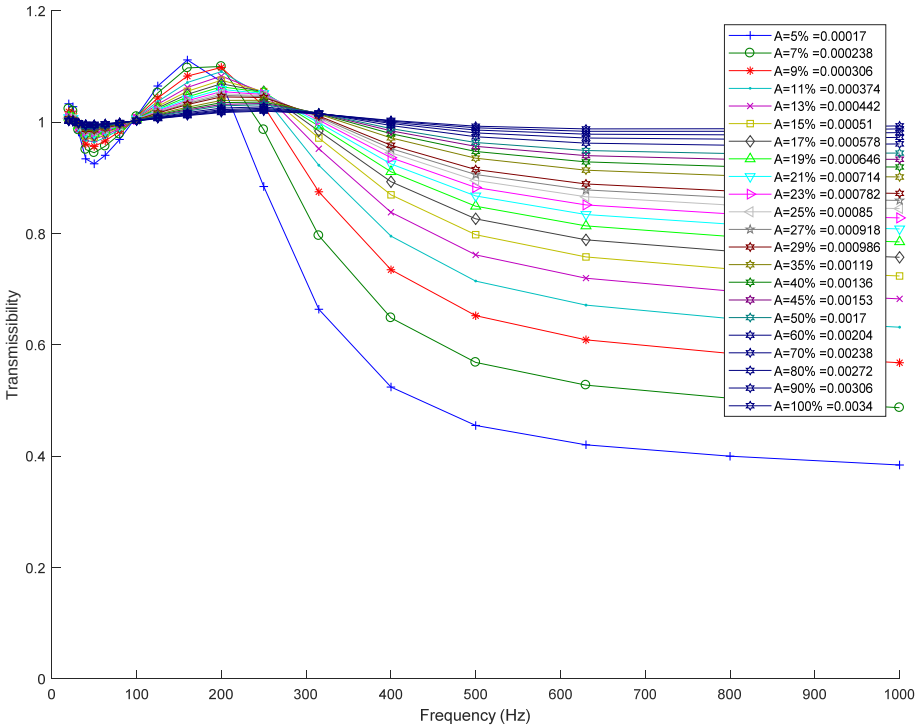

Figure A.6.10 - VT of glove at fingers side uses sample #1 vs area of resilient material at finger side

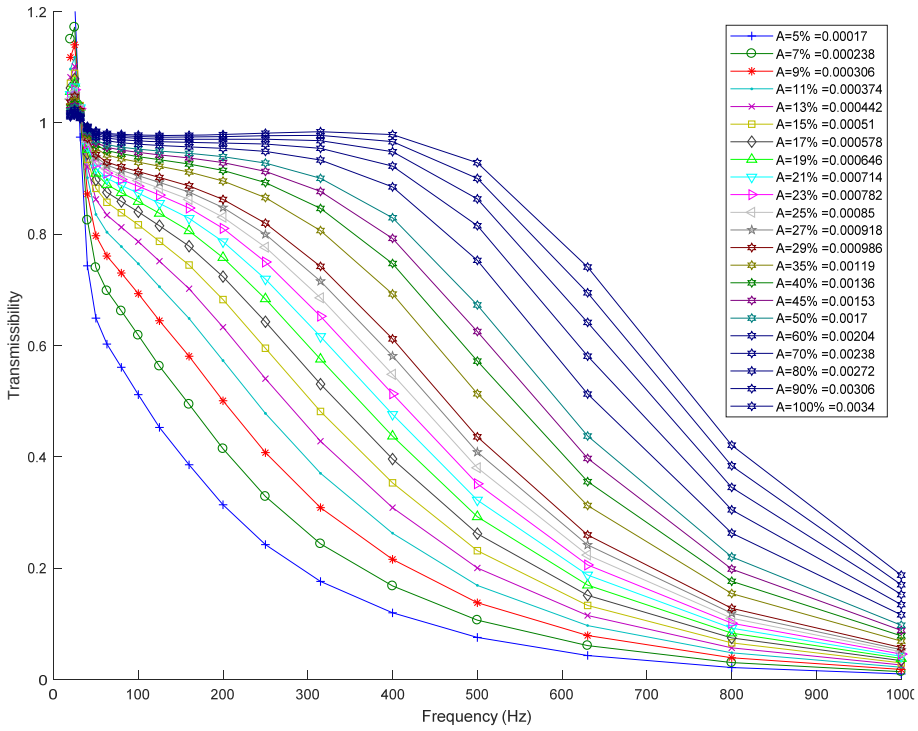

Figure A.6.11 - VT of glove at palm side uses sample #2 vs area of resilient material at palm side

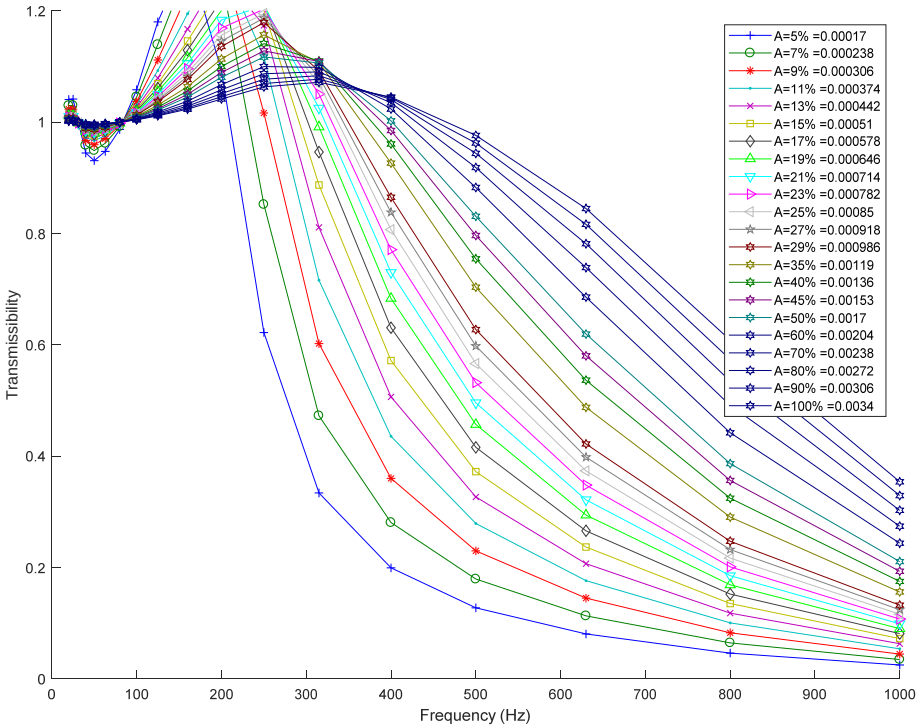

Figure A.6.12 - VT of glove at fingers side uses sample #2 vs area of resilient material at finger side

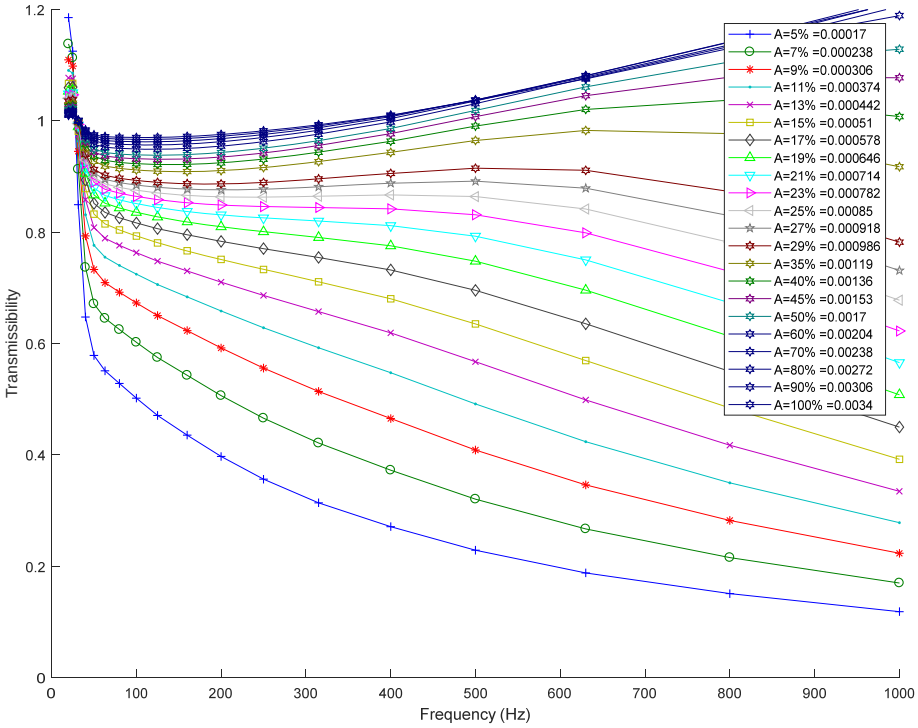

Figure A.6.13 - VT of glove at palm side uses sample #3 vs area of resilient material at palm side

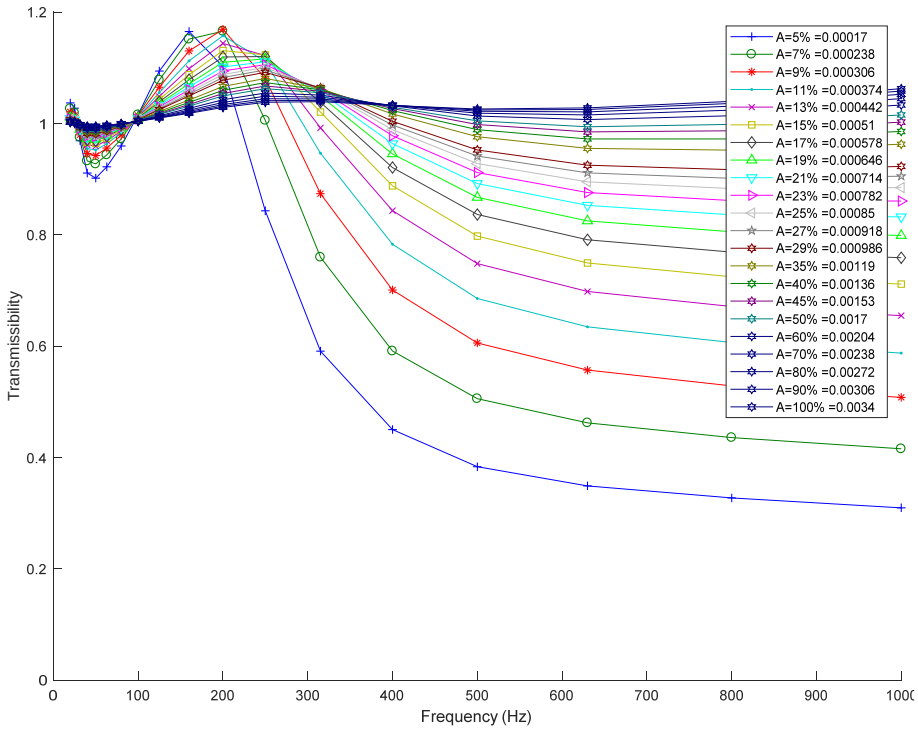

Figure A.6.14 - VT of glove at fingers side uses sample #3 vs area of resilient material at finger side

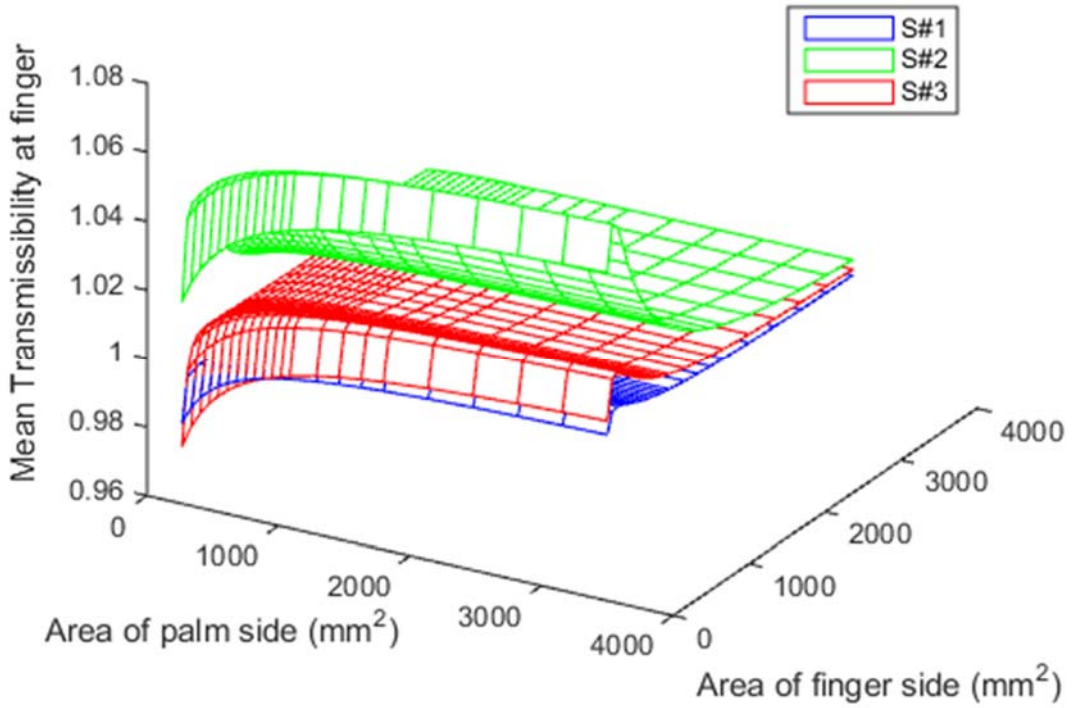

Figure A.6.15 - MVT at finger for medium frequency band

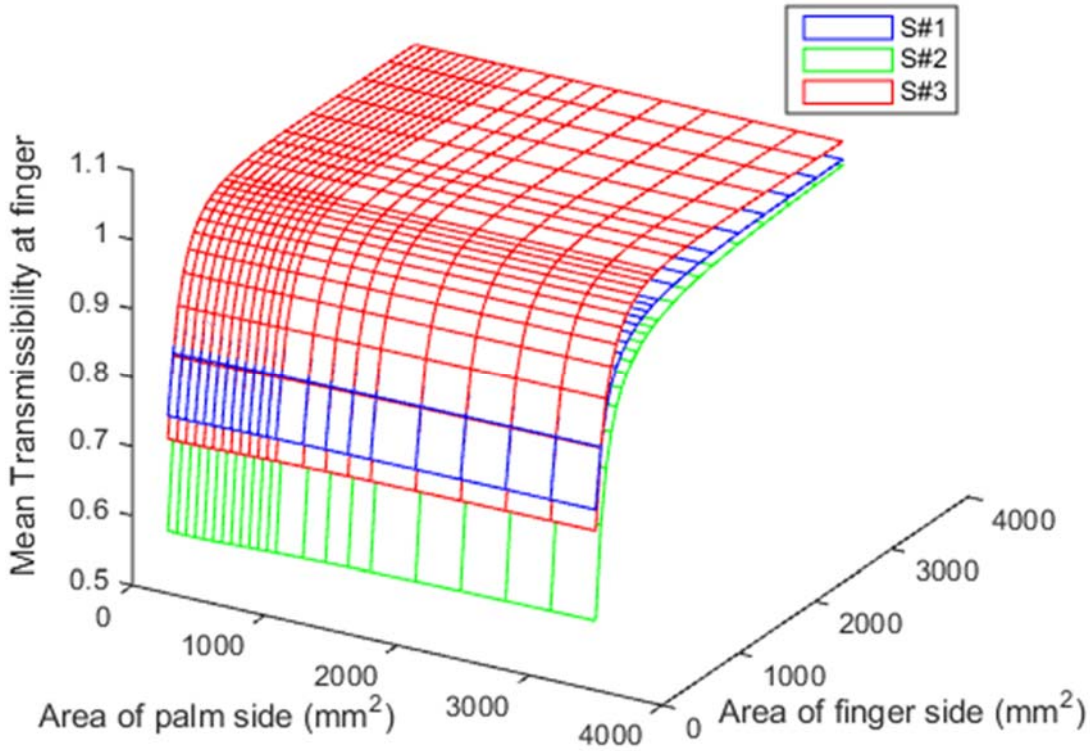

Figure A.6.16 - MVT at finger for high frequency band

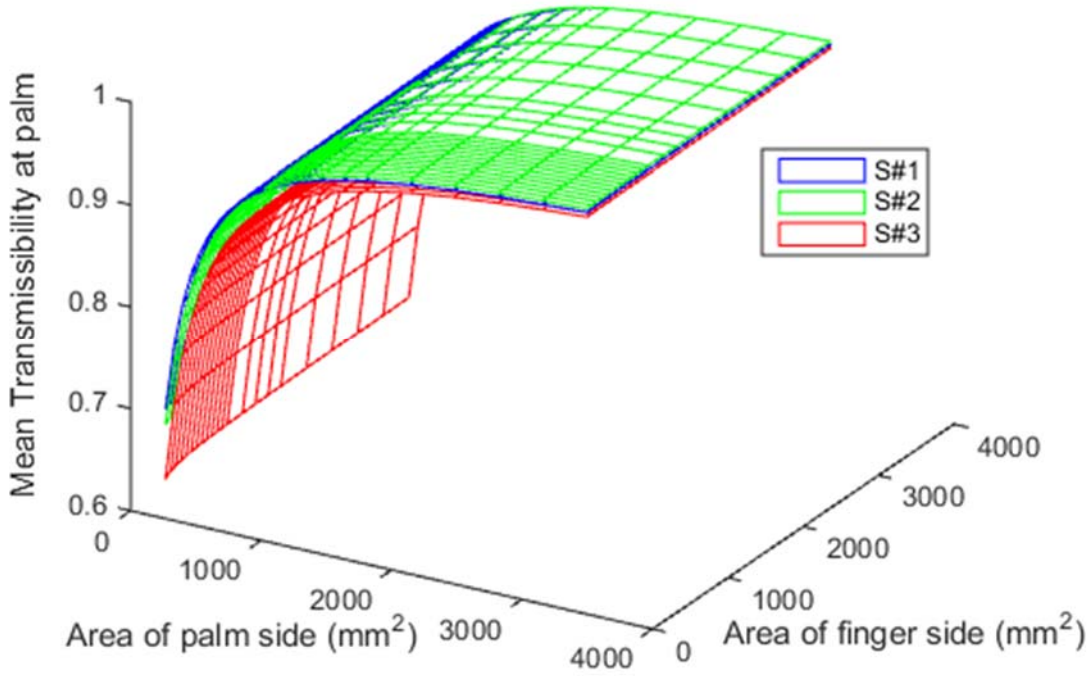

Figure A.6.17 - MVT at palm for medium frequency band

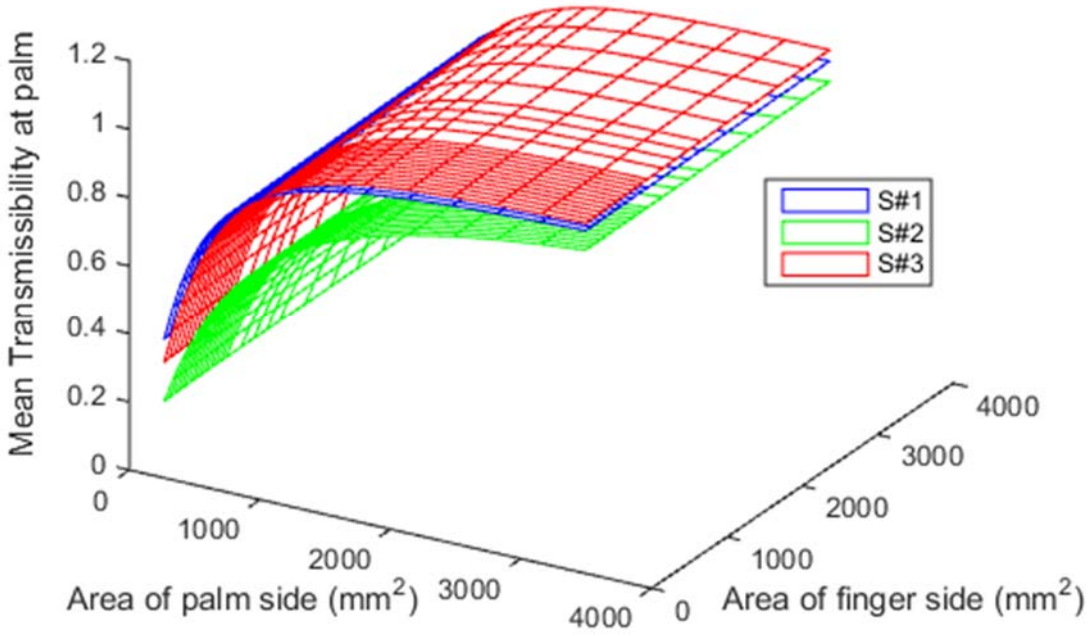

Figure A.6.18 - MVT at palm for high frequency band

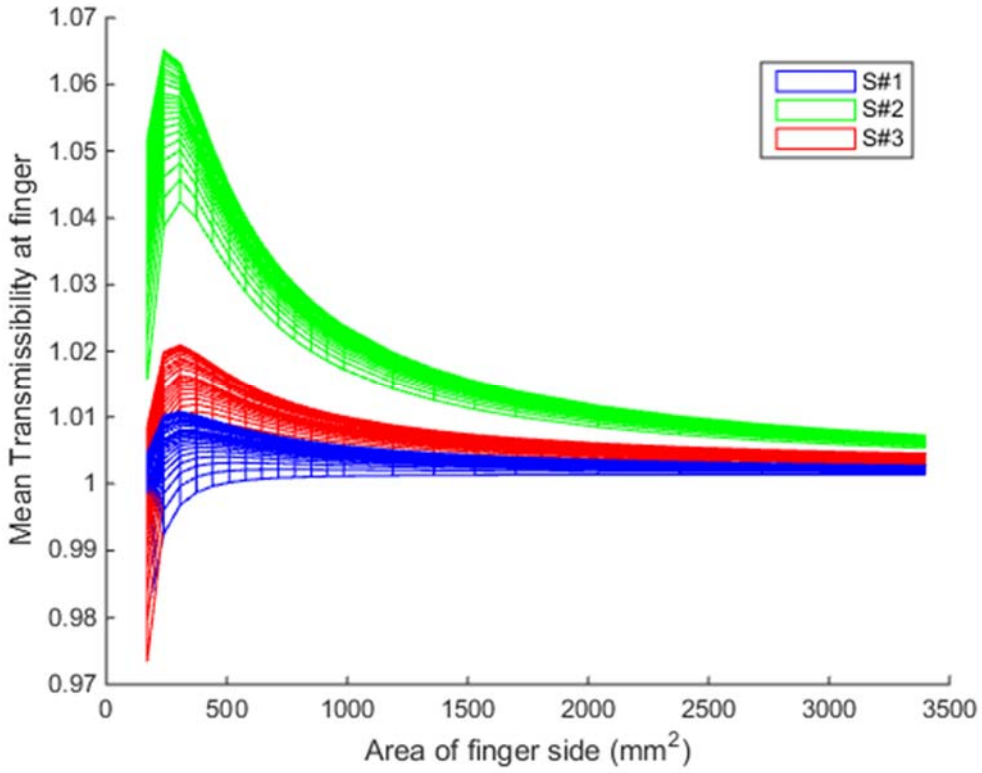

Figure A.6.19 - MVT at finger for medium frequency band vs area of resilient material at finger side

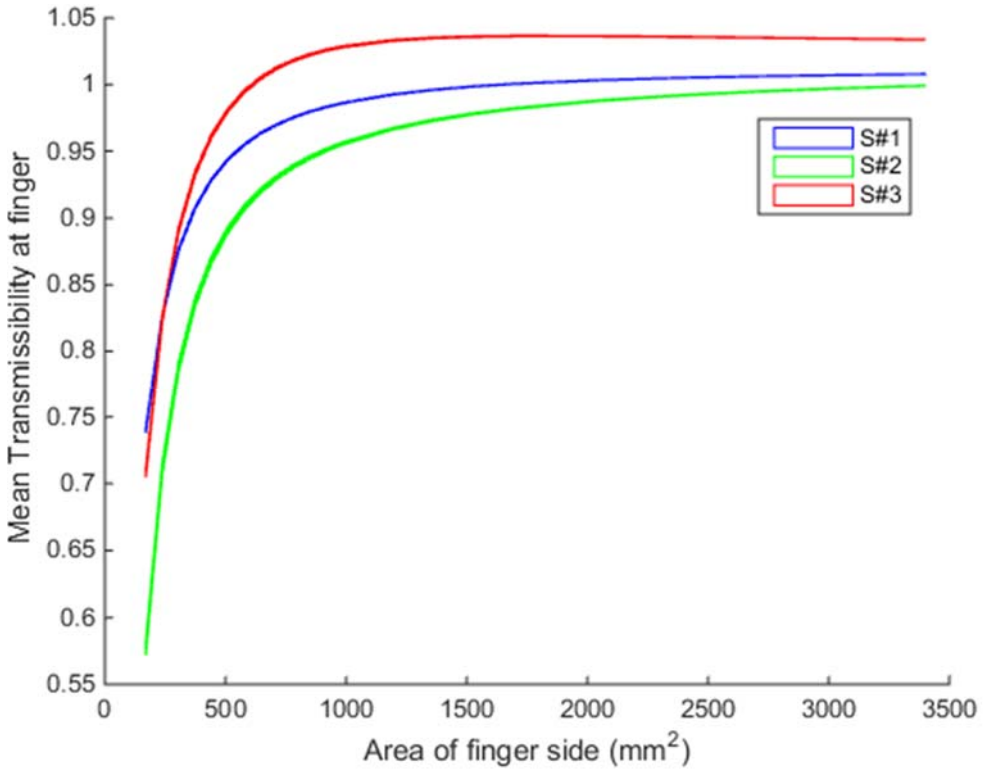

Figure A.6.20 - MVT at finger for high frequency band vs area of resilient material at finger side

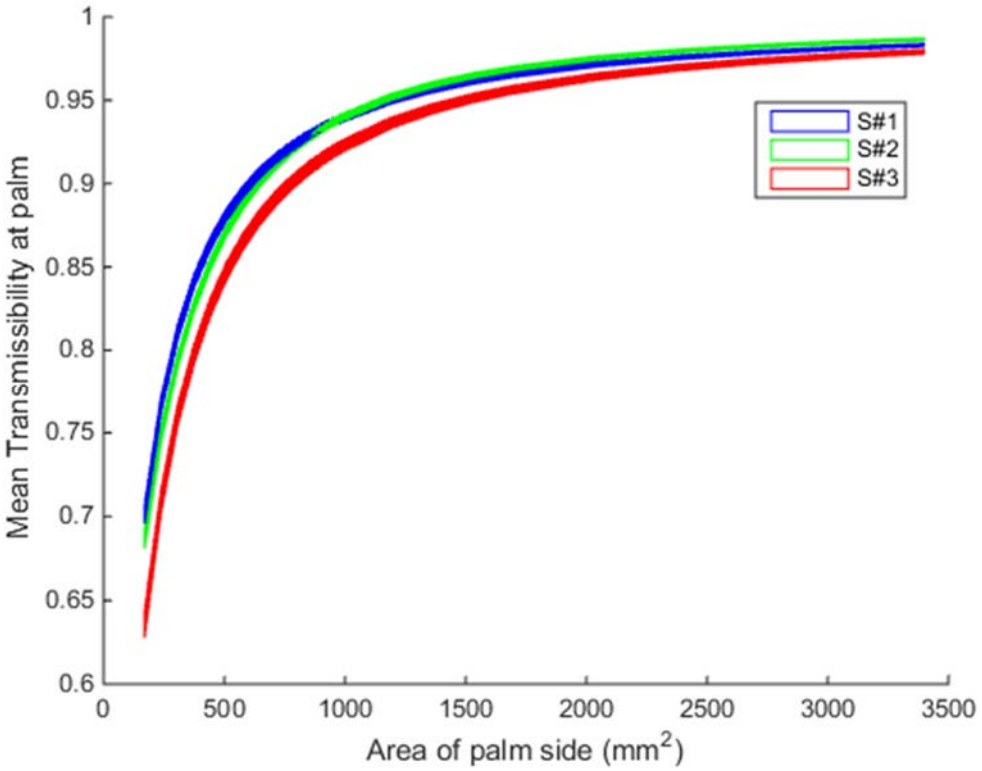

Figure A.6.21 - MVT at palm for medium frequency band vs area of resilient material at palm side

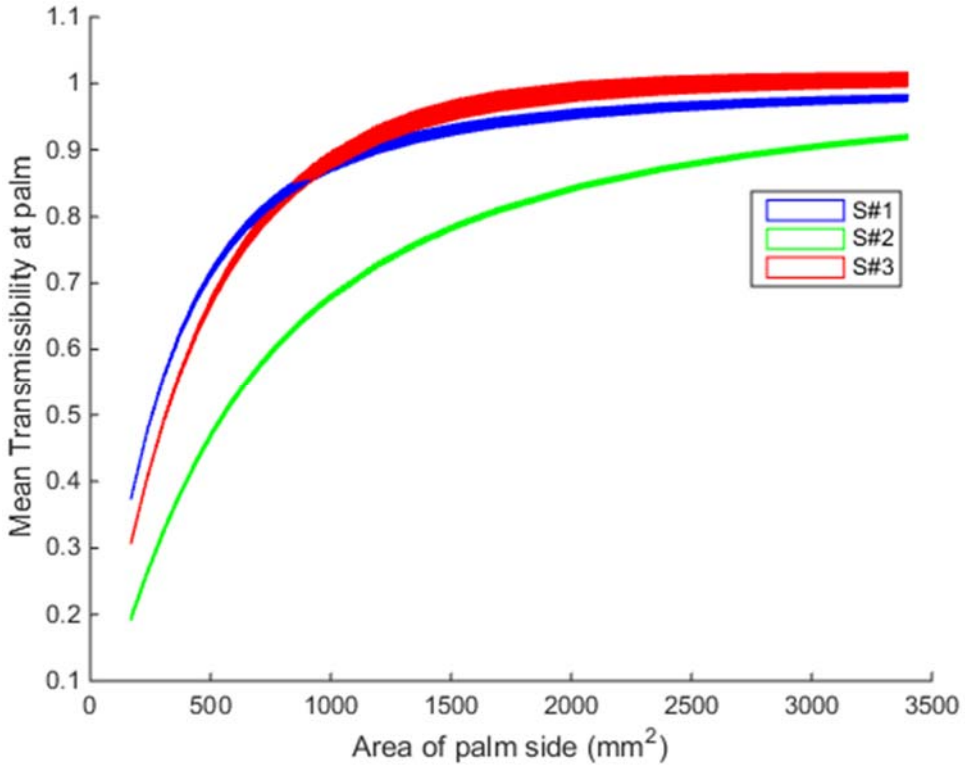

Figure A.6.22 - MVT at palm for high frequency band vs area of resilient material at palm side